



# UNIVERSITÀ DEGLI STUDI DI PALERMO

Dottorato di Ricerca in Scienze Molecolari e Biomolecolari

Dipartimento STEBICEF

Sezione di Chimica

S.S.D. - CHIM/06

## **SWEET IONIC LIQUIDS BASED MATERIALS FOR ENVIRONMENTAL APPLICATIONS**

**IL DOTTORE  
DOTT.SSA FLORIANA BILLECI**

**IL COORDINATORE  
PROF.SSA PATRIZIA DIANA**

**I TUTOR  
PROF.SSA FRANCESCA D'ANNA  
PROF. KENNETH R. SEDDON  
DOTT.SSA NATALIA V. PLECHKOVA  
DOTT. H. Q. NIMAL GUNARATNE**



To my Family.

To Ken, grateful to have known him.

## Table of Contents

List of Abbreviations and Acronyms.....	10
Abstract .....	13
1. Introduction .....	14
1.1 The sustainability issue in chemistry.....	14
1.2 About the solvent: the solution of Ionic Liquids .....	15
1.3 Greener Ionic Liquids: how to increase the biocompatibility .....	19
1.4 Sugar-based Ionic Liquids.....	22
1.5 Applications of sugar-based Ionic Liquids, a route toward the industry .....	28
1.6 The common aim.....	36
2. Gluconic derivatives: Synthesis and characterisation.....	39
2.1 Gluconic acid, a handy natural molecule.....	39
2.2 Sweet Ionic Liquids: synthesis and characterisation.....	42
2.3 Synthesis and characterisation of non-gluconic Ionic Liquids .....	60
2.4 Experimental section.....	65
2.4.1 Materials.....	65
2.4.2 Synthesis of the <i>N</i> -[2-(dimethylamino)ethyl]glucosamide intermediate .....	65
2.4.3 Synthesis of the <i>N</i> -[3-(dimethylamino)propyl]glucosamide intermediate ..	66
2.4.4 Synthesis of the <i>N</i> -[3-(imidazolyl)propyl]glucosamide intermediate .....	67
2.4.5 Synthesis of the <i>N</i> -[2-(dimethylamino)ethyl]glycolamide intermediate ..	67
2.4.6 Synthesis of the <i>N</i> -[2-(dimethylamino)ethyl]hexylamide intermediate ..	68
2.4.7 General quaternisation procedure to synthesise the $[C_{x y z(R)A w}]X$ ILs .....	68
2.4.8 $[N_{1 1 2GA 8}]Br$ .....	69
2.4.9 $[N_{1 1 3GA 8}]Br$ .....	69
2.4.10 $[N_{1 1 3GA 4}]I$ .....	70
2.4.11 $[N_{1 1 2GA 4}]I$ .....	70
2.4.12 $[Im_{3GA 4}]I$ .....	70
2.4.13 $[N_{1 1 2GA 4}]Br$ .....	71
2.4.14 $[N_{1 1 2GA 8L}]Br$ .....	71
2.4.15 $[N_{1 1 3GA 8L}]Br$ .....	72
2.4.16 $[N_{1 1 2GA 12}]Br$ .....	72
2.4.17 $[N_{1 1 2GlyA 8}]Br$ .....	72



2.4.18	[N <sub>1 1 2HexA 8</sub> ]Br .....	73
2.4.19	General methathesis procedure to synthesise the [N <sub>1 1 xGA 8</sub> ][NTf <sub>2</sub> ] ILs ....	73
2.4.20	[N <sub>1 1 2GA 8</sub> ][NTf <sub>2</sub> ] .....	74
2.4.21	[N <sub>1 1 3GA 8</sub> ][NTf <sub>2</sub> ] .....	74
2.4.22	General neutralisation reaction procedure to synthesise the gluconate salts .....	74
2.4.23	[P <sub>6 6 6 14</sub> ][Glu] .....	75
2.4.24	[P <sub>4 4 4 4</sub> ][Glu] .....	75
2.4.25	[N <sub>4 4 4 4</sub> ][Glu].....	75
2.4.26	[tmgH][Glu] .....	76
2.4.27	Differential Scanning Calorimetry (DSC).....	76
2.4.28	Thermogravimetric analysis (TGA) .....	76
2.4.29	POM measurements .....	76
2.4.30	NMR measurements .....	77
2.4.31	Mass spectrometric measurements.....	77
2.4.32	Conductivity measurements .....	77
3.	Novel “Sweet” Ionic Liquid Gels: combination of novel IL gelators and IL solvents .....	78
3.1	Gels in daily life.....	78
3.2	What is a Gel: definition and classification .....	79
3.3	How to combine gel concept and the Ionic Liquids to form Ionic Liquid Gels .....	83
3.4	Ionic Liquid Gels applications: a way to improve the Environmental Protection and Remediation.....	84
3.5	Gelation tests .....	90
3.6	Gel characterisations.....	93
3.7	Desulfurisation Process.....	112
3.8	Experimental Section.....	121
3.8.1.	Gelation Tests .....	121
3.8.2.	T <sub>gel</sub> determination.....	121
3.8.3.	POM measurements.....	121
3.8.4.	Opacity measurements.....	122
3.8.5.	RLS measurements .....	122
3.8.6.	NMR measurements .....	122
3.8.7.	Adsorption of sulfur compounds .....	123

4.	IL-Co complexes: a thermochromic and magnetic transition in a mild temperature range .....	124
4.1.	The Chromism phenomena .....	124
4.2.	Thermochromism: a common phenomenon for several compounds .....	125
4.3.	The thermochromism of metal complexes .....	128
4.3.1	Cobalt, an increasingly useful metal .....	130
4.3.2	The help of ILs to perform cobalt thermochromism.....	132
4.4.	Thermochromism of IL-Co complexes in IL: the achievement of the mild temperature range.....	135
4.4.1	Thermochromic behaviour and UV-Vis spectroscopy investigations .....	136
4.4.2	Magnetic moments of complexes in solution: the Evans method.....	151
4.4.3	A gaze on Cobalt: <sup>59</sup> Co NMR measurements .....	157
4.4.4	Designing a device: a thermochromic film .....	164
4.5.	Experimental Section .....	168
4.5.1	Materials .....	168
4.5.2	Thermochromic solution.....	168
4.5.3	Thermochromic film.....	168
4.5.4	Evans sample.....	169
4.5.5	VT UV-vis measurements.....	169
4.5.6	VT NMR measurements .....	169
	Conclusions.....	171
	Appendix.....	174
	Acknowledgements.....	183
	Curriculum Vitae.....	185

## Table of Figures

Figure 1 - Structures of common cations and anions in ILs. ....	17
Figure 2 - Some structures of the AAILs synthesised by Fukumoto <i>et al.</i> <sup>29</sup> .....	24
Figure 3 - Aliphatic cations tested by Fukumoto groups. ....	24
Figure 4 - CILs with hemi-, mesohemi-, meso- and D-tartrate. <sup>33</sup> .....	26
Figure 5 - ILs applications reported in this chapter. ....	28
Figure 6 - ILs structure employed by Schneider with CO <sub>2</sub> .....	31
Figure 7 - ILs combined with MDEA for CO <sub>2</sub> absorption. <sup>45</sup> .....	32
Figure 8 - Structures of the Cholinium ILs and of the antibiotics. <sup>47</sup> .....	34

Figure 9 - Structures of HILs. <sup>49</sup> .....	35
Figure 10 - Principal applications achieved. ....	37
Figure 11 - Aqueous equilibrium among gluconic acid, glucono- $\delta$ -lactone and glucono- $\gamma$ -lactone. ....	39
Figure 12 - POM images corresponding to [N <sub>4444</sub> ][Glu] (a) heating cycle; (b) cooling cycle.....	52
Figure 13 - POM images corresponding to [P <sub>4444</sub> ][Glu] (a) first heating cycle; (b) first cooling cycle; (c) second heating cycle; (d) second cooling cycle.....	53
Figure 14 - POM images corresponding to [P <sub>66614</sub> ][Glu] heating cycle. ....	54
Figure 15 - Gelators and solvents used to obtain ILGs for dyes adsorption. <sup>109</sup> .....	86
Figure 16 - Gelator used to obtain ILGs for dyes adsorption. <sup>110</sup> .....	87
Figure 17 - Structures of the phosphonium ILs to extract sulfur compounds. <sup>123</sup> .....	89
Figure 18 - Structures of gelators.....	90
Figure 19 - POM images of ILGs at 6.5 % wt. of gelator for: (a) [N <sub>4444</sub> ][Glu]/[N <sub>1444</sub> ][NTf <sub>2</sub> ] during the heating process until the isotropic solution, then the cooling process until formation of aggregates; (b) .....	96
Figure 20 -Strain sweep measurements at $f = 1$ Hz for: a) [P <sub>4444</sub> ][Glu]/[N <sub>2224</sub> ][NTf <sub>2</sub> ]; b) [P <sub>66614</sub> ][Glu]/[N <sub>1444</sub> ][NTf <sub>2</sub> ]. ....	100
Figure 21 - UV-Vis kinetic measurements at 568 nm for: a) [P <sub>4444</sub> ][Glu]/[N <sub>2224</sub> ][NTf <sub>2</sub> ]; b) [P <sub>66614</sub> ][Glu]/[N <sub>1444</sub> ][NTf <sub>2</sub> ]. ....	102
Figure 22 - RLS kinetic measurements for: a) [P <sub>4444</sub> ][Glu]/[N <sub>2224</sub> ][NTf <sub>2</sub> ]; b) [P <sub>66614</sub> ][Glu]/[N <sub>1444</sub> ][NTf <sub>2</sub> ]. ....	102
Figure 23 - VT <sup>1</sup> H NMR spectra for the [P <sub>4444</sub> ][Glu]/[N <sub>1444</sub> ][NTf <sub>2</sub> ] in the T range: 293 – 373 K. ....	105
Figure 24- Enlargement of the spectra reported in Figure 23, in the region 4.3-2.5 ppm. ....	106
Figure 25 - Enlarged region of VT <sup>1</sup> H NMR spectra of [P <sub>4444</sub> ][Glu]/[N <sub>1444</sub> ][NTf <sub>2</sub> ] at 12% wt. Protons are labelled on the gluconate structure (Ha: red marker; Hb: magenta marker; Hc: plum marker; Hd: blue marker). ....	107
Figure 26 – Trend and linear regression analysis of the chemical shift of Hc in the VT <sup>1</sup> H NMR for the gel a) [P <sub>4444</sub> ][Glu]/[N <sub>1444</sub> ][NTf <sub>2</sub> ]; b) [P <sub>66614</sub> ][Glu]/[N <sub>1444</sub> ][NTf <sub>2</sub> ]. ....	108
Figure 27 - FT-IR spectra for neat gelator, IL and corresponding ILG at 6.5 % wt. of gelator. ....	109
Figure 28 – AE of sulfur compounds on ILGs (6.5 % wt.) and the corresponding IL solvents at 20 °C. ....	116
Figure 29 - Plots of AE of sulfur compounds as a function of time for the ILGs: a) [P <sub>4444</sub> ][Glu]/[N <sub>2224</sub> ][NTf <sub>2</sub> ]; b) [P <sub>4444</sub> ][Glu]/[N <sub>1444</sub> ][NTf <sub>2</sub> ]. ....	116

Figure 30 – Comparison of AE of the solution of single compounds and mixed solutions of sulfur compounds (C = 1500 ppm) corresponding to: a) [P <sub>4444</sub> ][Glu]/[N <sub>224</sub> ][NTf <sub>2</sub> ]; b) [P <sub>4444</sub> ][Glu]/[N <sub>1444</sub> ][NTf <sub>2</sub> ].	117
Figure 31 - Comparison among the AE of the mixed solutions at different concentrations: a) [P <sub>4444</sub> ][Glu]/[N <sub>224</sub> ][NTf <sub>2</sub> ]; b) [P <sub>4444</sub> ][Glu]/[N <sub>1444</sub> ][NTf <sub>2</sub> ].	118
Figure 32 - Comparison among the AE of the mixed solutions at different volumes: a) [P <sub>4444</sub> ][Glu]/[N <sub>224</sub> ][NTf <sub>2</sub> ]; b) [P <sub>4444</sub> ][Glu]/[N <sub>1444</sub> ][NTf <sub>2</sub> ].	119
Figure 33 - Comparison among the AE obtained with a different contact area: a) [P <sub>444</sub> ][Glu]/[N <sub>224</sub> ][NTf <sub>2</sub> ]; b) [P <sub>4444</sub> ][Glu]/[N <sub>1444</sub> ][NTf <sub>2</sub> ].	119
Figure 34 - Cycles of reuse in the adsorption process for the ILG: a) [P <sub>4444</sub> ][Glu]/[N <sub>224</sub> ][NTf <sub>2</sub> ]; b) [P <sub>4444</sub> ][Glu]/[N <sub>1444</sub> ][NTf <sub>2</sub> ].	120
Figure 35 - Triazine ligands to form cobalt complexes. <sup>172</sup>	132
Figure 36 - Solution of [N <sub>112GA8</sub> ]Br/Co(NTf <sub>2</sub> ) <sub>2</sub> /[N <sub>224</sub> ][NTf <sub>2</sub> ] at 65 °C, varying the ligand/metal ratio from 1.5:1 to 7:1.	137
Figure 37 - Colour shades for the solution [N <sub>112GA8</sub> ]Br/Co(NTf <sub>2</sub> ) <sub>2</sub> /[N <sub>224</sub> ][NTf <sub>2</sub> ] in the concentration ratios: 3:1 -7:1. The range of temperature: 15-95 °C (the temperature increases of 5 °C- only in the ratio 7:1 the temperature increase of 10 °C up to 30°C)	138
Figure 38 - VT UV-Vis spectra of the solution [N <sub>112GA8</sub> ]Br/Co(NTf <sub>2</sub> ) <sub>2</sub> /[N <sub>224</sub> ][NTf <sub>2</sub> ] at different ratios: a) 3:1; b) 5:1; c) 6:1; d) 7:1.	139
Figure 39 - VT UV-Vis absorbance (725.0 nm) trends with the temperature of the solution [N <sub>112GA8</sub> ]Br/Co(NTf <sub>2</sub> ) <sub>2</sub> /[N <sub>224</sub> ][NTf <sub>2</sub> ] at different ratios: a) 3:1; b) 5:1; c) 6:1; d) 7:1.	141
Figure 40 - VT UV-Vis spectra for the system Co(NTf <sub>2</sub> ) <sub>2</sub> /[N <sub>224</sub> ][NTf <sub>2</sub> ].	143
Figure 41 - Colour shades for the solution [N <sub>112GA8</sub> ]Br/Co(NTf <sub>2</sub> ) <sub>2</sub> /[C <sub>1</sub> C <sub>4</sub> pyrr][NTf <sub>2</sub> ] and [N <sub>112GA8</sub> ]Br/Co(NTf <sub>2</sub> ) <sub>2</sub> /[N <sub>113</sub> ][NTf <sub>2</sub> ] at molar ratio 3:1, in the range of temperature: 20-95 °C (the temperature increases by 5 °C).	143
Figure 42 – VT UV-Vis spectra for the systems: a) [N <sub>112GA8</sub> ]Br/Co(NTf <sub>2</sub> ) <sub>2</sub> /[C <sub>1</sub> C <sub>4</sub> pyrr][NTf <sub>2</sub> ]; b) and [N <sub>112GA8</sub> ]Br/Co(NTf <sub>2</sub> ) <sub>2</sub> /[N <sub>113</sub> ][NTf <sub>2</sub> ].	144
Figure 43 - UV-Vis absorbance trends for the systems: a) [N <sub>112GA8</sub> ]Br/Co(NTf <sub>2</sub> ) <sub>2</sub> /[C <sub>1</sub> C <sub>4</sub> pyrr][NTf <sub>2</sub> ] (724.0 nm); b) and [N <sub>112GA8</sub> ]Br/Co(NTf <sub>2</sub> ) <sub>2</sub> /[N <sub>113</sub> ][NTf <sub>2</sub> ] (723.0 nm).	145
Figure 44 - Colour shades for the [N <sub>112GA8</sub> ][NTf <sub>2</sub> ]/ Co(NTf <sub>2</sub> ) <sub>2</sub> /[N <sub>224</sub> ][NTf <sub>2</sub> ] at variable temperature.	146
Figure 45 - VT UV-Vis investigation for the [N <sub>112GA8</sub> ][NTf <sub>2</sub> ]/ Co(NTf <sub>2</sub> ) <sub>2</sub> /[N <sub>224</sub> ][NTf <sub>2</sub> ] system: a) UV-Vis spectra; b) trend of the absorbance at 697.0 nm with the temperature.	147
Figure 46 - VT UV-Vis spectra for the system: a) [N <sub>112GlyA8</sub> ]Br/ Co(NTf <sub>2</sub> ) <sub>2</sub> /[N <sub>224</sub> ][NTf <sub>2</sub> ]; b) [N <sub>112HexA8</sub> ]Br/ Co(NTf <sub>2</sub> ) <sub>2</sub> /[N <sub>224</sub> ][NTf <sub>2</sub> ].	148

Figure 47 - Colour shades for the system $[N_{1.13GA8}]Br/Co(NTf_2)_2/[N_{2.224}][NTf_2]$ .....	149
Figure 48 - VT UV-Vis measurement for the system $[N_{1.13GA8}]Br/Co(NTf_2)_2/[N_{2.224}][NTf_2]$ : a) spectra at variable temperatures; b) trend of the absorbance at 725.5 nm with the temperature. ....	149
Figure 49 - Colour change for the system $[Im_{3GA4}]I$ .....	150
Figure 50 - VT UV-Vis measurement for the system $[Im_{3GA4}]I$ : a) spectra at variable temperature; b) trend of the absorbance at 782.5 nm. ....	150
Figure 51 - Simplified representation of the possible electronic distribution in the two complexes, (left) octahedral in pink and (right) tetrahedral in blue, for the system $[N_{1.12GA8}]Br/Co(NTf_2)_2/[N_{2.224}][NTf_2]$ (molar ratio [ligand]/[metal] = 3:1). ....	155
Figure 52 – Trends of: a) $\Delta\delta$ as a function of temperature; b) $\mu_{eff}$ as a function of the temperature for the system $[N_{1.12GA8}]Br/Co(NTf_2)_2/[N_{2.224}][NTf_2]$ . ....	156
Figure 53 – Trends of: a) $\Delta\delta$ as a function of temperature; b) $\mu_{eff}$ as a function of the temperature for the system $[N_{1.13GA8}]Br/Co(NTf_2)_2/[N_{2.224}][NTf_2]$ . ....	157
Figure 54 –VT $^{59}Co$ NMR for the system $[N_{1.12GA8}]Br/Co(NTf_2)_2/[N_{2.224}][NTf_2]$ in the range 20 – 90 °C ( $^{59}Co$ signal for $K_3[Co(CN)_6]$ fixed at 0 ppm).....	158
Figure 55 – Plot of $\Delta\delta$ as function of temperature in the range 20 – 90 °C for the system $[N_{1.12GA8}]Br/Co(NTf_2)_2/[N_{2.224}][NTf_2]$ .....	159
Figure 56 - VT $^{59}Co$ NMR for the system $[N_{1.12GA8}]Br/Co(NTf_2)_2/[N_{2.224}][NTf_2]$ at molar ratio [ligand]/[metal]=7 in the range 30 – 90 °C ( $^{59}Co$ signal for $K_3[Co(CN)_6]$ fixed at 0 ppm).....	160
Figure 57 - Trend of $\Delta\delta$ increasing the temperature for the system $[N_{1.12GA8}]Br/Co(NTf_2)_2/[N_{2.224}][NTf_2]$ at molar ratio [ligand]/[metal]=7:1 in the range 30 – 90 °C.....	160
Figure 58 - VT $^{59}Co$ NMR for the system $[N_{1.12GA8}][NTf_2]/Co(NTf_2)_2/[N_{2.224}][NTf_2]$ in the range 25 – 85 °C ( $^{59}Co$ signal for $K_3[Co(CN)_6]$ fixed at 0 ppm).....	161
Figure 59 - Trend of $\Delta\delta$ increasing the temperature in the range 25 – 85 °C for the system $[N_{1.12GA8}][NTf_2]/Co(NTf_2)_2/[N_{2.224}][NTf_2]$ . ....	161
Figure 60 - VT $^{59}Co$ NMR for the system $[N_{1.13GA8}]Br/Co(NTf_2)_2/[N_{2.224}][NTf_2]$ in the range 20 – 90 °C ( $^{59}Co$ signal for $K_3[Co(CN)_6]$ fixed at 0 ppm).....	162
Figure 61 - Trend of $\Delta\delta$ increasing the temperature in the range 20 – 90 °C for the system $[N_{1.13GA8}]Br/Co(NTf_2)_2/[N_{2.224}][NTf_2]$ .....	162
Figure 62 - VT $^{59}Co$ NMR for the system $[Im_{3GA4}]I/Co(NTf_2)_2/[N_{2.224}][NTf_2]$ in the range 25 – 85 °C ( $^{59}Co$ signal for $K_3[Co(CN)_6]$ fixed at 0 ppm).....	163
Figure 63 - Trend of $\Delta\delta$ increasing the temperature in the range 20 – 90 °C for the system $[Im_{3GA8}]Br/Co(NTf_2)_2/[N_{2.224}][NTf_2]$ . ....	163
Figure 64 - Thermochromic polymeric film $[N_{1.12GA8}]Br/Co(NTf_2)_2/PMMA$ : a) 25 °C; b) 60 °C.....	166

Figure 65 – VT UV-Vis measurement for the polymeric film  $[N_{112GA}][Br]/Co(NTf_2)_2/PMMA$ : a) spectra in the range of temperature 20-65 °C; b) trend of the absorbance increasing the temperature. .... 166

## Table of Schemes

Scheme 1 - Double alkylation of the imidazole to generate the imidazolium ILs. <sup>27</sup> .....	22
Scheme 2 - Synthesis of the Bz-His-OMe ILs. <sup>37</sup> .....	28
Scheme 3 - BASIL™ process using IL. ....	29
Scheme 4 - Oxidation of glucose by glucose oxidase ( <i>Aspergillus niger</i> ).....	40
Scheme 5 - The synthetic pathway to obtain new "sweet" ammonium ILs. ....	42
Scheme 6 - Metathesis to exchange the $[Br]^-$ anion with the $[NTf_2]^-$ anion. ....	44
Scheme 7 - The synthetic pathway to obtain the $[Im_{3AG4}]I$ IL.....	45
Scheme 8 - The synthetic pathway to obtain the gluconate ILs. ....	45
Scheme 9 - The synthetic pathway of the $[N_{112GlyA8}]Br$ IL. ....	61
Scheme 10 - The synthetic pathway of the $[N_{112HexA8}]Br$ IL. ....	62
Scheme 11 - Schematic illustration of the 3D-network formation.....	83
Scheme 12 - Equilibrium between: a) the ring-opened form (coloured); b) the ring-closed form (colourless) for the Crystal Violet Lactone. <sup>155</sup> .....	127
Scheme 13 - Dehydration of Ni(II) complex showing irreversible Thermochromism. <sup>157</sup> .....	128
Scheme 14 - Thermochromic equilibrium of the $[P_{4444}]_2[Co^{II}(sal)_2]$ complexes, in the hydrated (right) and anhydrous (left) form. <sup>175</sup> .....	134
Scheme 15 - Equilibrium of the Co-isothiocyanate complexes between the tetrahedral (left) and the octahedral (right) geometry depending on the change of the temperature. <sup>176</sup> .....	134

## Table of Tables

Table 1 – Thermal properties of Alanine-based Ionic Liquids. ....	25
Table 2 - Thermal properties of the tetrabutylphosphonium and the tetrabutylammonium AAILs. ....	25
Table 3 - Structures of ILs obtained with the synthesis reported in Scheme 5. ....	43
Table 4 - Structures of ILs obtained after the anion metathesis reported in Scheme 6. ....	44
Table 5 –Structure of new gluconate ILs. ....	46
Table 6 - Thermal properties (DSC and TGA) of the ILs with the gluconic moiety on the cation.....	47

Table 7 - Thermal properties (DSC and TGA) of the ILs and salt with the gluconate anion.....	50
Table 8 - Viscosity values, VFT parameters, fragility and fragility index.....	55
Table 9 - Conductivity values for ILs synthesised. ( <sup>a</sup> = This value was taken as known value to calculate the cell constant). .....	60
Table 10 - Thermal properties (DSC and TGA) of the [N <sub>1 1 2GlyA 8</sub> ]Br IL. ....	61
Table 11 - Thermal properties (DSC and TGA) of the [N <sub>1 1 2HexA 8</sub> ]Br IL.....	62
Table 12 - Viscosity values, VFT parameters, fragility and fragility index.....	63
Table 13 - Conductivity values for ILs synthesised. ( <sup>a</sup> = This value was taken as known value to calculate the cell constant) <sup>81</sup> .....	64
Table 14 - Gelation tests performed in conventional solvents for the gelators used (S= soluble after heating; I= insoluble; SC= soluble without heating; PG= gel like precipitate). *: wt. = $\frac{g_{gelator}}{g_{solution}}$ .....	92
Table 15 – ILGs obtained and relevant CGCs. *: wt. = $\frac{g_{gelator}}{g_{solution}}$ .....	93
Table 16 - CGC and $T_{gel-CGC}$ corresponding to gel phases obtained. $T_{gel-6.5\%wt.}$ , sol-gel temperature ( $T_{c-6.5\%wt.}$ ), gel-sol and sol-gel enthalpy ( $\Delta H_m$ and $\Delta H_c$ ) determined for gel phases at 6.5 % wt. by DSC measurements ( <sup>a</sup> : Determined by the lead-ball method. $T_{gel}$ were reproducible within $\pm 1$ °C. <sup>b</sup> : Determined by DSC). *: wt = $\frac{g_{gelator}}{g_{solution}}$ .....	94
Table 17 - Thixotropic and sonotropic behaviour of ILGs at 6.5% wt. (*= after 5 min of sonication, the gel phase persist.; / =the gel phase is too soft to detect the $T_{gel}$ ). .....	99
Table 18 - Yield strain at crossover point ( $\gamma$ ) values determined at 1Hz frequency and 25 °C for ILGs at 6.5% wt.. Error limits are based on an average of three different measurements.....	100
Table 19 - Gelation time ( $t_g$ ), RLS intensity ( $I_g$ ) and opacity ( $A_g$ ) of ILGs.....	103
Table 20 - Fitting parameters corresponding to chemical shift variation as a function of temperature for the Hc protons of the gluconate anion (R = correlation coefficient). .....	108
Table 21 - Stretching frequencies corresponding to gelator ( $\nu_{gelator}$ ) and ILGs ( $\nu_{ILG}$ ) and changes in stretching frequencies ( $\Delta\nu$ ) on going from gelator to gel phase..	111
Table 22 - AE% of sulfur compounds on ILGs (at 6.5% wt.) of gelator and corresponding ILs at 20 °C and 30 °C. ....	114
Table 23 - Temperature of the geometry switch for the system [N <sub>1 1 2GA 8</sub> ]Br/Co(NTf <sub>2</sub> ) <sub>2</sub> /[N <sub>2 4 4 4</sub> ][NTf <sub>2</sub> ] at different ratios. * = $T_{switch}$ s were reproducible within 1 °C. ....	142
Table 24 - Temperature of the switch for the system [N <sub>1 1 2GA 8</sub> ]Br/Co(NTf <sub>2</sub> ) <sub>2</sub> in different IL-solvent. * = $T_{switch}$ s were reproducible within 1 °C.....	145
Table 25 - Magnetic moments and relative temperatures for the system [N <sub>1 1 2GA 8</sub> ]Br/Co(NTf <sub>2</sub> ) <sub>2</sub> /[N <sub>2 2 2 4</sub> ][NTf <sub>2</sub> ] (molar ratio [ligand]/[metal] = 3:1). ....	154

Table 26 - Magnetic moments and relative temperatures for the system  $[N_{113GA}$   
 $_8]Br/Co(NTf_2)_2/[N_{2224}][NTf_2]$  (molar ratio [ligand]/[metal] = 3:1). ..... 156



## List of Abbreviations and Acronyms

<b>3D-network</b>	Three Dimensional Network
<b>AAILs</b>	Amino Acid Ionic Liquids
<b>ABS</b>	Aqueous Biphasic System
<b>AE</b>	Adsorption Efficiency
<b>BASIL™</b>	Biphasic Acid Scavenging utilising Ionic Liquids
<b>CGC</b>	Critical Gelation Concentration
<b>CILs</b>	Chiral Ionic Liquids
<b>COD</b>	Chemical Oxygen Demand
<b>DSC</b>	Differential Scanning Calorimetry
<b>FT-IR</b>	Fourier Transformation Infrared
<b>GntK</b>	Human gluconokinase
<b>HILs</b>	Herbicidal Ionic Liquids
<b>HPLC</b>	High-Performance Liquid Chromatography
<b>ILG</b>	Ionic Liquid Gel
<b>IL</b>	Ionic Liquid
<b>IPC-81</b>	rat cancer cells
<b>ISPRA</b>	Italian institute for the environmental researcher and protection
<b>ISTAT</b>	Italian national statistical institute
<b>LCA</b>	Life-Cycle Assessment
<b>LCS</b>	Luminescent Solar Concentrators
<b>LMMG</b>	Low Molecular Mass Gelator
<b>LMOG</b>	Low Molecular Organic Gelator
<b>LMWG</b>	Low Molecular Weight Gelator
<b>OECD</b>	Organisation for Economic Co-operation and Development
<b>PCBs</b>	Polychlorinated Biphenyls
<b>POM</b>	Polarised Optical Microscopy
<b>RTILs</b>	Room Temperature Ionic Liquids
<b>SPME</b>	Solid Phase Microextraction
<b>TGA</b>	Thermogravimetric Analysis
<b>ThCO<sub>2</sub></b>	Theoretical Carbon Dioxide Demand
<b>ThOD</b>	Theoretical Oxygen Demand
<b>TLC</b>	Thermochromic Liquid Crystal
<b>VFT</b>	Vogel-Fulcher-Tamman model
<b>VT <sup>1</sup>H NMR</b>	<sup>1</sup> H NMR at variable temperature
<b>VT <sup>59</sup>Co NMR</b>	<sup>59</sup> Co NMR at variable temperature
<b>VT UV-Vis</b>	UV-Vis at variable temperature
<b>A<sub>g</sub></b>	UV-Vis absorbance value corresponding to gel formation
<b>D</b>	Fragility
<b>G'</b>	Storage modulus
<b>G''</b>	Loss modulus
<b>G*</b>	Complex shear modulus

$I_g$	RLS intensity value corresponding to gel formation
$I_{RLS}$	RLS intensity
$m$	Fragility index
$T_{c-6.5 \% wt.}$	Temperature of gel formation at 6.5 % wt.
$t_g$	Time of gelation
$T_{gel}$	Melting temperature of the gel phase
$T_{gel-6.5 \% wt.}$	Melting temperature of the gel phase at 6.5 % wt.
$T_{gel-CGC}$	Melting temperature of the gel phase at CGC concentration
$T_{switch}$	Temperature corresponding to the colour change in the thermochromic solution
$\gamma$ at $G'=G''$	Strain at cross over point $G'=G''$
$\delta$	Chemical shift
$\Delta\delta$	Changes in chemical shift
$\Delta\nu$	Changes in stretching frequencies
$\mu_{eff}$	Effective magnetic moment
$\nu_{gelator}$	Stretching frequencies corresponding to gelator
$\nu_{ILG}$	Stretching frequencies corresponding to ILG
$\sigma$	Conductivity
$\chi_A$	Susceptibility per gram atom of paramagnetic ion
$\chi_g$	Mass of gram susceptibility
$\chi_m$	Molar susceptibility
$\chi_v$	Magnetic susceptibility per unit of volume
[aliquat]	Trioctylmethylammonium
$[C_4C_{1im}]_2NiCl_4$	Di-(1-butyl-3-methylimidazolium) tetrachloronickelate
$[C_{16}im][NTf_2]$	1-Hexadecyl-3-methylimidazolium bis{(trifluoromethyl)sulfonyl}imide
$[C_1C_2im][N(CN)_2]$	1-Ethyl-3-methylimidazolium dicyanoamide
$[C_1C_4pip][NTf_2]$	Butyl methyl piperidinium bis{(trifluoromethyl)sulfonyl}imide
$[C_1C_4pyrr][NTf_2]$	Butyl methyl pyrrolidinium bis{(trifluoromethyl)sulfonyl}imide
$[C_2C_{1im}][PF_6]$	1-Butyl-3-dimethylimidazolium hexafluorophosphate
$[C_2OHmim][BF_4]$	1-(3-Hydroxyethyl)-3-methylimidazolium tetrafluoroborate
$[C_4C_1C_{1im}][D-H-Tart]$	1-Butyl-2,3-dimethylimidazolium D-bitartrate monohydrate
$[C_8C_{1im}][BF_4]$	1-Octyl-3-methylimidazolium tetrafluoroborate
$[C_8C_{1im}]$	1-Octyl-3-methylimidazolium
$[C_8pyr][meso-H-Tart]$	1-Octylpyridinium meso-tartrate monohydrate
[Ch][Leu]	Cholinium leucinate
$[Co(NCS)_4]^{2-}$	Tetra(isothiocyanate) Cobalt(II)
$[Co(NCS)_6]^{6-}$	Hexa(isothiocyanate) Cobalt(II)
[DCA] <sup>-</sup>	Dicyanamide
$[N_{1113}][NTf_2]$	Trimethyl propyl ammonium bis{(trifluoromethyl)sulfonyl}imide
$[N_{1444}][NTf_2]$	Tributyl methyl ammonium bis{(trifluoromethyl)sulfonyl}imide
$[N_{2222}][L-Ala]$	Tetraethylammonium L-alaninate
$[N_{2222}][\beta-Ala]$	Tetraethylammonium $\beta$ -alaninate
$[N_{2224}][NTf_2]$	Trimethyl butyl ammonium bis{(trifluoromethyl)sulfonyl}imide
$[N_{4444}][Ala]$	Tetrabutylammonium alaninate

<b>[N<sub>4444</sub>][D-H-Tart]</b>	Tetrabutylammonium D-bitartrate monohydrate
<b>[N<sub>4444</sub>][Gly]</b>	Tetrabutylammonium glycinate
<b>[N<sub>4444</sub>][Val]</b>	Tetrabutylammonium valinate
<b>[N<sub>4446</sub>]<sup>+</sup></b>	Tributylhexylammonium
<b>[NH<sub>4</sub>][NO<sub>3</sub>]</b>	Ammonium nitrite
<b>[Ni(diam)<sub>2</sub>(NO<sub>2</sub>)<sub>2</sub>]</b>	Ni(diamine) <sub>2</sub> (NO <sub>2</sub> ) <sub>2</sub>
<b>[Ni(diam)<sub>2</sub>(ONO)<sub>2</sub>]</b>	Ni(diamine) <sub>2</sub> (ONO) <sub>2</sub>
<b>[P<sub>4444</sub>][Ala]</b>	Tetrabutylphosphonium alaninate
<b>[P<sub>4444</sub>][Co<sup>II</sup>(sal)<sub>2</sub>]</b>	Tetrabutylphosphonium cobalt(II)bis(salicylate)
<b>[P<sub>4444</sub>][Gly]</b>	Tetrabutylphosphonium glycinate
<b>[P<sub>4444</sub>][Val]</b>	Tetrabutylphosphonium valinate
<b>[P<sub>66614</sub>][Met]</b>	Trihexyltetradecylphosphonium methioninate
<b>[P<sub>66614</sub>][Pro]</b>	Trihexyltetradecylphosphonium proline
<b>[P<sub>66614</sub>]Cl</b>	Trihexyltetradecylphosphonium chloride
<b>[p-C<sub>12</sub>][Fum]</b>	3,3'-Di-n-decyl-1,1'(1,4-phenylenedimethylene)-diimidazolium Fumarate
<b>[TBCEP]Br</b>	Tributyl(1,2-dicarboxyethyl)phosphonium bromide
<b>[TBHPP]Cl</b>	Tributyl(2,3-dihydroxypropyl)phosphonium chloride
<b>[tmgH]Br</b>	Tetramethylguanidinium bromide
<b>[tmgH]Cl</b>	Tetramethylguanidinium chloride
<b>[tmgH]I</b>	Tetramethylguanidinium iodide
<b>34pba</b>	3-(4-pyridyl)benzoate
<b>Ala</b>	Alanine
<b>Arg</b>	Arginine
<b>Asn</b>	Asparagine
<b>BT</b>	Benzothiophene
<b>Co(NTf<sub>2</sub>)<sub>2</sub></b>	Cobalt(II) bis{(trifluoromethyl)sulfonyl}imide
<b>Cys</b>	Cysteine
<b>DBT</b>	Dibenzothiophene
<b>DMC</b>	Dichloromethane
<b>DMSO</b>	Dimethylsulfoxide
<b>FAD</b>	Flavin adenine dinucleotide
<b>His</b>	Histidine
<b>K<sub>3</sub>[Co(CN)<sub>6</sub>]</b>	Potassium hexacyanocobaltate(III)
<b>Leu</b>	Leucine
<b>LiNTf<sub>2</sub></b>	Lithium bis{(trifluoromethyl)sulfonyl}imide salt
<b>MDEA</b>	Methyldiethanoamine
<b>Met</b>	Methionine
<b>OPs</b>	Organophosphate esters
<b>PEMA</b>	Poly(ethylmethacrylate)
<b>PMMA</b>	Poly(methylmethacrylate)
<b>Pro</b>	Proline
<b>T</b>	Thiophene
<b>Trp</b>	Tryptophan

## Abstract

The fundamental role of Chemistry on the environmental fate is glaring and undeniable. Synthesis and applications between chemical compounds and systems produce waste and by-products which will have an impact on the ecosystem.

In this way, the compromise of the biodegradability and the toxicity of new compounds has to be considered. Environmental safety and remediation were taken into consideration in this Research Project. In particular, the synthesis of novel Ionic Liquids (ILs) was the base to set it up. ILs are a chemical class of compounds which consists of organic salts. The canonical definition of these compounds is based on having a melting point lower than 100 °C. These salts are characterised by attractive properties, such as low flammability and negligible vapour pressure. These ILs are widely employed as solvents to replace conventional solvents, as catalysts, as extractive and sorbent components. However, for a long time, these class of chemicals was described as “Green” and “Eco-friendly” without any investigation on their degradation. Indeed, only in the last decade, the pollution due to ILs was addressed. The biodegradation and the toxicity of these compounds became fundamental parameters to develop synthesis and applications.

Hence, in this Thesis, synthesis and applications of ILs were designed considering the sustainable Chemistry as a hinge point.

For this purpose, the gluconic acid was taken into account as starting material to obtain novel ILs. In particular, two groups of ILs were synthesised, taking advantage of the sugar moiety as part of the cation or the anion.

The applications of ILs were also conceived for a “Green” impact on the environment, believing that Chemistry can improve the human foot print on living ecosystem.

Therefore, these ILs were applied for environmental remediation designing Ionic Liquid Gels (ILGs) to remove sulfur compounds from fuels.

Furthermore, these ILs were also employed as ligands for metals, in order to generate thermochromic system for energetic storage devices.

# 1. Introduction

## 1.1 The sustainability issue in chemistry

Chemistry as a science, over the years, received adverse publicity due its perceived impact on the environment and human health. Chemistry is a dynamic science, which always has a strong biunivocal relationship with the society to which for example provides drugs (for therapeutic welfare of humans) and other useful chemicals for societal needs. In the XX century a new approach to chemistry, involving both the academic and industrial laboratories has been introduced.<sup>1</sup>

1998 was the year which determined the breakthrough taking into consideration the “Twelve Principles of the Green Chemistry”.<sup>2</sup> Before, the idea of a new approach to chemistry, which would take into account the value of the resources and the consequence of a science without rules, was an issue for few. After the birth of ‘green chemistry’, the impact of the chemistry on the environment and the use of the natural sources were, and still are, vital aspects of every new project that was taken into consideration.

These twelve principles paved the route for a new way of doing chemistry, and soon several indicators as the atom economy, the E-factor and the selectivity were defined.

Anastas and Warner formalised the Green Chemistry, in the “Report of the World Commission on Environment and Development: Our Common Future”, and the sustainable development was defined as: “development that meets the needs of the present without compromising the ability of future generations to meet their own needs”.<sup>3</sup> This concept will be later recovered and recast by James H. Clarke to describe the difference between Green Chemistry and Sustainable Chemistry. The principles of Green Chemistry define the “eco-friendly” reaction path, which has become increasingly important in chemical processes without the

---

1. Bernela, B.; Piccirilli, A.; Estrine, B.; Patouillard, N.; Guilbot, J.; Jerome, F., Sustainable chemistry: how to produce better and more from less? *Green Chem.* **2017**, *19* (21), 4973-4989.

2. Anastas, P. T.; Warner, J. C., *Green Chemistry: Theory and practice*. Oxford University press, New York: **1998**.

3. *Report of the World Commission on Environment and Development: Our Common Future*; Brundtland Commission report, United Nations: **1987**.

toxicity and the biodegradability concepts. The sustainability takes into account the whole process, from the raw materials to the disposal of unwanted by-products, and also, their economic and social impact.<sup>4</sup>

In the sustainability point of view, a synthetic process should be “eco-friendly”, using renewable or recyclable starting materials and respecting the principles of Green Chemistry; the synthesised products have to be non-toxic and recyclable, inducing improvements in the scientific research and, if it is possible, in the social economy. Moreover, the existing processes should be optimised, introducing renewable carbon sources.

It is always necessary to consider the whole chain of a process leading to the final objective. If a process based on a renewable source, which produces unnecessary co-products or spends more energy than the same process based on the fossil carbon, it is in conflict with the sustainable view, it could be better the use of fossil carbon as starting material and as alternative energy source. Every step can be crucial, therefore has to be considered.

Life-cycle assessment (LCA) analysis could be considered the practical approach at the sustainable chemistry. The “cradle to grave” approach identifies and considers all aspects of the environmental impact, from the raw materials and the product to the storage and the transportation, considering also the waste recovery recycle and its disposal, ending with the quantity of energy necessary for each part.<sup>1</sup> The objective to recycle or enhance the neglected materials is the base to move towards the circular economy, decreasing the waste and converting the valueless for one process into the raw material for another.<sup>4</sup>

## **1.2 About the solvent: the solution of Ionic Liquids**

A component almost omnipresent in chemical reactions and processes is the solvent, and on its use is based mostly on the known chemistry; purifications, extractions, phase-separations are only a few processes depending on the solvent. Moreover, the quantity used is often not moderate, and, if it is not recyclable, it

---

4. Clark, J. H., Chapter 1 Green and Sustainable Chemistry: An Introduction. In *Green and Sustainable Medicinal Chemistry: Methods, Tools and Strategies for the 21st Century Pharmaceutical Industry*, The Royal Society of Chemistry: **2016**; pp 1-11.

becomes problematic in terms of toxicity, pollution and environmental damage.<sup>5</sup> According to the principles of the Green Chemistry, the solvent should be reduced as much as possible. In the last decades, research was focused on finding the solvent system capable of replacing conventional organic solvents and water without compromising the efficiency of the processes in which they are used.

In order to begin the replacing, many solvents have been ranked taking into account the safety and health considerations. This ranking and the derived guides are an important tile in the sustainable development.<sup>6</sup>

Welton in “Solvents and sustainable chemistry” highlighted how a solvent could improve the sustainability of a chemical process, being both solvent and reagent, increasing the quality of the products and decreasing the number of the steps and the co-products formation.<sup>7</sup>

Ionic Liquids (ILs) were developed at the turn of the XIX and XX centuries. The first report was thanks to Atwood with his “red oil”, a stable intermediate in Friedel–Crafts reactions. Yoke was alert to realise that melts of copper(I) chloride and alkylammonium chlorides were liquid near to room temperature. Several other chemists contributed to the development of IL, as often happened in science, by the union of events and the perspicacity.<sup>8</sup>

---

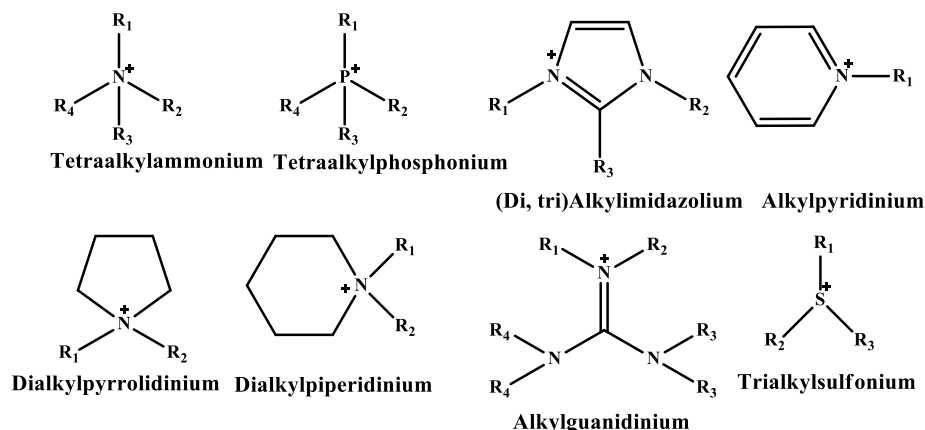
5. Turner, C.; Wang, J., Green solvents: A solution of air pollution and climatic changes. *Current Opinion in Green and Sustainable Chemistry* **2017**, *5*, ii-iii.

6. Capello, C.; Fischer, U.; Hungerbuhler, K., What is a green solvent? A comprehensive framework for the environmental assessment of solvents. *Green Chem.* **2007**, *9* (9), 927-934.

7. Welton, T., Solvents and sustainable chemistry. *Proceedings of the Royal Society A: Mathematical, Physical and Engineering Science* **2015**, *471* (2183).

8. Wilkes, J. S., A short history of ionic liquids—from molten salts to neoteric solvents. *Green Chem.* **2002**, *4* (2), 73-80.

### Cations:



### Anions:

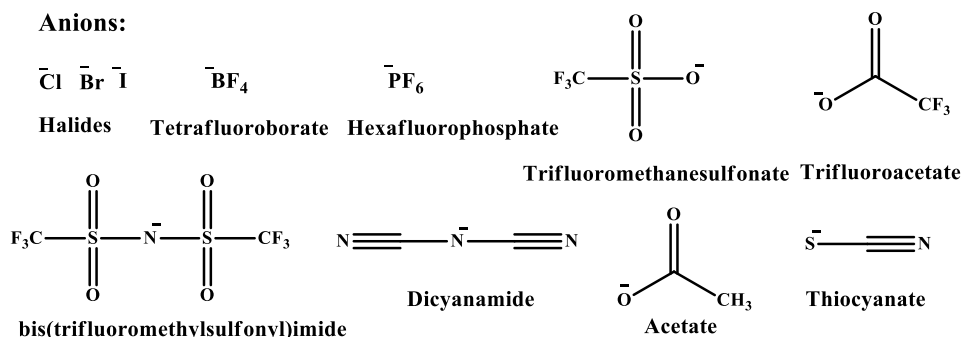


Figure 1 - Structures of common cations and anions in ILs.

ILs represent a class of chemical compounds, and they are defined as salts with a melting temperature below 100 °C; a subclass of ILs is represented by Room Temperature Ionic Liquids (RTILs) which are liquid at room temperature, as the same name implies. These salts, often formed by an organic cation and inorganic anion, present several particular properties which are the real reason for their success and proliferation in Chemistry (Figure 1). These properties are strongly correlated with the IL tuneable structure. The possibility to combine several cations and anions and to obtain new ILs with different properties is one of the most important features. The property more affected by the structure is the melting point, as it depends on the symmetry of the ions and their intermolecular interactions. In general, ILs show density higher than water and thermal stability can be closer to 400 °C; both these properties are correlated with the structure, especially the thermal decomposition. Moreover, ILs, being constituted by ions, have inherent conductivity, that is correlated with the viscosity, ionic size and ion



pairing ability.<sup>9</sup> They also present a negligible vapour pressure and they are generally not flammable.<sup>10</sup>

ILs characteristics can meet some of the necessary requirements to be “green solvent”. Considering what is said in the previous paragraph, the substitution of conventional organic solvents with ILs could be a step in the right direction for a greener process, but the whole chain has to be considered; for this purpose the cost, the number of synthetic steps, the toxicity and biodegradability of ILs are important aspects to take into account.

When the topic is to take care about the environment, the attention should be put on the use of materials which “could” poison and alter the ecosystem during the years. Often, the problem appears far away and is not immediately correlated with the current actions and choices. However, the reality is not like this and the story of Polychlorinated biphenyls (PCBs) helps to understand it. PCBs appeared for the first time in 1860 as a by-product of coal tar, and from 1929 were in large-scale produced and exported almost in every country. The wide diffusion was based on the properties, such as chemical and thermal stability, low volatility, dielectric properties, non-flammability, high boiling point and miscibility with organic solvents. In 1970 the first alarm on human health effect due to their use was launched.<sup>11</sup> During the time, several studies confirmed the correlation between PCBs and some human cancer forms.<sup>12</sup>

Some physico-chemical properties of PCBs and ILs are comparable, and the prominence of the latter in the last thirty years are the reasons leading Draye and co-workers to note the similarities.<sup>13</sup> However, if the general characteristics are similar, the variety of the ILs structures known until now, means different specific properties of ILs depend on the structure of the individual ILs. Many studies have

---

9. Every, H. A.; Bishop, A. G.; MacFarlane, D. R.; Oradd, G.; Forsyth, M., Transport properties in a family of dialkylimidazolium ionic liquids. *Phys. Chem. Chem. Phys.* **2004**, *6* (8), 1758-1765.

10. Singh, G.; Kumar, A., Ionic liquids: Physico-chemical, solvent properties and their applications in chemical processes. *Indian Journal of Chemistry sec. A* **2008**, *47A*, 495-503.

11. Gustafson, C. G., PCB's-prevalent and persistent. Intensified research is needed to minimize their dangers. *Environ. Sci. Technol.* **1970**, *4* (10), 814-819.

12. Kania-Korwel, I.; Lehmler, H.-J., Toxicokinetics of chiral polychlorinated biphenyls across different species—a review. *Environmental Science and Pollution Research* **2016**, *23* (3), 2058-2080.

13. Chatel, G.; Naffrechoux, E.; Draye, M., Avoid the PCB mistakes: A more sustainable future for ionic liquids. *J. Hazard. Mater.* **2017**, *324*, 773-780.

been focused on the environmental impact of ILs, studying the ecotoxicity and degradability.<sup>14</sup> For this purpose, at present, the synthesis of new classes of ILs, which includes cations and anions derived from natural sources, is the subject of several studies.

### **1.3 Greener Ionic Liquids: how to increase the biocompatibility**

Many classes of ILs are water soluble, therefore they could persist in the environment and interact with living organisms. The time of the biodegradation and the persistence of IL moieties in the environment depend on the structure of both cation and anion.<sup>15</sup> To understand if an IL could damage the ecosystem or behave as a biodegradable material, it is necessary to consider the Organisation for Economic Co-operation and Development (OECD) guidelines. These tests are internationally accepted to determine the effects of the chemicals on the ecosystem health.

The OECD guidelines define six different kinds of biodegradation, and among them, the primary biodegradation indicates the loss of specific properties of a substance due to the transformation of the structure by microorganisms, while the ready biodegradation is the rapid and complete degradation in aqueous media by the microorganism.<sup>16</sup> In other words, during the biodegradation, a complex and larger molecule is broken down and transformed into smaller molecules; these simpler derivatives became part of the metabolism of the microorganisms, converting them into essential nutrients for the life.

In particular, the Test No. 301 defines the “Ready Biodegradability” through six methods in aerobic aqueous media; these tests mainly use activated sludge derived from municipal wastewater.<sup>17</sup> The evaluated chemical can be defined biodegradable if the response of the test is 70 % removal of COD and 60 %

---

14. *Biodegradability and Toxicity of Ionic Liquids: BATIL-Meeting ; 6-8 May 2007, Berlin, Germany ; Book of Abstracts*. DECHEMA e. V.: **2007**.

15. Thuy Pham, T. P.; Cho, C.-W.; Yun, Y.-S., Environmental fate and toxicity of ionic liquids: A review. *Water Res.* **2010**, *44* (2), 352-372.

16. *Environmental risk assessment of ionisable compounds-Technical Report 123*; ECETOC-European Centre for Ecotoxicology and Toxicology of Chemicals: **2013**.

17. Ready Biodegradability, Guideline 301. *Organization for economic cooperation and development* **1992**.

removal of ThOD or ThCO<sub>2</sub> production for a time test of 28 days (where COD, ThOD and ThCO<sub>2</sub> are Chemical Oxygen Demand, Theoretical Oxygen and Theoretical Carbon Dioxide Demand, respectively). The biodegradation by microorganisms could happen via  $\omega$ -oxidation and subsequently  $\beta$ -oxidation of the alkyl side chain.<sup>18</sup>

Several studies took into account these tests and applied them on ILs. Those with longer alkyl chains on the cation ( $C \geq 6$ ) in aerobic media are more degradable than the same ion pairs but with a shorter side chain.<sup>19</sup> Moreover, the presence of oxygenated substituents also increases the biodegradability. The chemical functions such as ester, carboxyl and hydroxyl groups in the IL structure determine an improvement in the degradation results, providing sites for enzymatic attack and for the break of the bond between the cationic fragment and the possible corresponding alcohol, that is easily biodegradable.<sup>20</sup>

Hence, these chemical substituents are in the first place in the “biodegradation scale” (in particular ester group) followed by linear alkyl chains; finally also phenyl rings in the structure seems to increase the biodegradation.<sup>21</sup>

The side chain and related substituent are not the only parameters to be considered, indeed the cation head plays a fundamental role. For example, imidazolium cations are not completely biodegradable by microorganisms and they persist in the environment; conversely, pyrrolidinium and pyridinium ones are more biodegradable. For the other cations such as morpholinium, ammonium and phosphonium, the side chains and, even more, the nature of the anion are critical for the degradation.

The anions [PF<sub>6</sub>]<sup>-</sup> and [BF<sub>4</sub>]<sup>-</sup> are easily hydrolysable and show a higher degradability than [Br]<sup>-</sup> and [Cl]<sup>-</sup>; the organic anions such as acetate, naphthenic and ethyl or octyl sulphate are readily biodegradable.<sup>19,22</sup>

---

18. Markiewicz, M.; Stolte, S.; Lustig, Z.; Łuczak, J.; Skup, M.; Hupka, J.; Jungnickel, C., Influence of microbial adaption and supplementation of nutrients on the biodegradation of ionic liquids in sewage sludge treatment processes. *J. Hazard. Mater.* **2011**, *195*, 378-382.

19. Neumann, J.; Steudte, S.; Cho, C.-W.; Thoming, J.; Stolte, S., Biodegradability of 27 pyrrolidinium, morpholinium, piperidinium, imidazolium and pyridinium ionic liquid cations under aerobic conditions. *Green Chem.* **2014**, *16* (4), 2174-2184.

20. Gathergood, N.; Garcia, M. T.; Scammells, P. J., Biodegradable ionic liquids: Part I. Concept, preliminary targets and evaluation. *Ibid.* **2004**, *6* (3), 166-175.

21. Boethling, R. S.; Sommer, E.; DiFiore, D., Designing Small Molecules for Biodegradability. *Chem. Rev.* **2007**, *107* (6), 2207-2227.

However, biodegradable is not synonymous of “non-toxic”. Indeed, the toxicology defines the study of the effects of chemicals on living organisms. The toxicological research is focused on the consequence for the biochemical processes in the organisms, considering the vital mechanisms from the cellular to the molecular level. This is based on the relation between exposure and response. This relation permits to obtain information on the risk, namely the potential effects on the human and environmental health.<sup>23</sup>

Some features increase both biodegradation and toxicity; this is the case of the side alkyl chain. Longer alkyl chains, as above explained, show a better primary bio-oxidation than the shorter ones in aerobic media. However, a long alkyl chain can well interact with the lipidic bilayer of the cells, resulting toxic for the microorganisms. Moreover, the crucial role is not only played by the length but also by the number of long alkyl chains present in the structure. As for the biodegradability, also the toxicity depends on the head group considered. Although the response changes with the cells line studied, pyridinium cation is the least toxic in almost all cases, followed by the guanidinium. Also, in this case, the presence of hydroxyl substituents decreases its toxicity.<sup>24</sup>

Anions have a relevant role in the toxicity, and in aqueous media it follows the trend  $[\text{Br}^-] < [\text{DCA}^-] < [\text{Cl}^-] < [\text{BF}_4^-] < [\text{PF}_6^-] < [\text{NTf}_2^-]$ . However, the anion toxicity changes with the cation. To this aim, considering the  $[\text{C}_1\text{C}_4\text{pyrr}]^+$  cation combined with  $[\text{Cl}^-]$  or  $[\text{Br}^-]$  anions, the ILs show a lower impact on IPC-81 cells (rat cancer cells) than when the counter anion is  $[\text{NTf}_2^-]$  or, becoming more toxic, with  $[\text{BF}_4^-]$ . In an opposite way, ammonium and piperidinium are much less toxic with  $[\text{NTf}_2^-]$  than with halogen anion.<sup>25</sup> Similar results have been obtained for the

---

22. Abrusci, C.; Palomar, J.; Pablos, J. L.; Rodriguez, F.; Catalina, F., Efficient biodegradation of common ionic liquids by *Sphingomonas paucimobilis* bacterium. *Green Chem.* **2011**, *13* (3), 709-717.

23. Caserett, L. J.; Doull, J., *Casarett and Doull's Toxicology: The Basic Science of Poisons*. 7th ed.; McGraw-Hill: **2008**.

24. Frade, R. F.; Afonso, C. A., Impact of ionic liquids in environment and humans: An overview. *Human & Experimental Toxicology* **2010**, *29* (12), 1038-1054.

25. (a) Kumar, R. A.; Papaiconomou, N.; Lee, J.-M.; Salminen, J.; Clark, D. S.; Prausnitz, J. M., In vitro cytotoxicities of ionic liquids: Effect of cation rings, functional groups, and anions. *Environ. Toxicol.* **2009**, *24* (4), 388-395, (b) Stolte, S.; Matzke, M.; Arning, J.; Boschen, A.; Pitner, W.-R.; Welz-Biermann, U.; Jastorff, B.; Ranke, J., Effects of different head groups and functionalised side chains on the aquatic toxicity of ionic liquids. *Green Chem.* **2007**, *9* (11), 1170-1179.

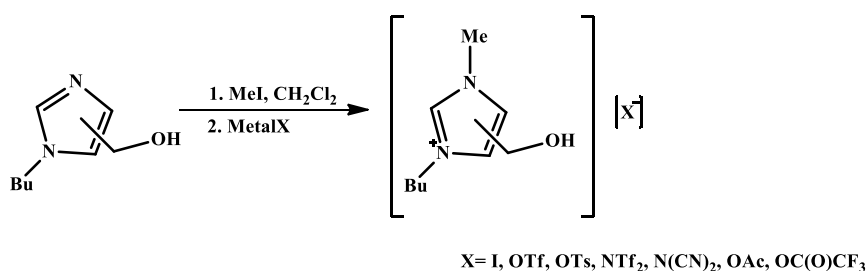
phosphonium cations. For example, trihexyl(tetradecyl)phosphonium chloride ( $[P_{6,6,14}][Cl]$ ) is more cytotoxic in S2 cells (deriving from a primary culture of late-stage *Drosophila Melanogaster* embryos), than the same cation but with bis(trifluoromethylsulfonyl)imide anion.<sup>26</sup>

The synthesis of new Ionic Liquids should consider, as far as possible, both the biodegradability and the toxicity, so that the health of the ecosystem should be the primary aim of the process and not a possible secondary consequence.

## 1.4 Sugar-based Ionic Liquids

An efficient and ideal way to synthesise greener ILs is using natural sources as starting materials.

Handy and co-workers in 2003 reported the first synthesis of sugar-derived ILs. They improved a previous work by Trotter and Darby, in which D-fructose was converted into hydroxymethyleneimidazole, and with alkylations, they obtained imidazolium cations (Scheme 1). The ILs obtained were employed as solvents for the Mizoroki–Heck reaction of methyl acrylate with several aryl iodides using palladium acetate as the catalyst.<sup>27</sup>



**Scheme 1 - Double alkylation of the imidazole to generate the imidazolium ILs.**<sup>27</sup>

26. Egorova, K. S.; Ananikov, V. P., Toxicity of Ionic Liquids: Eco(cyto)activity as Complicated, but Unavoidable Parameter for Task-Specific Optimization. *ChemSusChem* **2014**, 7 (2), 336-360.

27. Handy, S. T.; Okello, M.; Dickenson, G., Solvents from Biorenewable Sources: Ionic Liquids Based on Fructose. *Org. Lett.* **2003**, 5 (14), 2513-2515.

Natural sources such as carbohydrates and amino acids, apart from being biocompatible, are also chiral too. The use of chiral materials in the synthesis of IL led to a new IL class, the Chiral Ionic Liquids (CILs).

The first work on CILs dates back to 1999, in which the synthesis of several ILs for Diels-Alder reaction and, among them, the 1-butyl-3-methylimidazolium (S)-lactate was reported.<sup>28</sup> The synthesis of the CILs sheds light on the use of natural compounds, not only for the environmental safety, but also to obtain chiral products usable as chiral phase in chromatography, solvents or catalysts in asymmetric reactions, without the use of expensive chiral metal catalysts. The simple neutralisation reaction of the carboxylic acid function permits obtaining room temperature CILs. This is one of the reasons for the wide use of natural sources as anions in ILs synthesis. Amino acids as anions were largely studied for their properties, such as the possible coordination to transition metals. Moreover, functionalising the amino and carboxylic function could be useful to obtain a wide new class of ILs.

Fukumoto and co-workers, in 2005, synthesised 20 different Amino Acid ILs (AAILs) using the 1-ethyl-3-methylimidazolium ([C<sub>2</sub>C<sub>1</sub>im]) as cation, obtaining transparent, nearly colourless liquids at room temperature (Figure 2). However, they were not thermally stable (to 250 °C). Due to the proton at position 2 on the imidazolium ring, they evidenced a narrow electrochemical potential window. This work provided a starting point to develop the synthesis and the applications of this class of ILs, in which ILs are inherently chiral and endowed with the coordinating ability towards metal anions. They embed eco-friendly nature of the amino acids as well.<sup>29</sup>

---

28. Earle, J. M.; McCormac, B. P.; Seddon, R. K., Diels-Alder reactions in ionic liquids . A safe recyclable alternative to lithium perchlorate-diethyl ether mixtures. *Green Chem.* **1999**, *1* (1), 23-25.

29. Fukumoto, K.; Yoshizawa, M.; Ohno, H., Room Temperature Ionic Liquids from 20 Natural Amino Acids. *J. Am. Chem. Soc.* **2005**, *127* (8), 2398-2399.

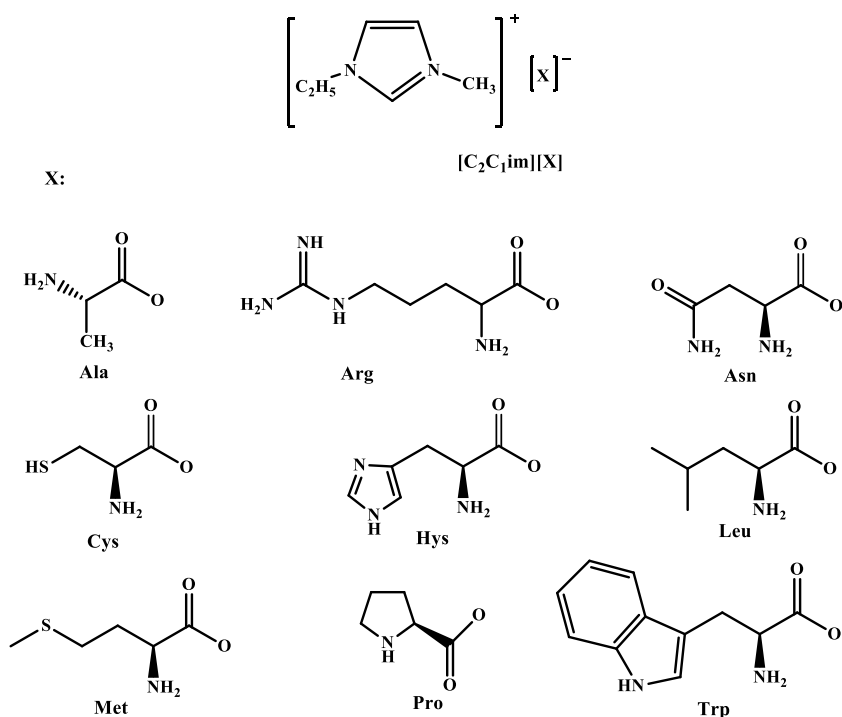


Figure 2 - Some structures of the AAILs synthesised by Fukumoto *et al.*<sup>29</sup>

For this purpose the same research group tested others cations. The reason was two-fold: on the one hand obtaining new AAILs, more thermally stable and less viscous, on the other hand decreasing the toxicology of the ILs and, at the same time, increase the biodegradability. In fact, the imidazolium cation was found to be not the best choice to achieve better biodegradability, while the synthesis with aliphatic cations, such as ammonium and phosphonium, could be the right direction (Figure 3).

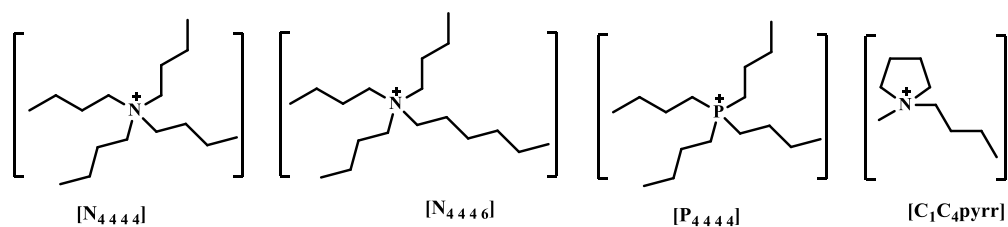


Figure 3 - Aliphatic cations tested by Fukumoto groups.

In Table 1, the comparison among thermal properties of alanine-based AAILs, as a function of the cation, is reported.

**Table 1 – Thermal properties of Alanine-based Ionic Liquids.**

Cation	$T_m/^\circ\text{C}$	$T_g/^\circ\text{C}$	$T_d/^\circ\text{C}$
$[\text{C}_2\text{C}_1\text{im}]^{+29}$	ND	-57	212
$[\text{N}_{4444}]^{+30}$	76	ND	162
$[\text{N}_{2226}]^{+30}$	ND	-40	150
$[\text{C}_4\text{C}_1\text{pyrr}]^+$	77	-64	176
$[\text{P}_{4444}]^{+30}$	ND	-70	286

ND: not determined (RTIL).

They synthesised the phosphonium ILs with amino acid anions combining the  $[\text{P}_{4444}]^+$  cation with the same 20 amino acids used for the  $[\text{C}_2\text{C}_1\text{im}]^+$ . They showed better properties, resulting in less viscous and, in 14 of 20 ILs, had a thermal stability higher than  $250^\circ\text{C}$ .<sup>30</sup> Table 2 displays the comparison among the AAILs having tetrabutyl-phosphonium and -ammonium cation, showing for the phosphonium ILs generally higher thermal stability and lower melting temperatures.<sup>31</sup>

**Table 2 - Thermal properties of the tetrabutylphosphonium and the tetrabutylammonium AAILs.**

AAILs	$T_m/^\circ\text{C}$	$T_g/^\circ\text{C}$	$T_d/^\circ\text{C}$
$[\text{P}_{4444}][\text{Gly}]^{30}$	13.6	-63.7	293
$[\text{N}_{4444}][\text{Gly}]^{31}$	16	-71	179
$[\text{P}_{4444}][\text{Val}]^{30}$	26	-59.1	286
$[\text{N}_{4444}][\text{Val}]^{31}$	25	-69	185
$[\text{P}_{4444}][\text{Ala}]^{30}$	ND	-70	286
$[\text{N}_{4444}][\text{Ala}]^{31}$	76	ND	162

ND: not determined (RTIL).

Generally, the trend of the decomposition temperatures for these AAILs increases in the following order, for a given anion:  $[\text{N}_{nnnn}]^+ < [\text{C}_n\text{mim}]^+ < [\text{P}_{nnnn}]^+$ .

In the case of tetraalkylphosphonium amino acid ILs, the  $T_d$  are similar to the corresponding amino acid and this could indicate that the first decomposition was the one of anion rather than the cation. The opposite seems to happen for the imidazolium and ammonium cations.

30. Kagimoto, J.; Fukumoto, K.; Ohno, H., Effect of tetrabutylphosphonium cation on the physico-chemical properties of amino-acid ionic liquids. *Chem. Commun.* **2006**, (21), 2254-2256.

31. Jiang, Y.-Y.; Wang, G.-N.; Zhou, Z.; Wu, Y.-T.; Geng, J.; Zhang, Z.-B., Tetraalkylammonium amino acids as functionalized ionic liquids of low viscosity. *Ibid.* **2008**, (4), 505-507.



Amino acids are not the only natural sources employed as anions for the CILs synthesis. Organic acids were largely used in this kind of synthesis. In this respect, Maschmeyer and co-workers obtained the tartrate, malate and mandelate-derived CILs coupled with tetrabutylammonium cation.<sup>32</sup> Several CILs were synthesised with tartrate anion changing the cations, from the cyclic aliphatic to the aromatic ones (Figure 4).<sup>33</sup> The use of organic acids did not increase the thermal stability of the ILs.

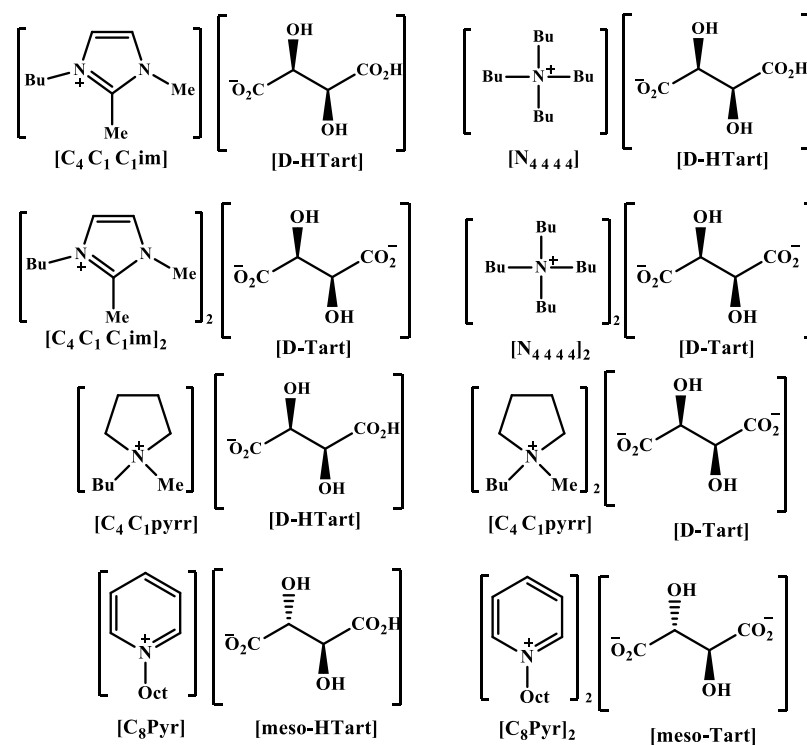


Figure 4 - CILs with hemi-, mesohemi-, meso- and D-tartrate.<sup>33</sup>

Pereira, Seddon and co-workers in 2010 designed, synthesised and studied Cholinium ILs ( $[\text{NMe}_3(\text{CH}_2\text{CH}_2\text{OH})]^+$ ), a non-toxic and biodegradable cation combined with alkanooates of systematically elongated chains. In addition to the properties of the ILs, they studied the toxicity and biodegradability, considering the importance of the anions, and specifically the length of the side chain in this

32. Allen, C. R.; Richard, P. L.; Ward, A. J.; van de Water, L. G. A.; Masters, A. F.; Maschmeyer, T., Facile synthesis of ionic liquids possessing chiral carboxylates. *Tetrahedron Lett.* **2006**, 47 (41), 7367-7370.

33. Rouch, A.; Castellan, T.; Fabing, I.; Saffon, N.; Rodriguez, J.; Constantieux, T.; Plaquevent, J.-C.; Genisson, Y., Tartrate-based ionic liquids: unified synthesis and characterisation. *RSC Adv.* **2013**, 3 (2), 413-426.

class of ILs. The toxicity increases with the length of the linear chain (see 1.2) also in this case, namely with the lipophilicity of the anion: ethanoate < propanoate < butanoate < pentanoate < hexanoate < octanoate < decanoate. However, these ILs result less toxic than their corresponding sodium salts. The thermal stability settles around 200 °C, as for the previous ILs described in this paragraph.<sup>34</sup>

Natural-based anions are not the unique sources for the synthesis of CILs. Indeed, natural-based cations can be used for the same purpose, expanding the CILs class and the application fields. Amino acids and amino acid ester salts can be employed as precursors in the cation design, because they represent a source of quaternary nitrogen.

One of the simplest synthesis is the protonation of the amine group of the amino acid, although often this is not a guarantee to obtain ILs. Indeed, the salts obtained show high melting points, while the decomposition temperatures do not show particular differences with respect the ones of the ILs made using natural-derived anions. The esterification and consecutive protonation permit to obtain room temperature CILs, without effects on the thermal stability.<sup>35</sup> The use of L-proline as a precursor for a cation, for example, permitted obtaining CIL ligands for Cu(II) also giving chiral selectors.<sup>36</sup>

The natural compounds in the ILs synthesis can also be “part” of the cation. For this purpose, Hannig *et al.* described the synthesis of new CILs used as chiral carbene precursor in palladium complexes. Hence, PG-His-OMe (where PG, the protector group, can be Bz or Boc) was used as starting material for the N-selective di-alkylation with propylbromide or isopropyl iodide, obtaining in both cases CILs with melting points not higher than 55 °C (Scheme 2).<sup>37</sup>

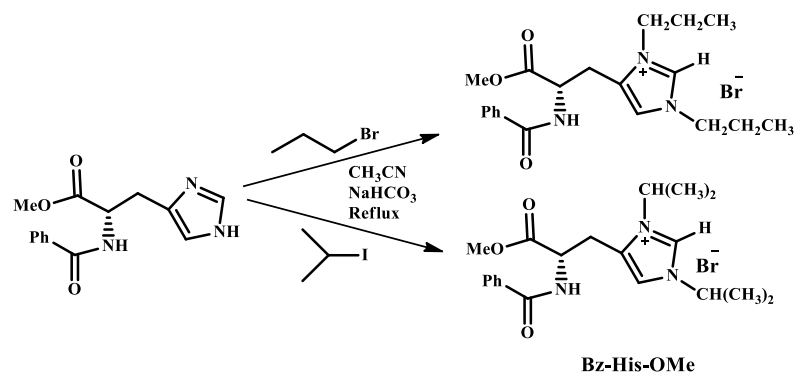
---

34. Petkovic, M.; Ferguson, J. L.; Gunaratne, H. Q. N.; Ferreira, R.; Leitao, M. C.; Seddon, K. R.; Rebelo, L. P. N.; Pereira, C. S., Novel biocompatible cholinium-based ionic liquids-toxicity and biodegradability. *Green Chem.* **2010**, *12* (4), 643-649.

35. Tao, G.-h.; He, L.; Sun, N.; Kou, Y., New generation ionic liquids: cations derived from amino acids. *Chem. Commun.* **2005**, (28), 3562-3564.

36. Mu, X.; Qi, L.; Zhang, H.; Shen, Y.; Qiao, J.; Ma, H., Ionic liquids with amino acids as cations: Novel chiral ligands in chiral ligand-exchange capillary electrophoresis. *Talanta* **2012**, *97*, 349-354.

37. Hannig, F.; Kehr, G.; Fröhlich, R.; Erker, G., Formation of chiral ionic liquids and imidazol-2-ylidene metal complexes from the proteinogenic amino acid L-histidine. *J. Organomet. Chem.* **2005**, *690* (24), 5959-5972.



Scheme 2 - Synthesis of the Bz-His-OMe ILs.<sup>37</sup>

## 1.5 Applications of sugar-based Ionic Liquids, a route toward the industry

The development, full characterisation and the tunability of ILs, have permitted the transition from the academic laboratories to the industrial applications.

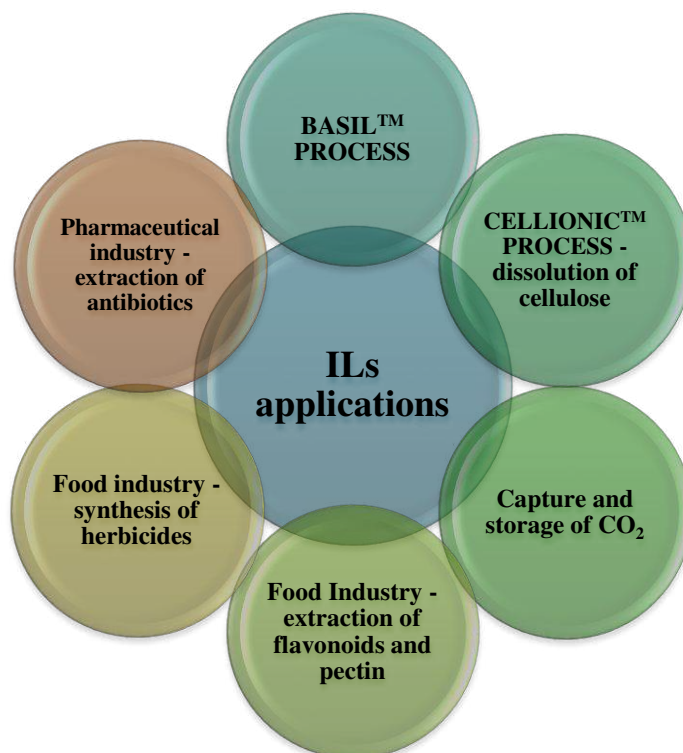
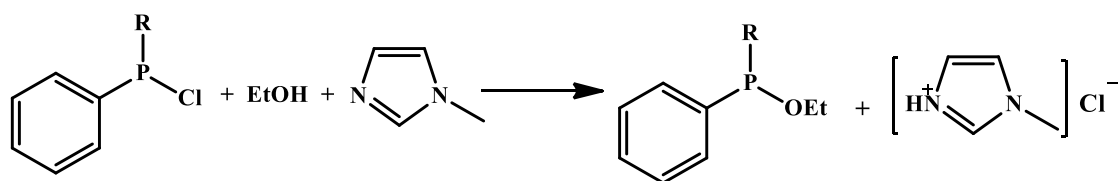


Figure 5 - ILs applications reported in this chapter.

At the beginning, among the companies which paved the way to the ILs application, BASF was the one which largely employed ILs for its processes, working with academia to extend the use of ILs as far as possible. BASIL™ (Biphasic Acid Scavenging utilising Ionic Liquids) is probably the most famous and successful process using ILs. The first publication of this application was in 2002. Through this process, the diethoxyphenylphosphine is produced, a photoinitiator intermediate. Originally, the process used triethylamine to counteract the HCl formed during the reaction between the dichlorophenylphosphine and ethanol, but the triethylammonium chloride formed a dense insoluble paste hampering efficient stirring. The substitution of the amine with the 1-methylimidazole led to the 1-methylimidazolium chloride formation (Scheme 3) resulting in phase separation. The BASIL™ process resulted in a better managed process due to several aspects.<sup>38</sup>



**Scheme 3 - BASIL™ process using IL.**

The good capability of ILs to solubilise biomass determined another step toward the industry, employing ILs for cellulose dissolution. The literature explained how both cation and anion are involved in the process, forming hydrogen bonds with cellulose hydrogen and oxygen atoms.<sup>39</sup> Also, in this case, BASF was at the forefront to improve the industrial process using ILs. The process using ILs does not need CS<sub>2</sub> as an auxiliary agent, decreasing the amount of waste compared with the Viscous Process. In addition, the CELLIONIC™

38. Plechkova, N. V.; Seddon, K. R., Applications of ionic liquids in the chemical industry. *Chem. Soc. Rev.* **2008**, 37 (1), 123-150.

39. Feng, L.; Chen, Z.-l., Research progress on dissolution and functional modification of cellulose in ionic liquids. *J. Mol. Liq.* **2008**, 142 (1), 1-5.

process employs [C<sub>2</sub>C<sub>1</sub>im][OAc] solutions to dissolve cellulose with a different degree of polymerisation.<sup>40</sup>

The cellulose polymer and its derivatives are employed in several fields, such as in the food, pharmaceutical and cosmetic industries. In the pharmaceutical industry, both ether and ester derivatives of cellulose are used in the coating of tablets, pills and similar, to stabilise the drug in contact with the air and also to regulate the release in the body.<sup>41</sup> The possibility to dissolve the cellulose in ILs permits to regenerate it in the form of fibers and films or to obtain gels and ionogels. They also can be incorporated into composite materials depending on the necessity.<sup>42</sup>

The research is designed towards the decrease of the human impact on the environment; the use of biomass to replace, for example, the carbon-derived fuels falls within this content.

The strong correlation between climate change and CO<sub>2</sub> emission is today evident and irrefutable. This topic is still on the top of the scientific research, and companies are working to find an efficient method to capture and store CO<sub>2</sub>, in order to decrease the human carbon footprint. Also, in this case, ILs have been playing a vital role. Blanchard *et al.* in a paper published in Nature reported the use of [C<sub>4</sub>C<sub>1</sub>im][PF<sub>6</sub>] to dissolve the CO<sub>2</sub>, and more important, the absence of contamination of CO<sub>2</sub> phase by the IL, frequently observed with conventional solvents.<sup>43</sup> This paper opened the way to a huge number of investigations and studies on this subject.

However, during the research development, the structure of ILs employed to dissolve CO<sub>2</sub> contained amino acids moieties, aided by the fact that aqueous amine solutions were commonly used for CO<sub>2</sub> dissolution. For this purpose, Schneider and Brennecke reported the synthesis and the application of

---

40. (a) Swatloski, R. P.; Spear, S. K.; Holbrey, J. D.; Rogers, R. D., Dissolution of Cellose with Ionic Liquids. *J. Am. Chem. Soc.* **2002**, *124* (18), 4974-4975, (b) Swatloski, R., Patrick; Rogers, R., Don; Holbrey, J., David Dissolution and Processing of Cellulose using Ionic Liquids. **2003**.

41. Shokri, J.; Adibkia, K., *Application of cellulose and cellulose derivatives in pharmaceutical industries*. InTech: **2013**; Vol. chapter 3.

42. Zhang, J.; Wu, J.; Yu, J.; Zhang, X.; He, J.; Zhang, J., Application of ionic liquids for dissolving cellulose and fabricating cellulose-based materials: state of the art and future trends. *Materials Chemistry Frontiers* **2017**, *1* (7), 1273-1290.

43. Blanchard, L. A.; Hancu, D.; Beckman, E. J.; Brennecke, J. F., Green processing using ionic liquids and CO<sub>2</sub>. *Nature* **1999**, *399*, 28.

[P<sub>6 6 6 14</sub>][Pro] (trihexyl(tetradecyl)phosphonium prolinat) and [P<sub>6 6 6 14</sub>][Met] (trihexyl(tetradecyl)phosphonium methioninat) in a 1:1 stoichiometry with CO<sub>2</sub> (Figure 6), showing a significant increase in adsorption of the gas and higher molar capacity than the ones previously reported with the cation-functionalised ILs and with the aqueous amine.<sup>44</sup>

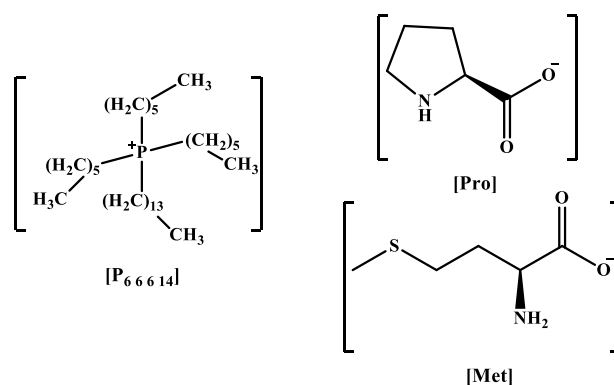


Figure 6 - ILs structure employed by Schneider with CO<sub>2</sub>.

Generally, the diffusivity of CO<sub>2</sub> is inversely proportional to the viscosity of the solvent used: the lower it is, the higher is the diffusivity and consequently the absorption of the gas.

Jiang *et al.* synthesised two AAILs which present viscosities lower than the ones usually reported. These two AAILs, the [N<sub>2 2 2 2</sub>][L-Ala] and the [N<sub>2 2 2 2</sub>][β-Ala] ( $\eta = 81$  and  $132$  mPa respectively), were employed for CO<sub>2</sub> absorption.

However, it is proved that the solubilisation of the AAILs in water can decrease their viscosities. For this purpose, the research group obtained other four AAILs maintaining the tetraalkylammonium cations and using the lysine and the glycine amino acids as anions (Figure 7).

44. Gurkan, B. E.; de la Fuente, J. C.; Mindrup, E. M.; Ficke, L. E.; Goodrich, B. F.; Price, E. A.; Schneider, W. F.; Brennecke, J. F., Equimolar CO<sub>2</sub> Absorption by Anion-Functionalized Ionic Liquids. *J. Am. Chem. Soc.* **2010**, *132* (7), 2116-2117.

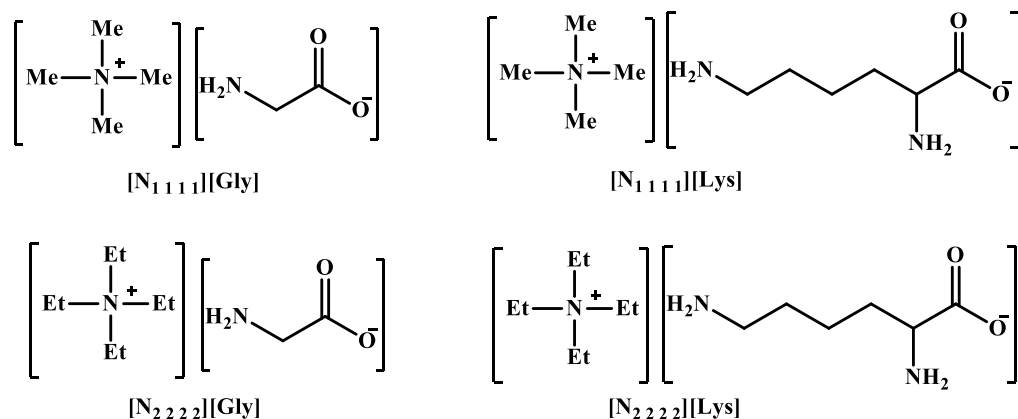


Figure 7 - ILs combined with MDEA for CO<sub>2</sub> absorption.<sup>45</sup>

These ILs combined with the MDEA (Methyldiethanolamine) aqueous solution gave better performance in the absorption of CO<sub>2</sub>. The best system out of the four ILs investigated in this study was the 15% IL + 15% MDEA mixture in water, in comparison to either the MDEA aqueous solution or the pure ILs.<sup>45</sup>

Although the use of ILs in cellulose dissolution and in CO<sub>2</sub> capture has been well known in the scientific world, they are also well known in several other fields of applications. There are literature reports on ILs used in other innovative fields of study. These fields are related to the bio-applications which are increasing their prevalence for diverse objectives. ILs are under study for the application in the pharmaceutical industry as well as in the food industry. The reason that opens the bio-field to ILs is the necessity to find new and easier method for the industries, because both of them daily face crucial issues for the social and economic progress.

Imidazolium ILs are commonly used in the food industry to extract compounds from food samples, and more importantly, from food waste; the main methods are the liquid-liquid, the solid-liquid and the vapour-liquid extractions. The use of pure ILs or their mixtures for this objective has extremely increased. Some known uses are the extraction of phenol compounds, caffeine and essential oils. However,

45. Feng, Z.; Cheng-Gang, F.; You-Ting, W.; Yuan-Tao, W.; Ai-Min, L.; Zhi-Bing, Z., Absorption of CO<sub>2</sub> in the aqueous solutions of functionalized ionic liquids and MDEA. *Chem. Eng. J. (Lausanne)* **2010**, *160* (2), 691-697.

the AAILs could gradually replace the imidazolium ILs.<sup>46</sup> Wand *et al.* synthesised and used Cholinium leucinate ([Ch][Leu]) to simultaneously extract flavonoids and pectin from ponkan peels. They found an efficient extractive method and consecutive isolation method using [Ch][Leu]-K<sub>3</sub>PO<sub>4</sub>-based ABS (aqueous biphasic system); flavonoids remained in the IL phase while the pectin floated in the salt phase. The first ones were isolated by precipitation after cooling, permitting to recycle the AAIL. The pectin was separated from the salt-phase under salt-out effect.<sup>47</sup>

The balance of the benefits and costs of each industrial process have to be determined before the start of production, including the product purification costs.

Shahriari *et al.* synthesised and studied cholinium based ILs, pointing their attention to the interaction with antibiotics and their purification.

---

46. Toledo Hijo, A. A. C.; Maximo, G. J.; Costa, M. C.; Batista, E. A. C.; Meirelles, A. J. A., Applications of Ionic Liquids in the Food and Bioproducts Industries. *ACS Sustainable Chemistry & Engineering* **2016**, *4* (10), 5347-5369.

47. Wang, R.; Chang, Y.; Tan, Z.; Li, F., Applications of choline amino acid ionic liquid in extraction and separation of flavonoids and pectin from ponkan peels. *Sep. Sci. Technol.* **2016**, *51* (7), 1093-1102.



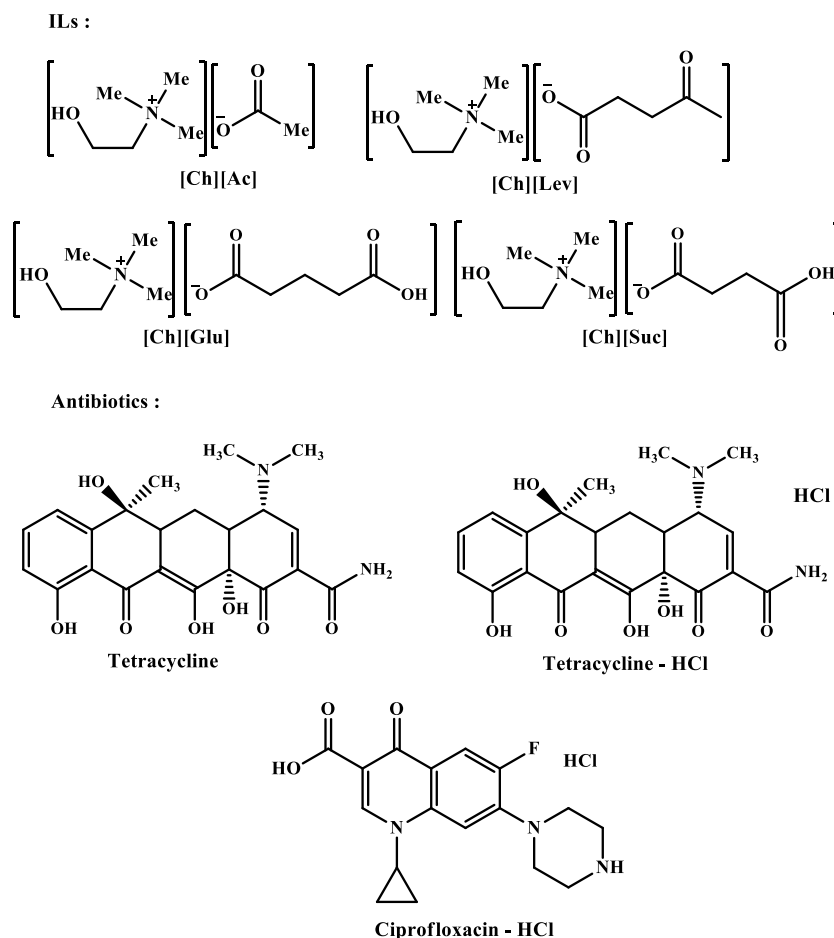


Figure 8 - Structures of the Cholinium ILs and of the antibiotics.<sup>47</sup>

They tested the cholinium-based ABS (with  $K_3PO_4$ ) using the ILs cholinium acetate ([Ch][Ac]), cholinium levulinate ([Ch][Lev]), cholinium glutarate ([Ch][Glu]), and cholinium succinate ([Ch][Suc]) (Figure 8); they also compared the results of the IL-systems with a cholinium chloride system. The antibiotics under study were the tetracycline, tetracycline·HCl and ciprofloxacin·HCl. The high partition coefficients obtained with cholinium-based ABS in this work provided a real alternative as extractive method for antibiotics, with a simpler and greener procedure, and these results are encouraging to focus more on this kind of studies.<sup>48</sup>

The sugar-based ILs have been employed also as herbicides. The HILs (ILs that present at least one component with herbicidal activity) present several

48. Shahriari, S.; Tome, L. C.; Araujo, J. M. M.; Rebelo, L. P. N.; Coutinho, J. A. P.; Marrucho, I. M.; Freire, M. G., Aqueous biphasic systems: a benign route using cholinium-based ionic liquids. *RSC Adv.* **2013**, 3 (6), 1835-1843.

advantages over the common herbicides on the market, such as the lower quantity required per hectare and lower toxicity. Pernak *et al.* synthesised high viscous ammonium ILs with glucose moiety on the cation, and coupled with anions derived from the 2-methyl-4-chlorophenoxyacetate (MCPA) or the 2,4-dichlorophenoxyacetate (2,4-D), which are used as herbicides (Figure 9).<sup>49</sup>

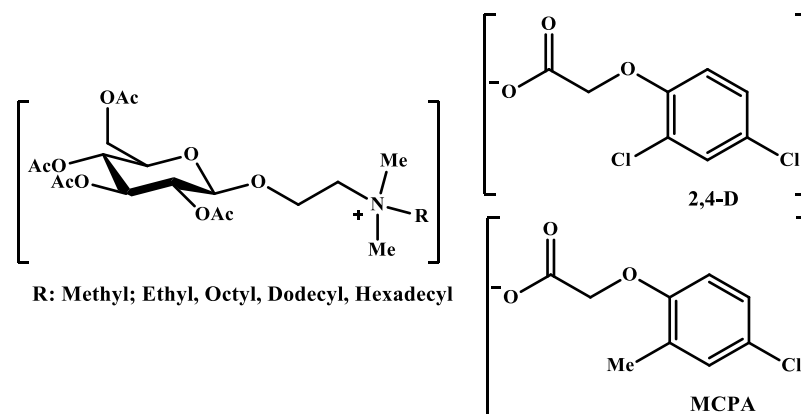


Figure 9 - Structures of HILs.<sup>49</sup>

The HILs properties investigated, such as the thermal stability and the surface activity, are interesting. The HILs show the herbicidal activity, even if the amount of herbicides is lower than the commercial one. Nevertheless, these HILs are a good starting-point to improve the synthesis in order to obtain new HILs with higher herbicidal effect and lower environmental contamination than the herbicides currently used.

The growth of industrial interest in ILs, in particular, the recyclable and the sugar-based ones, is apparent due the need to improve the processes both from the economic and environmental point of view. The use of ILs-based on natural sources is already a significant part of the scientific research and it is likely to become increasingly important in the future. Green and sustainable chemistry are the bases to devise new systems, utilising smart chemistry as a means to reach individual goals.

49. Pernak, J.; Czerniak, K.; Biedziak, A.; Marcinkowska, K.; Praczyk, T.; Erfurt, K.; Chrobok, A., Herbicidal ionic liquids derived from renewable sources. *RSC Adv.* **2016**, *6* (58), 52781-52789.

This is the context in which this research project has been developed, with the synthesis and the applications reaching towards the same common aim.

## **1.6 The common aim**

The introduction developed until now was focused on sustainable chemistry: its importance, the work performed as a human necessity as well as its developments during the years, without affecting the health of the ecosystems.

The second Chapter will present the ILs synthesised and characterised in this Research Project. In more detail, it will focus on the natural source used for the synthesis of the new ILs: gluconic acid. It can be produced from food waste and it is part of metabolic pathways also in the human organism.

Part of the objective of this Research Project, and consequently, of this final Thesis, is the synthesis of new eco-friendly ILs. The structures of these ILs will be shown in Chapter 2 and they share some general features to obtain safe compounds. The natural component will be deeply presented, showing the good match among the economic, chemical and environmental point of views. The choice of an aliphatic cation follows the same route, avoiding the persistence of aromatic moieties in the environment, like the imidazolium ILs. Moreover, also the length of the alkyl chain is not a casual choice, as alkyl chain with a number of carbon atoms between 4 and 8 were used, being this range a good compromise between hydrophilicity and hydrophobicity.

Each task of this Research Project has been built taking into account the “usefulness” from the synthesis to the possible applications. Why choose the gluconic acid among many natural molecules? The presence of five OH groups is not an accidental choice. These many OH groups permitted obtaining ILs which are able to establish hydrogen bond networks and coordinating interactions. These capabilities are the base of the successful applications achieved in this project.

Figure 10 shows the principal applications performed taking advantage of the structural characteristics of the ILs synthesised in this work.

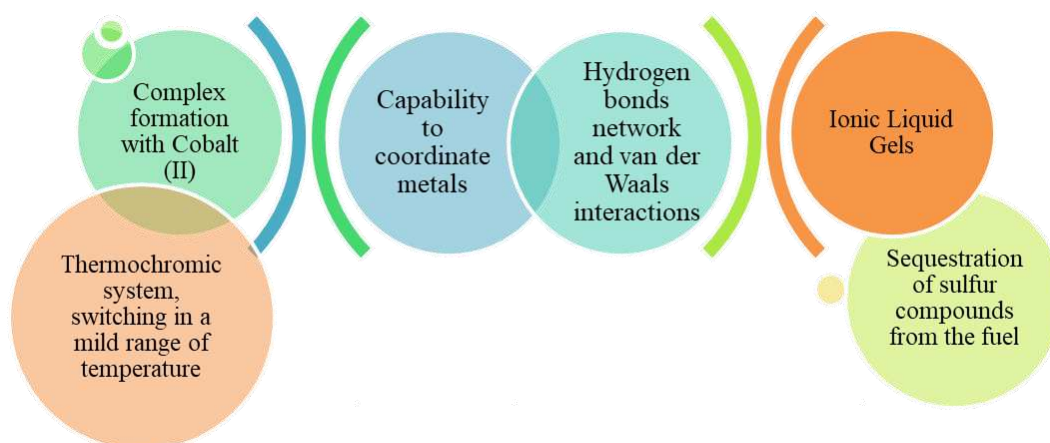


**Figure 10 - Principal applications achieved.**

The hydrogen bonds and the van der Waals interactions built by the gluconate ILs are the base on which the Ionic Liquid Gels (ILGs) have been obtained. The gluconate ILs were employed as gelator, capable of gelling in the appropriate solvent. These ILGs were employed as adsorbent materials to remove sulfur compounds (thiophene and derivatives) from the fuels.<sup>50</sup>

The OH groups, as it is specified in Figure 10, are also able to coordinate transition metals and lanthanides, forming complexes, whose geometry depends on the number of OH groups involved, but also on the physical features of the environment. This is the case of the thermochromic phenomena concerning the Co (II) –IL complexes. These complexes are constituted by the new natural IL-based, using these organic salts as ligand with a cobalt salt. The temperature affects the spin and the magnetic moments of the complexes, switching the configuration from the octahedral to the tetrahedral complex, visibly detected with a change in the colour of the solution, from pink to blue. The impressive detail is not the role of the temperature on the complex geometries, while, it is the mild temperature range employed to obtain this switching. Each aspect could lead to the creation of thermal sensors, spacing the applications in fields like storage of energy or bio-devices.

50. Billeci, F.; D'Anna, F.; Gunaratne, H. Q. N.; Plechkova, N. V.; Seddon, K. R., "Sweet" ionic liquid gels: materials for sweetening of fuels. *Green Chem.* **2018**, *20*, 4260-4276.

This brief overview on the ILs structures and principal applications sheds the light on the common aim of the project. From the synthesis to the applications, the objective is to induce an improvement and an innovation in the chemistry field, without compromising the delicate vital ecosystem.

## 2. Gluconic derivatives: Synthesis and characterisation

### 2.1 Gluconic acid, a handy natural molecule

Gluconic acid (pentahydroxyhexanoic acid) is naturally derived from glucose, through the oxidation of the aldehyde group on C-1 to a carboxyl group. In aqueous solution, the acid is in equilibrium with its cyclic forms. This equilibrium is ~100 times faster with the six-membered lactone than the five-membered one (Figure 11).<sup>51</sup>

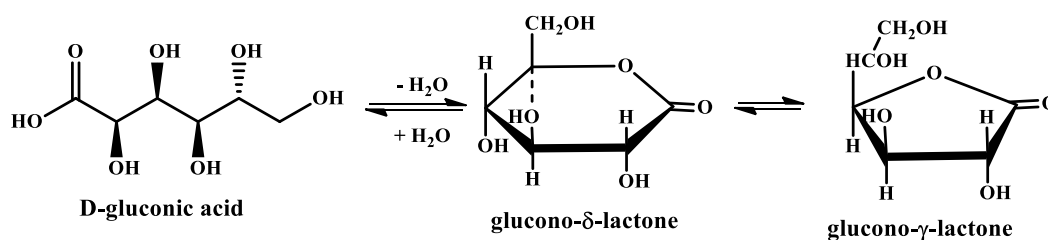


Figure 11 - Aqueous equilibrium among gluconic acid, glucono- $\delta$ -lactone and glucono- $\gamma$ -lactone.

Gluconic acid was reported for the first time in 1870 by Hlasiwetz and Habermann, who isolated the chlorine and barium gluconic salts as products of the glucose oxidation.<sup>52</sup> Ten years later, in 1880, Boutroux discovered the use of the *Acetobacter aceti* to oxidise glucose to obtain gluconic acid,<sup>53</sup> while, a little later, in 1922 Molliard identified this organic acid in cultures of *Aspergillus niger*.<sup>54</sup> During the years, several others bacteria and fungi capable of forming gluconic acid were identified, some examples are *Pseudomonas*, *Gluconobacter*

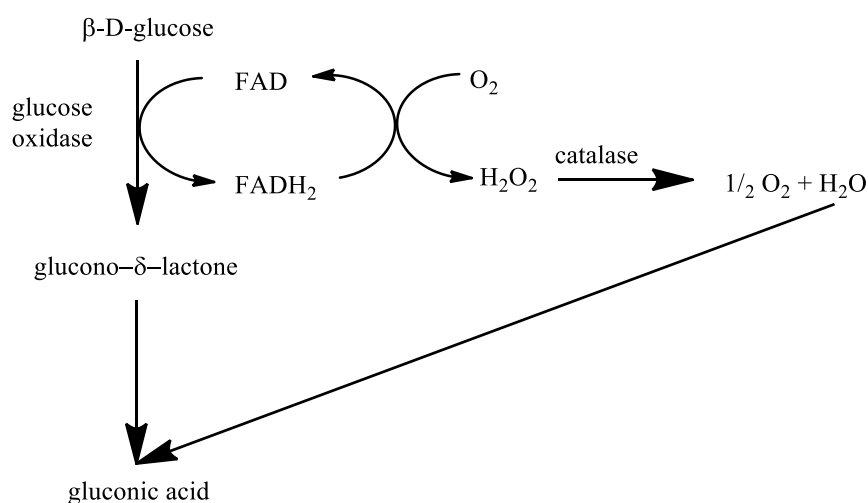
51. Hustede, H.; Haberstroh, H.-J.; Schinzig, E., Gluconic Acid. In *Ullmann's Encyclopedia of Industrial Chemistry*, **2000**.

52. Rohr, M.; Kubicek, C.; Kominek, J., Gluconic acid. In *Biotechnology, A Comprehensive Treatise in 8 Volumes. Vol. 3: Biomass, Microorganisms for Special Applications, Microbial Products I, Energy from Renewable Resources*, Rehm, H.; Reed, G., Eds. **1983**; Vol. 3, pp 455-465.

53. Henneberg, W., *Handbuch der Garungsbakteriologie*. II ed.; Springer Verlag: **1926**; Vol. 2.

54. Molliard, M., Survenue nouvelle fermentation acide produite par le *Sterigmatocystis nigra*. *C.R. Hebd. Seances Acad. Sci.* **1922**, (174), 881-883.

and *Penicillium luteum*.<sup>55</sup> The first report on the glucose oxidase activity is due to Muller in 1928 working on *Aspergillus niger* extracts.<sup>56</sup> The glucose oxidase enzyme is part of the oxidoreductase class. It is a homodimer and featuring one flavin adenine dinucleotide (FAD) per monomer, where each FAD is non-covalently bound. This enzyme catalyses the dehydrogenation of glucose to glucono- $\delta$ -lactone, reducing the FAD to FADH<sub>2</sub>. The biochemical process is schematically explained in Scheme 4.<sup>51</sup>



**Scheme 4 - Oxidation of glucose by glucose oxidase (*Aspergillus niger*).**

Gluconic acid is a natural organic acid traceable in foodstuffs such as honey, wine, rice, and vinegar.<sup>57,58,59</sup> The production can be chemical, electrochemical and biochemical.<sup>60</sup> In terms of commercial production, the chemical oxidation of

55. Ramachandran, S.; Nair, S.; Larroche, C.; Pandey, A., Gluconic acid. In *Current Developments in Biotechnology and Bioengineering Production, Isolation and Purification of Industrial Products*, Pandey, A.; Negi, S.; Soccol, C. R., Eds. Elsevier: **2017**; p 886.

56. Muller, D., studien uber ein neues Enzym, Glykoseoxydase. I. *Biochem. Z.* **1928**, (199), 136-170.

57. Barbe, J.-C.; de Revel, G.; Bertrand, A., Gluconic acid, its lactones, and SO<sub>2</sub> binding phenomena in musts from botrytized grapes. *J. Agric. Food Chem.* **2002**, *50* (22), 6408-6412.

58. Sanarico, D.; Motta, S.; Bertolini, L.; Antonelli, A., HPLC determination of organic acids in traditional balsamic vinegar of Reggio Emilia. *J. Liq. Chromatogr. Relat. Technol.* **2003**, *26* (13), 2177-2187.

59. Mato, I.; Huidobro, J. F.; Sánchez, M. P.; Muniategui, S.; Fernández-Muiño, M. A.; Sancho, M. T., Enzymatic determination of total d-Gluconic acid in honey. *J. Agric. Food Chem.* **1997**, *45* (9), 3550-3553.

60. Pal, P.; Kumar, R.; Banerjee, S., Manufacture of gluconic acid: A review towards process intensification for green production. *Chemical Engineering and Processing: Process Intensification* **2016**, *104*, 160-171.

glucose by hypochlorite solution is a one-step process, but it is not selective and environmentally safe. The electrochemical oxidation of glucose is not the industrial favourite process due to its cost, while, the fermentation of glucose containing biomass with specific microorganisms, such as *Aspergillus niger*, is the most attractive and inexpensive way to produce this organic acid.<sup>61,62</sup> Fang and co-workers obtained gluconic acid by potato pulp fermentation. Potato pulp is an agriculture waste, which contains cellulose, starch, and protein. This particular “waste” is easily hydrolysed to obtain sugars; for this reason, it is employed as crude starting material for gluconate and gluconic acid production. The research groups observed the successful use of the *Gluconobacter oxidans* DSM 2003 on the hydrolysed pulp, reaching a conversion from glucose to gluconic acid equal to 94.9%.<sup>63</sup> Gluconic acid and most of its derivatives are safe, non-toxic and readily biodegradable.<sup>64</sup> A study *in vivo* highlighted the fate of this natural organic acid in living organisms, demonstrating how a certain quantity of gluconic acid can be metabolised by rats, if introduced in their diet. The results showed the 57% of the total amount was excreted in the urine and another 14% was expired as CO<sub>2</sub>. The rest of the acid was found in the liver, both in the nucleic acid and in glycogen. The hypothesis of a role of gluconic acid (or phosphogluconic acid) as a precursor for the five-carbon sugars could be concrete.<sup>65</sup> Moreover, a recent study shed more light on gluconic acid metabolism in the human organism.

---

61. de Wilt, H. G. J., Part I. Oxidation of glucose to gluconic acid. Survey of techniques. *Ind. Eng. Chem. Prod. Res. Dev.* **1972**, *11* (4), 370-373.

62. Znad, H.; Markoš, J.; Baleš, V., Production of gluconic acid from glucose by *Aspergillus niger*: growth and non-growth conditions. *Process Biochem. (Amsterdam, Neth.)* **2004**, *39* (11), 1341-1345.

63. Jiang, Y.; Liu, K.; Zhang, H.; Wang, Y.; Yuan, Q.; Su, N.; Bao, J.; Fang, X., Gluconic Acid Production from Potato Waste by *Gluconobacter oxidans* Using Sequential Hydrolysis and Fermentation. *ACS Sustainable Chemistry & Engineering* **2017**, *5* (7), 6116-6123.

64. *Gluconic acid and derivatives. Screening Information Database (SIDS)*; Organisation for Economic Co-operation and Development (OECD): **2004**.

65. Stetten, M. R.; Stetten, D., The metabolism of gluconic acid. *J. Biol. Chem.* **1950**, *187* (1), 241-252.

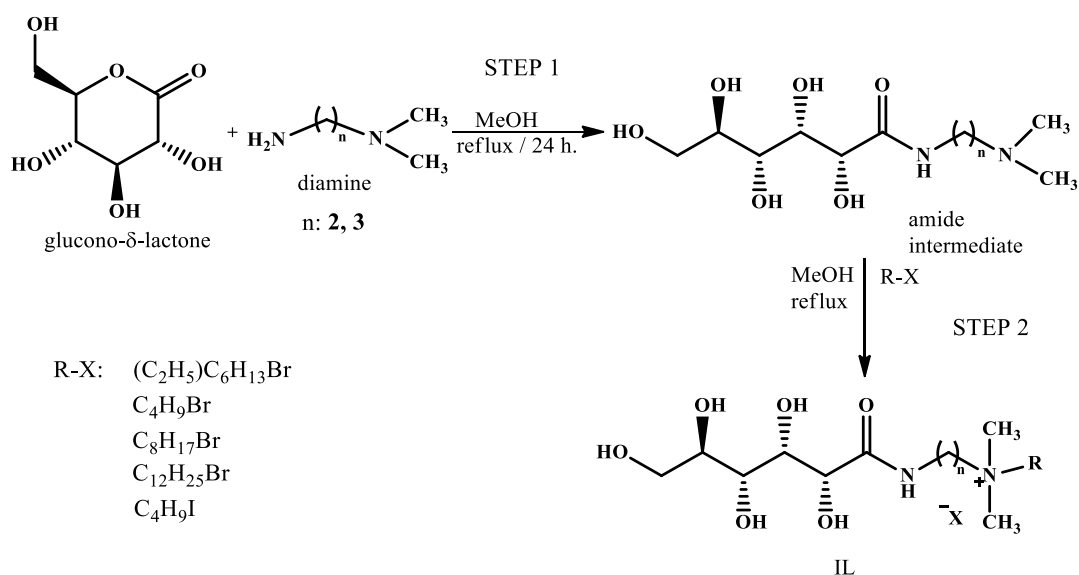


The existence of the Human Gluconokinase (GntK) and the evidence that its activity is written in human genome, support the possible role of this organic acid metabolism and synthesis of nucleotides and amino acids.<sup>66</sup>

## 2.2 Sweet Ionic Liquids: synthesis and characterisation

In the work reported in this thesis, gluconic acid has been used for the synthesis of 17 new organic salts, and with only one exception, these salts are new ILs. These new ILs can be divided into two different groups, the first one in which the gluconic moiety is part of the cation structure and a second group characterised by gluconate anion.

Scheme 5 shows the synthetic pathway to obtain the ammonium ILs with a “sweet” cation. The first step involves the cyclic form of gluconic acid, the glucono- $\delta$ -lactone, which is treated with an appropriate diamine to afford an amide intermediate (step 1). This intermediate is quaternised by reaction with the suitable alkyl halide (step 2).



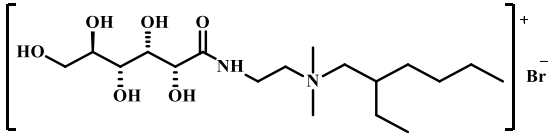
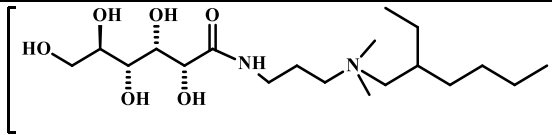
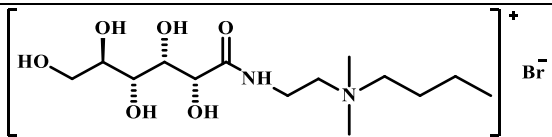
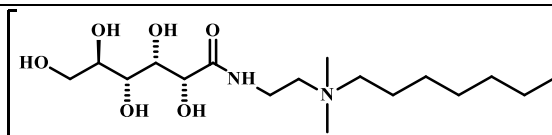
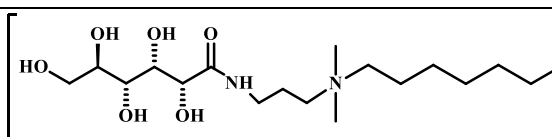
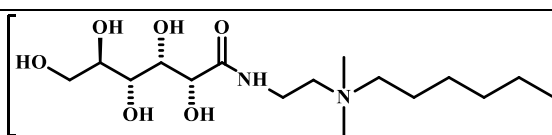
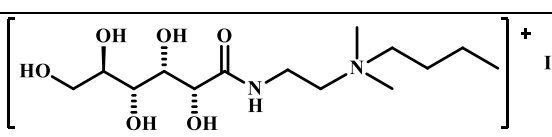
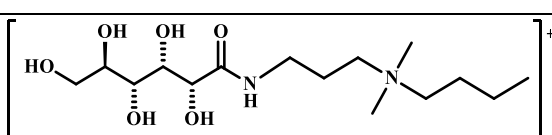
**Scheme 5 - The synthetic pathway to obtain new "sweet" ammonium ILs.**

66. Rohatgi, N.; Nielsen, T. K.; Bjørn, S. P.; Axelsson, I.; Paglia, G.; Voldborg, B. G.; Palsson, B. O.; Rolfsson, Ó., Biochemical characterization of human gluconokinase and the proposed metabolic impact of gluconic acid as determined by constraint based metabolic network analysis. *PLoS One* **2014**, 9 (6), e98760.

In Table 3, the ILs obtained with the above synthetic pathway are summarised.

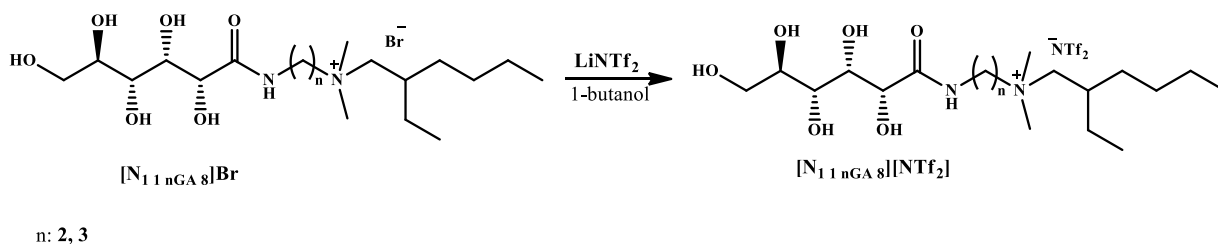
In all cases, the cation will be indicated as  $[N_{x,y,zGA,w}]^+$ , where x and y represent the length of alkyl groups borne on the diamine used, z the number of carbon atoms on the alkyl spacer of diamine, GA stands for gluconic amide and w represents the length of the alkyl chain used in the quaternisation step.

**Table 3 - Structures of ILs obtained with the synthesis reported in Scheme 5.**

	$[N_{112GA8}]Br$
	$[N_{113GA8}]Br$
	$[N_{112GA4}]Br$
	$[N_{112GA8L}]Br$
	$[N_{113GA8L}]Br$
	$[N_{112GA12}]Br$
	$[N_{112GA4}]I$
	$[N_{113GA4}]I$

These ILs differ for the length of the spacer between the amide and ammonium groups, for the alkyl chain length or the branching, and also for the anion.

In order to obtain ILs with fluorinated bistriflimide anion, the  $[N_{112GA8}Br]$  and the  $[N_{113GA8}Br]$  ILs were chosen for the metathesis with  $LiNTf_2$ , using the 1-butanol as the solvent (Scheme 6).



**Scheme 6 - Metathesis to exchange the  $[Br]^-$  anion with the  $[NTf_2]^-$  anion.**

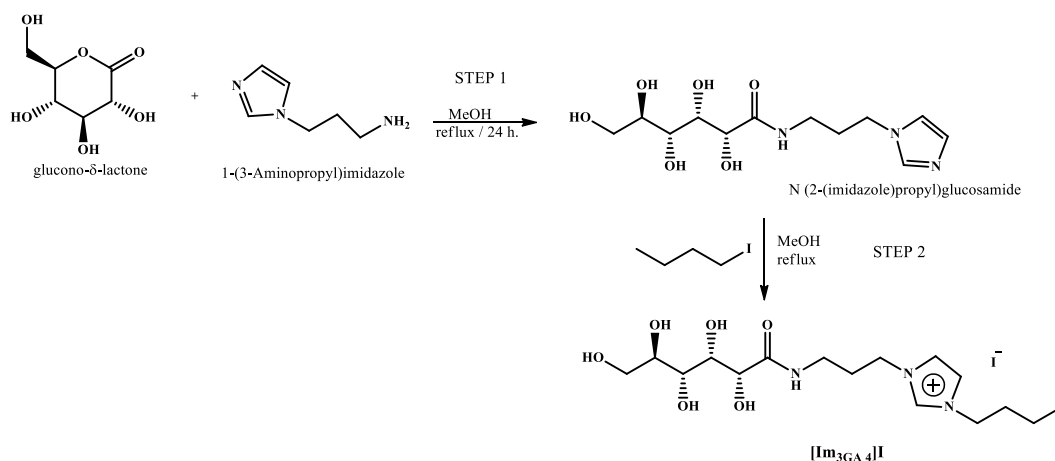
The structures of the ILs obtained after this metathesis are reported in Table 4.

**Table 4 - Structures of ILs obtained after the anion metathesis reported in Scheme 6.**

	$[NTf_2]^-$	$[N_{112GA8}][NTf_2]$
	$[NTf_2]^-$	$[N_{113GA8}][NTf_2]$

All the ILs show in Table 3 and 4 featured aliphatic cations. The choice of the ammonium cation is part of the main objective of this research project. Indeed, as above mentioned (introduction, paragraph 1.3), the choice for an aliphatic cation over the corresponding aromatic one takes into account the future disposal of the IL.

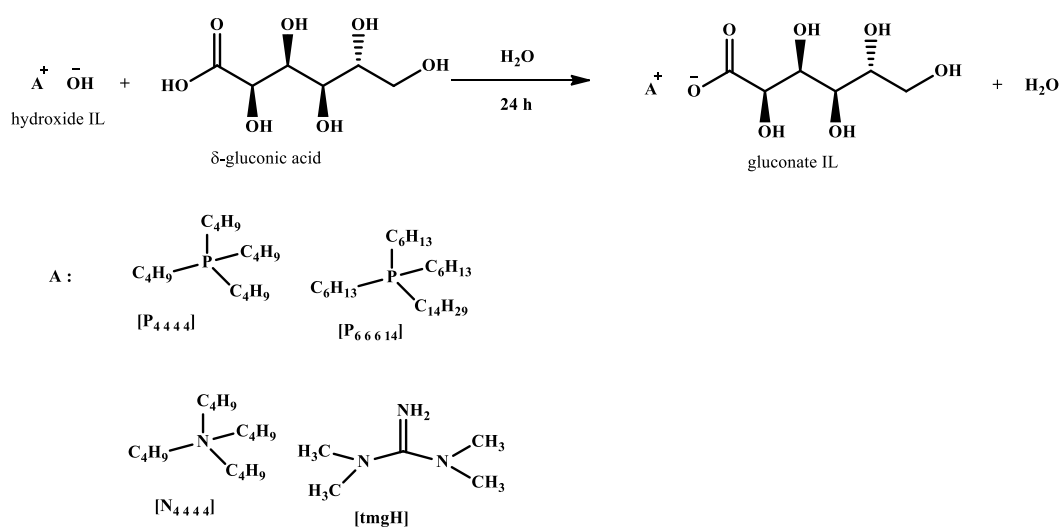
In Scheme 7, one IL synthesised incorporating the imidazolium cation is shown. This IL has been prepared with the aim of having an aromatic cationic unit to compare with the ammonium ILs. A comparative study of the properties of ILs resulting from change in structure can be envisaged.



**Scheme 7 - The synthetic pathway to obtain the [Im<sub>3AG 4</sub>]I IL.**

This synthesis resembles the one depicted in Scheme 5 with a two-step pathway. The first step is necessary to open the lactone and form the amide intermediate, the second step involves quaternisation of the imidazole to imidazolium. The notation given for the IL obtained is the **[Im<sub>3AG 4</sub>]I**.

The second group of new ILs synthesised in this work bears of the gluconate anion. In order to obtain new ILs with a simple synthesis, we took advantage of the acidic nature of the starting material; gluconic acid was treated with hydroxide ILs to achieve gluconate ILs through an acid base neutralisation reaction (Scheme 8).



**Scheme 8 - The synthetic pathway to obtain the gluconate ILs.**

The structures of the gluconate ILs are reported in Table 5.

**Table 5 –Structure of new gluconate ILs.**

$\left[ \begin{array}{c} \text{C}_6\text{H}_{13} \\   \\ \text{C}_6\text{H}_{13}-\text{P}-\text{C}_6\text{H}_{13} \\   \\ \text{C}_{14}\text{H}_{29} \end{array} \right]^+$	$\left[ \begin{array}{c} \text{O} \\    \\ \text{O}-\text{C}-\text{CH}(\text{OH})-\text{CH}(\text{OH})-\text{CH}(\text{OH})-\text{CH}_2\text{OH} \\   \quad   \quad   \\ \text{OH} \quad \text{OH} \quad \text{OH} \end{array} \right]^-$	<b>[P<sub>6 6 6 14</sub>][Glu]</b>
$\left[ \begin{array}{c} \text{C}_4\text{H}_9 \\   \\ \text{C}_4\text{H}_9-\text{P}-\text{C}_4\text{H}_9 \\   \\ \text{C}_4\text{H}_9 \end{array} \right]^+$	$\left[ \begin{array}{c} \text{O} \\    \\ \text{O}-\text{C}-\text{CH}(\text{OH})-\text{CH}(\text{OH})-\text{CH}(\text{OH})-\text{CH}_2\text{OH} \\   \quad   \quad   \\ \text{OH} \quad \text{OH} \quad \text{OH} \end{array} \right]^-$	<b>[P<sub>4 4 4 4</sub>][Glu]</b>
$\left[ \begin{array}{c} \text{C}_4\text{H}_9 \\   \\ \text{C}_4\text{H}_9-\text{N}-\text{C}_4\text{H}_9 \\   \\ \text{C}_4\text{H}_9 \end{array} \right]^+$	$\left[ \begin{array}{c} \text{O} \\    \\ \text{O}-\text{C}-\text{CH}(\text{OH})-\text{CH}(\text{OH})-\text{CH}(\text{OH})-\text{CH}_2\text{OH} \\   \quad   \quad   \\ \text{OH} \quad \text{OH} \quad \text{OH} \end{array} \right]^-$	<b>[N<sub>4 4 4 4</sub>][Glu]</b>
$\left[ \begin{array}{c} \text{NH}_2 \\    \\ \text{N}-\text{C}-\text{N} \\   \quad   \\ \text{ } \quad \text{ } \end{array} \right]^+$	$\left[ \begin{array}{c} \text{O} \\    \\ \text{O}-\text{C}-\text{CH}(\text{OH})-\text{CH}(\text{OH})-\text{CH}(\text{OH})-\text{CH}_2\text{OH} \\   \quad   \quad   \\ \text{OH} \quad \text{OH} \quad \text{OH} \end{array} \right]^-$	<b>[tmgH][Glu]</b>

The analysis of the properties of these new ILs can be divided into two sections recalling the structural differences, *i.e.* the function of the gluconic moiety, as part of the cation or the anion.

In Table 6 the thermal properties such as melting and decomposition temperatures, of the ILs where the gluconic motif is present on the cation, are reported.

**Table 6 - Thermal properties (DSC and TGA) of the ILs with the gluconic moiety on the cation.**

IL	DSC analysis		TGA analysis
	Heating $T_g$ (°C) ( $\Delta H$ )	Cooling $T_g$ (°C) ( $\Delta H$ )	95 % wt. $T_d$ (°C)
[N <sub>112GA8</sub> ]Br	-16.6	-22.6	168.4
[N <sub>113GA8</sub> ]Br	-0.1	-5.4	195.1
[N <sub>112GA4</sub> ]Br	-46.6	-49.0	127.8
[N <sub>112GA8L</sub> ]Br	-55.5	-60.6	200.6
[N <sub>113GA8L</sub> ]Br	-36.1	-43.6	200.6
[N <sub>112GA12</sub> ]Br	-22.8 (9.3 J g <sup>-1</sup> )	-19.6 (1.9 J g <sup>-1</sup> )	129.8
	87.1 (0.7 J g <sup>-1</sup> )	-28.2 (1.1 J g <sup>-1</sup> )	
[N <sub>113GA4</sub> ]I	-19.4	-25.7	191.7
[N <sub>112GA4</sub> ]I	-7.9		210.3
[N <sub>112GA8</sub> ][NTf <sub>2</sub> ]	-15.9		191.1
[N <sub>113GA8</sub> ][NTf <sub>2</sub> ]	-16.2	-44.4	188.5
[Im <sub>3AG4</sub> ]I	-3.7		197.3

The thermal stability for these ILs was determined with TGA measurements, considering for each sample the temperature corresponding to 5% loss in weight ( $T_d$ ). The highest temperature value is 210.3 °C for the [N<sub>112GA4</sub>]I. The increase in carbon atoms of the linker, between the amide function and the ammonium head group, is associated with a decrease in the thermal stability of about 19 °C for the [N<sub>113GA4</sub>]I. Greater change, however, is ascribable to the change of halide anion. The [Br<sup>-</sup>] determines a decrease of the thermal stability of about 80 °C for

the  $[\mathbf{N}_{1\ 1\ 2GA\ 4}]\mathbf{Br}$  compared to the iodide-based IL. The change of the cation head from ammonium to imidazolium induces less pronounced variations for the  $T_d$ ; the difference between  $T_d$ s in the case of  $[\mathbf{N}_{1\ 1\ 3GA\ 4}]\mathbf{I}$  and  $[\mathbf{Im}_{3AG\ 4}]\mathbf{I}$  ILs is only 5 °C. This behaviour was already observed by Afonso and co-workers, in their examination of properties of the [aliquat] and the  $[\mathbf{C}_8\mathbf{C}_{1im}]$  with different anions.<sup>67</sup>

The ILs considered until now carry a short (butyl) linear side chain on the cation. If this chain is substituted with a longer octyl chain, linear or branched, the thermal stability follows the series:  $[\mathbf{N}_{1\ 1\ 2GA\ 8L}]\mathbf{Br} \approx [\mathbf{N}_{1\ 1\ 3GA\ 8L}]\mathbf{Br} > [\mathbf{N}_{1\ 1\ 3GA\ 8}]\mathbf{Br} > [\mathbf{N}_{1\ 1\ 2GA\ 8}]\mathbf{Br} > [\mathbf{N}_{1\ 1\ 2GA\ 12}]\mathbf{Br} > [\mathbf{N}_{1\ 1\ 2GA\ 4}]\mathbf{Br}$ . The linear side chain determines a higher thermal stability compared with the same ILs, but with the branched side chain. This difference is more evident for the  $[\mathbf{N}_{1\ 1\ 2GA\ 8}]\mathbf{Br}$ , for which the  $T_d$  value is ~ 32 °C lower than that for  $[\mathbf{N}_{1\ 1\ 2GA\ 8L}]\mathbf{Br}$ . Moreover, in addition to the effect of the linear side chain, the linker length affects thermal stability in the case of the branched chain. Indeed, the  $[\mathbf{N}_{1\ 1\ 3GA\ 8}]\mathbf{Br}$  results in higher stability than the same IL with the shorter linker.

Also, the side chain length influences the  $T_d$ , with lower thermal stability, if the side chain length is long ( $[\mathbf{N}_{1\ 1\ 2GA\ 12}]\mathbf{Br}$ ) or short ( $[\mathbf{N}_{1\ 1\ 2GA\ 4}]\mathbf{Br}$ ). This seems to indicate that the octyl chain represents the best compromise in terms of thermal stability.

The length does not significantly affect the thermal stability in the case of  $[\mathbf{NTf}_2]^-$  based ILs, as accounted for by the comparison between  $T_d$  values corresponding to  $[\mathbf{N}_{1\ 1\ 2GA\ 8}][\mathbf{NTf}_2]$  and  $[\mathbf{N}_{1\ 1\ 3GA\ 8}][\mathbf{NTf}_2]$ . A more complex behaviour was detected as a function of the anion change, on going from  $[\mathbf{Br}]^-$  to  $[\mathbf{NTf}_2]^-$ . Indeed, in the case of  $[\mathbf{N}_{1\ 1\ 2GA\ 8}]^+$  cation, the above change induced a significant and parallel increase in  $T_d$  (~23 °C). Conversely, for the  $[\mathbf{N}_{1\ 1\ 3GA\ 8}]^+$  cation, the presence of the  $[\mathbf{NTf}_2]^-$  anion gave rise to a less significant decrease in thermal stability (~7 °C).

---

67. Kulkarni, P. S.; Branco, L. C.; Crespo, J. G.; Nunes, M. C.; Raymundo, A.; Afonso, C. A. M., Comparison of Physicochemical Properties of New Ionic Liquids Based on Imidazolium, Quaternary Ammonium, and Guanidinium Cations. *Chem. Eur. J.* **2007**, *13* (30), 8478-8488.

ILs are generally characterised by glass transitions ( $T_g$ ) and the corresponding temperatures are detected by DSC measurements ( $T_g$ , Table 6). The analysis of the data collected shows that the  $[\mathbf{N}_{1\ 1\ 2GA\ 4}]\mathbf{I}$  presents a higher  $T_g$  than the  $[\mathbf{N}_{1\ 1\ 3GA\ 4}]\mathbf{I}$  of about 10 °C. Moreover, differently from the other, for  $[\mathbf{N}_{1\ 1\ 3GA\ 4}]\mathbf{I}$ , it was possible to observe the glass transition also in the cooling cycle.

The change in the cation ( $[\mathbf{N}_{1\ 1\ 3GA\ 4}]\mathbf{I}$  and  $[\mathbf{Im}_{3GA\ 4}]\mathbf{I}$ ) determines a marked difference in the  $T_g$  of about 15 °C, this is different to what observed for thermal stability. The change of the anion for the  $[\mathbf{N}_{1\ 1\ 2GA\ 4}]^+$  cation, from the  $[\mathbf{I}]^-$  to the  $[\mathbf{Br}]^-$ , according to thermal stability, results in a decrease in  $T_g$ .

The  $T_g$ s for the bromide ILs need a different analysis in dependence on the length of the spacer, since both the length of the side chain and also its linear or branched nature have to be considered. The linear octyl side chain determines a lower glass transition temperature compared to the branched chain. This difference results in a symmetric trend with the glass temperatures of the  $[\mathbf{N}_{1\ 1\ 2GA\ 8L}]\mathbf{Br}$  and the  $[\mathbf{N}_{1\ 1\ 3GA\ 8L}]\mathbf{Br}$  differing, in absolute value, of about 40 °C from the  $T_g$  of the  $[\mathbf{N}_{1\ 1\ 2GA\ 8}]\mathbf{Br}$  and the  $[\mathbf{N}_{1\ 1\ 3GA\ 8}]\mathbf{Br}$ , both in the heating and cooling cycles. The same trend is traceable also considering the length of the spacer, as the addition of one  $\text{CH}_2$  determines an increase of the glass temperatures of about 20 °C when the side chain is linear ( $[\mathbf{N}_{1\ 1\ 2GA\ 8L}]\mathbf{Br}$  and  $[\mathbf{N}_{1\ 1\ 3GA\ 8L}]\mathbf{Br}$ ) or branched ( $[\mathbf{N}_{1\ 1\ 2GA\ 8}]\mathbf{Br}$  and  $[\mathbf{N}_{1\ 1\ 3GA\ 8}]\mathbf{Br}$ ). The elongation of the side chain, as expected,<sup>68</sup> increases the glass transition temperature and, in the case of  $[\mathbf{N}_{1\ 1\ 2GA\ 12}]\mathbf{Br}$ , determines the solid state of the ILs which is characterised by the occurrence of a melting process detected in the DSC curve. Finally, the change of the anion with a less coordinating and larger one, such as the  $[\mathbf{NTf}_2]^-$  anion, does not affect the glass transition temperature for the  $[\mathbf{N}_{1\ 1\ 2GA\ 8}]\mathbf{Br}$  and the  $[\mathbf{N}_{1\ 1\ 2GA\ 8}][\mathbf{NTf}_2]$ . Differently, for the  $[\mathbf{N}_{1\ 1\ 3GA\ 8}]\mathbf{Br}$  and the  $[\mathbf{N}_{1\ 1\ 3GA\ 8}][\mathbf{NTf}_2]$ , the anion change results in a decrease of the transition temperature of about 15 °C. This behaviour recalls the one observed for the  $T_d$ , showing a difference for the ILs with the propyl spacer, carrying the  $[\mathbf{Br}]^-$  and the  $[\mathbf{NTf}_2]^-$  anion. Conversely,  $T_d$

---

68. Machanová, K.; Wagner, Z.; Andresová, A.; Rotrekl, J.; Boisset, A.; Jacquemin, J.; Bendová, M., Thermal Properties of Alkyl-triethylammonium bis{(trifluoromethyl)sulfonyl}imide Ionic Liquids. *J. Solution Chem.* **2015**, *44* (3), 790-810.



does not change in the case of the ethyl spacer. The length of the linker for the [NTf<sub>2</sub>]<sup>-</sup> ILs does not influence the  $T_g$ .

The use of the gluconate anion determined the synthesis of other four organic salts, three of which were ILs with glass transitions or melting points lower than 100 °C. The structures of these salts are shown in Table 5. Their thermal and thermodynamic properties are reported in Table 7.

Table 7 - Thermal properties (DSC and TGA) of the ILs and salt with the gluconate anion.

IL	DSC analysis						TGA analysis
	Heating cycle			Cooling cycle			95 % wt. $T_d$ (°C)
	$T_g$ (°C) $T_m$ (°C)	$\Delta H_m$ (J g <sup>-1</sup> )	$\Delta S_m$ (J g <sup>-1</sup> K <sup>-1</sup> )	$T_c$ (°C)	$\Delta H_c$ (J g <sup>-1</sup> )	$\Delta S_c$ (J g <sup>-1</sup> K <sup>-1</sup> )	
[P <sub>4444</sub> ][Glu]	-21.8 80.2	78.7	0.22				155.0
[P <sub>66614</sub> ][Glu]	34.0	21.2	0.07	0.5	-28.1	-0.10	172.5
[N <sub>4444</sub> ][Glu]	120.0	105.3	0.26	73.4	-86.4	-0.25	161.8
[tmgH][Glu]	-24.1						103.1

All the salts reported in Table 7 are ILs, with the exception of the [N<sub>4444</sub>][Glu]. This latter and the phosphonium ILs are solid at room temperature, as demonstrated by their melting temperature ( $T_m$ ).

The guanidinium IL, [tmgH][Glu], is a highly viscous oil at room temperature and is characterised by a glass transition detected during the heating process, but not in the cooling cycle. ILs obtained with this cation and anions deriving from carboxylic acids, like acetic, formic and hexanoic acids are solid at room temperature ( $T_m$ : 77-83 °C, 90-97 °C and 43 °C respectively).<sup>69</sup> The change of the anion with the gluconate determines the change of the physical state of the IL.

69. King, A. W. T.; Asikkala, J.; Mutikainen, I.; Järvi, P.; Kilpeläinen, I., Distillable acid–base conjugate Ionic Liquids for cellulose dissolution and processing. *Angew. Chem., Int. Ed.* **2011**, *50* (28), 6301-6305.

Moreover, the corresponding halide salts, the **[tmgH]Cl**, **[tmgH]Br** and **[tmgH]I** are white solid salts with melting temperature over the canonical 100 °C (210 °C, 185 °C and 131 °C respectively),<sup>70</sup>  $T_m$  which defines an IL.

Table 7 also reports the thermodynamic parameters ( $\Delta H_m$ ,  $\Delta H_c$ ,  $\Delta S_m$  and  $\Delta S_c$ ) associated with the melting and the crystallisation transitions for the phosphonium ILs and the ammonium salt. The **[P<sub>4 4 4 4</sub>][Glu]** is the only one of them not showing any transition during the cooling process. The presence of the gluconate anion determines an increase in the melting temperature compared to the corresponding chloride salts, **[N<sub>4 4 4 4</sub>]Cl**, **[P<sub>4 4 4 4</sub>]Cl** and **[P<sub>6 6 6 14</sub>]Cl** (52, 62, -70 °C), as a possible consequence of the increased ability to form hydrogen-bonding networks. This is the opposite behaviour to the **[tmgH][Glu]**, for which the halide salts present higher  $T_m$ , and it could be ascribed to the different cation structure, determined by competitive interactions of guanidinium IL between the anion and the cation or another anion.

The melting temperature decreases on going from the tetrabutylammonium to the tetrabutylphosphonium IL. This could indicate the role of the cation in the solid lattice organisation, maintaining the same alkyl chains. However, the corresponding thermodynamic parameters highlight how this decrease in the  $T_m$  is ascribed to the strength of the cation-anion interactions rather than to differences in the solid lattice organisation, as accounted for by large gap in the  $\Delta H_m$  values. The elongation of the alkyl chains coupled with the asymmetry of the cation, maintaining the phosphonium head, it determines the decrease of about 50 °C in the melting temperature for the **[P<sub>6 6 6 14</sub>][Glu]** compared to **[P<sub>4 4 4 4</sub>][Glu]**.

The thermal stabilities reported in Table 7 show that the change from ammonium to phosphonium cation results in a thermal destabilisation, while the longer alkyl chain determines an increase in the thermal stability of the phosphonium IL.

The thermal behaviour of all the new salts was also analysed using polarised optical microscopy (POM). The gluconate ILs and the ammonium gluconate are

---

70. Anderson, M. L.; Hammer, R. N., Properties of 1,1,3,3-tetramethylguanidine as a nonaqueous solvent. *J. Chem. Eng. Data* **1967**, 12 (3), 442-447.

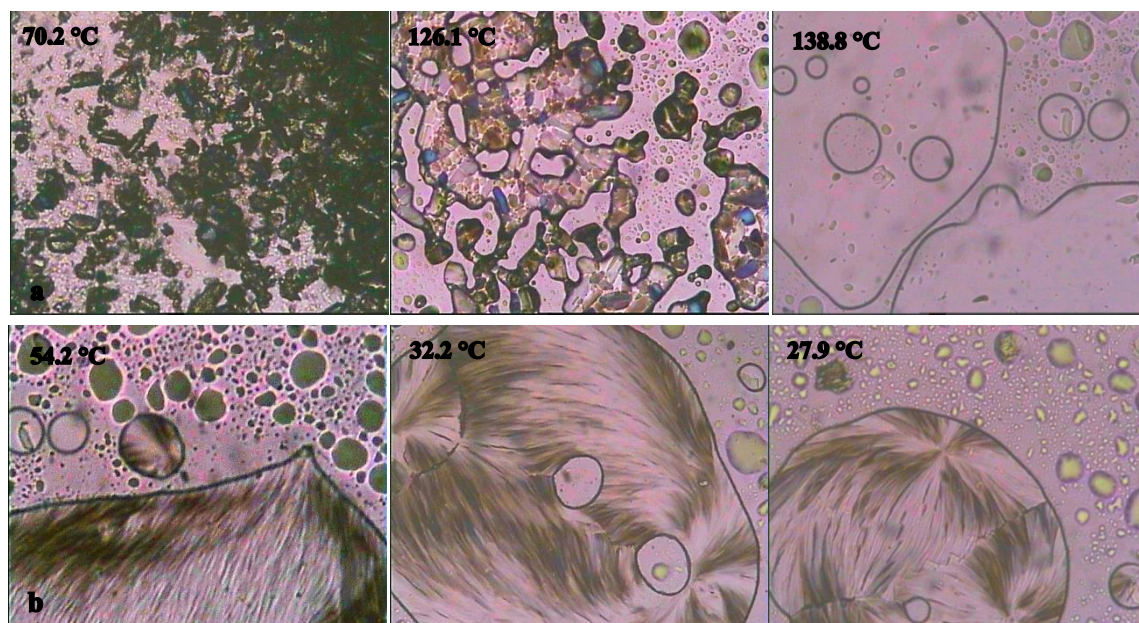


Figure 12 - POM images corresponding to  $[N_{4444}][Glu]$  (a) heating cycle; (b) cooling cycle.

the only ones showing different textures, exhibited during both heating and cooling cycles.

In the case of  $[N_{4444}][Glu]$ , the presence of discrete crystals was detected up to 120 °C, and above this temperature they melted giving an isotropic solution (Figure 12a). In the cooling process, the isotropic solution changed in well organised and oriented structures, already detected at ~55 °C (Figure 12b).

The pictures for the  $[P_{4444}][Glu]$  are reported in Figure 12a-d. In the first heating cycle, the crystals were detected until 68 °C. At ~80 °C, these crystals did not have well-defined contours anymore, and above this temperature the formation of an isotropic solution was observed (Figure 13a). In the cooling cycle, (Figure 13b) the isotropic solution was detected until ~30 °C while at 28.3 °C some crystals were appearing. These bright and coloured crystals were well-defined at room temperature. The second heating and cooling cycles highlight the reproducible formation of these crystals (Figure 13c-d).

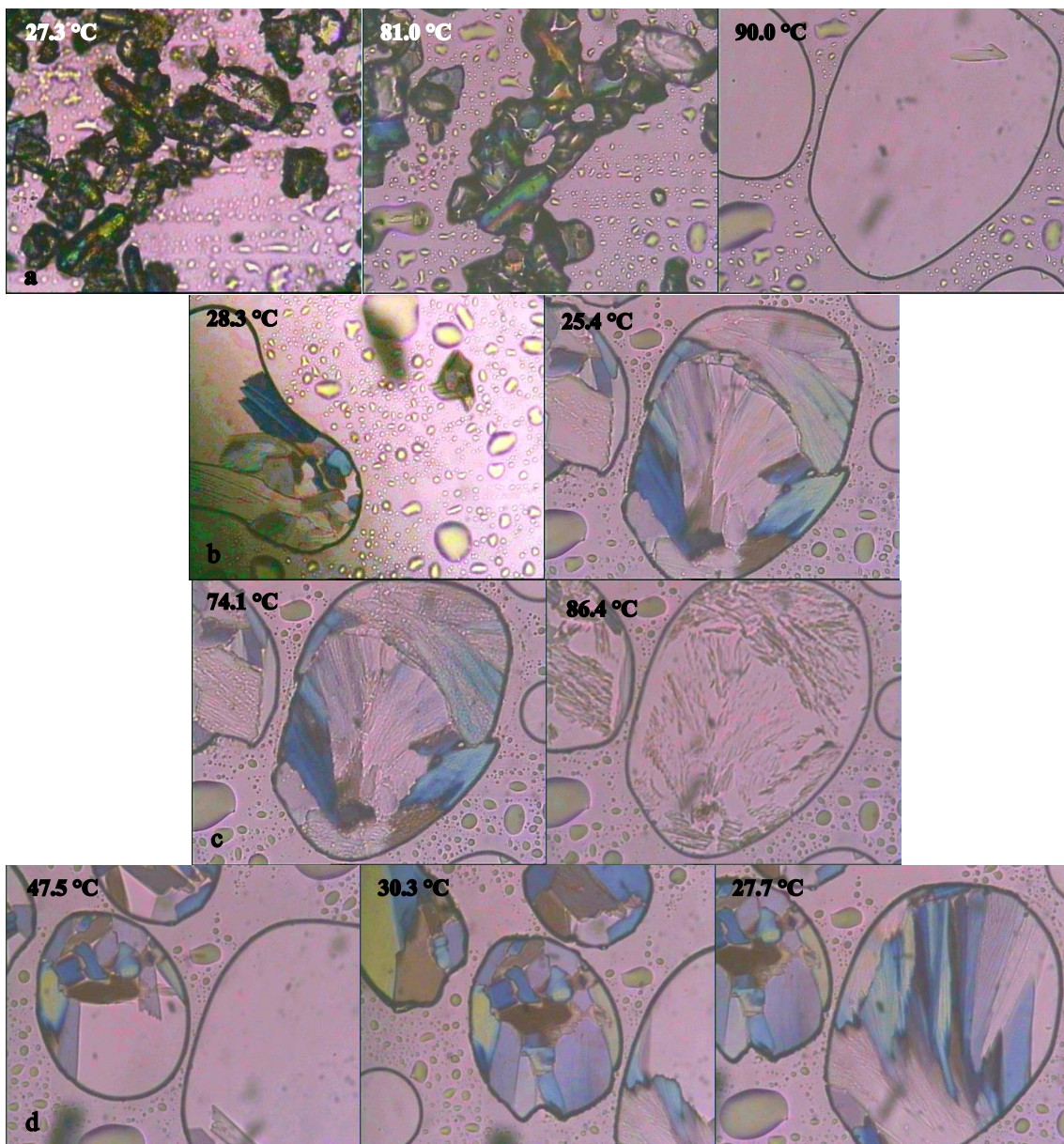


Figure 13 - POM images corresponding to [P<sub>4444</sub>][Glu] (a) first heating cycle; (b) first cooling cycle; (c) second heating cycle; (d) second cooling cycle.



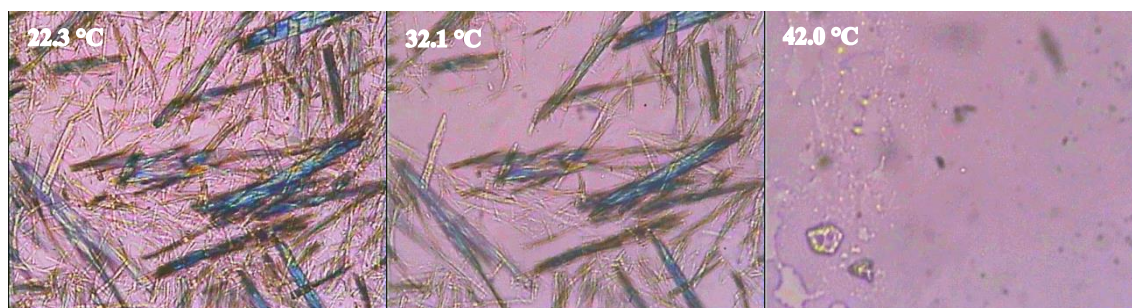


Figure 14 - POM images corresponding to [P<sub>6,6,6,14</sub>][Glu] heating cycle.

The lengthening of the alkyl chain for the phosphonium IL determines a decrease of the amount of crystals of [P<sub>6,6,6,14</sub>][Glu] and, in this case only some filamentous crystals were detected until ~33-34 °C during the heating cycle. After the melting, the isotropic solution persists and the recrystallisation is not observed.

The viscosity has been also determined for the ILs which were sufficiently fluid at room temperature, using a rheometer equipped with a temperature control. Table 8 reports the viscosity values obtained and the parameters connected to it through the Vogel-Fulcher-Tamman model fit (see page 55). The viscosity of ILs depends on several factors, such as van der Waals interactions, hydrogen bonding, the ion size and their polarisability, and also on the symmetry of the structure.<sup>71</sup>

Taking into consideration all the above factors, the difference among the ILs can be analysed considering the different anion, cation, the alkyl chain and the spacer lengths.

71. Branco, L. C.; Carrera, G. V. S. M.; Aires-de-Sousa, J.; Martin, I. L.; Frade, R.; Afonso, C. A. M., Physico-Chemical Properties of Task-Specific Ionic Liquids. In *Ionic Liquids: Theory, Properties, New Approaches*, Kokorin, A., Ed. IntechOpen: **February 2011**.

Table 8 - Viscosity values, VFT parameters, fragility and fragility index.

IL	$\eta$ (mPa*s) at 293.1 K	A (mPa*s)	B (K)	T <sub>0</sub> (K)	R <sup>2</sup>	D	m
[N <sub>1 1 2GA 8</sub> ]Br	34880	4.5*10 <sup>-5</sup>	1153.3	168.7	0.996	6.8	102.3
[N <sub>1 1 3GA 8</sub> ]Br	18120	1.4*10 <sup>-2</sup>	546.0	210.3	0.997	2.6	243.3
[N <sub>1 1 2GA 4</sub> ]Br	106.3	1.3*10 <sup>-5</sup>	850.2	176.0	0.999	4.8	138.1
[N <sub>1 1 3GA 8L</sub> ]Br	21980	4.9*10 <sup>-2</sup>	508.8	205.3	0.998	2.5	254.0
[N <sub>1 1 3GA 4</sub> ]I	31190	2.5*10 <sup>-4</sup>	997.5	174.9	0.999	5.7	119.5
[N <sub>1 1 2GA 4</sub> ]I	41700	4.2*10 <sup>-2</sup>	472.8	219.7	0.998	2.1	290.1
[N <sub>1 1 2GA 8</sub> ][NTf <sub>2</sub> ]	17420	4.5*10 <sup>-2</sup>	465.3	215.2	0.999	2.2	288.8
[N <sub>1 1 3GA 8</sub> ][NTf <sub>2</sub> ]	29030	1.2*10 <sup>-3</sup>	926.0	174.1	0.999	5.3	126.9
[Im <sub>3GA 4</sub> ]I	5569	8.7*10 <sup>-3</sup>	435.9	224.3	0.998	1.9	319.7

Among viscosity values, the highest was detected for [N<sub>1 1 2AG 4</sub>]I and the lowest for [N<sub>1 1 2AG 4</sub>]Br. Both ILs bear the shorter butyl chain on the ammonium cation. For them, the change of the bromide anion with the bigger iodide one determines an increase in viscosity of about 40000 mPa\*s. The spacer length affects the viscosities of about 10000 mPa\*s for the iodide ILs, [N<sub>1 1 2GA 4</sub>]I and [N<sub>1 1 3GA 4</sub>]I, with the higher value for the IL with the shorter spacer.

In contrast, the comparison between the [N<sub>1 1 3GA 4</sub>]I and the [Im<sub>3GA 4</sub>]I highlights the cation role in the IL properties, like the viscosity. The change in the cationic head nature determines a decrease in the viscosity of about 25000 mPa\*s.

Generally, the presence of the imidazolium cation permits obtaining less viscous ILs than the ammonium ones ( $[\text{Im}_{3\text{GA}4}]\text{I}$  and  $[\text{N}_{113\text{GA}4}]\text{I}$ ).<sup>25b</sup>

The viscosity is affected by spacer length also for the bromide ILs. Indeed, on going from the  $[\text{N}_{112\text{GA}8}]\text{Br}$ , leading the ethyl spacer, to the propyl one on the  $[\text{N}_{113\text{GA}8}]\text{Br}$ , the viscosity decreases to about 15000 mPa\*s. If the bromide anion is changed with the  $[\text{NTf}_2^-]$  one, the trend follows the opposite direction, with the higher viscosity for the  $[\text{N}_{113\text{GA}8}][\text{NTf}_2]$  than  $[\text{N}_{112\text{GA}8}][\text{NTf}_2]$ , although the difference between the viscosity values is lower than the one observed for the analogue bromide ILs. The change with a less coordinating anion, than the bromide, from  $[\text{N}_{112\text{GA}8}]\text{Br}$  to  $[\text{N}_{112\text{GA}8}][\text{NTf}_2]$  results in a decrease of the viscosity. This behaviour is expected for the  $[\text{NTf}_2^-]$  anion, determining weaker anion-cation charge interactions than the halide anion.<sup>72</sup> The trend is different for the  $[\text{N}_{113\text{GA}8}]\text{Br}$  and the  $[\text{N}_{113\text{GA}8}][\text{NTf}_2]$ , where the viscosity increases to about 10000 mPa\*s for the bistriflimide IL.

Finally, less significant changes in the ILs viscosity were detected as a function of the nature of the alkyl chain. Indeed, the change from the branched to the linear alkyl chain ( $[\text{N}_{113\text{GA}8}]\text{Br}$  and  $[\text{N}_{113\text{GA}8\text{L}}]\text{Br}$ ) determines a decrease in the viscosity values to about 3000 mPa\*s.

In general, the high viscosity values observed for these ILs could be justified by the presence of the gluconic moiety on the cation, which can establish multiple hydrogen bonding interactions.<sup>73</sup>

Each viscosity trend was fitted with the VFT (Vogel-Fulcher-Tammann) model, which describes the temperature dependence of the viscosity for a glass forming material. Indeed, in the DSC traces the crystallisation transition for the ILs is characterised by glass transitions, and a continuous raise in the viscosity associated with the decrease of the temperature. This model is expressed with the Eq. 1, which depends on three parameters:  $A$  (mPa\*s),  $B$  (K) and  $T_0$  (K). The  $A$

---

72. Yu, G.; Zhao, D.; Wen, L.; Yang, S.; Chen, X., Viscosity of ionic liquids: Database, observation, and quantitative structure-property relationship analysis. *AIChE J.* **2012**, *58* (9), 2885-2899.

73. (a) Ma, Y.; Yang, H.; Guo, J.; Wang, L.; Zhang, J., Effect of hydrogen bond on the viscosity of ionic liquid studied by combination of molecular dynamics and quantum chemistry. *Theor. Chem. Acc.* **2017**, *136* (9), 110, (b) Dong, K.; Zhang, S.; Wang, J., Understanding the hydrogen bonds in ionic liquids and their roles in properties and reactions. *Chem. Commun.* **2016**, *52* (41), 6744-6764.

parameter indicates the viscosity at the infinite temperature limit and  $T_0$  is the temperature at the infinite viscosity. This equation can be expressed in the logarithmic (10-base) or power form.<sup>74</sup>

$$\log \eta (T) = A + \frac{B}{(T-T_0)} \quad \text{Eq. 1}$$

The parameters  $B$  and  $T_0$  can be related to the fragility by equation Eq. 2:

$$D = \frac{B}{T_0} \quad \text{Eq. 2}$$

The fragility has been introduced by Angell,<sup>75</sup> and can be related to the VFT equation by mathematic manipulation (Eq. 3).

$$\log \eta (T) = A + \frac{D \cdot T_0}{(T-T_0)} \quad \text{Eq. 3}$$

The fragility  $D$  is a strength discriminant for the glass forming materials. A strong glass material presents a behaviour close to the Arrhenius law. It is a material characterised by strong interactions, which are not instantly broken down by heating. Oppositely, a fragile glass material is built on weak interactions and on hydrogen bonded network, and, its viscosity strongly depends on the temperature. These latter materials usually present a  $D < 10$ .<sup>76</sup>

The fragility can be used to obtain the fragility index,  $m$ , through the Eq. 4:

$$m = 16 + \frac{590}{D} \quad \text{Eq. 4}$$

---

74. (a) Zheng, Q.; Mauro, J. C., Viscosity of glass-forming systems. *J. Am. Ceram. Soc.* **2017**, *100* (1), 6-25, (b) Mauro, N. A.; Blodgett, M.; Johnson, M. L.; Vogt, A. J.; Kelton, K. F., A structural signature of liquid fragility. *Nature Communications* **2014**, *5*, 4616.

75. Angell, C. A., Relaxation in liquids, polymers and plastic crystals — strong/fragile patterns and problems. *J. Non-Cryst. Solids* **1991**, *131-133*, 13-31.

76. Böhmer, R.; Ngai, K. L.; Angell, C. A.; Plazek, D. J., Nonexponential relaxations in strong and fragile glass formers. *J. Chem. Phys.* **1993**, *99* (5), 4201-4209.



Glass forming materials are usually characterised by  $m$  values higher than 100. The value of this index is related to the structural stability of the material to thermal degradation.<sup>77</sup>

The  $D$  and  $m$  values are reported in Table 8. The reported ILs show fragility index over 100, highlighting the role played by hydrogen bonds and van der Waals interactions in this kind of structures.

The conductivity ( $\sigma$ ) of organic salts was also measured. Table 9 reports values obtained for ILs which are viscous liquids at room temperature.

A relation between the linker connecting the amide function and ammonium cation can be clearly identified. Although the difference in size of cations induced by linker of different length could be not significant for other properties, apparently this structural difference affects the ion mobility, resulting in a decrease of the available charge carriers on going from ethyl to propyl linker length.<sup>78</sup>

For all ILs here reported, the conductivity has to be considered on the grounds of the high viscous nature of these organic salts, being the conductivity inversely related to the viscosity.<sup>79</sup>

For all ILs bearing the same anion and alkyl chain, the conductivity of the salt with the ethyl linker is higher than the one of the salt with the propyl linker. The highest gap can be detected on going from  $[\text{N}_{112\text{GA}8}]\text{Br}$  to  $[\text{N}_{113\text{GA}8}]\text{Br}$ , for which the conductivity decreases to about 95 %. The difference between  $[\text{N}_{112\text{GA}8\text{L}}]\text{Br}$  and  $[\text{N}_{113\text{GA}8\text{L}}]\text{Br}$  is lower, while the conductivity is halved on going from  $[\text{N}_{112\text{GA}8}][\text{NTf}_2]$  to  $[\text{N}_{113\text{GA}8}][\text{NTf}_2]$  ILs.

The alkyl chain length plays also a role on the conductivity values; on going from branched alkyl chain ( $[\text{N}_{112\text{GA}8}]\text{Br}$ ) to the linear one ( $[\text{N}_{112\text{GA}8\text{L}}]\text{Br}$ ) an increase on the  $\sigma$  value occurs.

---

77. Moura Ramos, J. J.; Afonso, C. A. M.; Branco, L. C., Glass transition relaxation and fragility in two room temperature ionic liquids. *J. Therm. Anal. Calorim.* **2003**, *71* (2), 659-666.

78. Yuan, W.-L.; Yang, X.; He, L.; Xue, Y.; Qin, S.; Tao, G.-H., Viscosity, Conductivity, and Electrochemical Property of Dicyanamide Ionic Liquids. *Frontiers in chemistry* **2018**, *6*, 59-59.

79. Fitchett, B. D.; Knepp, T. N.; Conboy, J. C., 1-Alkyl-3-methylimidazolium Bis(perfluoroalkylsulfonyl) imide water-immiscible ionic liquids the effect of water on electrochemical and physical properties. *J. Electrochem. Soc.* **2004**, *151* (7), E219-E225.

If the alkyl chain is shortened from an octyl to a butyl chain, also in this case, an ethyl linker determines higher  $\sigma$  than the propyl one ( $[\text{N}_{1\ 1\ 2\text{GA}\ 4}]\text{I} - [\text{N}_{1\ 1\ 3\text{GA}\ 4}]\text{I}$ ). However, conductivity values for the  $[\text{N}_{1\ 1\ 3\text{GA}\ 8}]\text{Br}$  and  $[\text{N}_{1\ 1\ 3\text{GA}\ 4}]\text{I}$  resulted similar (0.002 and 0.005 S/m respectively).

The change of the anion determines a decrease of the conductivity on going from  $[\text{Br}]^-$  to  $[\text{NTf}_2]^-$ , for both  $[\text{N}_{1\ 1\ 2\text{GA}\ 8}]\text{Br}/[\text{N}_{1\ 1\ 2\text{GA}\ 8}][\text{NTf}_2]$  and  $[\text{N}_{1\ 1\ 3\text{GA}\ 8}]\text{Br}/[\text{N}_{1\ 1\ 3\text{GA}\ 8}][\text{NTf}_2]$ . This behaviour was not expected for the bistriflimide anion, considering the usual decrease of the viscosity due to this anion, and consequently, the increase of the conductivity. However, as already observed for the viscosity in this characterisation, this typical behaviour of IL is not always respected. Indeed, for conductivity the ion size and anionic charge delocalization have to be also considered.<sup>80</sup>

Finally, the aromatic cation determines an increase of the conductivity if compared with the corresponding ammonium IL ( $[\text{Im}_{3\text{GA}\ 4}]\text{I}/[\text{N}_{1\ 1\ 3\text{GA}\ 4}]\text{I}$ ). The higher conductivity for imidazolium ILs is usually described in previous literature reports.<sup>78</sup>

---

80. Hapiot, P.; Lagrost, C., Electrochemical Reactivity in Room-Temperature Ionic Liquids. *Chem. Rev.* **2008**, *108* (7), 2238-2264.

**Table 9 - Conductivity values for ILs synthesised. (<sup>a</sup>= This value was taken as known value to calculate the cell constant)<sup>81</sup>.**

IL	$\sigma$ (S/m) at 297.1 K
[N <sub>1 1 2GA 8</sub> ]Br	0.053
[N <sub>1 1 3GA 8</sub> ]Br	0.002
[N <sub>1 1 3GA 4</sub> ]I	0.005
[Im <sub>3GA 4</sub> ]I	0.022
[N <sub>1 1 2GA 4</sub> ]I	0.037
[N <sub>1 1 2GA 8</sub> ][NTf <sub>2</sub> ]	0.026
[N <sub>1 1 3GA 8</sub> ][NTf <sub>2</sub> ]	0.012
[N <sub>1 1 2GA 8L</sub> ]Br	0.122
[N <sub>1 1 3GA 8L</sub> ]Br	0.078
Standard [C <sub>8</sub> C <sub>1</sub> Im][BF <sub>4</sub> ]	0.059 <sup>a</sup>

### 2.3 Synthesis and characterisation of non-gluconic Ionic Liquids

Two other ILs were synthesised, which do not include the gluconic moiety but have similar alkyl chain length and a glycolic acid residue.

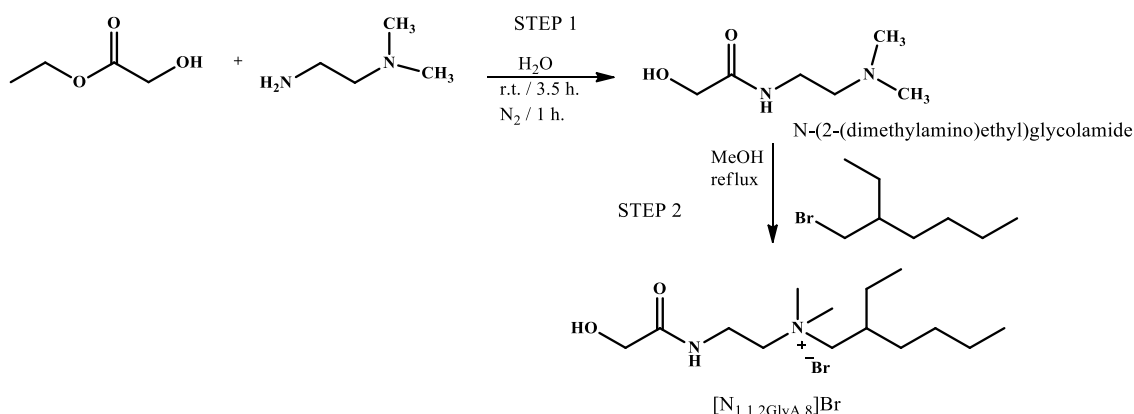
The synthesis of the [N<sub>1 1 2GLyA 8</sub>]Br is reported in Scheme 9. This IL differs from the [N<sub>1 1 2GA 8</sub>]Br for the length of hydroxylated chain and, consequently, the number of OH groups. The synthesis, also in this case, is composed by two steps. The first one considers the synthesis of an intermediate, the *N*-[2-(dimethylamino)ethyl]glycolamide, following a procedure already reported;<sup>82</sup> in

81. (a) Leys, J.; Wübbenhorst, M.; Menon, C. P.; Rajesh, R.; Thoen, J.; Glorieux, C.; Nockemann, P.; Thijs, B.; Binnemans, K.; Longuemart, S., Temperature dependence of the electrical conductivity of imidazolium ionic liquids. *J. Chem. Phys.* **2008**, *128* (6), 064509, (b) Stoppa, A.; Zech, O.; Kunz, W.; Buchner, R., The Conductivity of Imidazolium-Based Ionic Liquids from (−35 to 195) °C. A. Variation of Cation's Alkyl Chain. *J. Chem. Eng. Data* **2010**, *55* (5), 1768-1773.

82. Mower, M. P.; Blackmond, D. G., Mechanistic Rationalization of Unusual Sigmoidal Kinetic Profiles in the Machetti–De Sarlo Cycloaddition Reaction. *J. Am. Chem. Soc.* **2015**, *137* (6), 2386-2391.

the second step, the amino function is alkylated to obtain the IL. The relevant thermal properties are reported in Table 9.

The change in the structure from the gluconic to the glycolic moiety on the cation affects the thermal stability more than the glass transition (see also Table 6). The  $T_g$ s are 10 °C lower for the  $[N_{1.1}2GlyA_8]Br$ , while the  $T_d$  decreases by 39 °C.



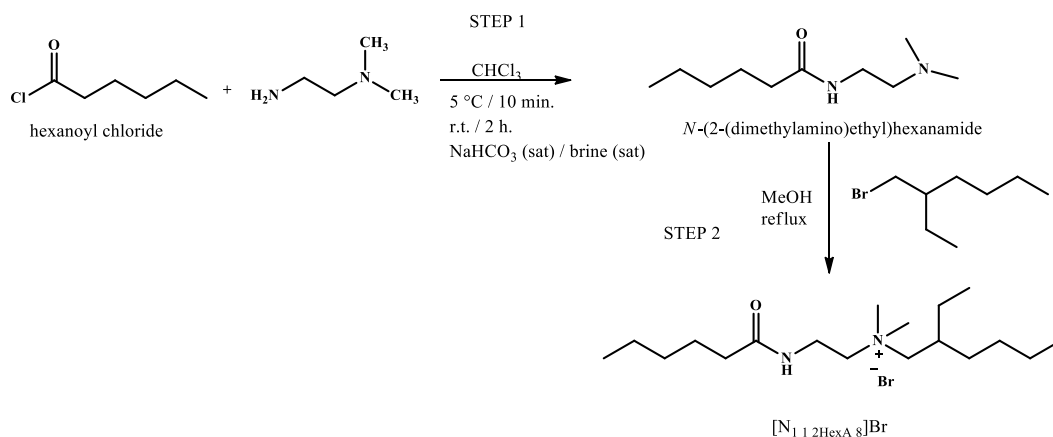
Scheme 9 - The synthetic pathway of the  $[N_{1.1}2GlyA_8]Br$  IL.

Table 10 - Thermal properties (DSC and TGA) of the  $[N_{1.1}2GlyA_8]Br$  IL.

IL	DSC analysis		TGA analysis
	Heating $T_g$ (°C)	Cooling $T_g$ (°C)	95 % wt. $T_d$ (°C)
$[N_{1.1}2GlyA_8]Br$	-25.5	-38.7	130.7

The synthesis of the  $[N_{1.1}2HexA_8]Br$  is reported in Scheme 10. This IL and the  $[N_{1.1}2GA_8]Br$  have the same alkyl chain length on the amide function, but the former does not bear OH groups. The synthesis involved two different steps. The first step consists of the synthesis of an intermediate, the *N*-[2-(dimethylamino)ethyl]hexanamide, obtained by a synthetic pathway already

reported;<sup>83</sup> the second step involved the alkylation of the amine in order to obtain the ammonium IL. The thermal properties of the  $[N_{1.1}2HexA_8]Br$  are reported in Table 11. The glass transition for this IL occurs at a lower temperature of about 30 °C than the one for  $[N_{1.1}2GA_8]Br$ . This can be ascribed to the lack of the OH groups that induces a decrease in both anion-cation and cation-cation interactions. In parallel, the same factor determines a decrease in the thermal stability.



Scheme 10 - The synthetic pathway of the  $[N_{1.1}2HexA_8]Br$  IL.

Table 11 - Thermal properties (DSC and TGA) of the  $[N_{1.1}2HexA_8]Br$  IL.

IL	DSC analysis		TGA analysis
	Heating $T_g$ (°C)	Cooling $T_g$ (°C)	95 % wt. $T_d$ (°C)
$[N_{1.1}2HexA_8]Br$	-48.7 0.4	-51.0	153.5

The viscosity of this IL was also determined and fitted with the VFT method. Obviously, the absence of the OH groups determines a drop in the viscosity value with respect to the one measured for the  $[N_{1.1}2GA_8]Br$  (see Table 8 and Table 12) and a corresponding increase in the fragility index.

83. Suzuki, Y.; Tsukahara, K. Antiaging and antiwrinkle cosmetics comprising amino group-containing compounds. JP 2009120515, **2009**.

Table 12 - Viscosity values, VFT parameters, fragility and fragility index.

IL	$\eta$ (mPa*s) at 293.1 K	A (mPa*s)	B (K)	$T_0$ (K)	$R^2$	D	m
[N <sub>1</sub> 1 <sub>2</sub> HexA <sub>8</sub> ]Br	260	4.2·10 <sup>-4</sup>	723.7	173.4	0.999	4.2	157.4

The conductivity for these ILs was also investigated. Table 13 reports the conductivity values for both the ILs devoid of all OH groups of the gluconic moiety and the conductivity for the [N<sub>1</sub>1<sub>2</sub>GA<sub>8</sub>]Br.

The  $\sigma$  values highlight the crucial role of OH groups. The decrease in the number of hydroxyl groups determines an increase on the conductivity. This results in the highest conductivity for [N<sub>1</sub>1<sub>2</sub>HexA<sub>8</sub>]Br, which does not bear any hydroxyl group in respect to all the ILs here reported. Also in this case, the relation between the viscosity and the conductivity is not observed. This behaviour is in agreement with the one already detected for the ILs bearing the hydroxylated alkyl chain, highlighting that the combination of different factors determines  $\sigma$  values of these ILs. However, similar findings were reported for alkanolammonium formate ILs, in which the increasing number of OH groups on the cation determines a decrease of the charge mobility and, obviously, a decrease of the conductivity value.<sup>84</sup>

84. Pinkert, A.; Ang, K. L.; Marsh, K. N.; Pang, S., Density, viscosity and electrical conductivity of protic alkanolammonium ionic liquids. *Phys. Chem. Chem. Phys.* **2011**, *13* (11), 5136-5143.

**Table 13 - Conductivity values for ILs synthesised. (<sup>a</sup>= This value was taken as known value to calculate the cell constant)<sup>81</sup>.**

<b>IL</b>	<b><math>\sigma</math> (S/m) at 297.1 K</b>
<b>[N<sub>1 1 2GA 8</sub>]Br</b>	0.053
<b>[N<sub>1 1 2GlyA 8</sub>]Br</b>	0.102
<b>[N<sub>1 1 2HexA 8</sub>]Br</b>	0.162
Standard <b>[C<sub>8</sub>C<sub>1</sub>Im][BF<sub>4</sub>]</b>	0.059 <sup>a</sup>

## 2.4 Experimental section

### 2.4.1 Materials

Glucono- $\delta$ -lactone (Sigma Aldrich,  $\geq 99.0\%$ ), *N,N*-dimethylethylenediamine (TCI,  $>98.0\%$ ), *N,N*-dimethyl-1,3-propanediamine (Sigma Aldrich,  $99.0\%$ ), 1-(3-aminopropyl)imidazole (Sigma Aldrich,  $\geq 97\%$ ), 2-ethylhexyl bromide (Sigma Aldrich,  $95.0\%$ ), 1-bromobutane (Sigma Aldrich,  $99.0\%$ ), 1-bromooctane (Sigma Aldrich,  $99\%$ ), 1-bromododecane (Sigma Aldrich,  $97\%$ ), 1-iodobutane (Sigma Aldrich,  $99\%$ ), ethyl glycolate (Sigma Aldrich,  $98\%$ ), hexanoyl chloride (Sigma Aldrich,  $97\%$ ), Co(NTf<sub>2</sub>)<sub>2</sub> (Alfa Aesar), poly(methyl methacrylate) (Sigma Aldrich), *N,N,N',N'*-tetramethylguanidine (Sigma Aldrich,  $99\%$ ), D-gluconic acid aqueous solution (Sigma Aldrich, 49-53 wt.% in H<sub>2</sub>O), tetrabutylphosphonium hydroxide solution (Sigma Aldrich, 40 wt.% in H<sub>2</sub>O), tetrabutylammonium hydroxide solution (Sigma Aldrich, 40 wt.% in H<sub>2</sub>O), trihexyltetradecylphosphonium chloride (Sigma Aldrich,  $\geq 95.0\%$ ), 1-butyl-1-methylpiperidinium chloride (Iolitec,  $99\%$ ), 1-butyl-1-methylpyrrolidinium chloride (Iolitec,  $99\%$ ), triethylmethylammonium bromide (Sigma Aldrich,  $\geq 99.0\%$ ), triethylmethylammonium bis{(trifluoromethyl)sulfonyl}imide (Iolitec,  $99.0\%$ ), tributylmethylammonium chloride (Sigma Aldrich,  $\geq 98.0\%$ ), and lithium bis{(trifluoromethyl)sulfonyl}imide salt (TCI,  $>98.0\%$ ) were purchased and used without further purification.

Dichloromethane (Merck,  $>99.8\%$ ), 1-butanol (Merck,  $>99.8\%$ ), methanol (Merck, HPLC grade), ethanol absolute (Merck, for analysis EMPARTA® ACS), acetonitrile (Merck, HPLC grade), ethyl acetate (Merck,  $98.8\%$ ) and *t*-butanol (Merck,  $99.5\%$ ) were purchased and used without further purification.

### 2.4.2 Synthesis of the *N*-[2-(dimethylamino)ethyl]glucosamide intermediate

Glucono- $\delta$ -lactone (8.42 mmol) was solubilised in methanol (70 mL) in two-neck round bottomed flask and placed in an oil bath at 60 °C. The *N,N*-



dimethylethylenediamine (9.26 mmol) was slowly added to the reaction mixture. After 24 h, the reaction was stopped and the solvent removed under vacuum. The yellow oil obtained was dissolved in a mixture of ethyl ethanoate/ethanol (50/50 v/v, 50 mL), obtaining a white solid. The solvent was removed under vacuum. To wash the solid product, ethyl ethanoate (50 mL) was added. The mixture was filtered using a Büchner funnel under vacuum, and the solid was collected. The product was dried *in vacuo* for 24 h.

Yield: 86.0%;  $T_m$  (DSC): 91.8 °C.

$^1\text{H}$  NMR (400 MHz; DMSO- $d_6$ );  $\delta$  (ppm): 7.53 (t, 1H,  $J = 8$  Hz); 5.42 (s, 1H); 4.31 (s, 1H); 3.97 (d, 1H); 3.89 (s, 1H); 3.56 (m, 1H); 3.47 (m, 2H); 3.35 (m, 2H); 3.18 (m, 2H); 2.31 (td, 2H,  $J = 4$  Hz); 2.14 (s, 6 H).  $^{13}\text{C}$  NMR (400 MHz; DMSO- $d_6$ );  $\delta$  (ppm): 173.8; 74.0; 72.5; 71.9; 70.6; 63.9; 58.4; 45.5; 36.6.

Mass for  $[\text{C}_{10}\text{H}_{23}\text{N}_2\text{O}_6]^+$ : 267.1556.

### 2.4.3 Synthesis of the *N*-[3-(dimethylamino)propyl]glucosamide intermediate

The glucono- $\delta$ -lactone (8.42 mmol) was solubilised in methanol (70 mL) in two-neck round bottomed flask and placed in an oil bath at 60 °C. The *N,N*-dimethyl-1,3-propanediamine (9.26 mmol) was slowly added to the reaction mixture. After 24 h, the reaction was stopped and the solvent removed under vacuum. The yellow oil obtained was dissolved in a mixture ethyl ethanoate/ethanol (50/50 v/v, 50 mL), resulting in a white solid. The solvent was removed under vacuum. To wash the solid product, ethyl ethanoate (50 mL) was added. The mixture was filtered using a Büchner funnel under vacuum, and the solid was collected. The product was dried *in vacuo* for 24 h.

Yield: 94.5%;  $T_m$  (DSC): 75.9 °C

$^1\text{H}$  NMR (400 MHz; DMSO- $d_6$ );  $\delta$  (ppm): 7.71 (t, 1H,  $J = 4$  Hz); 5.35 (d, 1H); 4.53 (s, 1H); 4.47 (s, 1H); 4.40 (d, 1H); 4.34 (s, 1H); 3.89 (d, 2H); 3.55 (d, 1H); 3.46 (s, 2H); 3.09 (m, 2H); 2.19 (t, 2H,  $J = 8$  Hz); 2.10 (s, 6H); 1.53 (m, 2H).  $^{13}\text{C}$  NMR (400 MHz; DMSO- $d_6$ );  $\delta$  (ppm): 172.6; 73.8; 72.5; 71.6; 70.3; 63.5; 57.0; 45.3; 37.0; 27.1.

Mass for  $[\text{C}_{11}\text{H}_{25}\text{N}_2\text{O}_6]^+$ : 281.1713.

#### 2.4.4 Synthesis of the *N*-[3-(imidazolyl)propyl]glucosamide intermediate

The glucono- $\delta$ -lactone (8.42 mmol) was solubilised in methanol (70 mL) in two-neck round bottomed flask and it was placed in an oil bath at 60 °C. The 1-(3-aminopropyl)imidazole (9.26 mmol) was slowly added to the reaction mixture. After 24 h, the reaction was stopped and the solvent removed under vacuum. The yellow oil obtained was dissolved in a mixture ethyl ethanoate/ethanol (50/50 v/v, 50 mL), obtaining a white solid. The solvent was removed under vacuum. To wash the solid product, ethyl ethanoate (50 mL) was added. The mixture was filtered using a Büchner funnel under vacuum, and the solid was collected. The product was dried *in vacuo* for 24 h.

Yield: 93.0%;  $T_m$  (DSC): 115.7 °C

$^1\text{H}$  NMR (600 MHz; DMSO- $d_6$ );  $\delta$  (ppm): 7.79 (t, 1H,  $J = 6$  Hz); 7.61 (t, 1H,  $J = 1.2$  Hz); 7.17 (t, 1H,  $J = 6$  Hz); 6.87 (t, 1H,  $J = 6$  Hz); 4.56 (d, 1H); 5.42 (d, 1H); 1.85 (m, 2H); 4.49 (d, 1H); 4.47 (d, 1H); 4.34 (t, 1H,  $J = 6$  Hz); 4.01 (q, 1H); 3.94 (m, 3H); 3.58 (m, 1H); 3.49 (m, 2H); 3.38 (m, 1H); 3.13 (m, 1H); 3.02 (m, 1H).  $^{13}\text{C}$  NMR (600 MHz; DMSO- $d_6$ );  $\delta$  (ppm): 173.2; 137.8; 128.7; 119.8; 74.1; 72.8; 71.9; 70.7; 63.8; 43.9; 35.8; 31.3.

Mass for  $[\text{C}_{12}\text{H}_{22}\text{N}_3\text{O}_6]^+$ : 304.1508.

#### 2.4.5 Synthesis of the *N*-[2-(dimethylamino)ethyl]glycolamide intermediate

The ethyl glycolate (10 mmol), *N,N*-dimethylethylenediamine (12 mmol) and distilled water (5 mL) were placed in a sealed screw cap tube. The reaction was stirred at room temperature for 3.5 hours. After this time, the reaction mixture was transferred in a round bottomed flask and  $\text{N}_2$  was blown into the reaction mixture

for 1 h. The residual solvent was removed under vacuum and a white solid was obtained. The product was dried *in vacuo* for 24 h.<sup>82</sup>

Yield: 70.0%.

<sup>1</sup>H NMR (400 MHz; DMSO-*d*<sub>6</sub>); δ (ppm): 7.55 (s, 1H); 5.52 (bs, 1H); 3.77 (s, 2H); 3.19 (q, 2H); 2.30 (t, 2H, *J* = 8 Hz); 2.14 (s, 6H). <sup>13</sup>C NMR (400 MHz; DMSO-*d*<sub>6</sub>); δ (ppm): 172.0; 58.5; 45.5; 36.4.

#### 2.4.6 Synthesis of the *N*-[2-(dimethylamino)ethyl]hexylamide intermediate

The *N,N*-dimethylethylenediamine (2.27 mmol) was dissolved in chloroform (10 mL) in a round bottomed flask and it was placed in ice to maintain the temperature equal to 5 °C. Hexanoyl chloride (2.29 mmol) was added dropwise in 8 minutes. The mixture was stirred at room temperature for two hours. After this time, the reaction was complete and chloroform was removed under vacuum. The oil obtained was subjected to extraction with ethyl ethanoate (30 mL). After the extraction, the mixture was washed with a saturated aqueous sodium bicarbonate solution (10 mL) and, then, with saturated brine (10 mL). After washing the residual solvent was removed under vacuum and a white solid was obtained. The product was dried *in vacuo* for 24 h.<sup>83</sup>

Yield: 70.9%.

<sup>1</sup>H NMR (300 MHz; CDCl<sub>3</sub>); δ (ppm): 6.04 (s, 1H); 3.30 (q, 2H, *J* = 3); 2.39 (t, 2H, *J* = 6 Hz); 2.22 (s, 6H); 2.14 (m, 2H); 1.62 (m, 2H); 1.30 (d, 4H); 0.88 (t, 3H, *J* = 6 Hz). <sup>13</sup>C NMR (300 MHz; CDCl<sub>3</sub>); δ (ppm): 172.9; 57.6; 44.8; 36.4; 36.3; 31.2; 25.2; 22.1 13.6.

#### 2.4.7 General quaternisation procedure to synthesise the [C<sub>x</sub>y z(R)<sub>A</sub>]<sub>w</sub>IX ILs

The suitable intermediate (3.0 mmol) was placed with methanol (4 mL) in a two-neck round bottomed flask and heated at 60 °C. The alkyl halide (4.5 mmol) was slowly added to the reaction mixture. The alkylation was stopped when the

$^1\text{H}$  NMR of the mixture did not show the signal of the amide related to the intermediate. The solvent was removed under vacuum and the IL was washed with ethyl ethanoate (20 mL). The ionic liquid was dried *in vacuo* for 24 h.

#### 2.4.8 $[\text{N}_{112\text{GA}8}]\text{Br}$

Chemical shift amide-intermediate: 7.53 ppm. Chemical shift amide-IL: 8.04 ppm. The product was obtained as light yellow oil. Yield: 90.2%;  $T_g$  (DSC): -16.6 °C (heating); -22.6 °C (cooling).

$^1\text{H}$  NMR (600 MHz, DMSO- $d_6$ );  $\delta$  (ppm): 8.04 (t, 1H,  $J = 6$  Hz); 5.48 (s, 1H); 4.34 (m, 4H); 3.96 (m, 1H); 3.87 (m, 1H); 3.50 (m, 3H); 3.42 (m, 4H); 3.32 (m, 4H); 2.96 (s, 6H); 1.80 (s, 1H); 1.27 (m, 10H); 0.82 (m, 6H).  $^{13}\text{C}$  NMR (600 MHz, DMSO- $d_6$ );  $\delta$  (ppm): 173.8; 74.0; 72.7; 72.0; 70.6; 69.1; 63.7; 62.9; 50.3; 33.4; 32.9; 32.8; 28.6; 28.0; 26.1; 22.8; 14.4; 10.6.

Mass for  $[\text{N}_{112\text{GA}8}]_2^+\text{Br}^-$ : 837.4880.

#### 2.4.9 $[\text{N}_{113\text{GA}8}]\text{Br}$

Chemical shift amide-intermediate: 7.71 ppm. Chemical shift amide-IL: 7.88 ppm. The product was obtained as light yellow oil. Yield: 83.0%;  $T_g$  (DSC): -0.1 °C (heating); -5.3 °C (cooling).

$^1\text{H}$  NMR (600 MHz, DMSO- $d_6$ );  $\delta$  (ppm): 7.88 (t, 1H,  $J = 6$  Hz); 5.47 (d, 1H); 4.59 (d, 1H); 4.53 (d, 1H); 4.48 (dd, 1H); 4.36 (t, 1H,  $J = 6$  Hz); 4.02 (t, 1H,  $J = 6$  Hz); 3.92 (m, 1H); 3.57 (m, 1H); 3.50 (m, 2H); 3.41 (m, 1H); 3.27 (t, 3H,  $J = 6$  Hz); 3.13 (m, 3H); 2.97 (s, 5H); 1.86 (m, 2H); 1.31 (m, 8H); 0.87 (m, 6H).  $^{13}\text{C}$  NMR (600 MHz, DMSO- $d_6$ );  $\delta$  (ppm): 173.5; 73.9; 72.5; 71.9; 70.8; 68.8; 63.7; 62.3; 50.0; 35.6; 32.8; 28.0; 26.1; 23.2; 22.8; 22.7; 14.4; 11.1; 10.5.

Mass for  $[\text{N}_{113\text{GA}8}]_2^+\text{Br}^-$ : 865.5101.

#### 2.4.10 [N<sub>1 1 3GA 4</sub>]I

Chemical shift amide-intermediate: 7.71 ppm. Chemical shift amide-IL: 7.87 ppm. The product was obtained as light yellow oil. Yield: 96.0%;  $T_g$  (DSC): -19.4 °C (heating); -25.7 °C (cooling).

<sup>1</sup>H NMR (600 MHz, DMSO-*d*<sub>6</sub>);  $\delta$  (ppm): 7.87 (t, 1H,  $J = 6$  Hz); 5.46 (d, 1H); 4.58 (s, 1H); 4.51 (d, 1H); 4.47 (d, 1H); 4.36 (s, 1H); 4.00 (t, 1H,  $J = 6$  Hz); 3.90 (s, 1H); 3.56 (m, 1H); 3.48 (s, 2H); 3.39 (m, 1H); 3.25 (m, 1H); 3.21 (m, 4H); 3.08 (m, 1H); 3.02 (s, 1H); 2.96 (s, 6H); 1.83 (m, 2H); 1.61 (m, 2H); 1.28 (q, 2H); 0.92 (t, 3H,  $J = 6$  Hz). <sup>13</sup>C NMR (600 MHz, DMSO-*d*<sub>6</sub>);  $\delta$  (ppm): 173.5; 73.9; 72.5; 71.9; 70.8; 63.7; 63.4; 61.6; 50.6; 49.0; 35.5; 24.1; 23.0; 19.7; 14.0.

Mass for [N<sub>1 1 3GA 4</sub>]<sub>2</sub><sup>+</sup> I: 801.3722.

#### 2.4.11 [N<sub>1 1 2GA 4</sub>]I

Chemical shift amide-intermediate: 7.53 ppm. Chemical shift amide-IL: 8.12 ppm. The product was obtained as light yellow oil. Yield: 97.4%;  $T_g$  (DSC): -7.9 (heating).

<sup>1</sup>H NMR (600 MHz, DMSO-*d*<sub>6</sub>);  $\delta$  (ppm): 8.12 (t, 1H,  $J = 6$  Hz); 5.54 (s, 1H); 4.46 (m, 4H); 4.04 (d, 1H); 3.95 (s, 1H); 3.50 (m, 15H); 3.17 (s, 1H); 3.10 (d, 1H); 3.05 (s, 6H); 1.66 (m, 2H); 1.32 (m, 2H); 0.94 (t, 3H,  $J = 6$  Hz). <sup>13</sup>C NMR (600 MHz, DMSO-*d*<sub>6</sub>);  $\delta$  (ppm): 173.8; 72.7; 70.6; 63.7; 61.6; 51.0; 33.3; 24.1; 19.6; 14.0.

Mass for [N<sub>1 1 2GA 4</sub>]<sub>2</sub><sup>+</sup> I: 773.3409.

#### 2.4.12 [Im<sub>3GA 4</sub>]I

Chemical shift amide-intermediate: 7.17 ppm. Chemical shift amide-IL: 9.12 ppm. The product was obtained as light yellow oil. Yield: 97.1%;  $T_g$  (DSC): -3.7 (heating).

<sup>1</sup>H NMR (400 MHz, DMSO-*d*<sub>6</sub>);  $\delta$  (ppm): 9.12 (s, 1H); 7.90 (t, 1H,  $J = 4$  Hz); 7.80 (d, 2H); 5.50 (s, 1H); 4.56 (s, 3H); 4.41 (q, 1H); 4.27 (t, 1H,  $J = 8$  Hz); 4.02

(s, 1H); 3.93 (s, 1H); 3.15 (s, 2H); 3.02 (m, 1H); 1.97 (m, 2H); 1.77 (q, 2H,  $J = 8$  Hz); 1.27 (m, 2H); 0.89 (t, 3H,  $J = 8$  Hz).  $^{13}\text{C}$  NMR (400 MHz, DMSO- $d_6$ );  $\delta$  (ppm): 173.4; 136.5; 122.8; 122.7; 73.8; 72.4; 71.8; 70.6; 63.5; 49.0; 46.6; 46.4; 34.8; 31.6; 29.8; 27.9; 19.1; 13.7.

Mass for  $[\text{Im}_{1.3\text{GA}4}]_2^+ \text{I}^-$ : 847.3314.

#### 2.4.13 $[\text{N}_{1.12\text{GA}4}]\text{Br}$

Chemical shift amide-intermediate: 7.53 ppm. Chemical shift amide-IL: 8.10 ppm. The product was obtained as light yellow oil. Yield: 85.5%;  $T_g$  (DSC): -46.6 °C (heating); -49.0 °C (cooling).

$^1\text{H}$  NMR (400 MHz, DMSO- $d_6$ );  $\delta$  (ppm): 8.10 (t, 1H,  $J = 8$  Hz); 5.51 (s, 1H); 4.41 (m, 4H); 4.02 (d, 1H); 3.93 (s, 1H); 3.49 (m, 7H); 3.03 (s, 6H); 1.31 (m, 2H); 0.93 (t, 3H,  $J = 8$  Hz).  $^{13}\text{C}$  NMR (400 MHz, DMSO- $d_6$ );  $\delta$  (ppm): 174.3; 74.5; 73.2; 72.5; 71.1; 64.2; 51.3; 43.6; 33.7; 24.6; 20.1; 14.4.

Mass for  $[\text{N}_{1.12\text{GA}4}]_2^+ \text{Br}^-$ : 727.3533.

#### 2.4.14 $[\text{N}_{1.12\text{GA}8\text{L}}]\text{Br}$

Chemical shift amide-intermediate: 7.53 ppm. Chemical shift amide-IL: 8.05 ppm. The product was obtained as light yellow oil. Yield: 85.5%;  $T_g$  (DSC): -55.5 °C (heating); -60.6 °C (cooling).

$^1\text{H}$  NMR (400 MHz, DMSO- $d_6$ );  $\delta$  (ppm): 8.05 (s, 1H); 4.41 (q, 1H); 4.06 (m, 1H); 3.34 (m, 17H); 3.08 (s, 2H); 3.04 (t, 2H,  $J = 4$  Hz); 2.84 (s, 2H); 2.09 (t, 1H,  $J = 8$  Hz); 1.66 (s, 1H); 1.51 (q, 1H); 1.28 (m, 7H); 0.87 (m, 3H).  $^{13}\text{C}$  NMR (400 MHz, DMSO- $d_6$ );  $\delta$  (ppm): 173.8; 74.0; 72.7; 63.9; 63.7; 61.7; 51.2; 51.0; 33.6; 33.2; 31.6; 28.9; 26.2; 22.4; 14.4.

Mass for  $[\text{N}_{1.12\text{GA}8\text{L}}]_2^+ \text{Br}^-$ : 837.4800.

#### 2.4.15 [N<sub>1</sub>1<sub>3GA</sub>8L]Br

Chemical shift amide-intermediate: 7.71 ppm. Chemical shift amide-IL: 8.10 ppm. The product was obtained as light yellow oil. Yield: 85.5%;  $T_g$  (DSC): -36.1 °C (heating); -43.6 °C (cooling).

<sup>1</sup>H NMR (400 MHz, DMSO-*d*<sub>6</sub>);  $\delta$  (ppm): 8.10 (t, 1H,  $J = 4$  Hz); 5.53 (d, 1H); 4.55 (d, 2H); 4.43 (d, 1H); 4.37 (s, 1H); 4.04 (t, 1H,  $J = 4$  Hz); 3.94 (s, 1H); 3.47 (m, 6H); 3.17 (0.8, 1H); 3.08 (s, 1H); 3.03 (s, 6H); 1.66 (s, 2H); 1.27 (d, 12H); 0.87 (t, 3H,  $J = 8$  Hz). <sup>13</sup>C NMR (400 MHz, DMSO-*d*<sub>6</sub>);  $\delta$  (ppm): 173.8; 74.0; 72.7; 63.9; 63.7; 61.7; 51.2; 51.0; 33.6; 33.2; 31.6; 28.9; 26.2; 25.3; 22.5; 14.4.

Mass for [N<sub>1</sub>1<sub>2GA</sub>8L]<sub>2</sub><sup>+</sup> Br<sup>-</sup>: 867.5101.

#### 2.4.16 [N<sub>1</sub>1<sub>2GA</sub>12]Br

Chemical shift amide-intermediate: 7.53 ppm. Chemical shift amide-IL: 8.09 ppm. The product was obtained as light yellow oil. Yield: 85.5%;  $T_m$  (DSC): 87.1 °C (heating).

<sup>1</sup>H NMR (400 MHz, DMSO-*d*<sub>6</sub>);  $\delta$  (ppm): 8.09 (t, 1H,  $J = 8$  Hz); 5.51 (s, 1H); 4.54 (s, 2H); 4.41 (m, 1H); 4.03 (d, 1H); 3.93 (s, 1H); 3.49 (m, 5H); 3.30 (m, 8H); 3.19 (s, 1H); 3.03 (s, 4H); 2.79 (s, 1H); 1.65 (s, 1H); 1.24 (s, 21 H); 0.84 (m, 3H). <sup>13</sup>C NMR (400 MHz, DMSO-*d*<sub>6</sub>);  $\delta$  (ppm): 172.9; 73.1; 72.7; 71.8; 71.4; 71.0; 69.7; 63.8; 55.7; 50.0; 42.2; 32.3; 31.8; 30.8; 28.6; 28.4; 28.2; 28.0; 27.0; 25.3; 21.6; 21.2; 13.5.

Mass for [N<sub>1</sub>1<sub>2GA</sub>12]<sub>2</sub><sup>+</sup> Br<sup>-</sup>: 951.6026.

#### 2.4.17 [N<sub>1</sub>1<sub>2GlyA</sub>8]Br

Chemical shift amide-intermediate: 7.55 ppm. Chemical shift amide-IL: 8.14 ppm. The product was obtained as light yellow oil. Yield: 98%;  $T_g$ : - 25.5 °C (heating); -38.7 °C (cooling).

$^1\text{H}$  NMR (400 MHz,  $\text{DMSO-}d_6$ );  $\delta$  (ppm): 8.14 (t, 1H,  $J = 8$  Hz); 5.61 (d, 1H); 3.83 (s, 2H); 3.55 (q, 2H); 3.42 (m, 2H); 3.22 (m, 2H); 3.06 (s, 6H); 2.71 (s, 1H); 1.28 (m, 8H); 0.88 (m, 6H).  $^{13}\text{C}$  NMR (400 MHz;  $\text{DMSO-}d_6$ );  $\delta$  (ppm): 172.9; 68.9; 62.7; 61.9; 50.3; 33.0; 32.9; 32.7; 28.0; 26.0; 22.8; 14.4; 10.5.

Mass for  $[\text{N}_{112}\text{GlyA}_8]_2^+ \text{Br}^-$ : 599.3939.

#### 2.4.18 $[\text{N}_{112}\text{HexA}_8]\text{Br}$

Chemical shift amide-intermediate: 6.04 ppm. Chemical shift amide-IL: 8.14 ppm. The product was obtained as light yellow oil. Yield: 69.8%;  $T_g$ :  $-48.7$  °C (heating);  $-51.0$  °C (cooling).

$^1\text{H}$  NMR (400 MHz,  $\text{DMSO-}d_6$ );  $\delta$  (ppm): 8.14 (t, 1H,  $J = 8$  Hz); 3.47 (m, 2H); 3.22 (t, 2H,  $J = 4$  Hz); 3.06 (s, 6H); 2.80 (s, 1H); 2.10 (t, 2H,  $J = 8$  Hz); 1.90 (s, 1H); 1.50 (q, 3H,  $J = 8$  Hz); 1.27 (m, 11H); 0.88 (m, 9H).  $^{13}\text{C}$  NMR (400 MHz;  $\text{DMSO-}d_6$ );  $\delta$  (ppm): 172.1; 67.7; 61.6; 49.1; 41.8; 34.5; 32.1; 31.8; 31.6; 30.2; 26.9; 24.9; 24.1; 21.7; 21.2; 13.2; 13.1; 9.4.

Mass for  $[\text{N}_{112}\text{HexA}_8\text{L}]_2^+ \text{Br}^-$ : 677.5308.

#### 2.4.19 General methathesis procedure to synthesise the $[\text{N}_{11x}\text{GA}_8]_2^+[\text{NTf}_2]^-$ ILs

The  $[\text{N}_{11x}\text{GA}_8]\text{Br}$  IL (0.60 mmol) was dissolved in 1-butanol (4 mL) in a round bottomed flask and stirred at room temperature for 24 h.  $\text{Li}(\text{NTf}_2)$  (0.64 mmol) was slowly added to the solution and white precipitate was formed. This precipitate was separated by filtration and the solution was passed through alumina oxide. The organic phase was placed in a separatory funnel and washed with distilled water. The organic phase was recovered and the sodium sulfate anhydrous was added to remove the residue of water. Sodium sulfate was removed by filtration. The organic solvent was removed under vacuum. The ionic liquid was dried *in vacuo* for 24 h.



#### 2.4.20 [N<sub>112GA8</sub>][NTf<sub>2</sub>]

The product was obtained as yellow oil. Yield: 72.6%.  $T_g$  (DSC): -15.9 °C.

<sup>1</sup>H NMR (600 MHz; DMSO-*d*<sub>6</sub>);  $\delta$  (ppm): 7.88 (t, 1H,  $J = 6$  Hz); 5.48 (d, 1H); 4.60 (d, 1H); 4.55 (d, 1H); 4.50 (d, 1H); 4.36 (s, 1H); 4.00 (t, 1H,  $J = 6$  Hz); 3.92 (s, 1H); 3.59 (d, 1H); 3.50 (s, 2H); 3.26 (t, 3H,  $J = 6$  Hz); 3.14 (m, 3H); 2.97 (s, 6H); 1.33 (m, 10H); 0.87 (m, 6H). <sup>13</sup>C NMR (600 MHz; DMSO-*d*<sub>6</sub>);  $\delta$  (ppm): 173.8; 123.1; 121.0; 118.9; 116.7; 74.0; 72.7; 72.0; 70.6; 69.1; 63.7; 60.8; 50.3; 35.1; 33.4; 32.8; 28.0; 26.1; 22.8; 19.1; 14.4; 10.5.

Mass for [N<sub>112GA8</sub>]<sub>2</sub><sup>+</sup>[NTf<sub>2</sub>]<sup>-</sup>: 1038.4789.

#### 2.4.21 [N<sub>113GA8</sub>][NTf<sub>2</sub>]

The product was obtained as yellow oil. Yield: 68.1%.  $T_g$  (DSC): -16.2 °C (heating); -44.4 °C (cooling).

<sup>1</sup>H NMR (600 MHz; DMSO-*d*<sub>6</sub>);  $\delta$  (ppm): 7.87 (t, 1H,  $J = 6$  Hz); 0.86 (m, 6H); 5.46 (d, 1H); 4.58 (d, 1H); 4.53 (d, 1H); 4.47 (dd, 1H); 4.35 (t, 1H,  $J = 6$  Hz); 4.00 (t, 1H,  $J = 6$  Hz); 3.91 (m, 1H); 3.28 (m, 1H); 3.49 (m, 1H); 3.38 (m, 1H); 3.24 (t, 2H,  $J = 6$  Hz); 3.12 (m, 3H); 2.95 (s, 6H); 1.87 (m, 3H); 1.28 (m, 10H). <sup>13</sup>C NMR (600 MHz; DMSO-*d*<sub>6</sub>);  $\delta$  (ppm): 172.8; 122.4; 120.3; 118.1; 73.1; 71.7; 71.2; 70.1; 68.1; 63.0; 61.6; 60.1; 49.2; 34.9; 32.0; 27.3; 25.3; 22.4; 22.0; 18.3; 13.6; 9.7.

Mass for [N<sub>113GA8</sub>]<sub>2</sub><sup>+</sup>[NTf<sub>2</sub>]<sup>-</sup>: 1066.5133.

#### 2.4.22 General neutralisation reaction procedure to synthesise the gluconate salts

The hydroxide salt aqueous solution (0.020 mol of salt) and the gluconic acid aqueous solution (0.024 mol of gluconic acid) were placed in a round bottomed flask and stirred for 24 hours. After this time, the neutralisation reaction was stopped and water was removed under vacuum. The white solid obtained was dried *in vacuo* overnight.

#### 2.4.23 [P<sub>66614</sub>][Glu]

The first step of this synthesis was the anion exchange to replace the Cl<sup>-</sup> anion with [OH]<sup>-</sup> anion using the Amberlite™ IRN-78 ion-exchange resin, OH-form, according to a previously reported procedure.<sup>85</sup> Yield: 89.4%; white solid;  $T_m$  (DSC): 35.6 °C; <sup>1</sup>H NMR (600 MHz; DMSO-*d*<sub>6</sub>);  $\delta$  (ppm): 3.73 (dd, 1H); 3.57 (m, 2H); 3.50, (m, 1H); 3.41 (dd, 2H); 3.31 (m, 3H); 2.17 (m, 7H); 1.56 (m, 3H); 1.30 (m, 46H); 0.88 (m, 12H). <sup>13</sup>C NMR (600 MHz, DMSO-*d*<sub>6</sub>);  $\delta$  (ppm): 176.4; 72.8; 72.4; 72.1; 71.6; 64.2; 31.8; 30.7; 30.3; 30.1; 29.5; 29.2; 29.1; 28.5; 22.6; 22.3; 21.0; 18.2; 17.7; 14.4; 14.3.

Mass for [P<sub>66614</sub>]<sub>2</sub><sup>+</sup>[Glu]<sup>-</sup>: 1162.0623.

#### 2.4.24 [P<sub>4444</sub>][Glu]

Yield: 97.9%; white solid;  $T_m$  (DSC): 81.5 °C; <sup>1</sup>H NMR (600 MHz; DMSO-*d*<sub>6</sub>);  $\delta$  (ppm): 4.63 (s, 1H); 4.50 (d, 1H); 4.41 (s, 1H); 4.17 (s, 1H); 3.71 (m, 1H); 3.55 (d, 1H); 3.48 (t, 1H, J = 6 Hz); 3.40 (s, 1H); 3.30 (m, 1H); 2.18 (m, 6H); 1.45 (m, 16H); 0.92 (t, 12H, J = 12 Hz). <sup>13</sup>C NMR (600 MHz, D<sub>2</sub>O);  $\delta$  (ppm): 178.5; 74.0; 72.5; 71.1; 70.9; 62.6; 23.3; 23.2; 22.7; 17.8; 17.4; 12.5.

Mass for [P<sub>4444</sub>]<sub>2</sub><sup>+</sup>[Glu]<sup>-</sup>: 713.5614.

#### 2.4.25 [N<sub>4444</sub>][Glu]

Yield: 95.0%; white solid;  $T_m$  (DSC): 134.9 °C; <sup>1</sup>H NMR (400 MHz; D<sub>2</sub>O);  $\delta$  (ppm): 4.11 (d, 1H); 4.01 (t, 1H, J=4 Hz); 3.82 (m, 1H); 3.80 (d, 1H); 3.75 (m, 2H); 3.65 (m, 1H); 3.19 (m, 8H); 1.64 (m, 8H); 1.36 (st, 8H); 0.94 (t, 12H, J=8 Hz). <sup>13</sup>C NMR (400 MHz, CDCl<sub>3</sub>);  $\delta$  (ppm): 175.5; 72.8; 72.4; 72.0; 71.5; 70.8; 64.2; 57.9; 30.2; 23.5; 19.7; 14.0.

Mass for [N<sub>4444</sub>]<sub>2</sub><sup>+</sup>[Glu]<sup>-</sup>: 632.3885.

---

85. Taylor, S. F. R.; McCrellis, C.; McStay, C.; Jacquemin, J.; Hardacre, C.; Mercy, M.; Bell, R. G.; de Leeuw, N. H., CO<sub>2</sub> Capture in Wet and Dry Superbase Ionic Liquids. *J. Solution Chem.* **2015**, *44* (3), 511-527.

#### 2.4.26 [tmgH][Glu]

Yield: 95.5%; white solid;  $T_g$  (DSC): -24.1 °C (heating).  $^1\text{H}$  NMR (600 MHz; DMSO- $d_6$ );  $\delta$  (ppm): 7.94 (s, 1H); 3.75 (dd, 1H); 3.57 (m, 2H); 3.55 (d, 1H); 3.46 (m, 3H); 3.41 (d, 1H); 3.40 (d, 1H); 3.32 (m, 2H); 2.89 (s, 12H).  $^{13}\text{C}$  NMR (600 MHz; DMSO- $d_6$ ): 175.6; 161.5; 73.0; 72.6; 72.0; 71.3; 64.1.

Mass for  $[\text{tmgH}]_2^+[\text{Glu}]$ : 427.2880.

#### 2.4.27 Differential Scanning Calorimetry (DSC).

DSC measurements were carried out using TA Instruments Modulated DSC Q 2000 V24.4 Build 116 with a refrigerated cooling system RCS 90, capable of controlling the temperature down to 220 K. Samples were weighed and hermetically sealed in aluminum pans. Heating and cooling rates were 10 °C  $\text{min}^{-1}$  for the ionic liquid sample. The maximum heating temperature was varied depending on the thermal stability of the sample. The minimum cooling temperature was set at -50 °C under dinitrogen atmosphere. Two heating-cooling cycles were performed.

#### 2.4.28 Thermogravimetric analysis (TGA)

Thermogravimetric analysis was performed using a TGA/DSC thermogravimetric analyser from Mettler-Toledo, Inc. The samples were measured in alumina crucibles, at a heating rate of 5 K  $\text{min}^{-1}$ , under a dinitrogen atmosphere. The onset of the weight loss in each thermogram was used as a measure of the decomposition temperature (point at 5 % wt. loss of the sample).

#### 2.4.29 POM measurements

The POM images of the salts were recorded using an Olympus BX50 microscope equipped with JVC TK-1085E camera. For all experiments, the 0.25 10X MD PLAN lens was used. For a typical sample, the salt samples were cast

between two glasses to record the POM images. In all cases, two consecutive heating-cooling cycles were performed. The samples were heated until melting and then cooled. Heating and cooling rates were  $5\text{ }^{\circ}\text{C min}^{-1}$ .

#### **2.4.30 NMR measurements**

$^1\text{H}$  NMR and  $^{13}\text{C}$  NMR spectra were recorded using Bruker AV-300, Bruker ultrashield 400 plus, Bruker-spectroscopin 400 ultrashield and Ascend™ 600 Bruker nuclear magnetic resonance spectrometers. Chemical shifts were reported relative to  $\text{SiMe}_4$ .

#### **2.4.31 Mass spectrometric measurements**

ESMS-mass spectrometric measurements were carried out on a Waters ICI Premier instrument with an Adylon Triversa NanoMate injection system (cone voltage 50 V, source  $120\text{ }^{\circ}\text{C}$ ). Both positive and negative ions were detected. For each sample, a methanol solution was prepared.

#### **2.4.32 Conductivity measurements**

The electrical conductivity  $\sigma$  (S/m) of the liquid salts was measured with a Keithley 2000 Multimeter in a two-points configuration on pure salts, at  $T = 297.15\text{ K}$ . Due to the small amount of sample to be analysed, a home-made cell with two microelectrodes was used; the cell constant was calculated using a commercial IL,  $[\text{C}_8\text{C}_1\text{Im}][\text{BF}_4]$ , whose conductivity is already reported in literature.<sup>81</sup> The conductivity values are the average between three measures.

## 3. Novel “Sweet” Ionic Liquid Gels: combination of novel IL gelators and IL solvents

### 3.1 Gels in daily life

Chemistry is ubiquitous in everyday life. Substances in all physical states are materials of daily necessity, considering for example the liquid coffee or the solid detergents. These substances and materials are so common, that every person has familiarity with chemicals as liquids, solids and gels. These latter are more common than we think. Gels are soft materials that can be found in cosmetics, in drugs, lubricants and food.<sup>86</sup> This latter is the one immediately associated to a gel concept. Indeed, gelatine, jelly and jam are probably the most common gels that we know and they are usually the first idea in mind when someone asks: what is a gel?

For example, gelatine formed by hydrolysed collagen, is able to gel in water. Collagen is a protein, which can establish intra and intermolecular hydrogen bond networks forming triple-helix structure, composed of three  $\alpha$ -chains. In the manufacturing process, heating denatures the original structure of collagen, while, during the cooling cycles, the helices are partially reformed allowing to trap water and to obtain a gel. The structure of gelatine depends on collagen concentration, on the temperature ramp of the cooling process and on the energy given to the system.<sup>87</sup>

This common phenomenon is useful to understand how a gel, usually associated with a simple material, owes its structural characteristics and properties to several factors.

---

86. Okesola, B. O.; Smith, D. K., Applying low-molecular weight supramolecular gelators in an environmental setting – self-assembled gels as smart materials for pollutant removal. *Chem. Soc. Rev.* **2016**, *45* (15), 4226-4251.

87. Duconseille, A.; Astruc, T.; Quintana, N.; Meersman, F.; Sante-Lhoutellier, V., Gelatin structure and composition linked to hard capsule dissolution: A review. *Food Hydrocolloids* **2015**, *43*, 360-376.

### 3.2 What is a Gel: definition and classification

Defining a gel is not as easy as defining a common chemical system like a solution or a mixture, although its characteristics are immediately recognisable, as Dorothy Jordan Lloyd expressed in the far 1926 “*The colloidal condition, the gel, is one which is easier to recognize than to define*”. In spite of this difficulty to define a gel, she gave some advice about the composition and the structural properties: “*Only one rule seems to hold for all gels, and that is that they must be built up from two components, one of which is a liquid at the temperature under consideration, and the other of which, the gelling substance proper, often spoken of as the gelator, is a solid. The gel itself has the mechanical properties of a solid, i.e., it can maintain its form under the stress of its own weight, and under any mechanical stress, it shows the phenomenon of strain*”.<sup>88</sup> Over the years, other attempts to define gels had been done,<sup>89</sup> where a material is identified as a gel if it “(1) has a continuous microscopic structure with macroscopic dimensions that is permanent on the time scale of an analytical experiment and (2) is solid-like in its rheological behavior despite being mostly liquid”<sup>90</sup> as reported in the book “*Molecular Gels*” edited by R. Weiss and P. Terech.

The first empirical procedure to identify a gel is the “tube inversion” test. This procedure consists of the manual inversion of the tube of the vial containing the system which has to be tested. If this material resists to its own weight and does not flow, it could be defined as a gel.<sup>91</sup>

However, two different aspects *viz* the rheological and the thermodynamic properties can give more information and determine if the system is a gel in an absolute way.

---

88. Lloyd, D. J., In *Colloid Chemistry*, Alexander, J., Ed. New York: The Chemical Catalog Co: **1926**; Vol. vol 1, pp 767–782.

89. (a) Hermans, P. H., *Colloid Science*. Elsevier Pub. Co.: **1949**; Vol. II, (b) Flory, P. J., Introductory lecture. *Faraday Discussions of the Chemical Society* **1974**, 57 (0), 7-18, (c) Gelbart, W. M.; Ben-Shaul, A., The “New” Science of “Complex Fluids”. *J. Phys. Chem.* **1996**, 100 (31), 13169-13189.

90. Weiss, R. G.; Terech, P., *Molecular Gels: Materials with Self-Assembled Fibrillar Networks*. Springer: **2006**.

91. Raghavan, S. R.; Cipriano, B. H., Gel Formation: Phase Diagrams Using Tabletop Rheology and Calorimetry. In *Molecular Gels: Materials with Self-Assembled Fibrillar Networks*, Weiss, R. G.; Terech, P., Eds. Springer Netherlands: Dordrecht, **2006**; pp 241-252.

In the former, the rheological behaviour is defined by the response of a material when it is submitted to stress (for example placed in the plate of a rheometer and it is subjected to shear stress).

The viscoelastic gel behaviour can be considered in an intermediate status, between liquid- and solid-like behaviour.<sup>92</sup> How much a particular gel is close to one behaviour than the other can be determined by rheological investigation. Indeed, for a viscoelastic material the rheological properties depend on two parameters,  $G'$  and  $G''$ , the storage and the loss moduli respectively. The storage modulus,  $G'$ , indicates the capacity of the material to store energy elastically (in-phase, elastic behaviour), while, the loss modulus,  $G''$ , indicates the capacity of the material to dissipate energy through heat (out of phase, viscous behaviour). These two moduli are the components of  $G^*$ , the complex shear modulus.<sup>93</sup>

This modulus,  $G^*$ , provides information about the nature of a gel, its strength and structure. In an oscillation shear stress experiment, the strain amplitude at a fixed frequency depends on the components of the  $G^*$  modulus,  $G'$  and  $G''$ , making it possible to study the viscoelastic properties of a gel. Initially, both moduli increase linearly with deformation (strain%), but, after a critical point of strain ( $\gamma$  at  $G'=G''$ ), this behaviour changes, showing a structural response of the gel. The linear trend showing  $G'>G''$  corresponds to a solid-like behaviour. Oppositely, when  $G''>G'$  a liquid-like behaviour can be determined. These different responses and the critical point depend on the network and interactions forming the gel. The ratio  $G''/G'$  corresponds to  $\tan \delta$ , which can give additional information about the strength of the gel. A value of  $\tan \delta$  higher than 1 indicates a weak gel network, while a value lower than 1 a strong gel. In addition, the gel network is defined by a frequency measurement at fixed strain (below the crossover point of  $\gamma$ ). In the oscillation frequency mode, both  $G'$  and  $G''$  result independent on the increase of frequency, oppositely, a more fluid-like material shows a more pronounced dependence of  $G'$  and  $G''$  on the frequency sweep.<sup>94</sup>

---

92. Marr, P. C.; Marr, A. C., Ionic liquid gel materials: applications in green and sustainable chemistry. *Green Chem.* **2016**, *18* (1), 105-128.

93. Dawn, A.; Kumari, H., Low Molecular Weight Supramolecular Gels Under Shear: Rheology as the Tool for Elucidating Structure–Function Correlation. *Chem. Eur. J.* **2018**, *24* (4), 762-776.

94. Almdal, K.; Dyre, J.; Hvidt, S.; Kramer, O., Towards a phenomenological definition of the term 'gel'. *Polymer Gels and Networks* **1993**, *1* (1), 5-17.

The gel phase, which consists of the solid component dissolved in the liquid component is formed by a 3D network. This network can be destroyed, by heating the gel phase. A gel can be defined as thermo-reversible or thermo-irreversible if it is or not capable of reforming the gel phase.

The thermodynamic aspect is referred to this behaviour, and in particular, to the first order transition of a solution obtained when a gel is melted. Usually, gels show an exothermic formation and an endothermic melting, when analysed in a calorimetric investigation.<sup>95</sup>

The gel classification can be dated to 1974, when Flory, during the *Faraday Discussion Meeting on Gel and Gelling Processing*, classified four different types of gels depending on the network structure:<sup>89b</sup>

1. Well-ordered lamellar structure.
2. Covalent polymeric structure. The network is formed by covalent interactions and results in a disordered gel.
3. Polymer network formed by physical interactions.
4. Particulate disordered structure, where the involved interactions form different clusters of aggregates.

The classification of gels was changed, improved and conformed in parallel with the scientific research and the discoveries in this field.<sup>96,97</sup> More recent classifications have differentiated the nature of the cross-linking connections,<sup>98</sup> optical behaviour, and thermal properties to make an order in the gel field.<sup>99,100</sup>

---

95. Guenet, J.-M., *Organogels Thermodynamics, Structure, Solvent Role, and Properties*. Springer International Publishing: **2016**.

96. Keller, A., Introductory lecture. Aspects of polymer gels. *Faraday Discuss.* **1995**, 101 (0), 1-49.

97. Nishinari, K., Some Thoughts on The Definition of a Gel. In *Gels: Structures, Properties, and Functions*, Tokita, M.; Nishinari, K., Eds. Springer-Verlag Berlin Heidelberg: **2009**.

98. Tanaka, F., Theory of molecular association and thermoreversible gelation. In *Molecular Gels Materials with Self-Assembled Fibrillar Networks*, Weiss, R. G.; Terech, P., Eds. Springer Netherlands: **2006**.

99. Nishinari, K., Rheological and DSC study of sol-gel transition in aqueous dispersions of industrially important polymers and colloids. *Colloid Polym. Sci.* **1997**, 275 (12), 1093.

100. Clark, A. H.; Ross-Murphy, S. B. In *Structural and mechanical properties of biopolymer gels*, Berlin, Heidelberg, Springer Berlin Heidelberg: Berlin, Heidelberg, **1987**; pp 57-192.



In general, a gel can be classified on the nature of interactions, of the gelator and of the solvent.

The nature of the interaction can be distinguished between physical and chemical. In the first case, the 3D gel network is built on hydrogen bonds, van der Waals interaction and  $\pi$ - $\pi$  stacking. The chemical interaction involves covalent bonds. However, it is not rare a joint occurrence of the covalent bonds with physical interactions to form the gel phase.

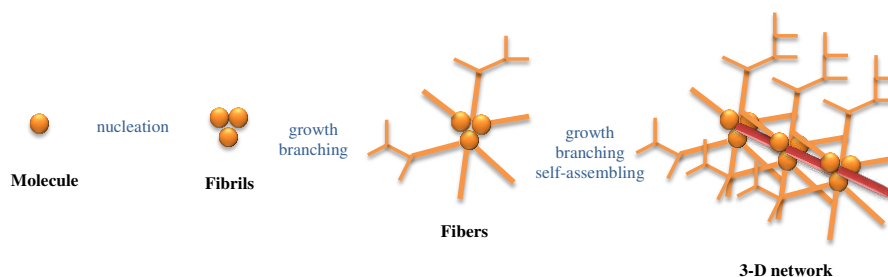
The nature of the gelator, the solid component, has been partially explained in the Flory classification (*vide supra*). The nature of the solid, usually, could be polymeric, colloidal and molecular. Polymeric gels are often the result of the combination of physical and chemical interactions, where the chain of the polymer builds a matrix where the liquid medium is trapped. The colloidal gelator can be a solid with size between nano and micrometers. In this case, the liquid medium is dispersed in the colloidal solid and the gel phase is formed.

In the latter case, we are dealing with molecular, or most commonly called supramolecular gels, in which the gelator is a small molecule known as Low Molecular Weight Gelator (LMWG) or Low Molecular Mass Gelator (LMMG). In this gel, the 3D network is characterised by aggregates which trap the liquid molecules. These gelators generally present a molecular weight lower than 3000 a.u.. The gel phase consists of a network where hydrogen bonds, van der Waals and  $\pi$ - $\pi$  interactions are involved.

The nucleation of the gelator is the starting point from which all the gelation processes can occur. The interaction of the gelator-nuclei leads to the fibrils formation. The branching and growing of these fibrils, due to further interactions, determine the fibers formation. The additional self-assembly of these fibers can occur through strands or tubular structure building. The size of this “fibrous” aggregates, and the time required to establish the connections, determine the supramolecular gel properties. A simplified representation is reported in Scheme 11.<sup>90,101</sup>

---

101. Li, J.-L.; Liu, X.-Y., Architecture of Supramolecular Soft Functional Materials: From Understanding to Micro-/Nanoscale Engineering. *Adv. Funct. Mater.* **2010**, *20* (19), 3196-3216.



**Scheme 11 - Schematic illustration of the 3D-network formation.**

The last classification takes into account the nature of the liquid medium. Hence, considering the solvent component, it is possible to discriminate among organogels, hydrogels, oleogels, polymer gels and Ionic Liquid gels, in which the liquid medium is an organic solvent, water, an oil, a liquid polymer or an Ionic Liquid respectively.<sup>92</sup>

This brief overview on the gel classification highlights how these systems are not as simple as they appear, and often, to describe a gel accurately it is necessary to match more than one classification.

### **3.3 How to combine gel concept and the Ionic Liquids to form Ionic Liquid Gels**

In the first Chapter, IL properties and characteristics were depicted. The possibility to design and synthesise a structure which could satisfy the required applications sometimes is not enough. The physical state is a fundamental parameter that has to be considered in any application or device. Thus, a solid-like phase can find more applicability than the liquid one. The first advantage is an easier handling of the material. Indeed, a gel features a solid dispersed in a trapped liquid phase, and can maintain both characteristics. The inclusion of ILs in the gel results in a solid-like material with the thermal stability, the negligible vapour pressure, the conductivity and the spatial organisation ascribable to the IL. The IL can be the gelator or/and solvent, obtaining in this way the Ionic Liquids Gels (ILGs).

Applying the tunable structures of the ILs to the gel is a scientific challenge, having witnessed fast growing of the interest on the ILGs.<sup>92</sup>

Recalling the gel classifications, ILGs can be polymeric, colloidal or supramolecular. In the first case, gelation can occur through the polymerisation *in situ* or with the dispersion (swelling) of the polymer in the IL phase. In both cases, the IL is used as the solvent in the gel formation.<sup>102</sup> However, polymers with the IL moiety incorporated in the polymeric structure were also synthesised.<sup>103</sup> Colloidal ILGs are often obtained with silica particles, dispersed in the IL phase. Usually, in this kind of gels, the concentration of the particles is low and does not affect the properties of the IL, such as the conductivity.<sup>104</sup> Often, hydrogen bonds and van der Waals interactions can be established easily in the IL medium. Both spatial organisation and structural characteristics support the supramolecular ILGs formation.<sup>105</sup> In this case, both solvent and gelator can be ILs and the possible applications depend on their structures.<sup>106</sup>

### 3.4 Ionic Liquid Gels applications: a way to improve the Environmental Protection and Remediation

In 2016 in Italy 30 116 605 tons of urban waste were produced. To this amount, the industrial one, 135 100 000 tons, has to be added (data from the Italian Institute for the Environmental Research and Protection – ISPRA). The waste problem and the pollution of the environment are connected. The quantity

---

102. Li, M.; Li, J.; Na, H.; Vlassak, J. J., Mechanical behavior of poly(methyl methacrylate)-based ionogels. *Soft Matter* **2014**, *10* (40), 7993-8000.

103. Briones O, X.; Tapia, R. A.; Campodónico, P. R.; Urzúa, M.; Leiva, Á.; Contreras, R.; González-Navarrete, J., Synthesis and characterization of poly (ionic liquid) derivatives of N-alkyl quaternized poly(4-vinylpyridine). *Reactive and Functional Polymers* **2018**, *124*, 64-71.

104. Ueno, K.; Hata, K.; Katakabe, T.; Kondoh, M.; Watanabe, M., Nanocomposite Ion Gels Based on Silica Nanoparticles and an Ionic Liquid: Ionic Transport, Viscoelastic Properties, and Microstructure. *J. Phys. Chem. B* **2008**, *112* (30), 9013-9019.

105. Shen, X.; Chen, Q.; Zhang, J.; Fu, P., Supramolecular Structures in the Presence of Ionic Liquids. In *Ionic Liquids - Theory, Properties, New Approaches*, Kokorin, A., Ed. IntechOpen: **2011**.

106. (a) Yu, Q.; Wu, Y.; Li, D.; Cai, M.; Zhou, F.; Liu, W., Supramolecular ionogel lubricants with imidazolium-based ionic liquids bearing the urea group as gelator. *J. Colloid Interface Sci.* **2017**, *487*, 130-140, (b) Rizzo, C.; Arrigo, R.; Dintcheva, N. T.; Gallo, G.; Giannici, F.; Noto, R.; Sutura, A.; Vitale, P.; D'Anna, F., Supramolecular Hydro- and Ionogels: A Study of Their Properties and Antibacterial Activity. *Chem. Eur. J.* **2017**, *23* (64), 16297-16311.

of waste increases faster than its recycling or disposal treatments. The consequence is an increase of waste in the environment without any treatment. It is even not rare that disposal of the municipal and industrial wastewaters is directed to sea, lakes or rivers without imposing any chemical and biological control. Indeed, the control of pollution comes from the management of waste. However, ordinary treatments of waste are not a universal solution. Wastewater recycling and purification treatments generate secondary waste. Big amount of waste is due to primary and secondary sludge used for the treatment of the water. However, the problem of waste disposal and recovery is not confined to wastewaters, but can be extended to every single material or substance.

It is necessary to remember that every process generates waste, which includes by-products, energy spent during the process, the reagents required for the treatments, and so on. This implies that a completely cleaned process cannot exist.<sup>107</sup>

Considering that, Chemistry has a twofold responsibility, on one hand the design of new processes which generate less waste, on the other hand, a timely intervention for the environmental remediation.

In this way, ILs can be useful in the field of environmental remediation. Their unique and advantageous properties and the tunable structures permit synthesising and applying ILs to extract, separate and capture pollutants from water, oil or other liquid systems. Moreover, as mentioned before, the possibility of gelling the ILs permits expanding the application for this purpose.

D'Anna and co-workers used ILGs for the adsorption of dyes from wastewaters. Dyes can derive from textile, paper and cosmetic industries and their presence in wastewaters caused pollution due to the persistence in the environment.<sup>108</sup> Diimidazolium ILs with anions deriving from natural resources were used as gelators to obtain ILGs in imidazolium ILs (solvents) and the obtained materials were applied as sorbents for dyes. Figure 15 reports the organic salts used as gelators and the IL solvents used in this study.

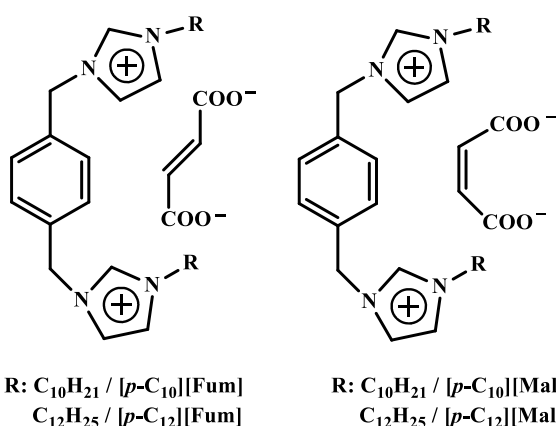
---

107. Sanghi, R.; Singh, V., *Green Chemistry for Environmental Remediation*. Wiley: **2012**.

108. Hassaan, M. A.; Nemr, A. E., Health and Environmental Impacts of Dyes: Mini Review. *American Journal of Environmental Science and Engineering* **2017**, *1* (3).

The ILGs showed a good affinity for Rhodamine B dye. The best sorbent systems were  $[p\text{-C}_{12}][\text{Fum}]/[\text{C}_4\text{C}_1\text{Im}][\text{PF}_6]$  and  $[p\text{-C}_{12}][\text{Fum}]/[\text{C}_4\text{C}_1\text{Im}][\text{NTf}_2]$ , which showed 95% and 97% of removal efficiencies in 6 h of contact. These materials can be also recycled and reused. The  $[p\text{-C}_{12}][\text{Fum}]/[\text{C}_4\text{C}_1\text{Im}][\text{PF}_6]$  was used 20 times without loss of performance.<sup>109</sup>

**Gelators:**



**Solvents:**

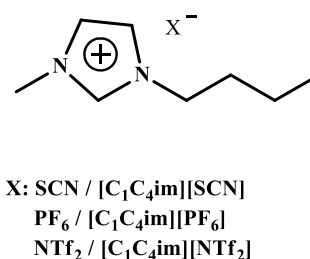


Figure 15 - Gelators and solvents used to obtain ILGs for dyes adsorption.<sup>109</sup>

Das and co-workers synthesised a gelator (Figure 16) which gelled in the hydrophobic  $[\text{C}_1\text{C}_4\text{im}][\text{PF}_6]$ . This ILG adsorbs anionic and cationic dyes (crystal violet and naphthol blue-black) from water. The ILG showed higher efficiency than the organogel obtained with toluene using the same gelator, or the neat IL alone, adsorbing more than 90% of the cationic and the anionic dyes in 8 and 20 h, respectively.<sup>110</sup>

These studies highlight the advantage of the ionic character of the ILGs in the dyes adsorption.

109. Marullo, S.; Rizzo, C.; Dintcheva, N. T.; Giannici, F.; D'Anna, F., Ionic liquids gels: Soft materials for environmental remediation. *J. Colloid Interface Sci.* **2018**, *517*, 182-193.

110. Dutta, S.; Das, D.; Dasgupta, A.; Das, P. K., Amino Acid Based Low-Molecular-Weight Ionogels as Efficient Dye-Adsorbing Agents and Templates for the Synthesis of TiO<sub>2</sub> Nanoparticles. *Chemistry - A European Journal* **2010**, *16* (5), 1493-1505.

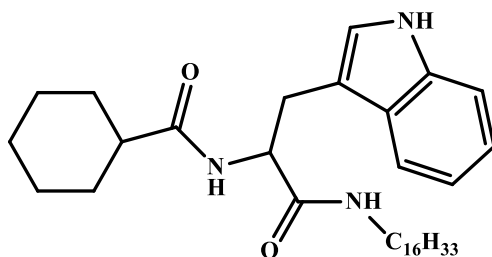


Figure 16 - Gelator used to obtain ILGs for dyes adsorption.<sup>110</sup>

Pang *et al.* studied a new method to determine the presence of organophosphate esters in water.<sup>111</sup> Organophosphate esters (OPs) are employed as flame retardants (chlorinated OPs), plasticizers and lubricants (non-halogenated OPs).<sup>112</sup> These substances have been classified as pollutants and their traces can be found in municipal waters, aquatic and atmospheric ecosystems.<sup>113</sup> At present OPs are considered as cancers-causing and mutagens.<sup>114</sup> To investigate the presence of OPs in water, an ionogel SPME fibres, (Solid Phase Microextraction) based on the  $[C_1C_{16}im][NTf_2]$  was obtained by sol-gel technology. The method and the ILG applied to determine the OPs in wastewater proved both accurate and with a low limit of detection.

The examples reported until now highlight the possibility to apply ILGs to remediate the undesirable actions against the ecosystem and the environment. However, as mentioned before, scientific research has to find new processes to prevent pollution. The application of ILGs to overcome such issues is addressed in this Thesis. The ILGs which will be fully described and characterised in the next paragraphs of this Chapter, have been applied for the desulfurisation of fuels,

111. Pang, L.; Pang, R.; Ge, L.; Zheng, L.; Zhao, J.; Zhang, H., Trace determination of organophosphate esters in environmental water samples with an ionogel-based nanoconfined ionic liquid fiber coating for solid-phase microextraction with gas chromatography and flame photometric detection. *J. Sep. Sci.* **2016**, 39 (22), 4415-4421.

112. Andresen, J. A.; Grundmann, A.; Bester, K., Organophosphorus flame retardants and plasticisers in surface waters. *Sci. Total Environ.* **2004**, 332 (1), 155-166.

113. Lai, S.; Xie, Z.; Song, T.; Tang, J.; Zhang, Y.; Mi, W.; Peng, J.; Zhao, Y.; Zou, S.; Ebinghaus, R., Occurrence and dry deposition of organophosphate esters in atmospheric particles over the northern South China Sea. *Chemosphere* **2015**, 127, 195-200.

114. Lin, K., Joint acute toxicity of tributyl phosphate and triphenyl phosphate to *Daphnia magna*. *Environ. Chem. Lett.* **2009**, 7 (4), 309-312.

in particular, to adsorb the more recalcitrant sulfur compounds (thiophene (T), benzothiophene (BT) and dibenzothiophene (DBT)) *via* extraction processes.<sup>115</sup>

Sulfur compounds in fuels, especially in diesel, determine an important and serious contamination of air and environment. The combination of sulfur with water forms acids that contribute to acid rains, that are corrosive and destructive for the environment. During fuel combustion, sulfur compounds form oxyacids; also, the sulfur compounds released in the air can negatively affect the human respiratory apparatus.<sup>116</sup>

Another negative aspect due to these contaminants is the detrimental effects on the vehicle engines and the fuel cells. The consequences of these effects justify the regulation which fixes sulfur concentration in fuel at 10 ppm.<sup>117</sup>

To this aim, supramolecular gels have never been explored. The conventional approach to decrease the level of sulfur is the hydrodesulfurisation generating H<sub>2</sub>S. Although the process can be efficient, the formation of sulfydric acid remains a problem, being this a component of acid rains. Moreover, this method loses efficiency in the presence of aromatic sulfur compounds. Several other methods have been studied in order to find an efficient alternative, like oxidative, adsorptive and extractive desulfurisation.<sup>118</sup> Sorbents materials as carbon beads,<sup>119</sup> graphene oxides,<sup>120</sup> functionalised polymers<sup>121</sup> and metal oxides<sup>122</sup> have been

---

115. Billeci, F.; D'Anna, F.; Gunaratne, H. Q. N.; Plechkova, N. V.; Seddon, K. R., "Sweet" ionic liquid gels: materials for sweetening of fuels. *Green Chem.* **2018**, *20* (18), 4260-4276.

116. (a) Chandra Srivastava, V., An evaluation of desulfurization technologies for sulfur removal from liquid fuels. *RSC Adv.* **2012**, *2* (3), 759-783, (b) Maricq, M. M.; Chase, R. E.; Xu, N.; Laing, P. M., The Effects of the Catalytic Converter and Fuel Sulfur Level on Motor Vehicle Particulate Matter Emissions: Light Duty Diesel Vehicles. *Environ. Sci. Technol.* **2002**, *36* (2), 283-289, (c) Kampa, M.; Castanas, E., Human health effects of air pollution. *Environ. Pollut.* **2008**, *151* (2), 362-367.

117. Dharaskar, S. A.; Wasewar, K. L.; Varma, M. N.; Shende, D. Z.; Tadi, K. K.; Yoo, C. K., Synthesis, characterization, and application of novel trihexyl tetradecyl phosphonium bis (2,4,4-trimethylpentyl) phosphinate for extractive desulfurization of liquid fuel. *Fuel Process. Technol.* **2014**, *123*, 1-10.

118. (a) Alipoor, Z.; Behrouzifar, A.; Rowshanzamir, S.; Bazmi, M., Electrooxidative Desulfurization of a Thiophene-Containing Model Fuel Using a Square Wave Potentiometry Technique. *Energy Fuels* **2015**, *29* (5), 3292-3301, (b) Hernández-Maldonado, A. J.; Yang, R. T., Desulfurization of Diesel Fuels by Adsorption via  $\pi$ -Complexation with Vapor-Phase Exchanged Cu(I)-Y Zeolites. *J. Am. Chem. Soc.* **2004**, *126* (4), 992-993.

119. Prajapati, Y. N.; Verma, N., Adsorptive desulfurization of diesel oil using nickel nanoparticle-doped activated carbon beads with/without carbon nanofibers: Effects of adsorbate size and adsorbent texture. *Fuel* **2017**, *189*, 186-194.

120. Abdi, G.; Ashokkumar, M.; Alizadeh, A., Ultrasound-assisted oxidative-adsorptive desulfurization using highly acidic graphene oxide as a catalyst-adsorbent. *Ibid.* **210**, 639-645.

used. Among these substances and materials, also ILs have been investigated to extract sulfur compounds from fuels by liquid-liquid extraction.

Zolfigol and co-workers reported the extractive study using phosphonium ILs (Figure 17).

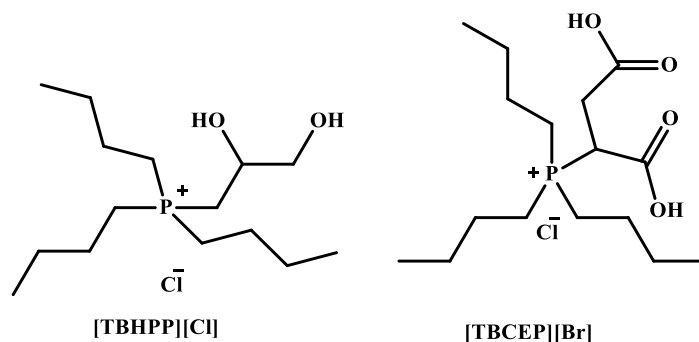


Figure 17 - Structures of the phosphonium ILs to extract sulfur compounds.<sup>123</sup>

After 30 minutes of contact with an heptane solution containing DBT, the extraction efficiency is about 59% for both [TBHPP][Cl] and [TBCEP][Br] ILs.<sup>123</sup>

Chen and co-workers synthesised and applied dicyanamide-based IL, [C<sub>1</sub>C<sub>2</sub>im][N(CN)<sub>2</sub>], to extract T and DBT from solutions which mimic gasoline and diesel. The first solution was prepared to dissolve thiophene in a mixture of *n*-hexane and toluene (85% and 15%). The diesel model was prepared to dissolve dibenzothiophene in *n*-hexane. The extraction efficiency was 41.7% and 56.5% for T and DBT after 20 min of contact. However, interesting results were collected about the extraction rate that reached almost the equilibrium after about 5 min. The IL was reused for at least 5 times with a removal efficiency close to 97%.<sup>124</sup>

121. Wang, J.; Wei, J., Selective and simultaneous removal of dibenzothiophene and 4-methyldibenzothiophene using double-template molecularly imprinted polymers on the surface of magnetic mesoporous silica. *J. Mater. Chem. A* **2017**, 5 (9), 4651-4659.

122. Iravani, A. A.; Gunda, K.; Ng, F. T. T., Adsorptive removal of refractory sulfur compounds by tantalum oxide modified activated carbons. *AIChE J.* **2017**, 63 (11), 5044-5053.

123. Moghadam, F. R.; Azizian, S.; Bayat, M.; Yarie, M.; Kianpour, E.; Zolfigol, M. A., Extractive desulfurization of liquid fuel by using a green, neutral and task specific phosphonium ionic liquid with glyceryl moiety: A joint experimental and computational study. *Fuel* **2017**, 208, 214-222.

124. Yu, G.; Li, X.; Liu, X.; Asumana, C.; Chen, X., Deep Desulfurization of Fuel Oils Using Low-Viscosity 1-Ethyl-3-methylimidazolium Dicyanamide Ionic Liquid. *Ind. Eng. Chem. Res.* **2011**, 50 (4), 2236-2244.



Even if ILs can be recycled and reused with multiple extractions, with high efficiency, the reason to develop better desulfurisation methods can be ascribed to some contamination of fuel with the extractant. Indeed, when a liquid/liquid extraction is operated with the ILs, a quantity of the fuel contaminates the extractive solvents and *vice versa*.

The amount of ILs involved in the mutual solubility depends on its structure; long alkyl chains can improve the extraction ability, but, at the same time, increase the mutual solubility of the ILs and fuel.<sup>125</sup>

To overcome the above issue, the use of ILGs may represent a solution as a consequence of the solvent entrapment in the gelatinous network.

### 3.5 Gelation tests

In order to achieve the desulfurisation aim, the gelling ability of the gluconate ILs were tested (Figure 18).

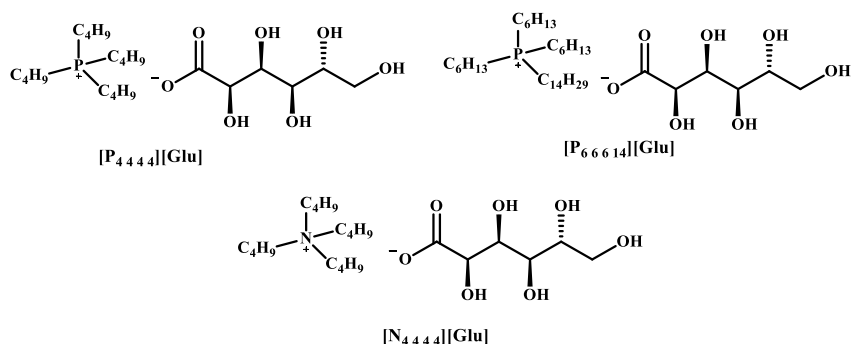


Figure 18 - Structures of gelators.

The phosphonium ILs and the ammonium salt were dissolved in several solvents, including organic solvents, oils, ILs and water, differing for polarity and viscosity. Table 14 reports the results of the gelation tests, which were performed

125. (a) Kianpour, E.; Azizian, S.; Yarie, M.; Zolfigol, M. A.; Bayat, M., A task-specific phosphonium ionic liquid as an efficient extractant for green desulfurization of liquid fuel: An experimental and computational study. *Chem. Eng. J. (Lausanne)* **2016**, 295, 500-508. (b) Ferreira, A. R.; Freire, M. G.; Ribeiro, J. C.; Lopes, F. M.; Crespo, J. G.; Coutinho, J. A. P., Ionic liquids for thiols desulfurization: Experimental liquid-liquid equilibrium and COSMO-RS description. *Fuel* **2014**, 128, 314-329.

using the heating/cooling method. Firstly, the gelator and the solvent were weighed in a vial and heated until a clear solution was obtained. Then, it was kept at 4 °C overnight. The temperature for the heating step changed depending on the nature of the solvent and was about 10 °C lower than its boiling point.

The tube inversion test (*vide supra*) was adopted as the first assessment of gel formation.

The organic salts were soluble at room temperature in protic polar solvents, such as alcohols and water. On the other hand, they were also soluble in several hot oils such as olive oil, sweet corn oil and engine oil. Conversely, they were insoluble in mixed seed oil.  $[\text{P}_{4444}][\text{NTf}_2]$  was soluble in silicon oil and paraffin oil, whereas  $[\text{P}_{66614}][\text{NTf}_2]$  was dissolved in diesel. Finally, as for low polar organic solvents, salts proved insoluble in hot cyclohexane.

The above results for the conventional solvents and the more common oils induced us to verify the possibility to obtain ILGs fully composed by ILs. The exclusion of conventional solvents was a good chance to form completely new materials, which take advantage from the ILs and do not need to refill the solvent after several uses.

Taking into account all the positive implications due to the use of ILs both as gelator and solvent, their behaviour in ILs was tested.

However, the essence of this Ph.D. Project has to be considered as the base on which all the experimental work is built. The consequence to this consideration is the choice of ILs used as gelation solvents. Indeed, we paid attention to the environmental impact of solvents used, so aliphatic rather than aromatic ILs were favoured. In particular  $[\text{N}_{2224}][\text{NTf}_2]$ ,  $[\text{N}_{1444}][\text{NTf}_2]$ ,  $[\text{C}_1\text{C}_4\text{pip}][\text{NTf}_2]$  and  $[\text{C}_1\text{C}_4\text{pyrr}][\text{NTf}_2]$  were chosen to carry out the study.

$[\text{P}_{66614}][\text{Glu}]$  showed the best gelling ability, giving gels in all ILs tested. Differently,  $[\text{P}_{4444}][\text{Glu}]$  gave gel phases only in ammonium-based ILs, whereas  $[\text{N}_{4444}][\text{Glu}]$  gelled only in  $[\text{N}_{1444}][\text{NTf}_2]$ . This different behaviour can be related to the nature of the organic salts tested. The phosphonium salts, which are ILs, showed stronger interactions with the ILs used as solvent, being able to build the network to form the gel phase.

**Table 14 - Gelation tests performed in conventional solvents for the gelators used (S= soluble after heating; I= insoluble; SC= soluble without heating; PG= gel like precipitate). \*: wt. =  $\frac{g_{gelator}}{g_{solution}}$ .**

Solvent	C / % wt.*	[P <sub>66614</sub> ][Glu]	[P <sub>4444</sub> ][Glu]	[N <sub>4444</sub> ][Glu]
methanol	1 - 3	SC	SC	SC
ethanol	1 - 3	SC	SC	SC
1-propanol	1 - 3	SC	SC	SC
2-propanol	1 - 3	SC	SC	SC
butanol	1 - 3	SC	SC	SC
pentanol	1 - 3	SC	SC	SC
hexanol	1 - 3	SC	SC	SC
octanol	1 - 3	SC	SC	SC
distilled water	1 - 3	SC	SC	SC
sea water	1 - 3	SC	SC	SC
1,3-propanediol	1 - 3	SC	SC	SC
triethylene glycol	1 - 3	SC	SC	SC
n-hexane	1 - 3	I	I	I
n-heptane	1	I	I	I
cyclohexane	1	SC	SC	SC
petroleum ether	1	SC	I	I
R-limonene	0.5 - 1	I	I	I
ethyl lactate	1 - 3	S	S	S
olive oil	1 - 5	S	S	S
sweet corn oil	1 - 5	S	S	S
mixed seeds oil	1 - 5	I	I	I
silicon oil	1 - 5	I	S	I
paraffin oil	1 - 5	PG	S	I
engine oil	1 - 5	S	S	S
diesel	1 - 5	S	I	I

Seven gels were obtained and, critical gelation concentrations (CGC), *i.e.* the minimum amount of gelator necessary to obtain a gel phase, are reported in Table 15. The gels appear homogeneously opaque and white. They, show thermo-reversibility and are stable for a long time (at least four months) at room temperature.

**Table 15 – ILGs obtained and relevant CGCs. \*: wt. =  $\frac{g_{gelator}}{g_{solution}}$ .**

IL	Gelator	CGC % wt.*
[N <sub>2 2 2 4</sub> ][NTf <sub>2</sub> ]	[P <sub>6 6 6 14</sub> ][Glu]	3.0
	[P <sub>4 4 4 4</sub> ][Glu]	5.0
[N <sub>1 4 4 4</sub> ][NTf <sub>2</sub> ]	[P <sub>4 4 4 4</sub> ][Glu]	5.5
	[N <sub>4 4 4 4</sub> ][Glu]	5.0
[C <sub>1</sub> C <sub>4</sub> pip][NTf <sub>2</sub> ]	[P <sub>6 6 6 14</sub> ][Glu]	5.5
	[P <sub>6 6 6 14</sub> ][Glu]	5.0
[C <sub>1</sub> C <sub>4</sub> pyrr][NTf <sub>2</sub> ]	[P <sub>6 6 6 14</sub> ][Glu]	5.0

All the CGC values fell in the range 2-5.5 % wt. The best gelator, [P<sub>6 6 6 14</sub>][Glu], shows an increase of the CGC going from the [N<sub>2 2 2 4</sub>][NTf<sub>2</sub>] to the [N<sub>1 4 4 4</sub>][NTf<sub>2</sub>], according to the increase on the alkyl chain length borne on the IL solvent cation. Differently, the values for ILs having cyclic cations (pyrrolidinium and piridinium) are the same. The change of the cation head going from phosphonium ([P<sub>4 4 4 4</sub>][Glu]) to ammonium ([N<sub>4 4 4 4</sub>][Glu]) slightly affects the gelling ability, as accounted for by the increase in CGC. In general, the lowest CGC value was found for the system [P<sub>6 6 6 14</sub>][Glu]/[N<sub>2 2 2 4</sub>][NTf<sub>2</sub>].

### 3.6 Gel characterisations

The determination of CGC value is the first step to characterise a gel, which comprises several investigations. Table 16 reports the  $T_{gel}$ s for all the gels

obtained, both at the CGC value and at 6.5 % wt.. The  $T_{\text{gel}}$  corresponds to the temperature of the melting of the gel phase.

In particular the method applied here to obtain  $T_{\text{gel}}$  is the “lead-ball method”,<sup>126</sup> which consists in placing a lead-ball (weighting less than 100 mg) on the top of the gel phase. The system is heated, at a constant rate, and  $T_{\text{gel}}$  corresponds to the temperature at which the lead-ball reaches the bottom of the vial passing through the gel phase.

**Table 16 - CGC and  $T_{\text{gel-CGC}}$  corresponding to gel phases obtained.  $T_{\text{gel-6.5%wt.}}$ , sol-gel temperature ( $T_{\text{c-6.5%wt.}}$ ), gel-sol and sol-gel enthalpy ( $\Delta H_{\text{m}}$  and  $\Delta H_{\text{c}}$ ) determined for gel phases at 6.5 % wt. by DSC measurements (<sup>a</sup>: Determined by the lead-ball method.  $T_{\text{gel}}$  were reproducible within  $\pm 1$  °C. <sup>b</sup>: Determined by DSC). \*: wt =  $\frac{g_{\text{gelator}}}{g_{\text{solution}}}$ .**

Gel	CGC % wt.*	$T_{\text{gel-CGC}}$ °C <sup>a</sup>	$T_{\text{gel-6.5%wt.}}$ °C	$\Delta H_{\text{m}}$ Jg <sup>-1 b</sup>	$T_{\text{c-6.5%wt.}}$ °C <sup>b</sup>	$\Delta H_{\text{c}}$ Jg <sup>-1 b</sup>
[P <sub>66614</sub> ][Glu]/[N <sub>2224</sub> ][NTf <sub>2</sub> ]	3.0	29	25 <sup>a</sup> 30.1 <sup>b</sup>	1.72	3.51	1.43
[P <sub>4444</sub> ][Glu]/[N <sub>2224</sub> ][NTf <sub>2</sub> ]	5.0	21	22 <sup>a</sup>			
[P <sub>4444</sub> ][Glu]/[N <sub>1444</sub> ][NTf <sub>2</sub> ]	2.0	29	26 <sup>a</sup> 25.1 <sup>b</sup>	44.60		
[N <sub>4444</sub> ][Glu]/[N <sub>1444</sub> ][NTf <sub>2</sub> ]	5.0	20	21 <sup>a</sup> 13.7 <sup>b</sup>	22.10		
[P <sub>66614</sub> ][Glu]/[N <sub>1444</sub> ][NTf <sub>2</sub> ]	5.5	23	26 <sup>a</sup> 18.2 <sup>b</sup>	3.49	-5.76	0.94
[P <sub>66614</sub> ][Glu]/[C <sub>1</sub> C <sub>4</sub> pip][NTf <sub>2</sub> ]	5.0	25	27 <sup>a</sup> 20.9 <sup>b</sup>	1.41		
[P <sub>66614</sub> ][Glu]/[C <sub>1</sub> C <sub>4</sub> pyrr][NTf <sub>2</sub> ]	5.0	25	28 <sup>a</sup> 24.6 <sup>b</sup>	2.46		

The  $T_{\text{gel}}$  values, determined at CGC ( $T_{\text{gel-CGC}}$ ) change between 20 and 29 °C. Table 16 permits comparing the trend of CGC and  $T_{\text{gel-CGC}}$ , showing an inverse correlation between the two parameters both for the [P<sub>66614</sub>][Glu] and the [P<sub>4444</sub>][Glu]; at higher CGC correspond lower  $T_{\text{gel-CGC}}$ .

However, a dependence on the alkyl chain length of IL solvents and the one of IL gelators can be detected. Indeed, among the IL solvents used in this work, long alkyl chain on the gelator ([P<sub>66614</sub>][Glu]) assembled stronger gel phase in the IL

126. Takahashi, A.; Sakai, M.; Kato, T., Melting Temperature of Thermally Reversible Gel. VI. Effect of Branching on the Sol–Gel Transition of Polyethylene Gels. *Polym. J.* **1980**, *12*, 335.

carrying the shorter alkyl chains ( $[N_{2224}][NTf_2]$ ). Conversely, the stronger ILG for the  $[P_{4444}][Glu]$  gelator is obtained in the IL solvent which carries the butyl chains ( $[N_{1444}][NTf_2]$ ). The change of the cation head from ammonium to phosphonium gelator ( $[N_{4444}]$ ,  $[P_{4444}]$ ) shows an increase in the CGC values in correspondence of a decrease in the  $T_{gel-CGC}$  ones.

To homogeneously compare gel properties, a common concentration of 6.5% wt. was chosen and this was used both for characterisation and application of gel phases. This concentration allows having gel phases from all gelators.

In this case,  $T_{gel}$  determination was carried out using both DSC and the lead-ball method. These two methods observe different situations: in the case of the lead-ball method, the initial loss of consistency of the gelatinous network was observed, whereas in the case of DSC investigation, it allowed detecting complete breakdown of the gel.

The comparison between the  $T_{gel}$ s collected at the CGC (% wt.) and at 6.5 % wt. shows a dependence on the concentration. Generally, the increase in the gelator concentration induces only small increases in the  $T_{gel}$  values. However, this is not the case for the most stable gels, the  $[P_{66614}][Glu]/[N_{2224}][NTf_2]$  and the  $[P_{4444}][Glu]/[N_{1444}][NTf_2]$ , for which the raising of the concentration caused a  $T_{gel}$  decrease of 4 and 3 °C respectively.

In the case of DSC measurements, the  $T_{gel-6.5\%wt.}$ s show values lower than the ones detected with the lead-ball method. The only exception is the  $[P_{66614}][Glu]/[N_{2224}][NTf_2]$ , for which the DSC  $T_{gel}$  is higher of 5 °C than the lead-ball one. On the other hand, in the case of  $[P_{66614}][Glu]/[N_{2224}][NTf_2]$  and  $[P_{66614}][Glu]/[N_{1444}][NTf_2]$ , during the cooling cycles, gel phase formation was observed. Corresponding temperature of gel formation ( $T_c$ ) are different from the melting ones, due to the hysteresis phenomena. In general, the trend detected for  $T_{gel-6.5\%wt.}$ , perfectly recalls the ones observed for values at CGC.

Considering the common solvent,  $[N_{1444}][NTf_2]$ , to all three gelators, the transition temperature decreases following the trend  $[P_{4444}][Glu] > [P_{66614}][Glu] > [N_{4444}][Glu]$ . Finally, DSC measurements account for an effect deriving from the geometry of the IL cation, as demonstrated by the increase in

$T_{\text{gel-6.5\%wt.}}$  on going from  $[\text{P}_{66614}][\text{Glu}]/[\text{C}_1\text{C}_4\text{pip}][\text{NTf}_2]$  to  $[\text{P}_{66614}][\text{Glu}]/[\text{C}_1\text{C}_4\text{pyrr}][\text{NTf}_2]$ .

The morphology of gel phases was analysed using polarized optical microscopy (POM). For each gel, the heating process was conducted until the temperature reached 90 °C (the temperature used to form the gel phase) and, obviously, at a temperature so higher than the melting temperature, an isotropic solution was obtained in all cases. However, as all materials were thermoreversible, aggregates were detected during the cooling cycle down to room temperature.

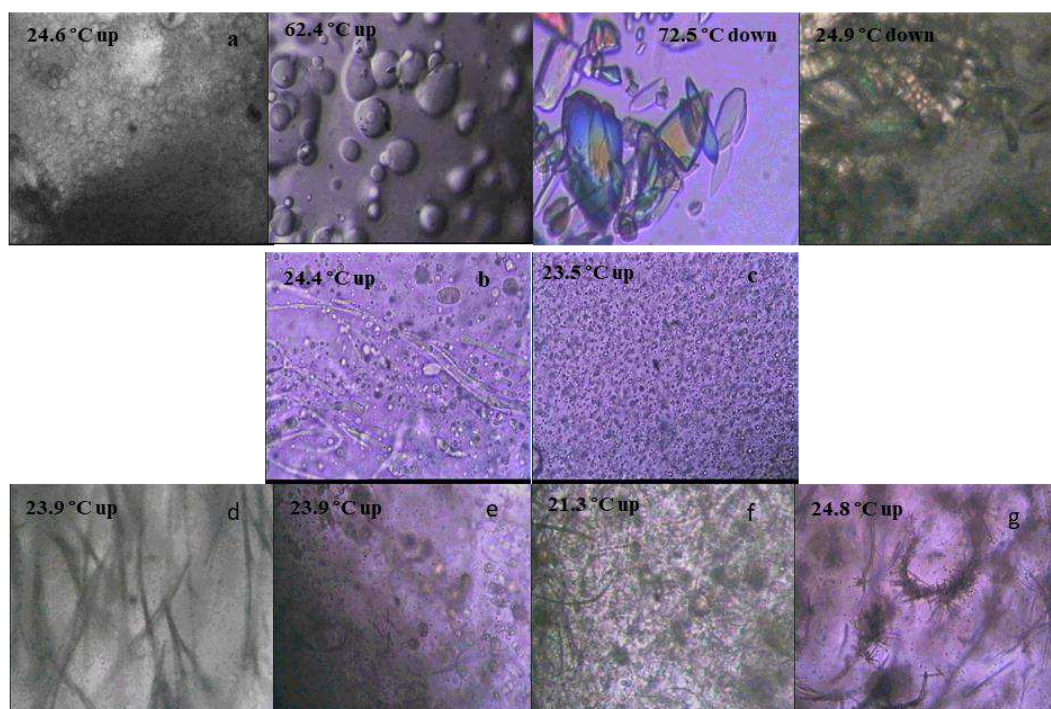


Figure 19 - POM images of ILGs at 6.5 % wt. of gelator for: (a)  $[\text{N}_{4444}][\text{Glu}]/[\text{N}_{1444}][\text{NTf}_2]$  during the heating process until the isotropic solution, then the cooling process until formation of aggregates; (b)  $[\text{P}_{4444}][\text{Glu}]/[\text{N}_{1444}][\text{NTf}_2]$  on heating process; (c)  $[\text{P}_{4444}][\text{Glu}]/[\text{N}_{1222}][\text{NTf}_2]$  on heating process; (d)  $[\text{P}_{66614}][\text{Glu}]/[\text{N}_{1444}][\text{NTf}_2]$  on heating process (e)  $[\text{P}_{66614}][\text{Glu}]/[\text{N}_{2224}][\text{NTf}_2]$  on heating process; (f)  $[\text{P}_{66614}][\text{Glu}]/[\text{C}_1\text{C}_4\text{pip}][\text{NTf}_2]$  on heating process; (g)  $[\text{P}_{66614}][\text{Glu}]/[\text{C}_1\text{C}_4\text{pyrr}][\text{NTf}_2]$  on heating process.

Figure 19 reports the POM pictures for all the gels. In general, textures resulted more compact for ammonium gels than phosphonium ones. Indeed, a thick texture (19-a) was observed for  $[\text{N}_{4444}][\text{NTf}_2]/[\text{N}_{1444}][\text{Glu}]$ , whereas fibrous texture

were obtained for  $[P_{4444}][Glu]/[N_{1444}][NTf_2]$  and  $[P_{66614}][Glu]/[N_{1444}][NTf_2]$  (19-b, 19-d). Furthermore, for phosphonium gels, fibres were defined for  $[P_{66614}]$  and only sketched for  $[P_{4444}]$  (Figure 19-b and 19-d). Interestingly, the cooling process for the  $[N_{4444}][Glu]/[N_{1444}][NTf_2]$  gel was characterised by the formation of coloured crystals at 35.7 °C (19-a).

The comparison between the morphology in the different ammonium IL solvents,  $[N_{2224}][NTf_2]$  and  $[N_{1444}][NTf_2]$ , shows a significant change in texture for the phosphonium ILGs. Indeed, the morphology is characterised by thick texture in the less viscous IL (19-c, 19-e) and fibrous texture in the more viscous IL (19-b, 19-d). Finally, the morphology is affected also by the cation structure of the IL solvent. Indeed, the comparison among the ILGs obtained for the  $[P_{66614}][Glu]$  in the different ILs shows a mixed texture, characterised by the presence of both fibrous and spherulitic motifs for the cyclic IL cations,  $[C_1C_4pip]^+$  and  $[C_1C_4pyrr]^+$  (19-f, 19-g). However, also in this case, the more fibrous texture is detected for the  $[P_{66614}][Glu]/[C_1C_4pyrr][NTf_2]$  gel.

The ILGs at 6.5 % wt. were characterised also for their self-repairing ability, *i.e.* their ability to reform spontaneously after the action of an external stimulus. In particular, gel phases were subjected to magnetic stirring and ultrasound irradiation, to have information about their thixotropic and sonotropic behaviour.

The thixotropic behaviour is a more common feature for organo-, hydro- and IL gels than the sonotropic one. However, both can be related to the ILGs in the literature.<sup>127,128,129</sup>

Weiss and co-workers reported the unusual and good response of organogel to the thixotropic stimulus. They observed that LMOG-based (low molecular-mass

---

127. Yu, X.; Chen, L.; Zhang, M.; Yi, T., Low-molecular-mass gels responding to ultrasound and mechanical stress: towards self-healing materials. *Chem. Soc. Rev.* **2014**, *43* (15), 5346-5371.

128. Rizzo, C.; Arrigo, R.; Dintcheva, N. T.; Gallo, G.; Giannici, F.; Noto, R.; Sutera, A.; Vitale, P.; D'Anna, F., Supramolecular Hydro- and Ionogels: A Study of Their Properties and Antibacterial Activity. *Chem. Eur. J.* **2017**, *23* (64), 16297-16311.

129. Rizzo, C.; Arcudi, F.; Đorđević, L.; Dintcheva, N. T.; Noto, R.; D'Anna, F.; Prato, M., Nitrogen-Doped Carbon Nanodots-Ionogels: Preparation, Characterization, and Radical Scavenging Activity. *ACS Nano* **2018**, *12* (2), 1296-1305.



organic gelators) organogels were able to restore the viscoelastic properties without the necessity to previously heat the gel to obtain the sol phase.<sup>130</sup>

Shen *et al.*, on the other hand, took advantage from the sonotropic response of nanogels. Indeed, their nanogel drug-delivery systems were stimulated by ultrasound to release the drug encapsulated inside the gel phase.<sup>131</sup>

Table 17 reports the results obtained. Considering the thixotropic investigation, with the only exception of the  $[P_{4444}][Glu]/[N_{1444}][NTf_2]$ , all the ILGs are able to reform after mechanical disruption of the gel phase. However, the comparison among the  $T_{gel}$ s obtained before and after the mechanical stimulus for the  $[P_{66614}][Glu]$ , shows that the reformed gel phases are less thermally stable.

As far as sonotropic behaviour is concerned, with the only exceptions of  $[P_{66614}][Glu]/[N_{2224}][NTf_2]$  and the  $[P_{66614}][Glu]/[C_1C_4pyrr][NTf_2]$  that are not affected by the ultrasound irradiation, and  $[P_{4444}][Glu]/[N_{2224}][NTf_2]$  that is not sonotropic, in all other cases, gel phases reformed after the action of the stimulus, demonstrating  $T_{gel}$ s comparable to the ones determined before the ultrasound action.

---

130. Mallia, V. A.; George, M.; Blair, D. L.; Weiss, R. G., Robust Organogels from Nitrogen-Containing Derivatives of (R)-12-Hydroxystearic Acid as Gelators: Comparisons with Gels from Stearic Acid Derivatives. *Langmuir* **2009**, *25* (15), 8615-8625.

131. Shen, N.; Lei, B.; Wang, Y.; Xu, S.; Liu, H., Redox/ultrasound dual stimuli-responsive nanogel for precisely controllable drug release. *New J. Chem.* **2018**, *42* (12), 9472-9481.

**Table 17 - Thixotropic and sonotropic behaviour of ILGs at 6.5% wt. (\*= after 5 min of sonication, the gel phase persist.; / =the gel phase is too soft to detect the  $T_{gel}$ ).**

ILG	$T_{gel}$	Thixotropic	$T_{gel-tix}$	Sonotropic	$T_{gel-son}$
[P <sub>6 6 6 14</sub> ][Glu]/ [N <sub>2 2 2 4</sub> ][NTf <sub>2</sub> ]	25	Yes	/	Stable*	26
[P <sub>4 4 4 4</sub> ][Glu]/ [N <sub>2 2 2 4</sub> ][NTf <sub>2</sub> ]	22	Yes	25	No	
[P <sub>6 6 6 14</sub> ][Glu]/ [N <sub>1 4 4 4</sub> ][NTf <sub>2</sub> ]	26	Yes	24	Yes	28
[P <sub>4 4 4 4</sub> ][Glu]/ [N <sub>1 4 4 4</sub> ][NTf <sub>2</sub> ]	26	No		Yes	27
[N <sub>4 4 4 4</sub> ][Glu]/ [N <sub>1 4 4 4</sub> ][NTf <sub>2</sub> ]	21	Yes	20	Yes	19
[P <sub>6 6 6 14</sub> ][Glu]/ [C <sub>1</sub> C <sub>4</sub> pip][NTf <sub>2</sub> ]	27	Yes	23	Yes	26
[P <sub>6 6 6 14</sub> ][Glu]/ [C <sub>1</sub> C <sub>4</sub> pyrr][NTf <sub>2</sub> ]	28	Yes	23	Stable*	28

In the introduction of this Chapter, it has been highlighted how the definition of a gel was related to its rheological and thermodynamic properties.

The latter were already shown in Table 16, while the rheological investigation was performed with a thermo-controlled rheometer. The first investigation was the strain sweep measurements, in which the strain applied to the gel was increased constantly at a fixed frequency (1 Hz).  $G'$  was higher than  $G''$  at lower values of strain, indicating solid-like behaviour and the increasing of the strain was coupled with a drop of the storage modulus, which crossed the loss modulus at a value of  $\gamma$  called the crossover point. This change of the gel moduli determined by  $G'' > G'$ , is related to a liquid-like behaviour. This visco-elastic trend usually is the “typical” behaviour to define a gel.<sup>132</sup>

However, not all the gels obtained were rheologically characterised. Unfortunately, the [P<sub>6 6 6 14</sub>][Glu]/[N<sub>2 2 2 4</sub>][NTf<sub>2</sub>], [P<sub>6 6 6 14</sub>][Glu]/[C<sub>1</sub>C<sub>4</sub>pyrr][NTf<sub>2</sub>] and [P<sub>6 6 6 14</sub>][Glu]/[C<sub>1</sub>C<sub>4</sub>pip][NTf<sub>2</sub>] were too soft and collapsed before obtaining reliable data.

132. Garai, A.; Nandi, A. K., Rheology of ( $\pm$ )-camphor-10-sulfonic acid doped polyaniline-m-cresol conducting gel nanocomposites. *Journal of Polymer Science Part B: Polymer Physics* **2008**, 46 (1), 28-40.

Figure 20 reports the strain sweep experiments for  $[P_{4444}][Glu]/[N_{2224}][NTf_2]$  and  $[P_{66614}][Glu]/[N_{1444}][NTf_2]$ , as representative examples.

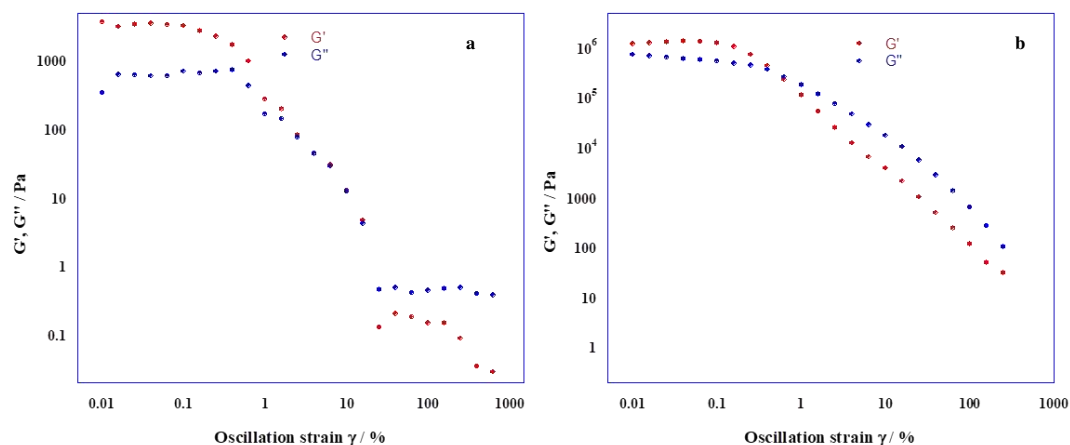


**Figure 20** -Strain sweep measurements at  $f = 1\text{Hz}$  for: a)  $[P_{4444}][Glu]/[N_{2224}][NTf_2]$ ; b)  $[P_{66614}][Glu]/[N_{1444}][NTf_2]$ .

As mentioned before, the crossover point is a parameter that provides information about the strength of the gel under study; it represents the level of stress needed to detect the flow of materials. Consequently, an increase in gel strength induces a corresponding increase in  $\gamma$  values at crossover point. Table 18 reports the values obtained for the gels used in this Thesis.

**Table 18** - Yield strain at crossover point ( $\gamma$ ) values determined at 1Hz frequency and 25 °C for ILGs at 6.5% wt.. Error limits are based on an average of three different measurements.

ILGs	Yield Strain at crossover point $\gamma$ (%)
$[N_{4444}][Glu]/[N_{1444}][NTf_2]$	$0.40 \pm 0.01$
$[P_{4444}][Glu]/[N_{1444}][NTf_2]$	$0.37 \pm 0.02$
$[P_{66614}][Glu]/[N_{1444}][NTf_2]$	$25.3 \pm 0.1$
$[P_{4444}][Glu]/[N_{2224}][NTf_2]$	$2.46 \pm 0.01$

The results reported in Table 18 permit analysing the mechanical properties of the gels related to nature of the gelators and the solvents used. Indeed, considering the gels in the  $[N_{1444}][NTf_2]$  solvent,  $\gamma$  follows the trend:  $[N_{4444}][Glu] \sim [P_{4444}][Glu] \ll [P_{66614}][Glu]$ . This trend does not follow any correlation with the nature of the cation. However, a stronger effect can connect the lengthening of the

alkyl chains with the strength of the gel, as accounted for by the increase in  $\gamma$  values on going from  $[\mathbf{P}_{4444}][\mathbf{Glu}]/[\mathbf{N}_{1444}][\mathbf{NTf}_2]$  to  $[\mathbf{P}_{66614}][\mathbf{Glu}]/[\mathbf{N}_{1444}][\mathbf{NTf}_2]$ .

The comparison between the  $[\mathbf{P}_{4444}][\mathbf{Glu}]/[\mathbf{N}_{1444}][\mathbf{NTf}_2]$  and the  $[\mathbf{P}_{4444}][\mathbf{Glu}]/[\mathbf{N}_{2224}][\mathbf{NTf}_2]$ , indicates the role of the IL solvent played in the rheological properties that the gels. In this case, the  $\gamma$  increases with the decrease in IL viscosity ( $\eta = 104.1$  cP for  $[\mathbf{N}_{2224}][\mathbf{NTf}_2]$  and 538.9 cP for  $[\mathbf{N}_{1444}][\mathbf{NTf}_2]$ ). Moreover, gelator being the same,  $[\mathbf{P}_{4444}][\mathbf{Glu}]$ , the different response to the increase in strain can be related to the different morphology, such as spherulitic and thick texture in the case of  $[\mathbf{P}_{4444}][\mathbf{Glu}]/[\mathbf{N}_{1444}][\mathbf{NTf}_2]$  and  $[\mathbf{P}_{4444}][\mathbf{Glu}]/[\mathbf{N}_{2224}][\mathbf{NTf}_2]$ , respectively.

At a first glance, a gel can be described by its appearance, that could be transparent or opaque, white or coloured. However, an arbitrary and subjective evaluation of the gel appearance is not suitable to define and characterise a gel. Hence, each ILG used in this Thesis has been characterised considering the trend of the absorbance (568 nm) during the sol-gel transition. This was studied as a function of the time. This measurement results in the definition of the opacity of the gel, and can be also correlated to the formation kinetics of the gel phase.<sup>133</sup>

Moreover, this is not the only investigation able to give information on the sol-gel transition; Resonance Light Scattering (RLS) measurements can give more information about both the kinetics of the gel matrix formation, and the size of the aggregates featuring the gel phase. RLS is an elastic scattering that originates from fluctuation of the refractive index of the solution.<sup>134</sup> RLS intensity ( $I_{\text{RLS}}$ ) increases during the sol-gel transition, to reach a constant value ( $I_g$ ), corresponding to the gel formation. Furthermore, the plateau value gives

---

133. Terech, P.; Pasquier, D.; Bordas, V.; Rossat, C., Rheological Properties and Structural Correlations in Molecular Organogels. *Langmuir* **2000**, *16* (10), 4485-4494.

134. Lu, W.; Fernández Band, B. S.; Yu, Y.; Geng Li, Q.; Chuan Shang, J.; Wang, C.; Fang, Y.; Tian, R.; Ping Zhou, L.; Li Sun, L.; Tang, Y.; Hua Jing, S.; Huang, W.; Ping Zhang, J., Resonance light scattering and derived techniques in analytical chemistry: past, present, and future. *Microchim. Acta* **2007**, *158* (1), 29-58.

information about the size of the aggregates. Indeed,  $I_{RLS}$  is directly proportional to the square of the molecular volume of aggregates.<sup>135</sup>

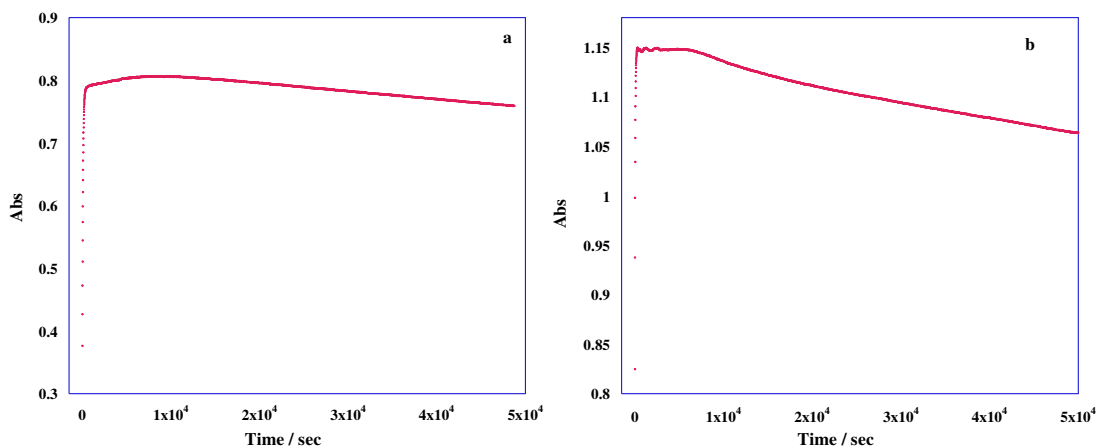


Figure 21 - UV-Vis kinetic measurements at 568 nm for: a)  $[P_{4\ 4\ 4\ 4}][Glu]/[N_{2\ 2\ 2\ 4}][NTf_2]$ ; b)  $[P_{6\ 6\ 6\ 14}][Glu]/[N_{1\ 4\ 4\ 4}][NTf_2]$ .

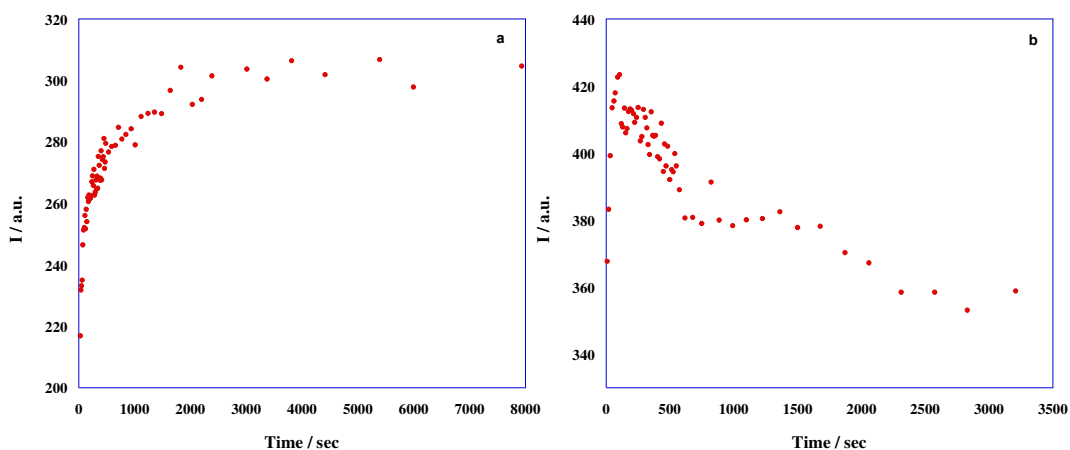


Figure 22 - RLS kinetic measurements for: a)  $[P_{4\ 4\ 4\ 4}][Glu]/[N_{2\ 2\ 2\ 4}][NTf_2]$ ; b)  $[P_{6\ 6\ 6\ 14}][Glu]/[N_{1\ 4\ 4\ 4}][NTf_2]$ .

The investigations for all ILGs were performed, with the exception of  $[P_{6\ 6\ 6\ 14}][Glu]/[N_{2\ 2\ 2\ 4}][NTf_2]$  and  $[P_{6\ 6\ 6\ 14}][Glu]/[C_1C_4pyrr][NTf_2]$ , whose formation was too slow to collect reliable data.

135. Zheng, J.; Wu, X.; Wang, M.; Ran, D.; Xu, W.; Yang, J., Study on the interaction between silver nanoparticles and nucleic acids in the presence of cetyltrimethylammonium bromide and its analytical application. *Talanta* **2008**, 74 (4), 526-532.

Figures 21 and 22 report the plots related to the UV-vis and RLS measurements for the  $[P_{4444}][Glu]/[N_{2224}][NTf_2]$  and the  $[P_{66614}][Glu]/[N_{1444}][NTf_2]$ , as representative examples.

Analysis of RLS trends, evidences the occurrence of a two-step mechanism for the following gels:  $[P_{4444}][Glu]/[N_{1444}][NTf_2]$ ,  $[P_{66614}][Glu]/[N_{2224}][NTf_2]$ ,  $[P_{66614}][Glu]/[C_1C_4pip][NTf_2]$ . In the first step, the  $I_{RLS}$  increases reaching a maximum value, then, it decreases down to  $I_g$ .

$I_g$  and opacity values ( $A_g$ ) corresponding to gel phase formation are compared in Table 19. In this Table, the time of gelation ( $t_g$ ) is also reported, *i. e.* the time necessary for the sol-gel transition to occur.

**Table 19 - Gelation time ( $t_g$ ), RLS intensity ( $I_g$ ) and opacity ( $A_g$ ) of ILGs.**

ILGs	$I_g$ / a. u.	$t_g$ /s	$A_g$ at 568 nm
$[P_{4444}][Glu]/[N_{2224}][NTf_2]$	400	2000	0.8
$[P_{66614}][Glu]/[N_{1444}][NTf_2]$	370	1900	1.1
$[P_{4444}][Glu]/[N_{1444}][NTf_2]$	580	1500	1.3
$[N_{4444}][Glu]/[N_{1444}][NTf_2]$	470	3800	1.5
$[P_{66614}][Glu]/[C_1C_4pip][NTf_2]$	420	1400	1.3

The comparison of results reported for the  $[N_{4444}][Glu]/[N_{1444}][NTf_2]$  and the  $[P_{4444}][Glu]/[N_{1444}][NTf_2]$  sheds light on the role of the cation on the aggregation and the formation of the 3D gel network. The  $I_g$  highlights the decrease of the aggregate size on going from the phosphonium to ammonium gelator.

Considering the  $[P_{4444}][Glu]$ -based gels, the IL solvent nature has to be considered. In particular, the viscosity of the IL influences the size of the aggregates featuring the gel phases. Indeed, a more organised system is obtained in more viscous IL ( $\eta = 104.1$  cP for  $[N_{2224}][NTf_2]$  and 538.9 cP for  $[N_{1444}][NTf_2]$ ).<sup>136,137</sup> Moreover, for the  $[P_{66614}][Glu]$ -based gels, the cyclic

136. Bhattacharjee, A.; Luís, A.; Santos, J. H.; Lopes-da-Silva, J. A.; Freire, M. G.; Carvalho, P. J.; Coutinho, J. A. P., Thermophysical properties of sulfonium- and ammonium-based ionic liquids. *Fluid Phase Equilib.* **2014**, *381*, 36-45.

137. Lee, C.-P.; Peng, J.-D.; Velayutham, D.; Chang, J.; Chen, P.-W.; Suryanarayanan, V.; Ho, K.-C., Trialkylsulfonium and tetraalkylammonium cations-based ionic liquid electrolytes for quasi-solid-state dye-sensitized solar cells. *Electrochim. Acta* **2013**, *114*, 303-308.

structure of the IL cation,  $[\text{C}_1\text{C}_4\text{pip}]^+$ , allows fast formation of a gel having more extended aggregates with respect to the one obtained in  $[\text{N}_{1444}][\text{NTf}_2]$ . The same trend is observed for the opacity measurements with less pronounced differences. In general, the phosphonium ILGs show faster gel network formation than the ILGs with the ammonium gelator. Finally, the length of the alkyl chains on the  $[\text{P}_{4444}][\text{Glu}]$  and the  $[\text{P}_{66614}][\text{Glu}]$  was taken into account. Our results also indicate that the gelation process is slow for longer alkyl chains associated with the cation. This phenomenon could be connected to the spatial hindrance of the chains and their difficult organisation in the network.

Interestingly, the size of the aggregates can be correlated to the mechanical response of the phosphonium ILGs. Indeed, the strongest  $[\text{P}_{66614}][\text{Glu}]$ -based gel is characterised by smaller aggregates. Similarly, the  $[\text{P}_{4444}][\text{Glu}]$ -based gel resists more to the strain when it is composed of smaller aggregates.

The characterisations shown until now are related to the properties of the gel phase. However, it could be important identify the nature of the interactions which underpin the self-assembly of the network.

To this aim, Escuder *et al.*<sup>138,139</sup> studied the useful application of NMR measurements to probe the nature of the intermolecular interactions, the thermodynamic parameters and, also, to determine the CGC value of supramolecular gel phases.

However, to perform these studies, the concentration and the physical state of the sample have to be considered. Indeed, the gelator results cannot be observed by NMR spectroscopy if it is immobilised and involved in the self-assembled network. This phenomenon could be due to the large correlation time of the assemblies, and as consequence, to the short  $T_2$  (transversal relaxation time), which results in small broad signals.

---

138. Escuder, B.; Llusar, M.; Miravet, J. F., Insight on the NMR Study of Supramolecular Gels and Its Application to Monitor Molecular Recognition on Self-Assembled Fibers. *J. Org. Chem.* **2006**, *71* (20), 7747-7752.

139. Hirst, A. R.; Coates, I. A.; Boucheteau, T. R.; Miravet, J. F.; Escuder, B.; Castelletto, V.; Hamley, I. W.; Smith, D. K., Low-Molecular-Weight Gelators: Elucidating the Principles of Gelation Based on Gelator Solubility and a Cooperative Self-Assembly Model. *J. Am. Chem. Soc.* **2008**, *130* (28), 9113-9121.

For this reason, the VT  $^1\text{H}$  NMR of the gel phases was performed. The concentration of the gelator was increased to 12 % wt. to obtain reliable data.

Hence, raising the temperature causes the collapse of the gel phase and the peaks of gelator become visible. Furthermore, the chemical shifts of the signals change with the temperature. In particular, the relation between the temperature and the chemical shift variation provides information about the strength of supramolecular forces involved in the aggregation.<sup>140</sup>

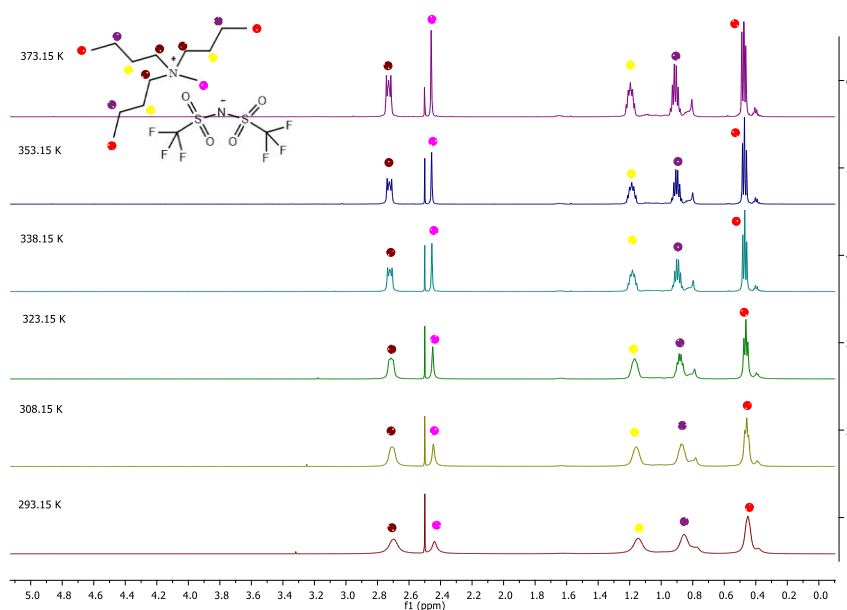


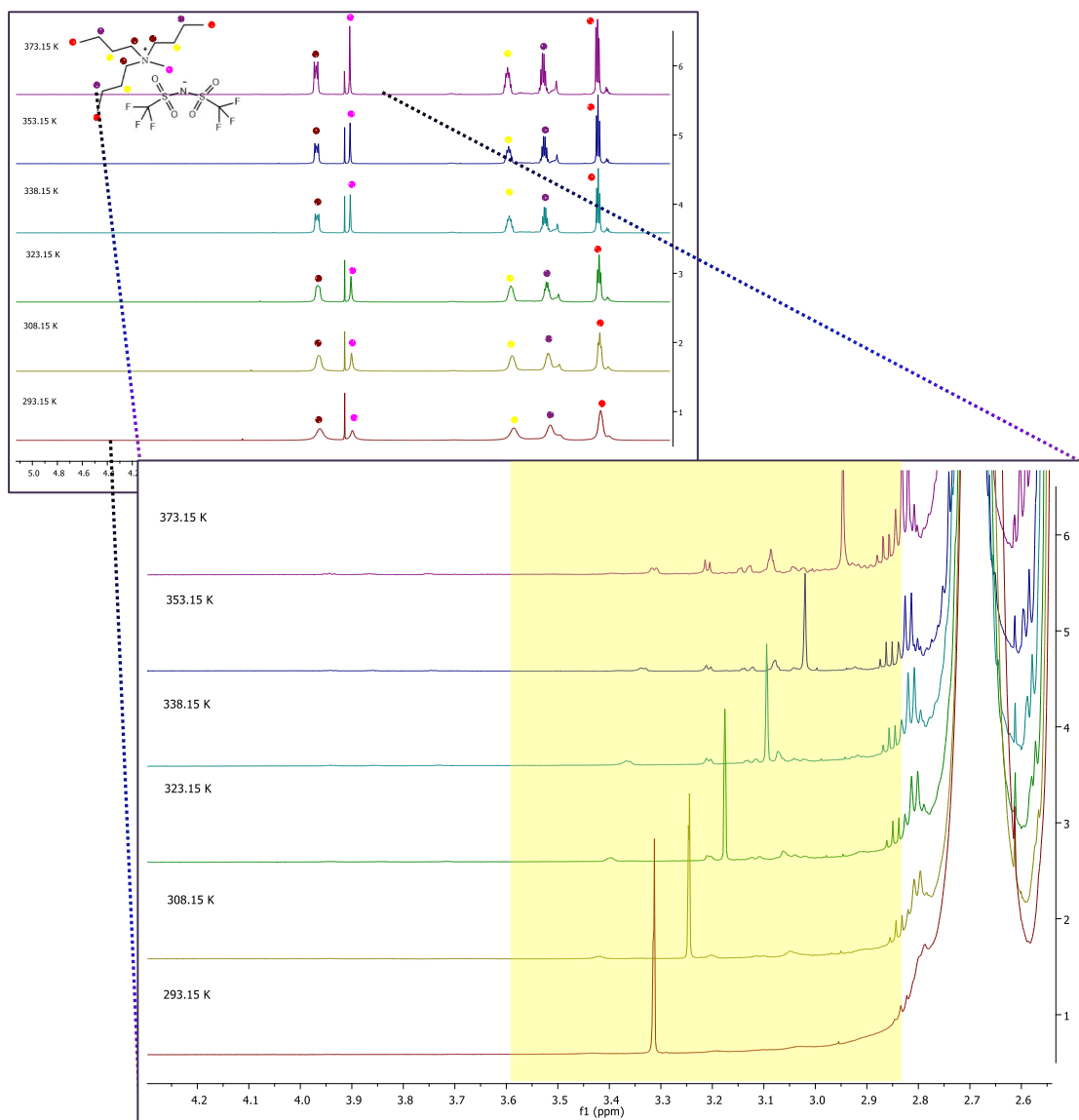
Figure 23 - VT  $^1\text{H}$  NMR spectra for the  $[\text{P}_{4444}][\text{Glu}]/[\text{N}_{1444}][\text{NTf}_2]$  in the T range: 293 – 373 K.

Figure 23 reports the VT  $^1\text{H}$  NMR for the  $[\text{P}_{4444}][\text{Glu}]/[\text{N}_{1444}][\text{NTf}_2]$  in the temperature range 293 – 373 K. This shows only the peaks related to the IL solvent. These signals become more resolved at higher temperature, although they do not show any chemical shift variation.

However, enlarging the region between the 4.3 and 2.5 ppm, the peaks relative to the gelator are identified. Moreover, with the increase in temperature, the peaks become more defined and, in this case, a significant change in chemical shift is observed (Figure 24).

140. Tena-Solsona, M.; Escuder, B.; Miravet, J. F.; Castelleto, V.; Hamley, I. W.; Dehsorkhi, A., Thermodynamic and Kinetic Study of the Fibrillization of a Family of Tetrapeptides and Its Application to Self-Sorting. What Takes So Long? *Chem. Mater.* **2015**, 27 (9), 3358-3365.





**Figure 24-** Enlargement of the spectra reported in Figure 23, in the region 4.3-2.5 ppm.

In order to identify which protons are involved in the chemical shift variation, the VT <sup>1</sup>H NMR spectra for the of  $[P_{4444}][Glu]/[N_{1444}][NTf_2]$  were performed and analysed at a concentration of the gelator lower than the CGC (3 % wt.) (A.5).

Considering this, in Figure 25 we report the enlarged spectra with each signal of the proton in the gluconate anion labelled.

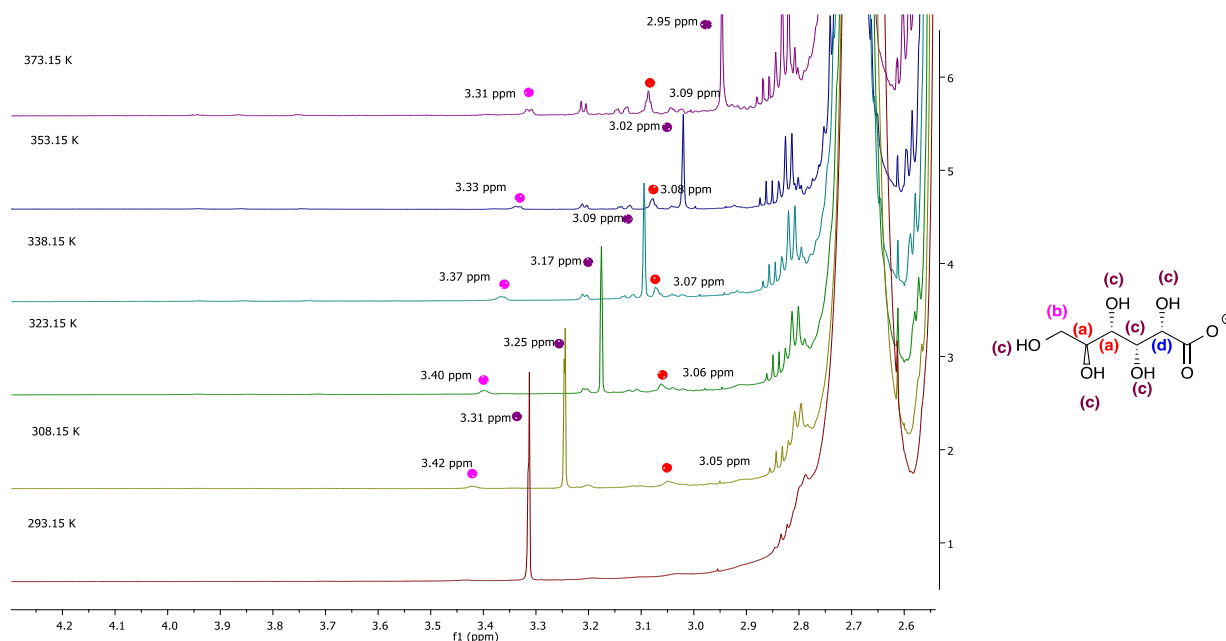


**Figure 25 - Enlarged region of VT  $^1\text{H}$  NMR spectra of  $[\text{P}_{4444}][\text{Glu}]/[\text{N}_{1444}][\text{NTf}_2]$  at 12% wt. Protons are labelled on the gluconate structure (Ha: red marker; Hb: magenta marker; Hc: plum marker; Hd: blue marker).**

The Hb and Hc protons show a downfield shift, while the Ha protons an upfield shift. Furthermore, the Hc, which corresponds to OH groups, is the signal which shows the highest chemical shift change. Consequently, summarising the above results, a relevant role of the hydrogen bonds as driving force in the gel network formation can be assumed.

The chemical shift of the Hc can be correlated in all cases as a function of temperature, showing a linear trend which can be fitted with linear regression analysis (Figure 26, Eq. 5):

$$\delta H_c = m_1 * T + m_2 \quad . \text{ Eq. 5}$$

The only exception is represented by the  $[\text{N}_{4444}][\text{Glu}]/[\text{N}_{1444}][\text{NTf}_2]$ , for which  $\delta H_c$  reaches a constant value at 338 K. The results of linear regression analysis results are reported in Table 20.

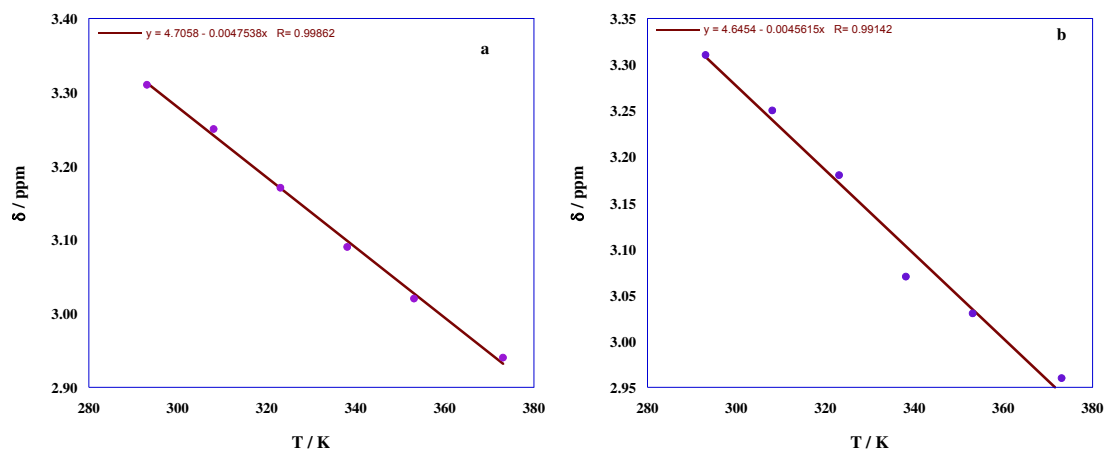


Figure 26 – Trend and linear regression analysis of the chemical shift of Hc in the VT  $^1\text{H}$  NMR for the gel a)  $[\text{P}_{4444}][\text{Glu}]/[\text{N}_{1444}][\text{NTf}_2]$ ; b)  $[\text{P}_{66614}][\text{Glu}]/[\text{N}_{1444}][\text{NTf}_2]$ .

Table 20 - Fitting parameters corresponding to chemical shift variation as a function of temperature for the Hc protons of the gluconate anion ( $R$  = correlation coefficient).

ILGs	$10^3 \cdot (m_1 \pm \delta m_1)$	$m_2 \pm \delta m_2$	$R$
$[\text{P}_{66614}][\text{Glu}]/[\text{N}_{1444}][\text{NTf}_2]$	$-4.56 \pm 0.30$	$4.64 \pm 0.09$	0.991
$[\text{P}_{66614}][\text{Glu}]/[\text{N}_{2224}][\text{NTf}_2]$	$-1.12 \pm 0.12$	$3.78 \pm 0.04$	0.982
$[\text{P}_{66614}][\text{Glu}]/[\text{C}_1\text{C}_4\text{pyrr}][\text{NTf}_2]$	$-5.33 \pm 0.40$	$4.84 \pm 0.12$	0.992
$[\text{P}_{66614}][\text{Glu}]/[\text{C}_1\text{C}_4\text{pip}][\text{NTf}_2]$	$-4.43 \pm 0.32$	$4.56 \pm 0.10$	0.989
$[\text{P}_{4444}][\text{Glu}]/[\text{N}_{1444}][\text{NTf}_2]$	$-4.75 \pm 0.12$	$4.71 \pm 0.04$	0.999
$[\text{P}_{4444}][\text{Glu}]/[\text{N}_{2224}][\text{NTf}_2]$	$-6.01 \pm 0.58$	$5.09 \pm 0.19$	0.982

The slope value ( $m_2$ ) can be inversely correlated to the case with which supramolecular interactions are broken down by raising the temperature. Indeed, the higher this value is, the weaker is the fibrillar network. Accordingly, the  $[\text{P}_{66614}][\text{Glu}]/[\text{N}_{2224}][\text{NTf}_2]$  results the ILG with the strongest network, and, this result matches the thermodynamic one, as this gel has the highest  $T_{\text{gel-6.5\%wt}}$ .

Also in this case, the results in Table 20 permit considering the relation between the IL solvent and the properties of the ILG. In particular, as shown by  $m_2$  values collected for  $[\text{P}_{66614}][\text{Glu}]$  gelator, the viscosity of ILs plays a crucial role in the aggregation process. However, the viscosity affects in opposite way the features of gel phases formed by ILs having cyclic cations. Indeed, in these cases, the  $m_2$  value decreases with the increase of the viscosity ( $\eta = 84.33$  and  $255$  cP for  $[\text{C}_1\text{C}_4\text{pyrr}][\text{NTf}_2]$  and  $[\text{C}_1\text{C}_4\text{pip}][\text{NTf}_2]$ , respectively). Differently, in the case of the ammonium ILs, the relevance of hydrogen bond, in the self-assembled

network, decreases with the increase of the viscosity ( $\eta = 104.1$  and  $538.9$  cP, for  $[\text{N}_{2\ 2\ 2\ 4}][\text{NTf}_2]$  and  $[\text{N}_{1\ 4\ 4\ 4}][\text{NTf}_2]$ , respectively). In general, the differences detected among gels prepared using ammonium IL solvents are more pronounced than using the cyclic ones.

Moreover, gel phases formed in less viscous IL solvent  $[\text{N}_{2\ 2\ 2\ 4}][\text{NTf}_2]$  indicate changes in the gelator structure. Indeed, the comparison between  $m_2$  values collected for  $[\text{P}_{6\ 6\ 6\ 14}][\text{Glu}]$  and  $[\text{P}_{4\ 4\ 4\ 4}][\text{Glu}]$  shows significant differences, demonstrating that longer chains result in stronger gel network, probably due to the increase of van der Waals interactions.

The VT  $^1\text{H}$  NMR study permits considering the fundamental role of the hydrogen bonds in the self-assembly process and in the network stability. In order to validate this evidence, the infrared spectra (FT-IR) can be a useful tool.

Figure 27 reports the FT-IR spectra for  $[\text{P}_{6\ 6\ 6\ 14}][\text{Glu}]/[\text{N}_{1\ 4\ 4\ 4}][\text{NTf}_2]$  and  $[\text{P}_{4\ 4\ 4\ 4}][\text{Glu}]/[\text{N}_{2\ 2\ 2\ 4}][\text{NTf}_2]$ . The regions considered are the ones of -OH stretching ( $3550\text{-}3150\text{ cm}^{-1}$ ) and the  $\text{-COO}^-$  stretching bands ( $1650\text{-}1400\text{ cm}^{-1}$ ). These are diagnostic to investigate which groups are more involved in the hydrogen bond formation.

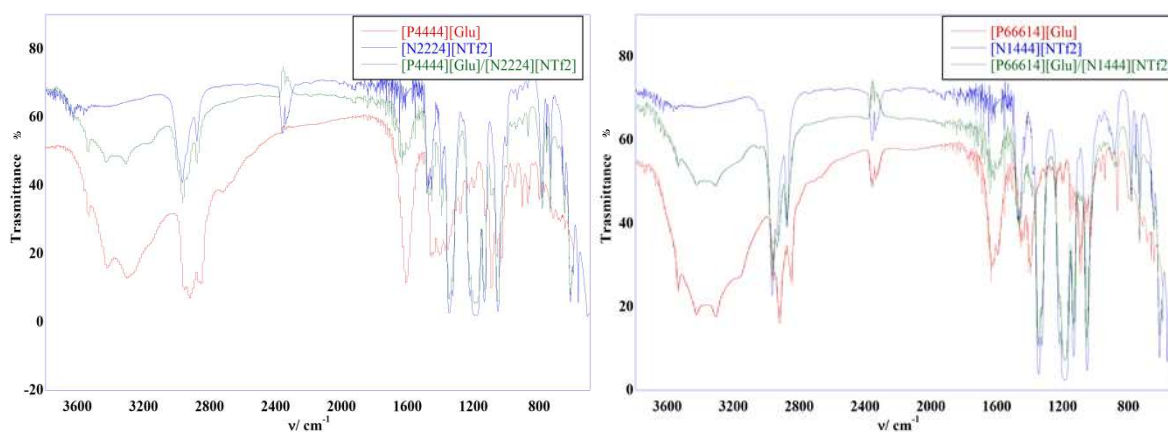


Figure 27 - FT-IR spectra for neat gelator, IL and corresponding ILG at 6.5 % wt. of gelator.

Table 21 reports the shifts in frequency on going from the gelator to the ILG. The accordance between the FT-IR and the VT  $^1\text{H}$  NMR shift, confirms the role of hydrogen bonds favouring the formation of gel networks. Moreover, results in Table 21 evidence the correlation among the gelators nature and changes in frequency values. Indeed, the ILGs formed by  $[\text{P}_{4444}][\text{Glu}]$  display the highest shift. Conversely, the ones with the  $[\text{P}_{66614}][\text{Glu}]$  gelator show the smallest shift. Furthermore, also the involvement of different functional groups changes as a function of the gelator nature. Indeed, higher  $\Delta\nu$  values were obtained for the  $-\text{COO}^-$  groups in the case of  $[\text{P}_{66614}][\text{Glu}]$  ILGs. Differently, in the case of  $[\text{P}_{4444}][\text{Glu}]$  and  $[\text{N}_{4444}][\text{Glu}]$  ILGs, the highest  $\Delta\nu$  values were obtained for  $-\text{OH}$  groups.

**Table 21 - Stretching frequencies corresponding to gelator ( $\nu_{\text{gelator}}$ ) and ILGs ( $\nu_{\text{ILG}}$ ) and changes in stretching frequencies ( $\Delta\nu$ ) on going from gelator to gel phase.**

ILGs	chemical group	$\nu_{\text{gelator}} / \text{cm}^{-1}$	$\nu_{\text{ILG}} / \text{cm}^{-1}$	$\Delta\nu / \text{cm}^{-1}$
[P <sub>66614</sub> ][Glu]/[N <sub>1444</sub> ][NTf <sub>2</sub> ]	-OH	3540	3540	0
		3428	3428	3
		3306	3314	-8
		3161	3166	-5
	-COO <sup>-</sup>	1618	1618	12
		1448	1462	-14
[P <sub>66614</sub> ][Glu]/[N <sub>2224</sub> ][NTf <sub>2</sub> ]	-OH	3540	3540	0
		3431	3428	3
		3306	3314	-8
		3161	3166	-7
	-COO <sup>-</sup>	1630	1621	9
		1448	1460	-12
[P <sub>66614</sub> ][Glu]/[C <sub>1</sub> C <sub>4</sub> pyrr][NTf <sub>2</sub> ]	-OH	3540	3545	-5
		3431	3428	3
		3306	3311	-5
		3161	3166	-5
	-COO <sup>-</sup>	2930	2969	-39
		2860	2883	-23
[P <sub>66614</sub> ][Glu]/[C <sub>1</sub> C <sub>4</sub> pip][NTf <sub>2</sub> ]	-OH	3540	3545	-5
		3431	3428	3
		3306	3311	-5
		3161	3166	6
	-COO <sup>-</sup>	2930	2964	-34
		2860	2880	-20
[P <sub>66614</sub> ][Glu]/[C <sub>1</sub> C <sub>4</sub> pip][NTf <sub>2</sub> ]	-COO <sup>-</sup>	1630	1621	9
		1448	1469	-21
		1398	1354	44

ILGs	chemical group	$\nu_{\text{gelator}} / \text{cm}^{-1}$	$\nu_{\text{ILG}} / \text{cm}^{-1}$	$\Delta\nu / \text{cm}^{-1}$
<b>[P<sub>4444</sub>][Glu]/[N<sub>1444</sub>][NTf<sub>2</sub>]</b>	-OH	3572	3629	-57
		3552	3554	-2
		3416	3433	-17
		3300	3312	-12
		3158	3166	-8
	-COO <sup>-</sup>	2929	2970	-41
		2862	2870	-8
<b>[P<sub>4444</sub>][Glu]/[N<sub>2224</sub>][NTf<sub>2</sub>]</b>	-OH	3572	3631	-59
		3552	3545	7
		3416	3432	-16
		3300	3311	-11
		3158	3167	-9
	-COO <sup>-</sup>	1613	1632	-19
	<b>[N<sub>4444</sub>][Glu]/[N<sub>1444</sub>][NTf<sub>2</sub>]</b>	-OH	3566	
3444				
3322			3344	-22
2977			2977	0
2933			2877	56
-COO <sup>-</sup>		2855		
		1638	1596	42
		1602		
	1447	1463	-16	
	1397	1353	44	

### 3.7 Desulfurisation Process

In the introduction of this Chapter, the ILs application for environmental remediation and preservation was mentioned, together with the possibility to apply the ILGs studied in this Thesis for this purpose.

The issue related to sulfur pollution of atmosphere and soil due to the presence of sulfur compounds, in particular aromatic ones, in fuels led to considering new possible removal materials for the removal of contaminants.

To achieve this goal, and to obtain reliable experimental results, the literature was taken into consideration to prepare the solution mimicking the fuel.<sup>123,124</sup> In particular, high amounts of thiophene, benzothiophene and dibenzothiophene can be present in diesel fuel. For this purpose, standard solutions of these aromatic compounds in hexane were prepared to reproduce the diesel mixture. The ILGs (also in this case at 6.5% wt.) used to adsorb the contaminants are featured by the presence of **[P<sub>4444</sub>][Glu]** and **[N<sub>4444</sub>][Glu]** IL gelators, as the solubility of the **[P<sub>66614</sub>][Glu]** in diesel does not allow its use (see Table 14).

Practically, a fixed amount of the solution at fixed concentration (500 µL at 500 ppm) was cast on the top of the ILG (250 mg) and rested in contact.

In Table 22 and Figure 28 the results of the adsorption after 24 h and 48 h are reported. Furthermore, to evaluate the capacity of adsorption of these soft materials, the Adsorption Efficiency (AE) was calculated as:

$$AE = \frac{C_0 - C_f}{C_0} \times 100 \quad \text{Eq. 6}$$

where  $C_0$  and  $C_f$  represent the concentration of the sulfur compound before and after contact with the gel phase, respectively. For a useful comparison, the above tests were also performed using pure ILs. The investigation, in all cases, was carried out using a thermo-control system fixed at 20 °C. However, to investigate the temperature effect, the same test was conducted also at 30 °C. Results are reported in Table 22. The comparison of the AEs permits considering the role of the temperature negligible, as accounted for by data collected for **[P<sub>4444</sub>][Glu]**/**[N<sub>2224</sub>][NTf<sub>2</sub>]** and **[P<sub>4444</sub>][Glu]**/**[N<sub>1444</sub>][NTf<sub>2</sub>]** ILGs, at 30 °C. This result perfectly agrees with data previously reported in literature about removal efficiency of sulfur compounds by ILs, using liquid-liquid extraction method.<sup>123</sup>



**Table 22 - AE% of sulfur compounds on ILGs (at 6.5% wt.) of gelator and corresponding ILs at 20 °C and 30 °C.**

Adsorbent ILG	AE (%) T		AE (%) BT		AE (%) DBT	
	<i>t</i> = 24 h	<i>t</i> = 48 h	<i>t</i> = 24 h	<i>t</i> = 48 h	<i>t</i> = 24 h	<i>t</i> = 48 h
[N <sub>2224</sub> ][NTf <sub>2</sub> ]	83.7	87.0	56.2	56.9	57.2	54.7
[P <sub>4444</sub> ][Glu]/ [N <sub>2224</sub> ][NTf <sub>2</sub> ]	49.5	60.4	57.7	67.2	46.8	68.0
[P <sub>4444</sub> ][Glu]/ [N <sub>2224</sub> ][NTf <sub>2</sub> ] (30 °C)	47.2	60.9				
[N <sub>1444</sub> ][NTf <sub>2</sub> ]	12.0	53.2	47.2	53.3	49.9	73.8
[N <sub>4444</sub> ][Glu]/ [N <sub>1444</sub> ][NTf <sub>2</sub> ]	22.9	86.4	45.0	52.8	27.5	46.2
[P <sub>4444</sub> ][Glu]/ [N <sub>1444</sub> ][NTf <sub>2</sub> ]	40.6	82.4	41.2	53.8	26.5	46.5
[P <sub>4444</sub> ][Glu]/ [N <sub>1444</sub> ][NTf <sub>2</sub> ] (30 °C)	57.6	65.3				

Data reported in Table 22, can be analysed considering neat ILs and gels differing in IL gelation solvent and gelators nature.

Firstly, in order to compare the performances of neat ILs and ILGs, the sulfur adsorption was tested for both systems, taking AE values after 24 and 48 h.

The less viscous IL, [N<sub>2224</sub>][NTf<sub>2</sub>], achieves AE close to 84% already after 24 h, and a prolonged contact with the hexane solution, does not affect significantly this value. However, a similar trend can be detected for ILG with this IL solvent, [P<sub>4444</sub>][Glu]/[N<sub>2224</sub>][NTf<sub>2</sub>], for which AE values at 24 h are closed to the ones achieved after 48 h of contact.

On the contrary, the more viscous IL, [N<sub>1444</sub>][NTf<sub>2</sub>], shows a more considerable gap, *i.e.* the difference in value between the adsorption at 24 and 48 h. However, for this IL, the difference in AE values is more evident for T adsorption compared to BT and DBT. ILGs in [N<sub>1444</sub>][NTf<sub>2</sub>], [P<sub>4444</sub>][Glu]/[N<sub>1444</sub>][NTf<sub>2</sub>] and [N<sub>4444</sub>][Glu]/[N<sub>1444</sub>][NTf<sub>2</sub>], show a similar behaviour to the one already described for the neat IL, with an increase of adsorption going from 24 to 48 h of contact.

Considering these data in detail, the adsorption of T results are affected by the viscosity of ILs. Indeed, if neat ILs or ILGs are considered, the adsorption efficiency changes in an opposite way. AE value for the  $[P_{4444}][Glu]/[N_{2224}][NTf_2]$  ILG, after 48 h, is lower than the T adsorption on the  $[P_{4444}][Glu]/[N_{1444}][NTf_2]$  ILG. This role of the viscosity in ILGs is mitigated for DB and DBT. Conversely, AE values related to the T adsorption by neat  $[N_{2224}][NTf_2]$  are higher, both at 24 and 48 h, compared to the values for neat  $[N_{1444}][NTf_2]$ .

Interestingly, these differences going from ILs to ILGs can be ascribed to the gel network, apparently, the gelatinous matrix adsorbs more if it is formed by a more viscous IL ( $[N_{1444}][NTf_2]$ ).

In some cases, the AE slightly decreases on going from the IL solvent to the ILG.  $[P_{4444}][Glu]/[N_{2224}][NTf_2]$  adsorbs less T than  $[N_{2224}][NTf_2]$ ,  $[P_{4444}][Glu]/[N_{1444}][NTf_2]$  adsorbs less DBT than  $[N_{1444}][NTf_2]$ , and  $[P_{4444}][Glu]/[N_{1444}][NTf_2]$  adsorbs less T and DBT compared to  $[N_{1444}][NTf_2]$ . For the other ILGs, the comparison among AEs measured at 48 h highlights the same or better performances with respect to the corresponding IL solvent.

These interesting results, prove not only the real opportunity to use ILGs as sorbent materials for desulfurisation processes but also the best adsorption for phosphonium gelator, in agreement with what observed by Zolfigol and co-workers.<sup>123</sup>

All these considerations can be better evidenced in the histogram reported in Figure 28.

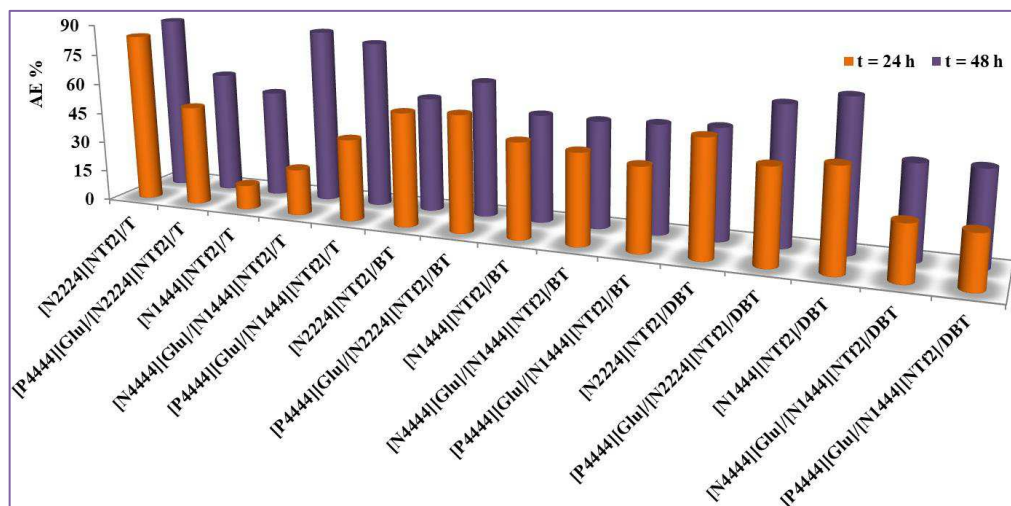


Figure 28 – AE of sulfur compounds on ILGs (6.5 % wt.) and the corresponding IL solvents at 20 °C.

The  $[P_{4444}][Glu]$  ILGs are chosen to evaluate parameters, like the optimum time of contact, the ratio between the volume of fuel and the amount of gel phase, the concentration of sulfur compounds in the fuel and the possibility to recycle the gel phase.

The aim of this study was to obtain an applicable system. For this purpose, the kinetic, of the adsorption was studied (Figure 29) to optimise the time of the contact.

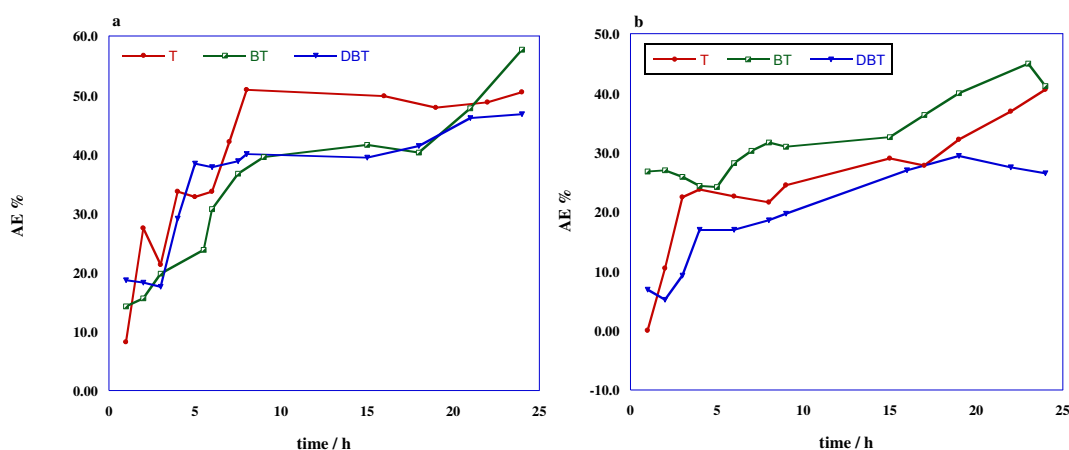


Figure 29 - Plots of AE of sulfur compounds as a function of time for the ILGs: a)  $[P_{4444}][Glu]/[N_{2224}][NTf_2]$ ; b)  $[P_{4444}][Glu]/[N_{1444}][NTf_2]$ .

As far as  $[P_{4444}][Glu]/[N_{2224}][NTf_2]$  ILG system is concerned, the plot of AE as a function of time highlights the better efficiency of this system in adsorbing T

from a hexane solution compared to BT and DBT. In contrast, the  $[P_{444}][Glu]/[N_{1444}][NTf_2]$  shows only negligible differences among the compounds.

The kinetic study permits identifying the highest AE after 7 h of contact, this time is more realistic for an applicative aim.

The investigation, after this optimisation, is conducted with a mixture of the three aromatic molecules. The choice to mix the contaminants arises from the same awareness to work with a system which can mimic the real fuel.

Surprisingly, the AE measured for the total sulfur concentration (1500 ppm) was higher than the adsorption of the single contaminant (Figure 30). This synergetic behaviour was not expected and not yet understood. However, the best results are obtained for the BT and DBT. Once again, the AE of the refractory compounds (BT and DBT) sheds a positive light on the systems under study.

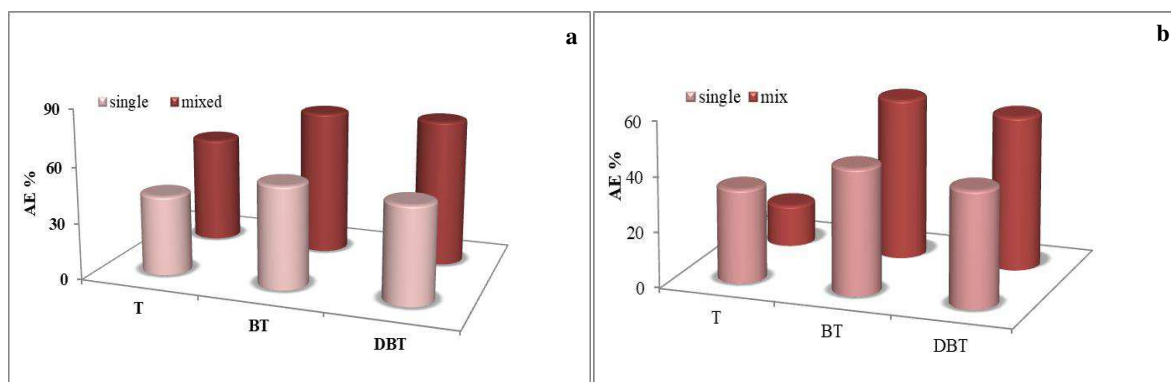


**Figure 30** – Comparison of AE of the solution of single compounds and mixed solutions of sulfur compounds (C = 1500 ppm) corresponding to: a)  $[P_{444}][Glu]/[N_{2224}][NTf_2]$ ; b)  $[P_{444}][Glu]/[N_{1444}][NTf_2]$

The possible presence of other aromatic contaminants could negatively affect the stability of the ILG system. In order to study this effect, the influence of benzene on the stability of the ILG was considered. Benzene solutions with two different concentrations were taken into account. The first one with the same concentration used for each sulfur molecule, and the other one four times more concentrated (500 – 2000 ppm). The  $^1H$  NMR investigation of the hexane solution does not show trace of ILG component as consequence of the stability of this system.

The concentration and volume of the hexane mixed solution cast on top of the ILG were also taken into account.

The concentration of the T+BT+DBT solution was varied between 900 and 3000 ppm (500  $\mu$ L), maintaining unchanged the amount and the composition of the ILGs. The histogram in Figure 31 reports these experiments with an interesting correlation between the concentration of the mixed solution and the AE of the ILGs. Indeed, the increased concentration caused the parallel increase of the AE, obtaining the best AE for the  $[P_{4444}][Glu]/[N_{2224}][NTf_2]$  ILG (Figure 31).

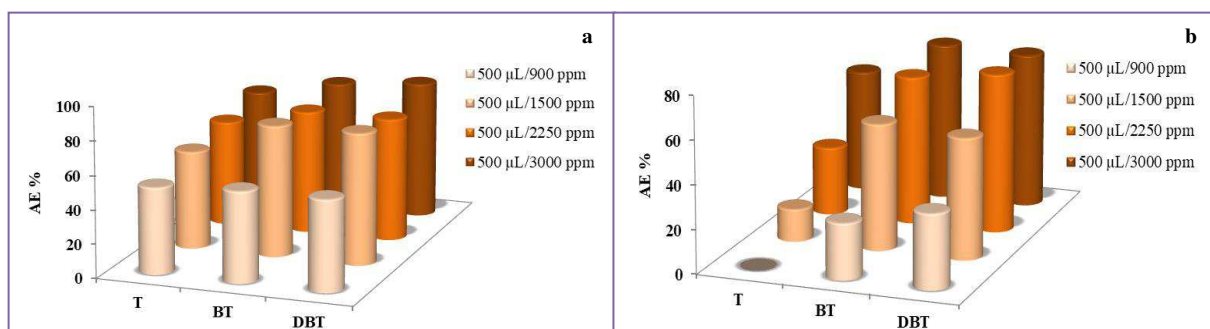


Figure 31 - Comparison among the AE of the mixed solutions at different concentrations: a)  $[P_{4444}][Glu]/[N_{2224}][NTf_2]$ ; b)  $[P_{4444}][Glu]/[N_{1444}][NTf_2]$ .

In addition, the volume of the mixed solution was changed between 300 and 700  $\mu$ L (1500 ppm), maintaining unvaried the quantity and the composition of the ILGs.

The gel phases did not collapse even after the contact with the 700  $\mu$ L of fuel. However, the AE stayed constant up to 500  $\mu$ L of fuel volume (Figure 32). It decreases only using 700  $\mu$ L of solution with evident difference for the ILG in the  $[N_{2224}][NTf_2]$ .

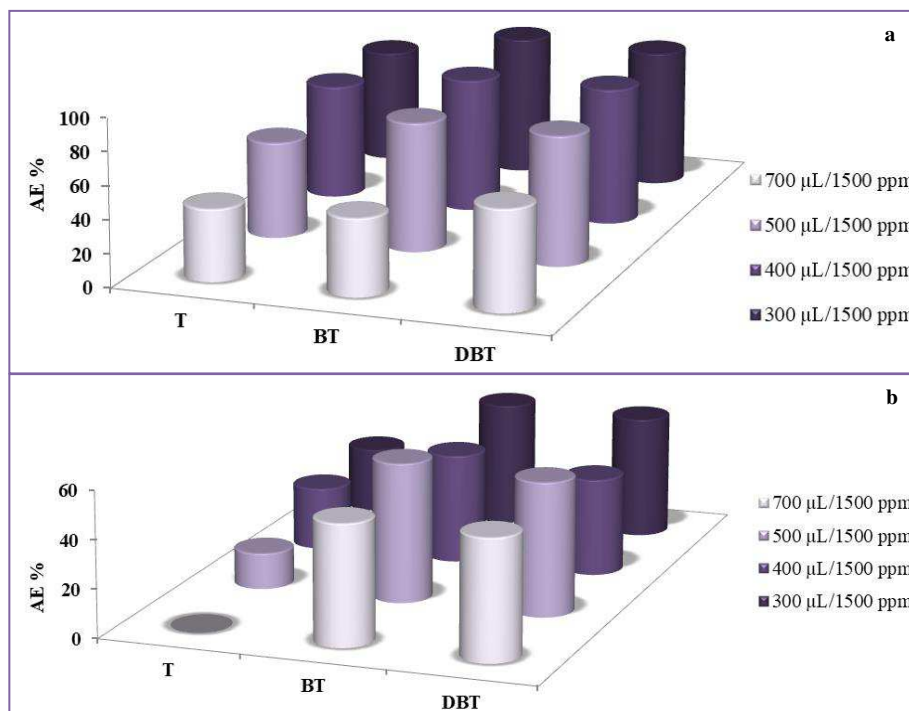


Figure 32 - Comparison among the AE of the mixed solutions at different volumes: a)  $[P_{4444}][Glu]/[N_{2224}][NTf_2]$ ; b)  $[P_{4444}][Glu]/[N_{1444}][NTf_2]$ .

The last parameter taken into account was the contact surface area. The effect on the AE of the increase in diameter of vial used to form the gel was investigated, maintaining the ratio  $V_{fuel} (\mu L) / m_{gel} (mg)$  equal to 2. The increase of the contact surface determines a drop of the AE, with a more drastic effect for the  $[P_{4444}][Glu]/[N_{2224}][NTf_2]$  compared to  $[P_{4444}][Glu]/[N_{1444}][NTf_2]$  (Figure 33).

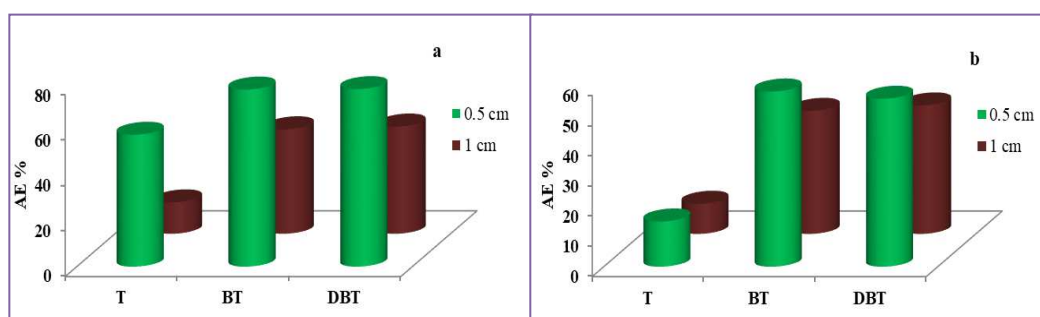
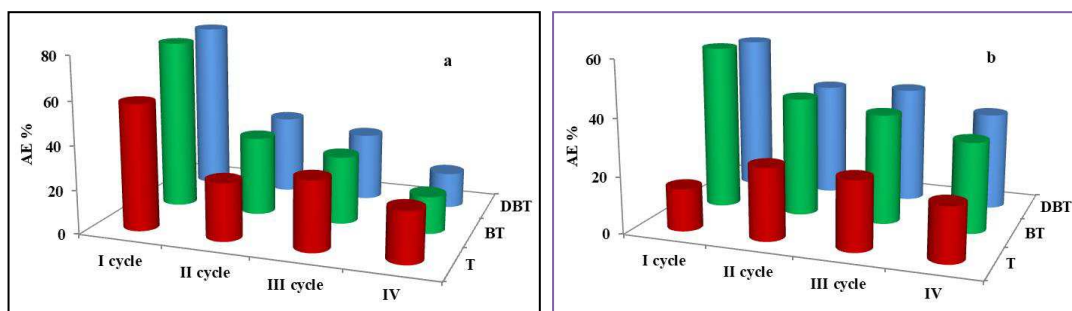


Figure 33 - Comparison among the AE obtained with a different contact area: a)  $[P_{4444}][Glu]/[N_{2224}][NTf_2]$ ; b)  $[P_{4444}][Glu]/[N_{1444}][NTf_2]$ .

Finally, the reuse of the ILGs was also considered and investigated. After the removal of the solution in contact with the gel phase, this was renovated and a fresh hexane solution was put in contact. Figure 34 shows the trend of the adsorption efficiency, and how many reuses could be performed. The ILGs retained 40 % of their adsorption ability up to the fourth cycle of use.



**Figure 34 - Cycles of reuse in the adsorption process for the ILG: a) [P<sub>4444</sub>][Glu]/[N<sub>2224</sub>][NTf<sub>2</sub>]; b) [P<sub>4444</sub>][Glu]/[N<sub>1444</sub>][NTf<sub>2</sub>].**

In the introduction, the use of ILs for environmental remediation and, in particular for desulfurisation of fuels, was highlighted. However, the problem related to the mutual solubility of ILs in fuel was also considered as the biggest limitation to the extractive process with the ILs.

To shed more light on the advantage of ILGs application for the desulfurisation through adsorption process, the possible mutual solubility was investigated. In particular, the HPLC and <sup>1</sup>H NMR did not show any contamination of the hexane solution by the ILG components. Moreover, neither the weight of the ILGs was changed after being in contact with the solution.

All the results discussed in this Chapter support the achievement of the experimental work. Indeed, the self-supporting and highly porous nature of ILGs make them suitable to adsorb contaminants both for environmental remediation and prevention of pollution in the low-impact Chemistry.

## **3.8 Experimental Section**

### **3.8.1. Gelation Tests**

The salt was weighed in a vial and a proper solvent was added; the first concentration considered was 1% wt. (2.5 mg of salt in 250 mg of solvent). If the salt was insoluble at room temperature, the solution was heated for 1.5 h at 10 °C lower than the boiling point of the solvent. After heating, the clear solution was immediately stored in the fridge (4 °C) overnight. After this time, if it was still a solution or would drip with the tube inversion test, the concentration of the salt was increased.

### **3.8.2. $T_{\text{gel}}$ determination**

The  $T_{\text{gel}}$  values were determined by the lead ball method. The lead ball (weighing 46.23 mg and 2 mm in diameter) was placed on top of the gel, and the vial was placed in a water bath. The temperature of the bath was increased at 2 °C  $\text{min}^{-1}$  till the lead ball, going through the gel phase, reached the bottom of the vial ( $T_{\text{gel}}$ ). The  $T_{\text{gel}}$  values were reproducible within 1 °C.

### **3.8.3. POM measurements**

The POM images of the gel phases were recorded using an Olympus BX50 microscope equipped with a JVC TK-1085E camera. For all experiments, a 0.25 10× MD PLAN lens were used. The gel phases were cast on a glass and were not covered with another glass above to avoid destroying the gel phase itself. The gels were heated until 90 °C and then cooled. The heating and cooling rates were 5 °C  $\text{min}^{-1}$ .



### **3.8.4. Opacity measurements**

Opacity measurements were recorded with a UV-Vis spectrophotometer (Beckman Coulter DU 800). The limpid hot solution of the salt was put in a quartz cuvette with a light path of 0.2 cm. The kinetics of gel formation was recorded at a wavelength of 568 nm and a temperature of 20 °C. Spectra were recorded until gel formation. The gel phase obtained at the end of the measurement was stable after the tube inversion test.

### **3.8.5. RLS measurements**

RLS measurements were carried out at 20 °C on a spectrofluorophotometer (JASCO FP-777 W) using a synchronous scanning mode. The RLS spectrum was recorded from 300 to 600 nm with both the excitation and emission slit widths set at 1.5 nm. The maximum intensity of the spectrum obtained was chosen as the working wavelength. The sample preparation was the same as that of the opacity measurements, putting the clear hot solution of the salt in the cuvette. The spectra were recorded until constant values of intensity (gel formation). The gel phase obtained at the end of the measurement was stable after the tube inversion test.

### **3.8.6. NMR measurements**

The VT  $^1\text{H}$  NMR were recorded using an Ascend™ 600 Bruker with an internal solvent reference ( $d_6$ -DMSO). Each gel was formed in the NMR tube containing the internal solvent reference inside. The spectra were recorded from 293 up to 373 K; for each temperature, the sample was equilibrated for 20 min. NMR spectra of hexane solutions put in contact with gel phases, to check a possible mutual solubility, were recorded using a 400 MHz spectrometer (Bruker ultrashield 400 plus). A coaxial capillary tube loaded with  $d_6$ -DMSO was used as the external magnetic field-frequency lock and its residual signal at  $\delta = 2.56$  ppm as the reference.

### 3.8.7. Adsorption of sulfur compounds

Each experiment was carried out at 20 °C. The solution, at a fixed concentration (500 µL), was cast on top of the gel (250 mg), and after the established time, 200 µL of the solution were used to run the HPLC measurements. The concentration of sulfur compound(s) still present in solution was determined using a previously obtained calibration curve. The adsorption efficiency of sulfur compounds was determined using an HPLC Shimadzu LC-10 AD equipped with an inverse phase C18 column. A binary mixture of ACN/H<sub>2</sub>O (80/20; v/v) was used as eluent at a flow rate of 1 mL min<sup>-1</sup>.

## 4. IL-Co complexes: a thermochromic and magnetic transition in a mild temperature range

### 4.1. The Chromism phenomena

Several animals are capable to change the colour of the skin in dependence of the colour of the environment of their habitat. Obviously, for these animals, such as chameleons, arctic foxes and seahorses, this phenomenon is a mimicry or an adjustment shaped genetically on nature, but the principle remains the same: a more or less drastic Chromism is due to an external change.

Chromism is a reversible change of the colour of a substance, due to an external stimulus. The substance can be organic or inorganic.

Considering this definition, the main phenomena which are comprised in the Chromism classification are Photochromism, Ionochromism, Electrochromism, Solvatochromism and Thermochromism.

Photochromism is a reversible transformation induced by the absorption of an electromagnetic radiation between two forms, A and B, having different absorption spectra. The A form is thermodynamically stable and can be converted into B by irradiation. The reverse reaction can occur thermally or photochemically.<sup>141</sup>

Ionochromism is the reversible colour change due to the interaction with ionic species. This phenomenon can be “additional” to the photochromic one and can cause an alteration in the conductivity of the substance. However, if the ion is the proton, the phenomenon is named Halochromism or Acidochromism, being, in this case, the external stimulus is the pH variation.<sup>142</sup>

The reversible colour change due to an electric current passage (potential difference) is associated with the electrochromic phenomenon. The electroactive

---

141. Bouas-Laurent, H.; Dürr, H., Organic photochromism (IUPAC Technical Report). *Pure Appl. Chem.* **2001**, 73 (4), 639-665.

142. Bamfield, P.; Hutchings, M., *Chromic Phenomena: Technological Applications of Colour Chemistry: Edition 3.* **2018**.

substance, changes its properties and, consequently, the colour when an oxidative or reductive process occurs.<sup>143</sup>

Solvatochromism can be identified in the change in the absorption or emission spectra of a substance when it is dissolved in solvents differing in polarity; as a consequence a colour variation is observed.<sup>144</sup>

Finally, thermochromism is the change of the colour of a substance induced by temperature variation.<sup>145</sup> More precisely, Jesse H. Day<sup>146</sup> defined it as: “*Thermochromism is defined operationally as an easily noticeable reversible colour change in the temperature range limited by the boiling point of each liquid, the boiling point of the solvent in the case of solution or the melting point for solids*”.

## 4.2. Thermochromism: a common phenomenon for several compounds

Thermochromism is a phenomenon that can involve several substances, from organic to inorganic ones such as polymers, transition metals and liquid crystals.<sup>142</sup>

This phenomenon is due to the heating and can be related to a charge transfer,<sup>147</sup> modification in the chemical structure,<sup>148</sup> change in the crystalline field,<sup>149</sup> or further, physical phenomena which involve the temperature, such as decomposition or phase transition.<sup>149</sup>

---

143. Monk, P. M. S.; Mortimer, R. J.; Rosseinsky, D. R., *Electrochromism: Fundamentals and Applications*. VCH Verlagsgesellschaft mbH and VCH Publishers, Inc.: **1995**.

144. Nigam, S.; Rutan, S., Principles and Applications of Solvatochromism. *Appl. Spectrosc.* **2001**, 55 (11), 362A-370A.

145. Crano, J. C.; Guglielmetti, R. J., *Organic Photochromic and Thermochromic Compounds: Volume 2: Physicochemical Studies, Biological Applications, and Thermochromism*. Springer US: **2006**.

146. Day, J. H., Thermochromism. *Chem. Rev.* **1963**, 63 (1), 65-80.

147. Yuan, T.; Xu, Y.; Zhu, C.; Jiang, Z.; Sue, H.-J.; Fang, L.; Olson, M. A., Tunable Thermochromism of Multifunctional Charge-Transfer-Based Supramolecular Materials Assembled in Water. *Chem. Mater.* **2017**, 29 (23), 9937-9945.

148. Kalnins, K. K., Structure and thermochromism of spiropyrans. Triplet mechanism of the thermal cleavage/closure of the pyran ring. *J. Struct. Chem.* **1998**, 39 (5), 642-650.

149. Seeboth, A.; Ruhmann, R.; Mühling, O., Thermotropic and Thermochromic Polymer Based Materials for Adaptive Solar Control. *Materials* **2010**, 3 (12), 5143-5168.

Nevertheless, a first classification can be done between the intrinsic colour change, where the heat is the unique cause of thermochromism, and the indirect colour change, in which the variation is due to the change in the environment around the system as consequence of the heat.<sup>150</sup>

In the first group, the system changes the colour without the “help” of an agent and, when the heating is stopped, the system should come back to the original state. Some compounds showing this type of thermochromism are spirooxazines, bianthrylidenes and Liquid Crystals.

The Thermochromic Liquid Crystals (TLCs) are the most famous and common systems showing thermo-responsive behaviour; their use is traceable in thermometers, biomedical devices, temperature-sensitive pigments and in cosmetics.<sup>151</sup> The colour change of TLC is due to the change in the space of the chiral nematic and cholesteric mesophases. As a consequence, certain wavelengths are reflected depending on the interlayer distance.<sup>152</sup>

The “thermo-spot” was one of the first medical devices composed of TLCs. This medical sensor monitors the neonates temperature in a really narrow range: 35.5 °C (black), 35.5-36.4 °C (brown) and 36.5 °C (green). This device has been useful to diagnose hypothermia of suffering neonates and children, with a sensitivity over 95 %.<sup>153</sup>

The indirect thermochromic system is composed of two fundamental elements, a pH-sensitive pigment and a proton donor. Several dyes are pH sensitive, and, the temperature determines the change of the environment, which results in different absorption. Usually, these systems are based on spiro lactone and fluoran compounds, and, the ring opening is usually associated with a change in colour.<sup>154</sup>

---

150. Towns, A. D., Thermochromic composite materials formulated from spiro lactone colour formers. In *ChemiChromics*, New Orleans, USA, 1999; Vol. Proceedings of ChemiChromics USA '99.

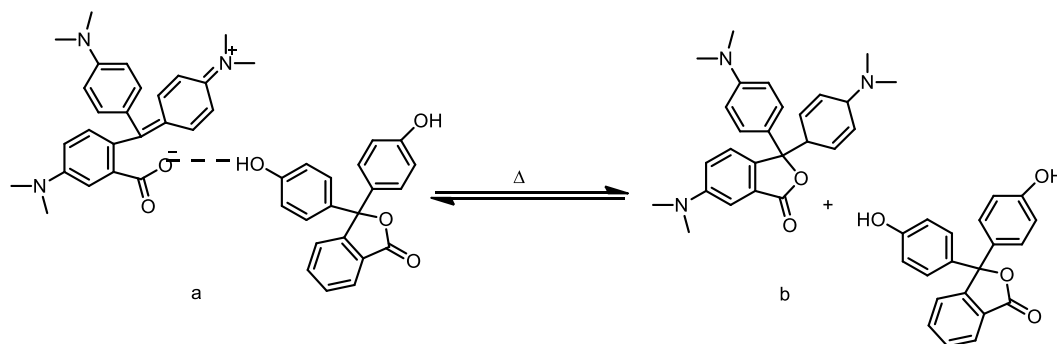
151. *Handbook of Thermochromic Liquid Crystal Technology*. LCRHallcrest: Pickwick Lane, Glenview, IL 60026, **2014**.

152. Smith, C. R.; Sabatino, D. R.; Praisner, T. J., Temperature sensing with thermochromic liquid crystals. *Experiments in Fluids* **2001**, *30* (2), 190-201.

153. Mole, T. B.; Kennedy, N.; Ndoya, N.; Emond, A., ThermoSpots to Detect Hypothermia in Children with Severe Acute Malnutrition. *PLoS One* **2012**, *7* (9), e45823.

154. Burkinshaw, M. S.; Griffiths, J.; Towns, D. A., Reversibly thermochromic systems based on pH-sensitive functional dyes. *J. Mater. Chem.* **1998**, *8* (12), 2677-2683.

Scheme 12 reports an explicative example of this kind of system, where the opened and closed form of the most studied Crystal Violet Lactone are in equilibrium, corresponding to a blue thermochromism due to hydrogen bond.<sup>155</sup>



**Scheme 12 - Equilibrium between: a) the ring-opened form (coloured); b) the ring-closed form (colourless) for the Crystal Violet Lactone.**<sup>155</sup>

Although from the beginning, the thermochromism is defined as a reversible phenomenon, several irreversible thermochromic effects can be included.

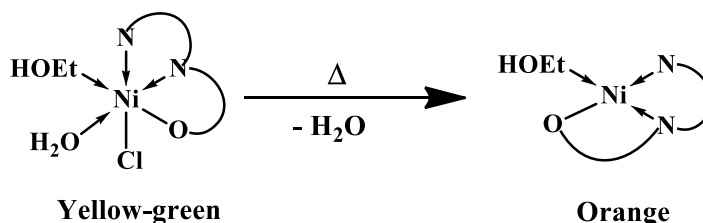
Usually, this kind of thermochromism occurs in the solid state, and, also in this case, a general distinction can be made. The colour change for some substances, can be definitely irreversible, *i.e.* there is no equilibrium and the final species is thermodynamically stable. In this case, the phenomenon is named “thermodynamically irreversible Thermochromism”. This situation is different from the colour change in the “kinetically irreversible thermochromism”, in which an equilibrium exists between the two coloured forms. In this case, the reverse reaction is relatively slow and only the kinetically stable system can be observed.<sup>156</sup>

A common and well known irreversible thermochromism is the dehydration of metal complexes. Scheme 13 reports the heating process for the yellow-green Ni(II) complex. This complex changes to orange when it is heated in the solid state at over 200 °C. The change from octahedral to a square planar geometry is

155. Raditoiu, A.; Raditoiu, V.; Nicolae, C. A.; Raduly, M. F.; Amariutei, V.; Wagner, L. E., Optical and structural dynamical behavior of Crystal Violet Lactone – Phenolphthalein binary thermochromic systems. *Dyes Pigm.* **2016**, *134*, 69-76.

156. Sone, K.; Fukuda, Y., *Inorganic Thermochromism*. Springer, Berlin, Heidelberg: **1987**; Vol. 10.

responsible for the orange colour of the compound, in which the chloride ion moves from the inner to the outer coordination sphere.<sup>157</sup>



Scheme 13 - Dehydration of Ni(II) complex showing irreversible Thermochromism.<sup>157</sup>

There are various thermochromic phenomena of metal complexes involving different mechanisms upon which their application is based.

### 4.3. The thermochromism of metal complexes

The thermochromism phenomena involving metal complexes are mainly related to the change in the ligand field strength or to the change in the coordination geometry. The colour change is usually associated with a  $d \rightarrow d$  transition, as consequence of changes in the interaction with the ligands, both in term of strength and number. In this case, interactions with other ligands present in the environment are brought about by the effect of temperature.<sup>158,156</sup>

The geometry of a complex depends on the strength of the ligand field, *i.e.* the capacity of the ligand to split the orbitals of the complex; the higher is the split, the higher is the energy an electron needs to transition from an orbital at lower energy to another one at higher energy. The ligand field strength increases along the spectrochemical series: (*weak*)  $I^- < Br^- < S^{2-} < [SCN]^- < Cl^- < [NO_3]^- < N_3^- < F^- < [OH]^- < C_2O_4^{2-} \approx H_2O < [NCS]^- < CH_3CN < py < NH_3 < en < bipy < phen < [NO_2]^- < PPh_3 < [CN]^- \approx CO$  (*strong*).<sup>159</sup>

157. Donia, A. M.; El-Boraey, H. A., Reversible and irreversible thermochromism of some Schiff base metal complexes. *Transition Met. Chem.* **1993**, 18 (3), 315-318.

158. Bloomquist, D. R.; Willett, R. D., Thermochromic phase transitions in transition metal salts. *Coord. Chem. Rev.* **1982**, 47 (1), 125-164.

159. Rodgers, G. E., *Introduction to coordination, solid state, and descriptive inorganic chemistry*. New York (N.Y.) : McGraw-Hill: **1994**.

A weak field ligand shows a small gap between the orbitals and determines a high spin complex, *i.e.* the distribution of the electrons in the complex orbitals firstly favours the filling of all orbitals before pairing the electrons. A strong field ligand displays an opposite situation, which generally leads to a low spin complex. The split of the orbitals derives from the crystal field theory, in which it is assumed that a metal shows degenerate *d*-orbitals. The presence of the ligands determines a change in the *d*-orbitals energy. The different split depends on the nature of the ligand and metal (*vide supra* the spectrochemical series). Indeed, ligands approach the metal from a different direction which induces a splitting of the orbitals. Strength and nature of the ligand, size and oxidation state of the metal affect crystal field splitting.

The different colours are related to the geometry of the complex and, to the ligand field. Low spin complexes absorb the light radiation at higher energy, corresponding to lower wavelengths, while high spin complexes absorb it at higher wavelengths.<sup>160</sup>

The spin configuration, however, can be affected by changes in pressure, temperature, light and by promoting the cross-over, *i.e.* the transition of one or more electrons in a higher energy free orbital.<sup>161</sup> Moreover, the variation of temperature and, the complex energy could induce changes in the number of ligand coordinating the metal centre and consequently the geometry of the complex, because of the interaction with another compound in solution which becomes new ligand, or oppositely, the loss of one or more ligands.

Curtis and House studied the behaviour of  $[\text{Ni}(\text{trien})(\text{py})_2]^{2+}$  in polar solvents, in which this compound establishes a thermochromic equilibrium, changing colour from violet to yellow. Violet corresponds to the octahedral coordination while yellow is the consequence of the loss of one molecule of pyridine.<sup>162</sup>

Goodgame and Hitchmann studied diamine complex of nickel in chloroform. In particular, the equilibrium which involves the nitro (red) and the nitrito (blue)

---

160. Wolfram, T.; Ellialtıođlu, Ő., Crystal-field theory. In *Applications of Group Theory to Atoms, Molecules, and Solids*, Wolfram, T.; Ellialtıođlu, Ő., Eds. Cambridge University Press: Cambridge, **2014**; pp 90-122.

161. *Spin Crossover in Transition Metal Compounds I*. 1 ed.; Springer-Verlag Berlin Heidelberg: **2004**.

162. Curtis, N. F.; House, D. A., 1153. Transition-metal complexes of triethylenetetramine. Part II. Some nickel(II) and copper(II) derivatives. *J. Chem. Soc.* **1965**, (0), 6194-6197.



complexes,  $[\text{Ni}(\text{diam})_2(\text{NO}_2)_2] \rightleftharpoons [\text{Ni}(\text{diam})_2(\text{ONO})_2]$ , was investigated. In solution of a suitable solvent, the conversion from -ONO to -NO<sub>2</sub> can occur and the solution appears red. However, upon heating the solution, the energy-rich nitrito complex is the predominant complex and the solution becomes blue.<sup>163</sup>

### 4.3.1 Cobalt, an increasingly useful metal

Cobalt is a ferromagnetic metal with a shiny appearance (m.p. 1493 °C, b.p. 3100 °C). Its magnetism is retained until 1100 °C, the highest temperature among metals. The valence shell electron configuration is  $(3d)^7(4s)^2$ . This metal was used since ancient times for its blue colour mainly in glass and porcelain decorations.<sup>164</sup> In recent time, cobalt was used to form superalloys with nickel and iron, obtaining excellent performance at high temperatures against the corrosion and powerful magnets.<sup>165</sup> Different type of alloys have been also applied in medical devices,<sup>166</sup> even if, in this field, titanium alloys are preferred to cobalt ones. Finally, cobalt is also used for the preparation of classical or film electrodes.<sup>167</sup>

Recently, cobalt is becoming more useful in storage energy devices. Poizot investigated and proposed a new anode for the Lithium-ion batteries, based on a nano-sized transition-metal oxide. Cobalt oxides showed the best electrochemical properties as storage materials in the lithium batteries.<sup>168</sup> The good performance in

---

163. Goodgame, D. M. L.; Hitchman, M. A., Studies of Nitro and Nitrito Complexes. III. Some Nitro Complexes of Nickel(II) and a Nitro-Nitrito Equilibrium. *Inorg. Chem.* **1966**, 5 (8), 1303-1307.

164. Rehren, T. H., Aspects of the Production of Cobalt-blue Glass in Egypt. *Archaeometry* **2001**, 43 (4), 483-489.

165. Crook, P. Cobalt superalloy. **1981**.

166. Lemons, J. E.; Niemann, K. M. W.; Weiss, A. B., Biocompatibility studies on surgical-grade titanium-, cobalt-, and iron-base alloys. *Journal of Biomedical Materials Research* **1976**, 10 (4), 549-553.

167. Fan, Y.; Fan, L.; Meng, S.; Guo, Y.; Liu, Y., Preparation of cobalt hydroxide film modified electrode and its analytical application. *J. Anal. Chem.* **2012**, 67 (4), 370-377.

168. Poizot, P.; Laruelle, S.; Grugeon, S.; Dupont, L.; Tarascon, J. M., Nano-sized transition-metal oxides as negative-electrode materials for lithium-ion batteries. *Nature* **2000**, 407, 496.

the energy storage led to the common use of this metal in laptop, computer and phone devices.<sup>169</sup>

The large number of studies about cobalt are not surprising, considering its properties; most insights are reported in organometallic and coordination chemistry fields.<sup>170</sup> In particular, cobalt has been widely studied for its thermochromic behaviour upon ligand exchange.

Mehalana *et al.* investigated pyridyl-benzoate complexes of cobalt at different stoichiometry ( $\{[Co(34pba)_2] \cdot DMF\}_n$ , where 34pba is 3-(4-pyridyl)benzoate), showing thermochromism at the temperature of 281 and 347 °C in dependence on the structure. The switch from pink to blue is related to the change in the coordination geometry from octahedral to tetrahedral.<sup>171</sup>

Shen *et al.* studied also the interaction of water as ligand for Co(II). They synthesised three new ligands for cobalt, based on the 1,3,5-triazine derivatives (Figure 35). With these ligands, four complexes with cobalt were obtained and all of them showed a thermochromic behaviour when heated under vacuum. In particular, three of them displayed the switch from pink to purple, at 150 °C, and only one from orange to purple, at 180 °C. The systems were reversible when exposed to air. Study of magnetic susceptibility permitted determining the octahedral geometry for the pink complexes at room temperature. The different colour of the fourth complex at room temperature (orange instead of pink) could be ascribed to a different role of water molecules in the coordination sphere of cobalt.<sup>172</sup>

---

169. Johnson, C. S.; Li, N.; Lefief, C.; Vaughey, J. T.; Thackeray, M. M., Synthesis, Characterization and Electrochemistry of Lithium Battery Electrodes:  $xLi_2MnO_3 \cdot (1 - x)LiMn_0.333Ni_0.333Co_0.333O_2$  ( $0 \leq x \leq 0.7$ ). *Chem. Mater.* **2008**, *20* (19), 6095-6106.

170. Kemmitt, R. D. W.; Russell, D. R., 34 - Cobalt. In *Comprehensive Organometallic Chemistry*, Wilkinson, G.; Stone, F. G. A.; Abel, E. W., Eds. Pergamon: Oxford, **1982**; Vol. 5, pp 1-276.

171. Mehlana, G.; Bourne, S. A.; Ramon, G.; Öhrström, L., Concomitant Metal Organic Frameworks of Cobalt(II) and 3-(4-Pyridyl)benzoate: Optimized Synthetic Conditions of Solvatochromic and Thermochromic Systems. *Cryst. Growth Des.* **2013**, *13* (2), 633-644.

172. Shen, C.; Sheng, T.; Zhu, Q.; Hu, S.; Wu, X., Four new cobalt(ii) coordination complexes: thermochromic switchable behavior in the process of dehydration and rehydration. *CrystEngComm* **2012**, *14* (9), 3189-3198.

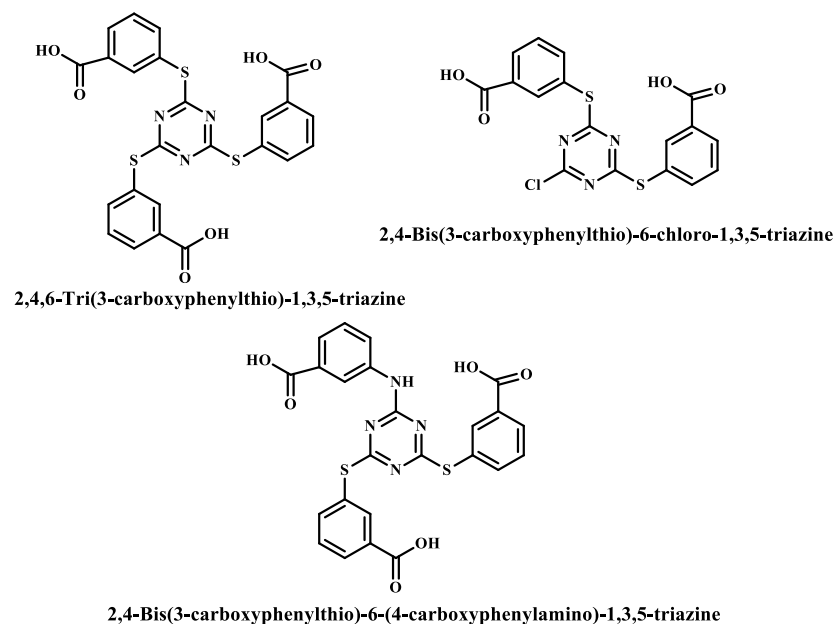


Figure 35 - Triazine ligands to form cobalt complexes.<sup>172</sup>

### 4.3.2 The help of ILs to perform cobalt thermochromism

In previous paragraphs the main principles of chromism and thermochromism were explained. In this context, the metal and the ligands were considered without deeply investigating the solvent. However, if a system is designed for a particular application also this factor has to be considered. For example, temperature reached in energy devices is fundamental for the right operation of device itself. In this case the solvent cannot be ignored and it becomes a priority in the design of system.

Cobalt thermochromism discussed above is featured by the switch between the octahedral and the tetrahedral coordination geometries, depending on the presence of the hydroxyl ligand (usually the water). However, to utilise all the advantages from a device based on cobalt thermochromism, the solvent should not evaporate during the heating process. In addition, the ligand should always be present in the system, without any need to refill it after every process.

A better way to avoid loss of solvent is to use a non-volatile one. ILs, also in this case, could be the solution. The thermal stability and the negligible vapour pressure determine their good performance in the heating process. Moreover,

another advantage is their capacity to dissolve many metal complexes and metallorganic compounds.<sup>173</sup>

Gadžurić and co-workers reported a thermochromic study in which the metal/ligand ratio determines the thermochromic behaviour. In particular, they came up with a system in which the  $[\text{NH}_4][\text{NO}_3]$  is mixed with a second component, such as an organic solvent. These solvent systems were used to dissolve different molar ratios of Co(II) and chloride ( $2 \leq \text{molar ratio} \leq 80$ ). The mixtures obtained were investigated at two different temperatures: 298.15 K and 323.15 K. However, only slight changes in colour, due to the system components and the temperature taken into consideration, were detected. The energy given to the complexes was not sufficient to switch the geometry from the octahedral (pink solution), at room temperature, to tetrahedral one (blue solution), at 323.15 K. The change in the colour was mainly achieved as a consequence of the concentration instead of the temperature.<sup>174</sup>

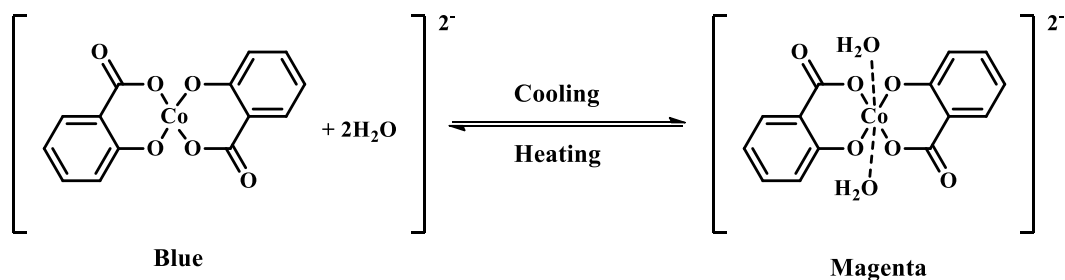
Konho *et al.* synthesised and studied the water-dependent thermochromism of the  $[\text{P}_{4444}]_2[\text{Co}^{\text{II}}(\text{sal})_2]$  square-planar complex (Scheme 14). This complex shows a blue coloration, which in presence of water, both in liquid or gas state, establishes two coordination bonds with two molecules of water. The new coordination sphere determines the switch of the colour to magenta and the consequent distortion of the complex geometry. The heating permits obtaining once again the original blue complex. However, also in this case, the thermochromism was more connected to the ligand than to the temperature. Indeed, the system is not self-contained and water is necessary as an external ligand to observe the thermochromism.<sup>175</sup>

---

173. Dyson, P. J., Transition metal chemistry in ionic liquids. *Transition Met. Chem.* **2002**, 27 (4), 353-358.

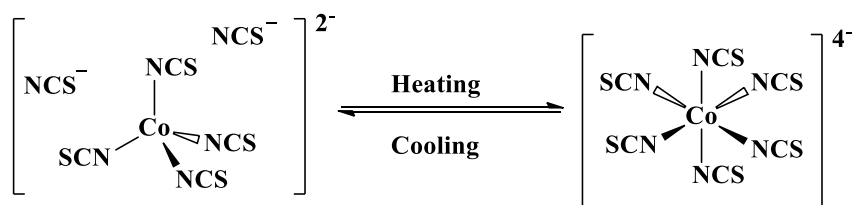
174. Gadžurić, S.; Vraneš, M.; Dožić, S., Thermochromic cobalt(II) chloro-complexes in different media: Possible application for auto-regulated solar protection. *Sol. Energy Mater. Sol. Cells* **2012**, 105, 309-316.

175. Kohno, Y.; Cowan, M. G.; Masuda, M.; Bhowmick, I.; Shores, M. P.; Gin, D. L.; Noble, R. D., A cobalt(ii) bis(salicylate)-based ionic liquid that shows thermoresponsive and selective water coordination. *Chem. Commun.* **2014**, 50 (50), 6633-6636.



Scheme 14 - Thermochemical equilibrium of the  $[P_{4444}]_2[Co^{II}(sal)_2]$  complexes, in the hydrated (right) and anhydrous (left) form.<sup>175</sup>

Thermochromic cobalt complexes were obtained by Osborne *et al.* using the isothiocyanate cobalt complex dissolved in thiocyanate ILs. The complex,  $[Co(NCS)_4]^{2-}$ , displays the blue colour related to the tetrahedral geometry. This changes colour and coordination sphere after heating (octahedral geometry, red complex,  $[Co(NCS)_6]^{4-}$ ). The two complexes established an equilibrium between the two coordination forms, showing a significant increase in the magnetic moments (of the complexes) as a consequence of coordination changes. However, to obtain the tetrahedral complex, it was necessary to cool the system in a temperature range between  $-25$  and  $-40$  °C (Scheme 15).<sup>176</sup>



Scheme 15 - Equilibrium of the Co-isothiocyanate complexes between the tetrahedral (left) and the octahedral (right) geometry depending on the change of the temperature.<sup>176</sup>

These examples related to cobalt demonstrate how the thermochromic behaviour usually involves the octahedral-tetrahedral coordination switch, adding or removing two ligands from the coordination sphere of cobalt. However, even if the coordination change has been deeply investigated, it is not easy to obtain a

176. Osborne, S. J.; Wellens, S.; Ward, C.; Felton, S.; Bowman, R. M.; Binnemans, K.; Swadzba-Kwasny, M.; Gunaratne, H. Q. N.; Nockemann, P., Thermochromism and switchable paramagnetism of cobalt(ii) in thiocyanate ionic liquids. *Dalton Trans.* **2015**, 44 (25), 11286-11289.

reversible thermochromic system in a mild temperature range. Indeed, the necessity of an external ligand or a strong change in the temperature range makes the system not suitable for some applications. Consequently, the achievement of self-contained systems, which show thermochromic behaviour in a mild temperature range could be the way to construct new thermochromic devices.

#### **4.4. Thermochromism of IL-Co complexes in IL: the achievement of the mild temperature range**

In Chapter 4, ILs and ILGs were presented as good materials for environmental remediation. However, another issue strongly related to environmental safety is the energy demand and production. The modern society is based on energy sources as in daily life every process consumes energy. If we start to think what we can do without energy, the answer is nothing, as we spend energy to produce food, use transports, communicate and work.

In Italy, for example, the average quantity of electrical energy consumed by a family is around 2300 kWh per year (data from the National Statistical Institute – ISTAT).<sup>177</sup>

In a global view, the demand for energy will increase, considering the growing dependence of the society on “smart” devices, such as smartphones, laptop and so on. The first step could be to optimise and “clean” the production of energy, for example, using less Carbon sources and enhancing use of natural ones, by improving the efficiency of solar panels, wind turbines, wave powers. The second step should be the production of devices which have longer “life” consuming less energy. To achieve this goal the design of new batteries is necessary.

In this context, the second part of the Research Project was developed. The structure of ILs synthesised and characterised make them amenable for interaction with metal ions, in particular transition metals and lanthanides.

Among transition metals, the interest was focused on cobalt. The presence of this metal in lithium batteries applied in new smart devices was briefly

---

177. ISTAT [http://dati.istat.it/Index.aspx?DataSetCode=DCCV\\_CNSENRG](http://dati.istat.it/Index.aspx?DataSetCode=DCCV_CNSENRG).

mentioned.<sup>178</sup> Cobalt is usually part of the cathode and at the moment its performance is unique. In lithium batteries, lithium cobalt oxide cathode consists of about 60 % of cobalt. The indicator of the essential role of cobalt in the “smart” era is its price per ton. In 2016 a ton of cobalt oscillated between \$20,000 and \$30,000 and in 2018 the price has already reached \$80,000.<sup>179</sup>

Taking into account all above considerations, the interaction of halide ILs bearing the gluconic moiety on the cation with cobalt was investigated. The choice of these ILs rather than gluconate ones, is based on the structure as the concomitant presence of the hydroxylated chain,<sup>180</sup> amide function<sup>181</sup> and the halide anion<sup>182</sup> can be useful in coordinating metals.

#### 4.4.1 Thermochromic behaviour and UV-Vis spectroscopy investigations

The [N<sub>11</sub>2GA8]Br was chosen as an IL to check its coordination capability in the presence of cobalt salt, Co(NTf<sub>2</sub>)<sub>2</sub>.

The initial idea was to use the IL-ligand in excess with respect to the metal, considering the possibility that the metal could coordinate more than one molecule at the same time.

---

178. (a) Scrosati, B.; Garche, J., Lithium batteries: Status, prospects and future. *J. Power Sources* **2010**, *195* (9), 2419-2430, (b) Whittingham, M. S., Lithium Batteries and Cathode Materials. *Chem. Rev.* **2004**, *104* (10), 4271-4302.

179. King, A., Battery builders get the cobalt blues. *Chemistry World* **2018**.

180. (a) Zheng, X.-J.; Jin, L.-P.; Gao, S., Synthesis and Characterization of Two Novel Lanthanide Coordination Polymers with an Open Framework Based on an Unprecedented [Ln7(μ<sub>3</sub>-OH)8]13+ Cluster. *Inorg. Chem.* **2004**, *43* (5), 1600-1602, (b) Tsyganenko, A. A.; Filimonov, V. N., Infrared spectra of surface hydroxyl groups and crystalline structure of oxides. *J. Mol. Struct.* **1973**, *19*, 579-589.

181. Sigel, H.; Martin, R. B., Coordinating properties of the amide bond. Stability and structure of metal ion complexes of peptides and related ligands. *Chem. Rev.* **1982**, *82* (4), 385-426.

182. (a) Schock, L. E.; Marks, T. J., Organometallic thermochemistry. Metal hydrocarbyl, hydride, halide, carbonyl, amide, and alkoxide bond enthalpy relationships and their implications in pentamethylcyclopentadienyl and cyclopentadienyl complexes of zirconium and hafnium. *J. Am. Chem. Soc.* **1988**, *110* (23), 7701-7715, (b) Stambuli, J. P.; Incarvito, C. D.; Bühl, M.; Hartwig, J. F., Synthesis, Structure, Theoretical Studies, and Ligand Exchange Reactions of Monomeric, T-Shaped Arylpalladium(II) Halide Complexes with an Additional, Weak Agostic Interaction. *Ibid.* **2004**, *126* (4), 1184-1194.

The  $[\text{N}_{1.12}\text{GA}_8]\text{Br}/\text{Co}(\text{NTf}_2)_2$  molar ratios taken into consideration were: 1.5:1; 3:1; 5:1; 6:1; 7:1.

However, as already explained in the Chapter 2, the ILs synthesised were very viscous. This is the reason why a “solvent” was necessary to solubilise the metal and the ligand to favour the interactions.

The solvent chosen was another IL, the  $[\text{N}_{2.224}][\text{NTf}_2]$ . The reason is again ascribed to the thermal stability and the negligible vapour pressure of this class of compounds. Moreover, IL nature was chosen considering the environmental sustainability of the cation and the non-coordinating ability of anion for cobalt.

The cobalt salt is a pink solid which maintains its colouration when is dissolved in IL-solvent. When IL-ligand was added and solubilised upon heating, all solutions at different ratio assumed a blue coloration (Figure 36).

However, when solutions were cooled down to room temperature, solutions at 3:1, 5:1, 6:1, 7:1 ratios came back to a pink colouration, while the 1.5:1 ratio solution remained blue.



**Figure 36 - Solution of  $[\text{N}_{1.12}\text{GA}_8]\text{Br}/\text{Co}(\text{NTf}_2)_2/[\text{N}_{2.224}][\text{NTf}_2]$  at 65 °C, varying the ligand/metal ratio from 1.5:1 to 7:1.**

To investigate the above phenomena, UV-Vis spectra were recorded in the temperature range 15-95 °C (VT UV-Vis). Colour shades during UV-Vis measurements and spectra for solutions with ratio 3:1 - 7:1 are reported in Figure 37 and 38, respectively.



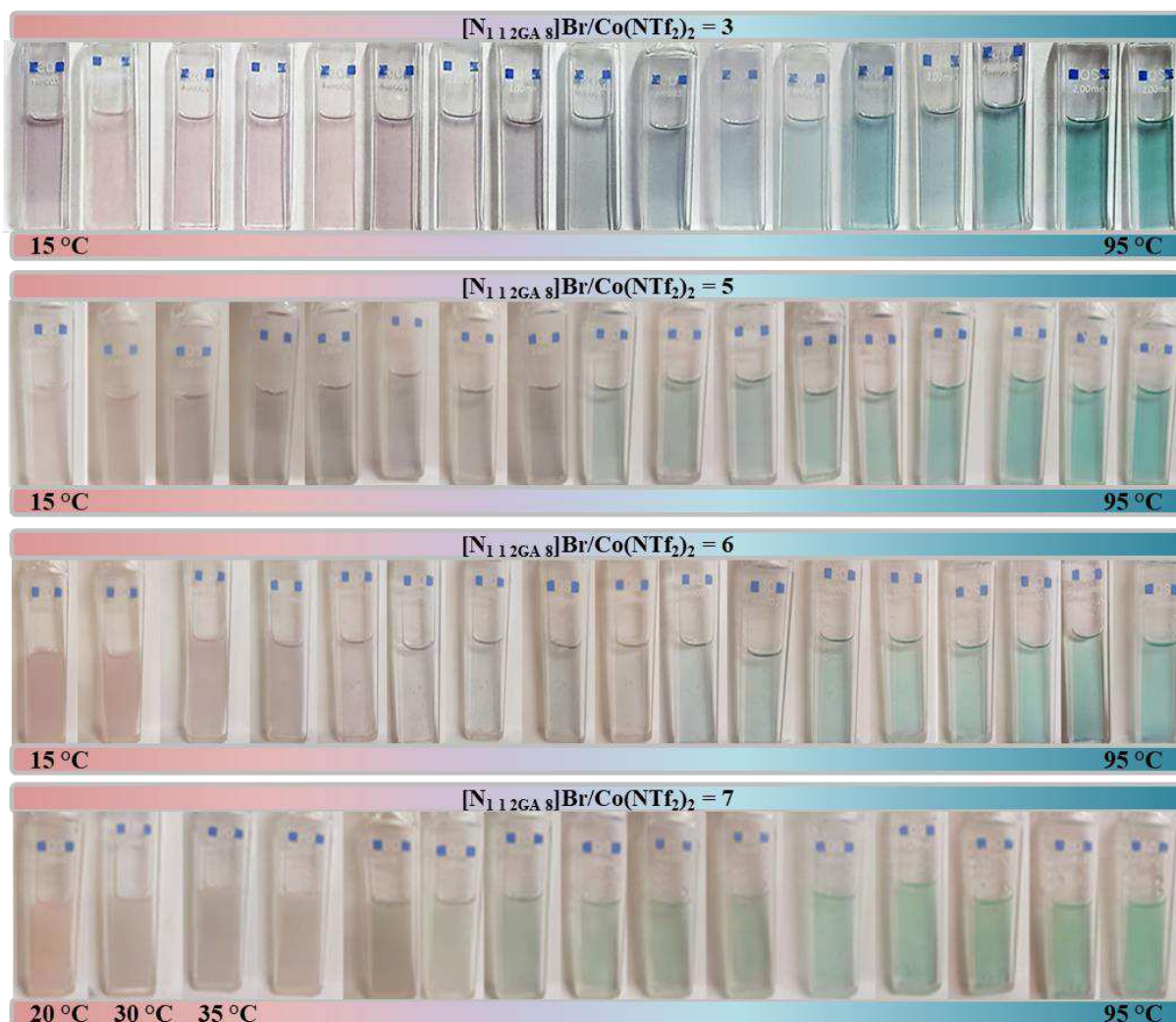
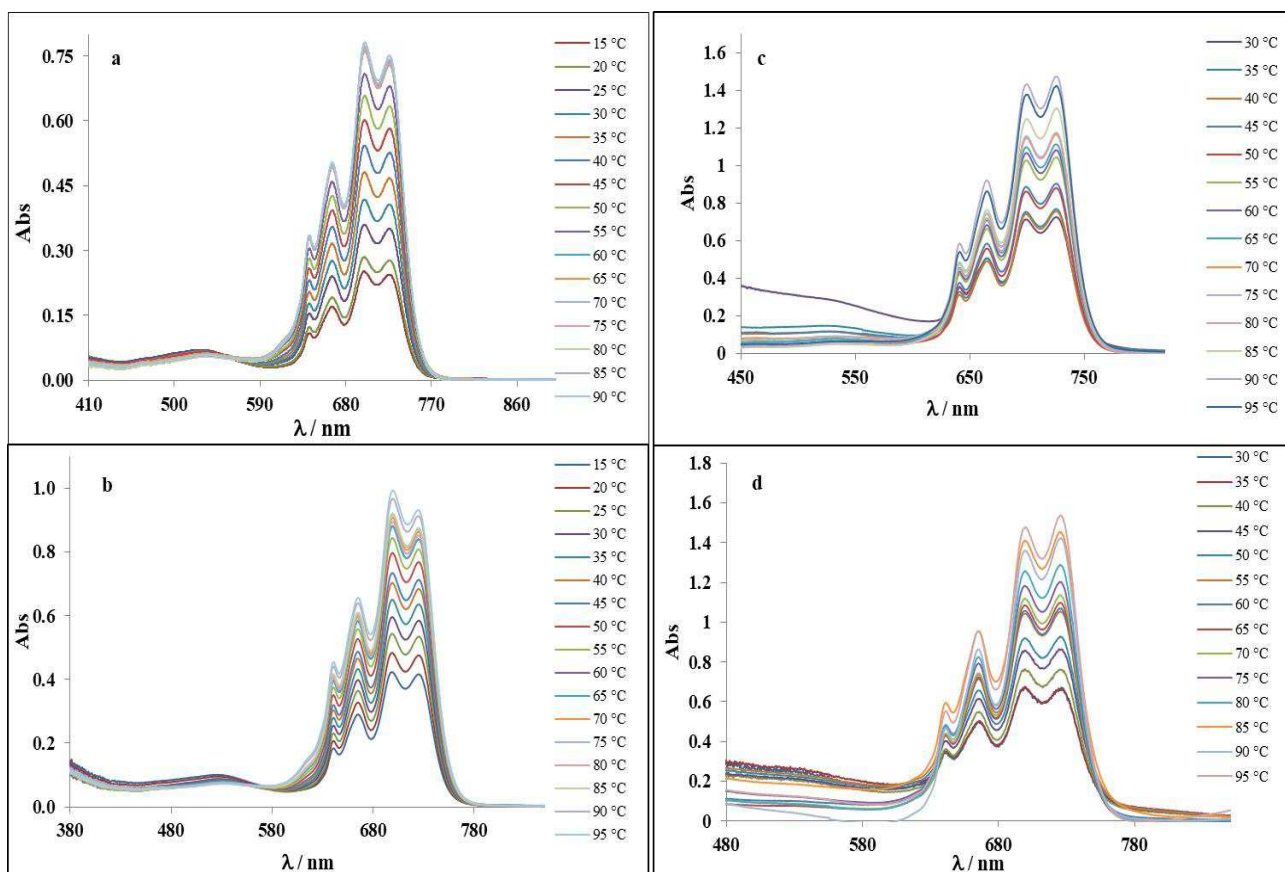


Figure 37 - Colour shades for the solution  $[N_{112GA8}]Br/Co(NTf_2)_2/[N_{2224}][NTf_2]$  in the concentration ratios: 3:1 -7:1. The range of temperature: 15-95 °C (the temperature increases of 5 °C- only in the ratio 7:1 the temperature increase of 10 °C up to 30°C) .

Preliminary information on the influence of concentration is provided by the appearance of each solution. Systems with [ligand]/[metal] ratio 3:1 and 5:1 showed clear solutions for each temperature considered, and the transition from pink to blue occurred at a different temperature depending on the ratio used.

In the case of systems with ratios 6:1 and 7:1, the higher concentration of the ligand is reflected in the opalescent appearance of solutions at 15 and 20 °C, respectively. Moreover, for the last ratio, the opalescence endures up to high temperatures, albeit with lower intensity.



**Figure 38 - VT UV-Vis spectra of the solution  $[N_{112GA8}]Br/Co(NTf_2)_2/[N_{2224}][NTf_2]$  at different ratios: a) 3:1; b) 5:1; c) 6:1; d) 7:1.**

Generally, spectra reported clearly show the relation between the concentration of the ligand and the absorbance, the increase of the first one corresponds also to the increase of the second. However, if for spectra in Figure 38-a and 38-b, the only difference can be detected in absorbance values, for the ones in Figure 38-c and 38-d some considerations have to be made. For these solutions, spectra in the range 15-25 °C cannot be satisfactorily recorded, due to their opalescence. Moreover, the base-line for spectra in Figures 38-c,d were still high.

For systems with ratio 3:1 and 5:1, the band in the range ~440-600 nm can be detected more clearly. Differently, the group of bands in the range ~600-790 appears in all spectra. These bands increase in absorbance upon raising the temperature. For the first band, at lower wavelengths (440-600 nm), absorbance drops at higher temperature.

According to the literature reports, the band at 400-600 nm corresponds to an octahedral complex in solution.<sup>176</sup> The weak absorption is due to a transition

forbidden by Laporte rule. Indeed, the octahedral complex features a centre of symmetry and, consequently,  $d \rightarrow d$  transition is not allowed. The absorption will proportionally increase with the distortion of the octahedral symmetry.<sup>183</sup>

As already said, the absorbance of the group of bands at longer wavelengths (600-800 nm) increases with the temperature. This should indicate the formation of a tetrahedral complex in solution, which lacks a centre of symmetry and, as consequence, Laporte rules do not apply. This results in a strong band in UV-Vis spectra.

In solution, an equilibrium between the octahedral and the tetrahedral coordination geometry could be established. This is shifted toward octahedral or tetrahedral geometry depending on the temperature and confirmed by the isosbestic point traceable in the spectra between the two groups of bands.

The isosbestic points move at longer wavelengths with the increase in ratio: 550 nm - 561 nm - 605 nm - 633 nm for systems using ratios 3:1 - 5:1 - 6:1 - 7:1, respectively. The shift should be related to change in the equilibrium due to the higher amount of ligand. This affects the availability of the ligand in solution and alters the interaction between the metal and the ligand.

The above behaviour was visually observed in the colour change of solutions differing for the [ligand]/[metal] ratios.

To deeply analyse the UV-Vis measurements, the absorbance at the maximum of the band of the tetrahedral complex is reported as a function of the temperature (Figure 39). Interestingly, the position of the longest wavelength band does not change along the whole range of ratios considered, and remains centered between 725.0-725.5 nm. Moreover, absorbances follow different trends depending on which [ligand]/[metal] ratio is used. Indeed, only with a [ligand]/[metal] ratio equal to 3:1, a clear plateau region is detected. This becomes less evident using a ratio equal to 5:1, whereas in the other two cases, more irregular trends with changes in slope can be observed. Such differences do not reflect in the visual appearance of the solutions, which in all cases goes from pink to blue. This phenomenon could be due to a reorganisation of the complexes in solution.

---

183. Miessler, G. L.; Tarr, D. A., *Inorganic Chemistry*. second ed.; Prentice Hall: 1998.

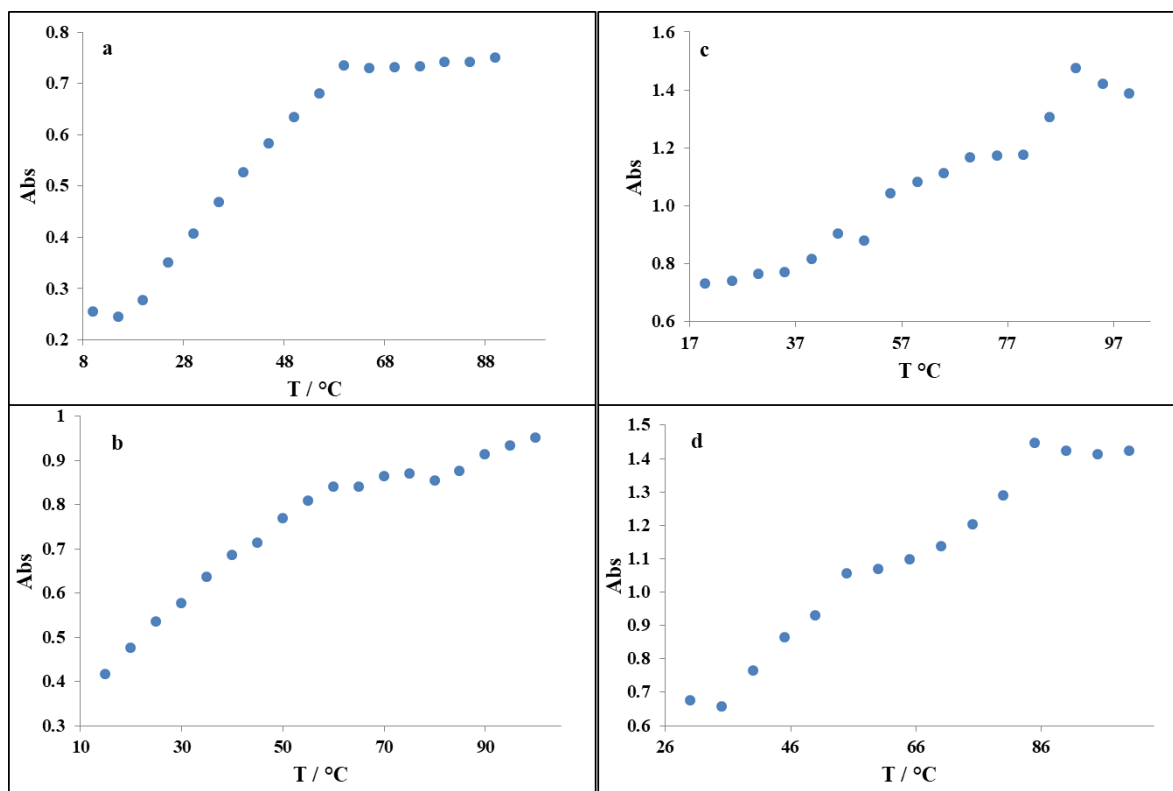


**Figure 39 - VT UV-Vis absorbance (725.0 nm) trends with the temperature of the solution  $[N_{1 1 2GA}]Br/Co(NTf_2)_2/[N_{2 2 2 4}][NTf_2]$  at different ratios: a) 3:1; b) 5:1; c) 6:1; d) 7:1.**

The plateau region should correspond to the presence in solution of the tetrahedral complex as the predominant species. The intersection of the two linear traits of the curve allows determining the temperature of the geometry switch ( $T_{switch}$ ). These values are reported in Table 23.

**Table 23 - Temperature of the geometry switch for the system  $[\text{N}_{112\text{GA}8}]\text{Br}/\text{Co}(\text{NTf}_2)_2/[\text{N}_{2224}][\text{NTf}_2]$  at different ratios. \* =  $T_{\text{switch}}$ s were reproducible within 1 °C.**

Thermochromic system	Ratio [ligand]/[metal]	$T_{\text{switch}}$ °C*
$[\text{N}_{112\text{GA}8}]\text{Br}/\text{Co}(\text{NTf}_2)_2/[\text{N}_{2224}][\text{NTf}_2]$	3:1	59
$[\text{N}_{112\text{GA}8}]\text{Br}/\text{Co}(\text{NTf}_2)_2/[\text{N}_{2224}][\text{NTf}_2]$	5:1	80
$[\text{N}_{112\text{GA}8}]\text{Br}/\text{Co}(\text{NTf}_2)_2/[\text{N}_{2224}][\text{NTf}_2]$	6:1	82
$[\text{N}_{112\text{GA}8}]\text{Br}/\text{Co}(\text{NTf}_2)_2/[\text{N}_{2224}][\text{NTf}_2]$	7:1	85

$T_{\text{switch}}$ s increase with the ligand/metal ratios. However, for ratios higher than 3:1,  $T_{\text{switch}}$  does not match with the visual colour change of the solution (Figure 37). Probably, in the above cases, initial tetrahedral complex formation occurs in a small quantity and it changes the colour of the solution. However, the change of metal coordination proceeds slower also as consequence of the increased viscosity of the solution.

Considering the results obtained in solution, a [ligand]/[metal] ratio equal to 3:1 was considered as the best condition and was used for further investigation.

We firstly ensure a that the IL-solvent did not induce any thermochromic phenomenon so, to achieve this goal, VT UV-Vis investigation was performed in absence of ligand,  $[\text{N}_{112\text{GA}8}]\text{Br}$ . It was observed that with the increase of temperature the solution did not change the colour, and maintained the pink colouration. Moreover, the spectra reported in Figure 40 highlight the absence of the tetrahedral complex, as only the band between 400-600 nm appears with an absorbance lower than the one detected for the system  $[\text{N}_{112\text{GA}8}]\text{Br}/\text{Co}(\text{NTf}_2)_2/[\text{N}_{2224}][\text{NTf}_2]$  using a ratio equal to 3:1.

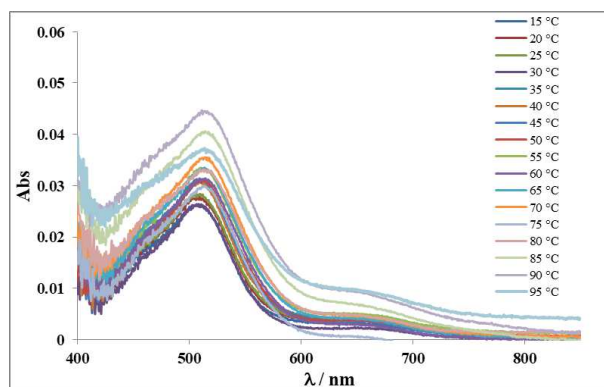


Figure 40 - VT UV-Vis spectra for the system  $\text{Co}(\text{NTf}_2)_2/[\text{N}_{2,2,4}][\text{NTf}_2]$ .

Subsequently, the effect due to the solvent nature was analysed. To this aim, the system  $[\text{N}_{1,1,2\text{GA},8}]\text{Br}/\text{Co}(\text{NTf}_2)_2$  was investigated in different solvents. In particular,  $[\text{N}_{1,1,1,3}][\text{NTf}_2]$  and  $[\text{C}_1\text{C}_4\text{pyrr}][\text{NTf}_2]$  were chosen.

Compared to  $[\text{N}_{2,2,4}][\text{NTf}_2]$ ,  $[\text{N}_{1,1,1,3}][\text{NTf}_2]$  bears shorter alkyl chain on the cation and is less viscous ( $\eta = 72.0$  cP and  $\eta = 104.1$  cP for  $[\text{N}_{1,1,1,3}][\text{NTf}_2]$  and  $[\text{N}_{2,2,4}][\text{NTf}_2]$ , respectively). On the other hand,  $[\text{C}_1\text{C}_4\text{pyrr}][\text{NTf}_2]$  has a viscosity comparable to  $[\text{N}_{1,1,1,3}][\text{NTf}_2]$  ( $\eta = 84.3$  cP), but it is characterised by the presence of a cyclic cation. The thermochromic behaviour, from the pink solution to the blue one, was retained also in different solvents (Figure 41) and the VT UV-Vis investigation is reported in Figure 42.



Figure 41 - Colour shades for the solution  $[\text{N}_{1,1,2\text{GA},8}]\text{Br}/\text{Co}(\text{NTf}_2)_2/[\text{C}_1\text{C}_4\text{pyrr}][\text{NTf}_2]$  and  $[\text{N}_{1,1,2\text{GA},8}]\text{Br}/\text{Co}(\text{NTf}_2)_2/[\text{N}_{1,1,1,3}][\text{NTf}_2]$  at molar ratio 3:1, in the range of temperature: 20-95 °C (the temperature increases by 5 °C).

Colour shades reported in Figure 41 highlight the sudden change in colour with temperature when the solvent was  $[\text{C}_1\text{C}_4\text{pyrr}][\text{NTf}_2]$  compared with the solution in  $[\text{N}_{2,2,2,4}][\text{NTf}_2]$ .

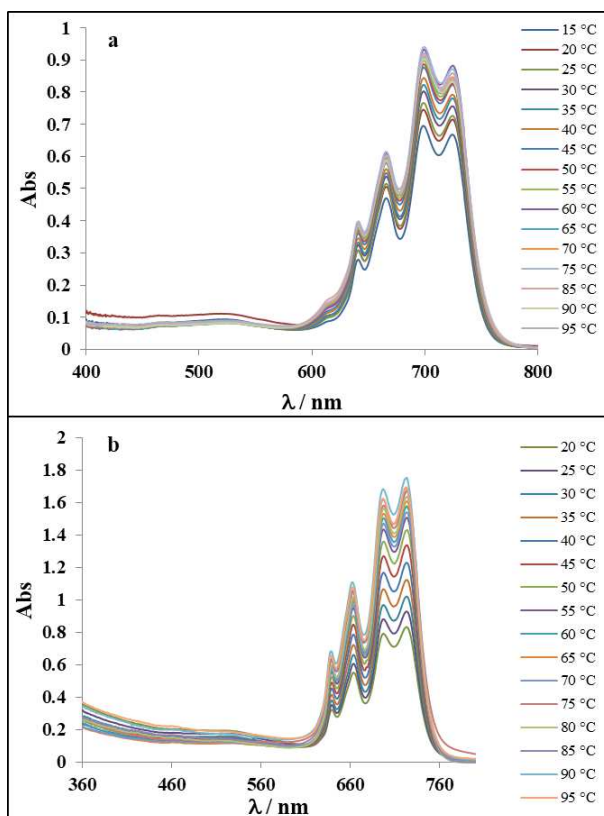


**Figure 42 – VT UV-Vis spectra for the systems: a)  $[\text{N}_{112\text{GA}8}]\text{Br}/\text{Co}(\text{NTf}_2)_2/[\text{C}_1\text{C}_4\text{pyrr}][\text{NTf}_2]$ ; b) and  $[\text{N}_{112\text{GA}8}]\text{Br}/\text{Co}(\text{NTf}_2)_2/[\text{N}_{1113}][\text{NTf}_2]$ .**

The band related to the octahedral coordination is very weak in these solutions, and is more evident for pyrrolidinium (Figure 42-a) than ammonium (Figure 42-b) IL. The trends of absorbance as a function of temperature are reported in Figure 43, and the relative  $T_{\text{switch}}$  in Table 24.



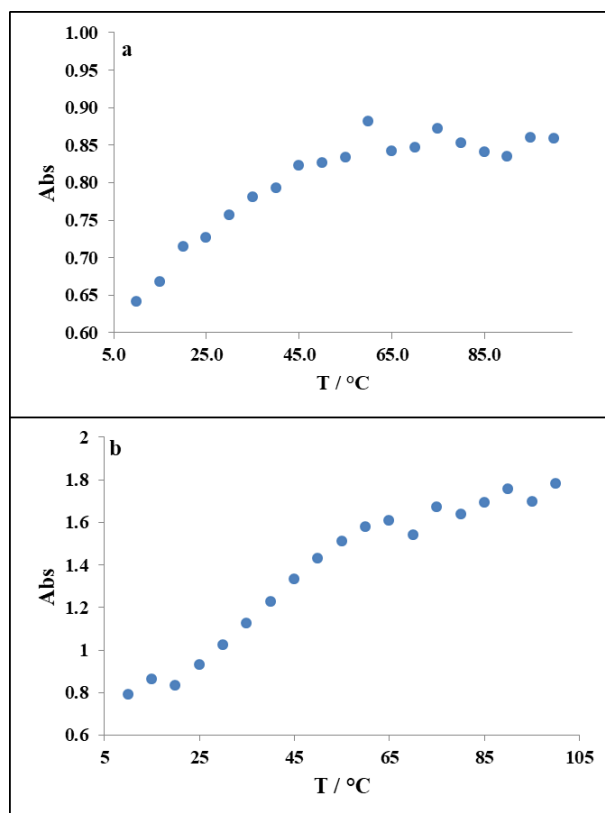


**Figure 43 - UV-Vis absorbance trends for the systems: a)  $[N_{112GA8}]Br/Co(NTf_2)_2/[C_1C_4pyrr][NTf_2]$  (724.0 nm); b) and  $[N_{112GA8}]Br/Co(NTf_2)_2/[N_{1113}][NTf_2]$  (723.0 nm).**

The plots reported in Figure 43 reveal a more gradual change in slope compared with the trend reported in Figure 39-a, highlighting a role of the solvent.

**Table 24 - Temperature of the switch for the system  $[N_{112GA8}]Br/Co(NTf_2)_2$  in different IL-solvent. \* =  $T_{switch}$ s were reproducible within 1 °C.**

Thermochromic system	Ratio [ligand]/[metal]	$T_{switch}$ °C*
$[N_{112GA8}]Br/Co(NTf_2)_2/[C_1C_4pyrr][NTf_2]$	3:1	44
$[N_{112GA8}]Br/Co(NTf_2)_2/[N_{1113}][NTf_2]$	3:1	57
$[N_{112GA8}]Br/Co(NTf_2)_2/[N_{2444}][NTf_2]$	3:1	59



The supposed influence of the IL-solvent on thermochromism is more evident, considering data reported in Table 24. Indeed,  $T_{\text{switch}}$  significantly varies as a function of a different IL cation nature (44 °C for piperidinium IL and ~58 °C for ammonium ones), while it is not affected by the solvent viscosity.

Afterwards, ligand properties in the thermochromic system were also considered. Firstly, the role of the anion was investigated. In the introduction section, the role of the  $[\text{Br}]^-$  anion has been highlighted hypothesizing how its absence should influence the tetrahedral complex formation. To prove this, the  $[\text{N}_{112\text{GA}8}][\text{NTf}_2]$  IL was applied as ligand for  $\text{Co}(\text{NTf}_2)_2$ , recording VT UV-Vis spectra for the system  $[\text{N}_{112\text{GA}8}][\text{NTf}_2]/\text{Co}(\text{NTf}_2)_2/[\text{N}_{2224}][\text{NTf}_2]$  (Figure 45).

The role of the bromide anion was confirmed by the fact that the solution maintained its pink colour up to 100 °C (Figure 44).

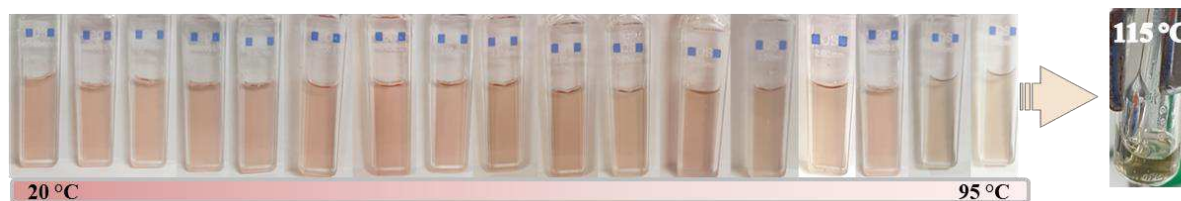


Figure 44 - Colour shades for the  $[\text{N}_{112\text{GA}8}][\text{NTf}_2]/\text{Co}(\text{NTf}_2)_2/[\text{N}_{2224}][\text{NTf}_2]$  at variable temperature.

A pale change of colour towards green was observed only at ~115 °C. This transition could be ascribed to the presence of fluoride-cobalt complex, according to previous reports.<sup>184</sup>

However, also this interaction is reversible, as demonstrated by the fact that the pink coloration is restored when the solution is cooled down.

184. Dugan, T. R.; Goldberg, J. M.; Brennessel, W. W.; Holland, P. L., Low-Coordinate Cobalt Fluoride Complexes: Synthesis, Reactions, and Production from C–F Activation Reactions. *Organometallics* **2012**, *31* (4), 1349-1360.

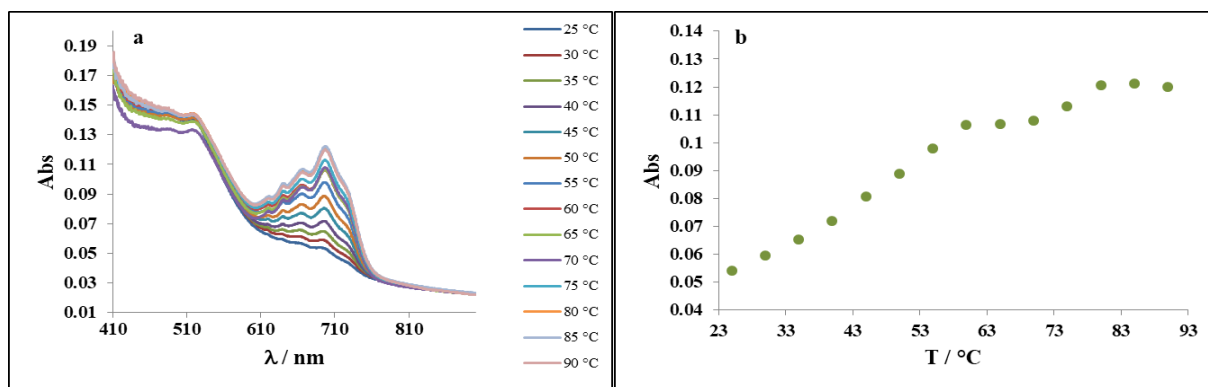


Figure 45 - VT UV-Vis investigation for the  $[N_{1 1 2GA 8}][NTf_2]/ Co(NTf_2)_2/[N_{2 2 2 4}][NTf_2]$  system: a) UV-Vis spectra; b) trend of the absorbance at 697.0 nm with the temperature.

Figure 45-b reports the trend of the absorbance as a function of the temperature for this system. Also in this case, different slopes can be detected although no colour changes is apparent below 95 °C indicating that, in this case, the geometry reorganisation in solution is more energy consuming.

A further investigation was focused on the cation structure. Firstly the alkyl chain was taken into account, so the branched octyl chain of  $[N_{1 1 2GA 8}]^+$  cation was changed with an octyl linear chain, using the  $[N_{1 1 2GA 8L}Br]$  as ligand in a ratio equal to 3:1 with cobalt salt. In this case, some difficulty in solubilising the ligand and obtaining a homogenous solution was encountered. This suspension at room temperature assumed a blue coloration, which did not change upon increasing the temperature. The same solubility problem was detected by using a ligand bearing a longer alkyl chain, such as  $[N_{1 1 2GA 12}Br]$ .

These results led to hypothesize that van der Waals interactions and steric hindrance in solution favours a tetrahedral complex formation with cobalt already at room temperature, avoiding the establishment of the thermochromic equilibrium between the two forms.

Also, the shortening of the alkyl chain using  $[N_{1 1 2GA 4}Br]$  IL-ligand does not determine any change in the solution colour. The blue coloration was visible already at room temperature and the increase of the temperature did not affect the solution. In addition, the spectra did not show any particular changes during the VT UV-Vis measurement.

On the other hand, the effect of the number of OH in the equilibrium was studied using the ligand with the branched octyl chain. For this purpose, the  $[N_{11}2_{\text{GlyA}8}]Br$  and the  $[N_{11}2_{\text{HexA}8}]Br$  were used as ligands with Cobalt salt.

In both cases, the blue coloration was detected already at room temperature. In Figure 46, the spectra for systems  $[N_{11}2_{\text{GlyA}8}]Br/Co(NTf_2)_2/[N_{22}224][NTf_2]$  and  $[N_{11}2_{\text{HexA}8}]Br/Co(NTf_2)_2/[N_{22}224][NTf_2]$  are reported. These spectra show the exclusive presence of the tetrahedral complex, which is highlighted by the high intensity of the bands in the wavelength range 600-800 nm, and by the absence of the band corresponding to the octahedral complex. Moreover, a difference in the band shape can be observed on going from the ligand with an OH group (Figure 46-a) to the ligand without OH groups (Figure 46-b). In the latter case, resolution decreases and the components of the band are partially overlapped.

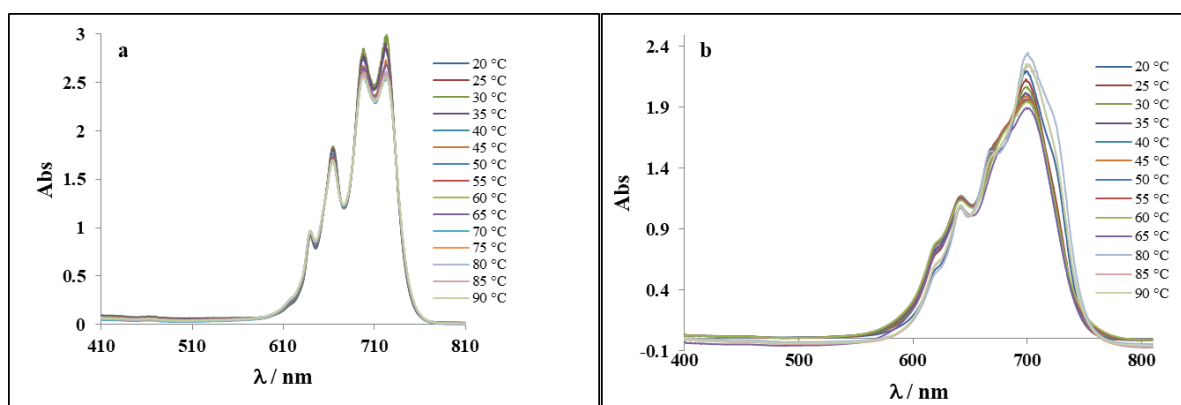


Figure 46 - VT UV-Vis spectra for the system: a)  $[N_{11}2_{\text{GlyA}8}]Br/Co(NTf_2)_2/[N_{22}224][NTf_2]$ ; b)  $[N_{11}2_{\text{HexA}8}]Br/Co(NTf_2)_2/[N_{22}224][NTf_2]$ .

The effect of the linker length between amide function and ammonium head was also investigated. To this aim, we used  $[N_{11}3_{\text{GA}8}]Br$  as ligand and recorded UV-Vis spectra in  $[N_{22}224][NTf_2]$  as a function of temperature. Also in this case, the thermochromism phenomenon was detected (Figure 47), as accounted for by spectra recorded for this system (Figure 48).



Figure 47 - Colour shades for the system  $[N_{1.13GA.8}]Br/Co(NTf_2)_2/[N_{2.22.4}][NTf_2]$ .

Spectra in Figure 48-a result similar to the ones detected for  $[N_{1.12GA.8}]Br$  ligand. The isosbestic point is around 576 nm, which corresponds to a bathochromic shift of about 30 nm with respect to the  $[N_{1.12GA.8}]Br/Co(NTf_2)_2$  system.

However, the trend of the absorbance (Figure 48-b) shows different changes in the slope upon increasing the temperature.

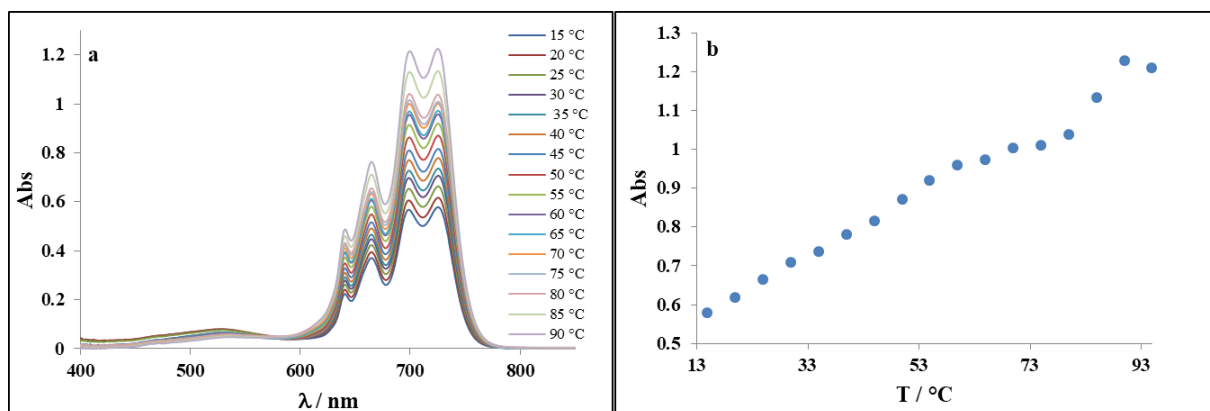
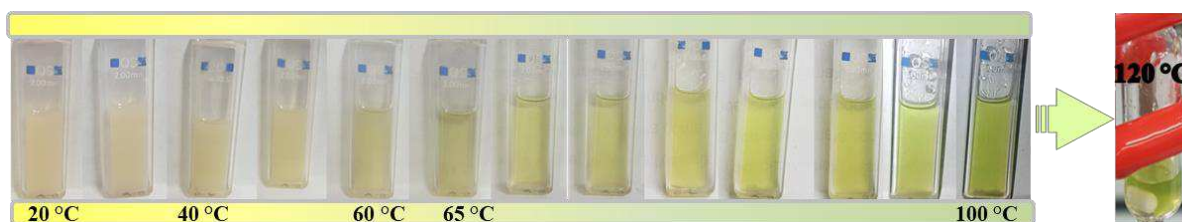


Figure 48 - VT UV-Vis measurement for the system  $[N_{1.13GA.8}]Br/Co(NTf_2)_2/[N_{2.22.4}][NTf_2]$ : a) spectra at variable temperatures; b) trend of the absorbance at 725.5 nm with the temperature.

Also in this case,  $T_{switch}$  was calculated and it was equal to 79 °C. Then, the increase in the length of the ligand spacer induced an increase in the  $T_{switch}$  of about 30 °C with respect to the one detected for  $[N_{1.12GA.8}]Br$ . The colour change was visible at a temperature about 45 °C lower than the one obtained determining the cross point. This could be again ascribed to an initial formation of the tetrahedral complex. However, also in this case the complete change of the geometry seems to occur slowly.

Finally, as the last factor, the nature of the cationic head of the ligand was taken into account. To this aim, we used [**Im<sub>3GA</sub> 4**]**I**. In this case, we observed a drastic change in the thermochromic phenomenon. Indeed, the colour of the solution at room temperature is a shade of yellow, and turns to green when the temperature increases (Figure 49).



**Figure 49 - Colour change for the system [**Im<sub>3GA</sub> 4**]**I**.**

The mixture appeared opalescent up to 65 °C and, then, a shining green solution was detected around 120 °C.

Spectra recorded up to 100 °C are reported in Figure 50.

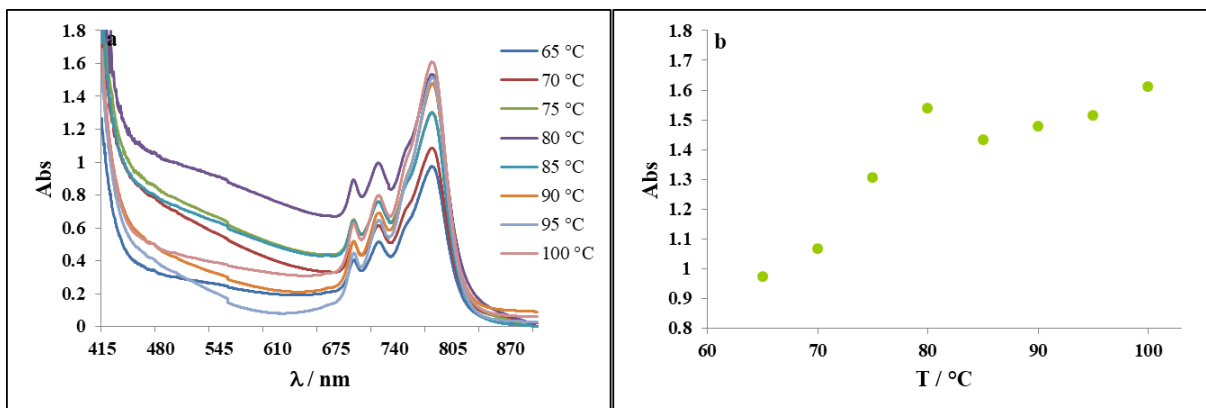


**Figure 50 - VT UV-Vis measurement for the system [**Im<sub>3GA</sub> 4**]**I**: a) spectra at variable temperature; b) trend of the absorbance at 782.5 nm.**

Spectra in Figure 50-a show a high baseline. However, this behaviour is not related to the opalescence of the solution, both because the solution at 65 °C appears clear, and also because the absorbance of the baseline increases with the temperature.

Moreover, the absorbance (Figure 50-b) increases with the temperature, and it is characterised by a change in slope at 75 °C, which can be related to the colour change of the solution (Figure 49).

#### **4.4.2 Magnetic moments of complexes in solution: the Evans method**

UV-Vis investigations, reported in the previous paragraph, allow hypothesising the geometry of complexes considering the position of the bands detected in the spectra. However, a way to confirm the geometries involved in solution, six-coordinated complex at room temperature and four-coordinated complex increasing the temperature, is through the calculation of magnetic moments.

Indeed, the magnetic characterisation of coordination complexes composed by transition metals can give information about the electronic distribution in the *d*-orbitals. Generally, transition metal ions feature incomplete *d*-shells, and the distribution of the unpaired electrons determines the properties of the complex formed.

The calculation of magnetic moment  $\mu$  is an indirect method, as it is obtained by magnetic susceptibility measurements.<sup>185</sup>

The magnetic susceptibility (per unit of volume) is defined as the ratio of the intensity,  $I$ , of the magnetisation induced in a substance by an external magnetic field, and the intensity of this magnetic field,  $H$ :<sup>186</sup>

$$\chi_v = \frac{I}{H} \quad \text{Eq. 7}$$

The mass of gram susceptibility is defined in the Eq. 8:

---

185. O'Handley, R. C., *Modern Magnetic Materials: Principles and Applications*. Wiley: **1999**.

186. Singh, A. K., Chapter 4 - Experimental Methodologies for the Characterization of Nanoparticles. In *Engineered Nanoparticles*, Singh, A. K., Ed. Academic Press: Boston, **2016**; pp 125-170.

$$\chi_g = \frac{\chi_v}{d} \quad \text{Eq. 8}$$

where  $d$  is the density of the substance, and the Eq. 9 results by the substitution of  $\chi_v$  defined in Eq. 7, in Eq. 8.

$$\chi_g = \frac{I}{H*d} \quad \text{Eq. 9}$$

The molar susceptibility will result, obviously, as:

$$\chi_m = \chi_g * MW \quad \text{Eq. 10}$$

where MW is the molecular weight of the substance, and the substitution of  $\chi_g$  in Eq. 10, defines the  $\chi_m$  as:

$$\chi_m = \frac{I*MW}{H*d} \quad \text{Eq. 11}$$

Diamagnetic compounds have negative  $\chi_m$ , while paramagnetic ones have positive magnetic susceptibility. However, for paramagnetic compounds the susceptibility per gram atom of paramagnetic ion ( $\chi_A$ ) must be considered, since it represents the diamagnetic correction of ligands or groups.

Taking into account all the considerations mentioned for the magnetic susceptibility, the effective magnetic moment  $\mu_{eff}$ , is defined as:

$$\mu_{eff} = \sqrt{\frac{3kT\chi_A}{N\beta^2}} \quad \text{Eq. 12}$$

where  $k$  is the Boltzmann's constant,  $T$  is the temperature in Kelvin,  $\beta$  is the Bohr Magneton and  $N$  is the Avogadro's number. The Eq. 12 can be reworked in Eq. 13:

$$\mu_{eff} = 2.828 \sqrt{T\chi_A} \quad \text{Eq. 13}$$

The effective magnetic moment will be expressed in Bohr Magneton unit, B.M.<sup>187,188</sup>

However, Eq. 13 reports the relation between  $\mu_{eff}$  and  $\chi_A$  based on the CGS (centimetre-gram-second) system. Magnetic properties can be also reported in SI (International System of Units) system, by using the following equation:<sup>189</sup>

$$\mu_{eff} = 797.8 \sqrt{T\chi_A} \quad \text{Eq. 14}$$

In 1959 Evans proposed a method to investigate and measure the magnetic susceptibility and, as consequence, calculate magnetic moments.<sup>190</sup>

The method proposed is based on <sup>1</sup>H NMR investigation. According to this method, it is possible to measure the magnetic susceptibility of a sample observing the “effect” of the magnetism on a probe compound, both in presence and in absence of the sample, when an external magnetic field is applied. The probe substance will change the NMR chemical shift when it is in contact with the magnetic sample in the magnetic field (the magnetic field of the NMR instrument).

The magnetic susceptibility is related to the change in chemical shift of the inert probe substance, due to the contact with the magnetic sample. The above change is calculated as the difference between the chemical shift of the inert probe in solution and the one placed inside a capillary.

The relation was firstly written by Evans, and later corrected by Schubert:<sup>191</sup>

$$\chi_g = \frac{3\Delta f}{2\pi f m} + \chi_0 + \frac{\chi_0(d_0 - d_s)}{m} \quad \text{Eq. 15}$$

---

187. Hoppe, J. I., Effective magnetic moment. *J. Chem. Educ.* **1972**, 49 (7), 505.

188. O'Connor, C. J., Magnetochemistry-Advances in Theory and Experimentation. In *Prog. Inorg. Chem.*, Wiley: **1982**; Vol. 29.

189. Blundell, S., Units in electromagnetism. In *Magnetism in Condensed Matter*, OUP Oxford: **2001**.

190. Evans, D. F., 400. The determination of the paramagnetic susceptibility of substances in solution by nuclear magnetic resonance. *J. Chem. Soc.* **1959**, (0), 2003-2005.

191. Schubert, E. M., Utilizing the Evans method with a superconducting NMR spectrometer in the undergraduate laboratory. *J. Chem. Educ.* **1992**, 69 (1), 62.



Where the  $\Delta f$  is the chemical shift difference,  $f$  is the frequency of the NMR instrument,  $m$  is the mass of the paramagnetic substance,  $\chi_0$  is the susceptibility of the solvent,  $d_0$  is the density of the solvent and  $d_s$  is the density of the solution.

Taking into account the above information, the Evans method was applied to thermochromic systems to calculate magnetic moments and, to study the effect of the temperature on the complex geometry and the electronic distribution.

Firstly, the method was applied to the system that gave the best results with UV-Vis spectroscopic investigation. As already highlighted in the previous paragraph, this system is  $[\text{N}_{112\text{GA}8}\text{Br}/\text{Co}(\text{NTf}_2)_2/[\text{N}_{2224}][\text{NTf}_2]$ , where the [ligand]/[metal] molar ratio is equal to 3:1.

The probe compound included in the system was the *t*-butanol. The choice of this solvent was based on the necessity to have a species unable to interact with the sample due to steric hindrance and having  $^1\text{H}$  NMR signals in a non-interfering region. The alcohol *t*-butanol seemed a good choice as the chemical shift of the OH proton was completely different from the one corresponding to protons of the sample and it was enough sterically hindered to weakly interact with cobalt.

In Table 23 the  $\mu_{\text{eff}}$  obtained for the  $[\text{N}_{112\text{GA}8}\text{Br}/\text{Co}(\text{NTf}_2)_2/[\text{N}_{2224}][\text{NTf}_2]$  system are reported and they show a regular trend with the increase in temperature.

**Table 25 - Magnetic moments and relative temperatures for the system  $[\text{N}_{112\text{GA}8}\text{Br}/\text{Co}(\text{NTf}_2)_2/[\text{N}_{2224}][\text{NTf}_2]$  (molar ratio [ligand]/[metal] = 3:1).**

T / K	$\mu_{\text{eff}}$ / B. M.
303.15	5.28
313.15	5.07
323.15	4.72
333.15	4.44
343.15	3.90

The moments can be related to cobalt complexes. In particular, the moment at 30 °C (5.28 B.M.) corresponds to an octahedral complex at high spin, which has 3 unpaired electrons in the orbitals. Moreover, the moment calculated at 60 °C (4.44 B.M.) corresponds to a tetrahedral complex having three unpaired electrons in the orbitals.<sup>192</sup> Figure 51 reports a simplified representation of the possible electronic distribution in the two complexes.

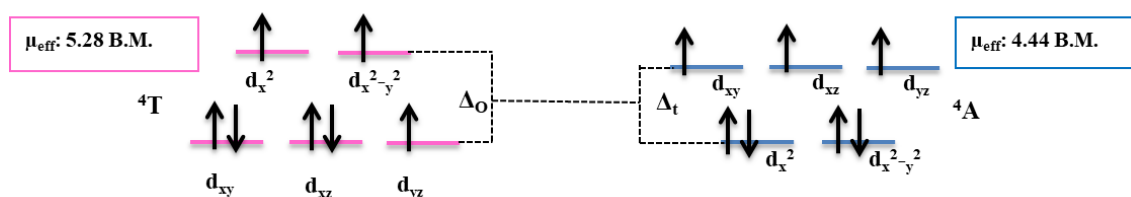


**Figure 51 - Simplified representation of the possible electronic distribution in the two complexes, (left) octahedral in pink and (right) tetrahedral in blue, for the system  $[N_{112GA8}]Br/Co(NTf_2)_2/[N_{2224}][NTf_2]$  (molar ratio [ligand]/[metal] = 3:1).**

The trend of the chemical shift difference ( $\Delta\delta$ ) as a function of temperature is reported in Figure 52. While the trend of magnetic moments as a function of temperature is reported in Figure 52-b. In this case, as the temperature increases, magnetic moments gradually decrease.

192. (a) Petriček, S., Octahedral and Tetrahedral Cobalt(II) Sites in Cobalt Chloride Complexes with Polyethers. *Croat. Chem. Acta* **2011**, *84* (4), 515-520, (b) Varga, F.; Rajnák, C.; Titiš, J.; Moncol, J.; Boča, R., Slow magnetic relaxation in a Co(II) octahedral–tetrahedral system formed of a  $[CoL_3]^{2+}$  core with L = bis(diphenylphosphano) methane and tetrahedral  $[CoBr_4]^{2-}$  counter anions. *Dalton Trans.* **2017**, *46* (13), 4148-4151, (c) de Berg, K. C.; Chapman, K. J., Determination of the Magnetic Moments of Transition Metal Complexes Using Rare Earth Magnets. *J. Chem. Educ.* **2001**, *78* (5), 670, (d) Yamada, S., Recent aspects of the stereochemistry of schiff-base-metal complexes. *Coord. Chem. Rev.* **1966**, *1* (4), 415-437.

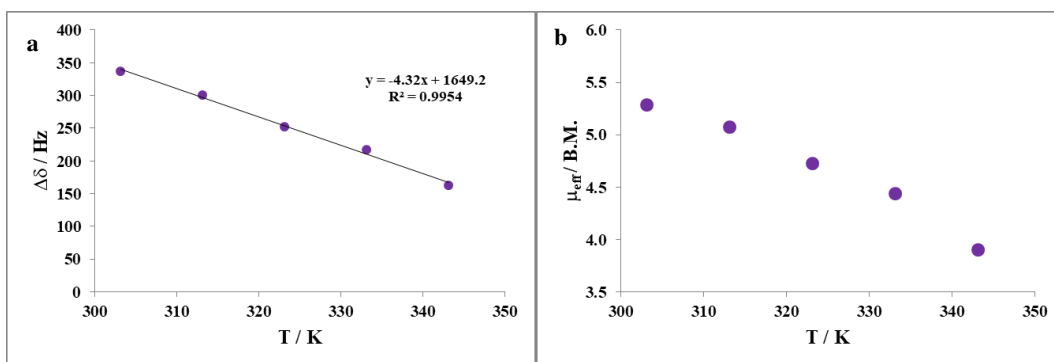


Figure 52 – Trends of: a)  $\Delta\delta$  as a function of temperature; b)  $\mu_{\text{eff}}$  as a function of the temperature for the system  $[\text{N}_{112\text{GA}8}]\text{Br}/\text{Co}(\text{NTf}_2)_2/[\text{N}_{2224}][\text{NTf}_2]$ .

Other interesting results were obtained in the case of  $[\text{N}_{113\text{GA}8}]\text{Br}/\text{Co}(\text{NTf}_2)_2/[\text{N}_{2224}][\text{NTf}_2]$ . Indeed, the solution turned blue immediately after the *t*-butanol addition. The VT  $^1\text{H}$  NMR was conducted and the  $\mu_{\text{eff}}$  values are reported in Table 26.

Table 26 - Magnetic moments and relative temperatures for the system  $[\text{N}_{113\text{GA}8}]\text{Br}/\text{Co}(\text{NTf}_2)_2/[\text{N}_{2224}][\text{NTf}_2]$  (molar ratio [ligand]/[metal] = 3:1).

T / K	$\mu_{\text{eff}}$ / B. M.
303.15	2.91
313.15	2.96
323.15	2.82
333.15	2.87
343.15	3.10

Magnetic moments obtained for this system were more compatible with a square planar coordination sphere around cobalt than the tetrahedral one.<sup>193</sup> However, the addition of the *t*-butanol plays a fundamental role in the colour switch. Apparently, alcohol influences the equilibrium in solution, favoring the formation of the tetra-coordinated complex. The different metal coordination modes could be related to the nature of the interaction between the sugar-based ligand and cobalt.

193. Hiroaki, N.; Shoichiro, Y., Planar Quadri-co-ordinate Complexes of Cobalt(II) with Schiff Bases Derived from Salicylaldehyde. *Bull. Chem. Soc. Jpn.* **1964**, 37 (1), 8-12.

However, these magnetic moments reported in Table 26 are similar to anomalous magnetic moments for cobalt.<sup>194</sup> For the above reason, an investigation should be carried out with a different probe.

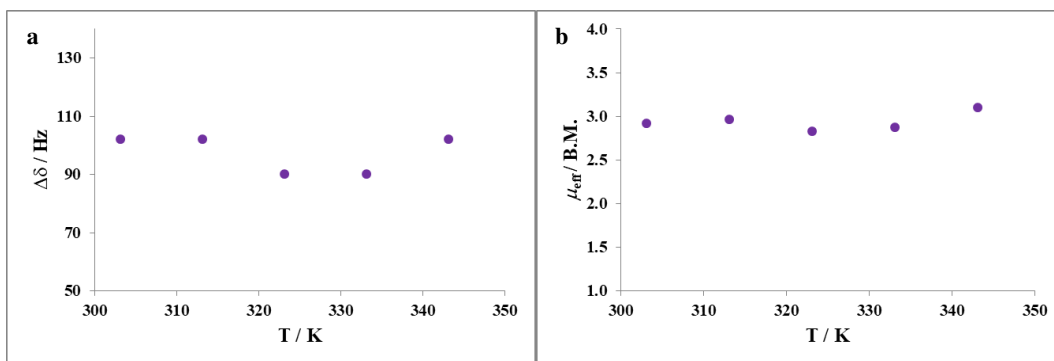


**Figure 53 – Trends of: a)  $\Delta\delta$  as a function of temperature; b)  $\mu_{\text{eff}}$  as a function of the temperature for the system  $[\text{N}_{113\text{GA}8}]\text{Br}/\text{Co}(\text{NTf}_2)_2/[\text{N}_{2224}][\text{NTf}_2]$ .**

Figure 53-a reports the trend of the  $\Delta\delta$  as a function of the temperature for  $[\text{N}_{113\text{GA}8}]\text{Br}$ . As above stated, the complex formed at room temperature with the alcohol is stable and does not change with the temperature. Consequently, Figure 53-b shows the independence of magnetic moment from the temperature.

The investigation for the system  $[\text{Im}_{3\text{GA}4}]\text{I}/\text{Co}(\text{NTf}_2)_2/[\text{N}_{2224}][\text{NTf}_2]$  was not performed. The impossibility to record the spectra was due to the formation of a biphasic system when the *t*-butanol was added. Moreover, as soon as two phases were obtained, a precipitate was visible on the bottom of the tube.

Finally, in the case of  $[\text{N}_{112\text{GA}8}][\text{NTf}_2]/\text{Co}(\text{NTf}_2)_2/[\text{N}_{2224}][\text{NTf}_2]$  the signal of the butanol in contact with the system was detected, but not the one corresponding to *t*-butanol in the capillary. This signal was obscured due to overlap with ligand signals.

#### 4.4.3 A gaze on Cobalt: <sup>59</sup>Co NMR measurements

The thermochromic system firstly investigated by UV-Vis measurements and then by applying the Evans method, was further analysed by using <sup>59</sup>Co NMR.

194. Barefield, E. K.; Busch, D. H.; Nelson, S. M., Iron, cobalt, and nickel complexes having anomalous magnetic moments. *Quarterly Reviews, Chemical Society* **1968**, 22 (4), 457-498.

The quadrupolar spin number of cobalt  $S = 7/2$  generates a broad peak which is difficult to observe. However,  $^{59}\text{Co}$  nucleus is magnetically active and it is a naturally abundant isotope. Consequently, NMR has been widely used to investigate a wide range of different complexes.<sup>195</sup>

The chemical shift range of the  $^{59}\text{Co}$  NMR spectrum covers over 18000 ppm with different regions of the spectrum corresponding to different coordination geometries of the metal in the complex.<sup>196</sup>

According to previous reports, a  $\text{K}_3[\text{Co}(\text{CN})_6]$  saturated solution in  $\text{D}_2\text{O}$  was chosen as external reference. Its  $\delta$  is arbitrarily assigned to 0 ppm.<sup>196,197</sup>

The VT  $^{59}\text{Co}$  NMR investigation was performed in the range of temperature of 20 – 90 °C, in line with the VT UV-Vis measurement range.

Figure 54 displays the spectra as a function of the temperature for the system  $[\text{N}_{112}\text{GA}_8]\text{Br}/\text{Co}(\text{NTf}_2)_2/[\text{N}_{2224}][\text{NTf}_2]$ .

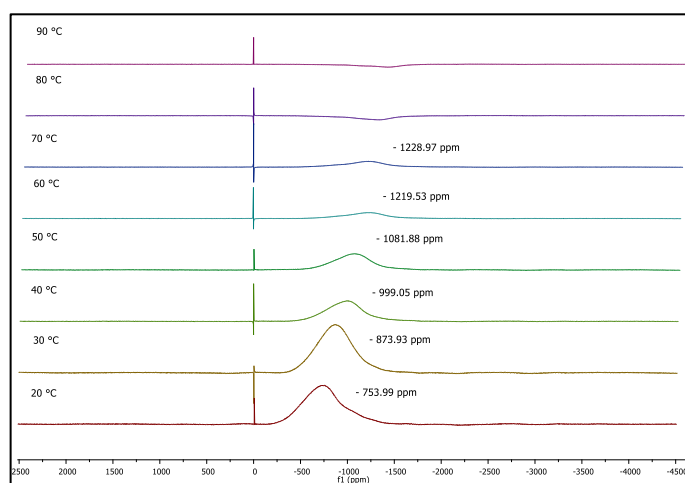


**Figure 54** –VT  $^{59}\text{Co}$  NMR for the system  $[\text{N}_{112}\text{GA}_8]\text{Br}/\text{Co}(\text{NTf}_2)_2/[\text{N}_{2224}][\text{NTf}_2]$  in the range 20 – 90 °C ( $^{59}\text{Co}$  signal for  $\text{K}_3[\text{Co}(\text{CN})_6]$  fixed at 0 ppm).

195. (a) McClintock, L. F.; Bagaria, P.; Kjaergaard, H. G.; Blackman, A. G., Co(III) complexes of the type  $[\text{L}]\text{Co}(\text{O}_2\text{CO})^+$  (L=tripodal tetraamine ligand): Synthesis, structure, DFT calculations and  $^{59}\text{Co}$  NMR. *Polyhedron* **2009**, 28 (8), 1459-1468, (b) Medek, A.; Frydman, V.; Frydman, L., Solid and liquid phase  $^{59}\text{Co}$  NMR studies of cobalamins and their derivatives. *Proc. Natl. Acad. Sci. U. S. A.* **1997**, 94 (26), 14237-14242.

196. Goodfellow, R. J., Group VIII Transition Metals. In *Multinuclear NMR*, 1 ed.; Mason, J., Ed. Springer US: **1987**.

197. (a) Sharrad, C. A.; Cavigliasso, G. E.; Stranger, R.; Gahan, L. R., Embracing ligands. Synthesis, characterisation and the correlation between  $^{59}\text{Co}$  NMR and ligand field parameters of Co(III) complexes with a new class of nitrogen–thioether multidentate ligand. *Dalton Trans.* **2004**, (5), 767-777, (b) Munro, O. Q.; Shabalala, S. C.; Brown, N. J., Structural, Computational, and  $^{59}\text{Co}$  NMR Studies of Primary and Secondary Amine Complexes of Co(III) Porphyrins. *Inorg. Chem.* **2001**, 40 (14), 3303-3317.

A significant change in the chemical shift of  $^{59}\text{Co}$  was detected upon increasing the temperature. Furthermore, changing the temperature from 20 up to 70 °C, the signal intensity decreased and at 70 °C it almost disappeared. This behaviour is more evident in Figure 55, which shows the change in chemical shift ( $\Delta\delta$ ) of  $^{59}\text{Co}$  versus temperature.

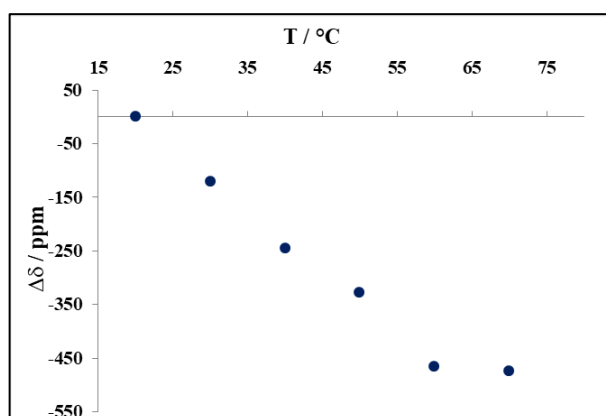


Figure 55 – Plot of  $\Delta\delta$  as function of temperature in the range 20 – 90 °C for the system  $[\text{N}_1 \text{ 1 2GA}_8]\text{Br}/\text{Co}(\text{NTf}_2)_2/[\text{N}_{2 \text{ 2 2 4}}][\text{NTf}_2]$ .

The trend clearly demonstrates the upfield shift of the signal up to 60 °C. At 70 °C, it remains unchanged, but at higher temperatures the signal disappears.

The temperature corresponding to change in slope of  $\Delta\delta$  values, perfectly matches with value calculated by UV-Vis measurements and with the colour switch of the solution (60 °C).

With the above results in mind, we verified if also the signal of hexacyanocobaltate showed a shift as a function of the temperature. According to previous reports, it has a temperature coefficient of 6.2 Hz/°C. The correction of the chemical shift, in the spectra reported before, should be operated. However, the changes in chemical shift for these IL system are so large that a correction would not be significant. In fact, the frequency values of signal corresponding to IL-Co complex is about three orders of magnitude larger than the changes of the reference signal. The chemical shift of the reference remains constant within 0.25 %.

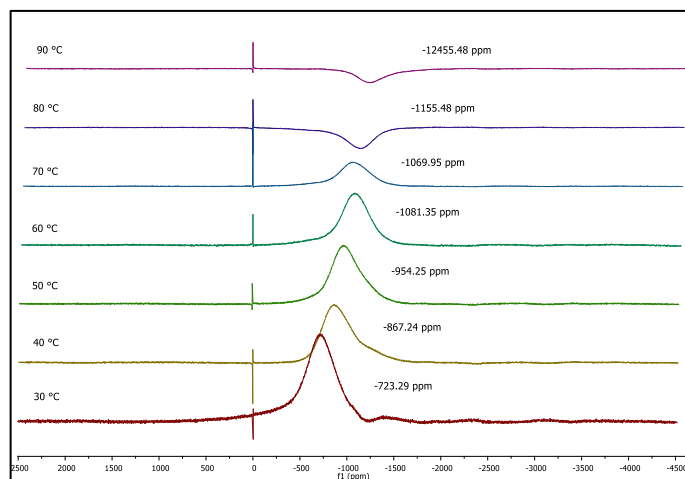


Figure 56 - VT  $^{59}\text{Co}$  NMR for the system  $[\text{N}_{1\ 1\ 2\text{GA}\ 8}]\text{Br}/\text{Co}(\text{NTf}_2)_2/[\text{N}_{2\ 2\ 2\ 4}][\text{NTf}_2]$  at molar ratio  $[\text{ligand}]/[\text{metal}]=7$  in the range  $30 - 90\ ^\circ\text{C}$  ( $^{59}\text{Co}$  signal for  $\text{K}_3[\text{Co}(\text{CN})_6]$  fixed at  $0\ \text{ppm}$ ).

A different trend was detected using a  $[\text{ligand}]/[\text{metal}]$  molar ratio equal to 7:1. Indeed, in this case, the change in chemical shift was observed up to  $90\ ^\circ\text{C}$ , but in the range  $70\text{-}80\ ^\circ\text{C}$ , signal inverted its phase lending a negative peak. Figure 57 reports trend of  $\Delta\delta$  as a function of the temperature. Before the inversion of the signal, a plateau can be evidenced ( $60\text{-}70\ ^\circ\text{C}$ ). Incidentally, this change in the NMR signal occurs close to the plateau region obtained with the aid of the VT UV-Vis investigation (Figure 39).

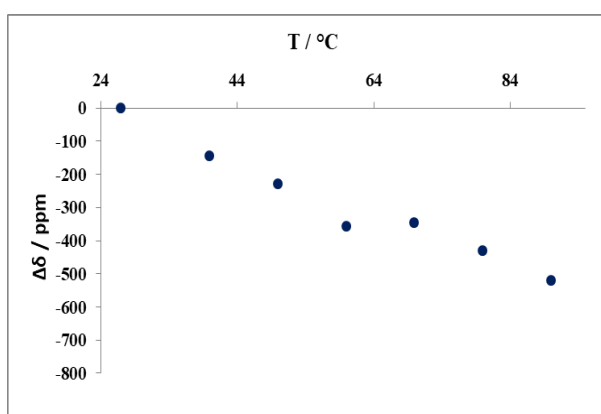
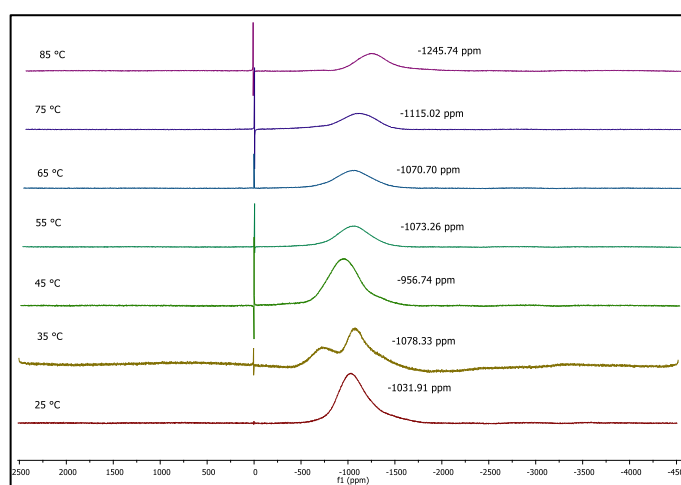


Figure 57 - Trend of  $\Delta\delta$  increasing the temperature for the system  $[\text{N}_{1\ 1\ 2\text{GA}\ 8}]\text{Br}/\text{Co}(\text{NTf}_2)_2/[\text{N}_{2\ 2\ 2\ 4}][\text{NTf}_2]$  at molar ratio  $[\text{ligand}]/[\text{metal}]=7:1$  in the range  $30 - 90\ ^\circ\text{C}$ .

In Figure 58 and 59,  $^{59}\text{Co}$  NMR spectra, and trend seen for  $\Delta\delta$  as a function of the temperature for the  $[\text{N}_{1\ 1\ 2\text{GA}\ 8}][\text{NTf}_2]/\text{Co}(\text{NTf}_2)_2/[\text{N}_{2\ 2\ 2\ 4}][\text{NTf}_2]$  system are

reported, respectively. In this case, the signal was detected until the highest temperature was reached. However, the  $\Delta\delta$  change was significantly lower than the one detected in the presence of  $[\text{N}_{112\text{GA}8}]\text{Br}$  ligand, confirming the significant role played by the anion of the ligand in determining the occurrence of the thermochromic phenomenon.

In this case,  $\Delta\delta$  values increase in parallel with temperature and this result perfectly matches the one obtained by UV-Vis investigation and only a pale change in colour for the solution was observed.



**Figure 58** - VT  $^{59}\text{Co}$  NMR for the system  $[\text{N}_{112\text{GA}8}][\text{NTf}_2]/\text{Co}(\text{NTf}_2)_2/[\text{N}_{2224}][\text{NTf}_2]$  in the range 25 – 85 °C ( $^{59}\text{Co}$  signal for  $\text{K}_3[\text{Co}(\text{CN})_6]$  fixed at 0 ppm).

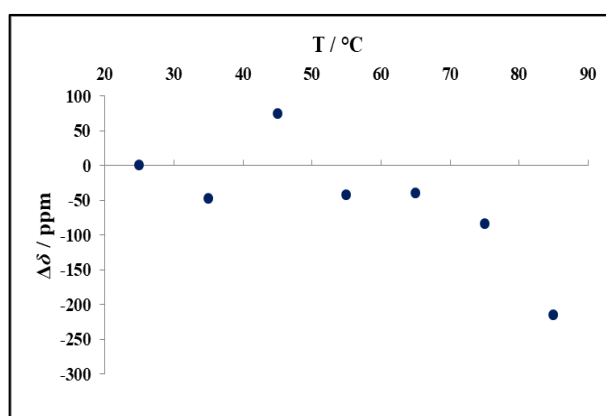


**Figure 59** - Trend of  $\Delta\delta$  increasing the temperature in the range 25 – 85 °C for the system  $[\text{N}_{112\text{GA}8}][\text{NTf}_2]/\text{Co}(\text{NTf}_2)_2/[\text{N}_{2224}][\text{NTf}_2]$ .



Figure 60 reports the results for the other system which showed the thermochromic behaviour,  $[N_{1.13GA8}]Br/Co(NTf_2)_2/[N_{2.224}][NTf_2]$ . The signal of  $^{59}Co$ , also in this case, was shifted upfield by the increase in temperature. At 80 °C, the intensity of the signal decreased and completely disappeared at 90 °C.

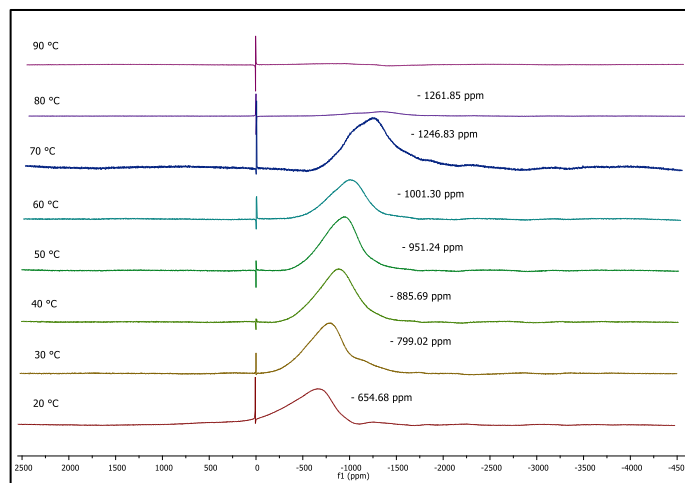


Figure 60 - VT  $^{59}Co$  NMR for the system  $[N_{1.13GA8}]Br/Co(NTf_2)_2/[N_{2.224}][NTf_2]$  in the range 20 – 90 °C ( $^{59}Co$  signal for  $K_3[Co(CN)_6]$  fixed at 0 ppm).

Figure 61 displays the trend of the  $\Delta\delta$  as a function of temperature.  $\Delta\delta$  gradually increased up to 70 °C, then a plateau region was reached. Also in this case, the change in slope in  $\Delta\delta$  trend occurs in a temperature range that perfectly matches the one detected by UV-Vis measurements. This supports the hypothesis that the phenomenon observed in solution can be related to the change of the electronic configuration of the metal ion in the complex.

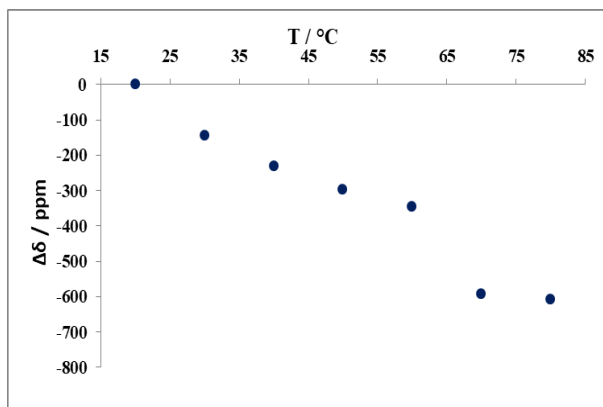


Figure 61 - Trend of  $\Delta\delta$  increasing the temperature in the range 20 – 90 °C for the system  $[N_{1.13GA8}]Br/Co(NTf_2)_2/[N_{2.224}][NTf_2]$ .

Finally, the last investigation was carried out for the  $[\text{Im}_{3\text{GA}}\text{4}]\text{I}/\text{Co}(\text{NTf}_2)_2/[\text{N}_2\text{224}][\text{NTf}_2]$  system. In this case, spectra show the inversion of the signal already at 55 °C. However, the chemical shift of the signal was detected up to 75 °C, the temperature at which the signal almost disappeared.

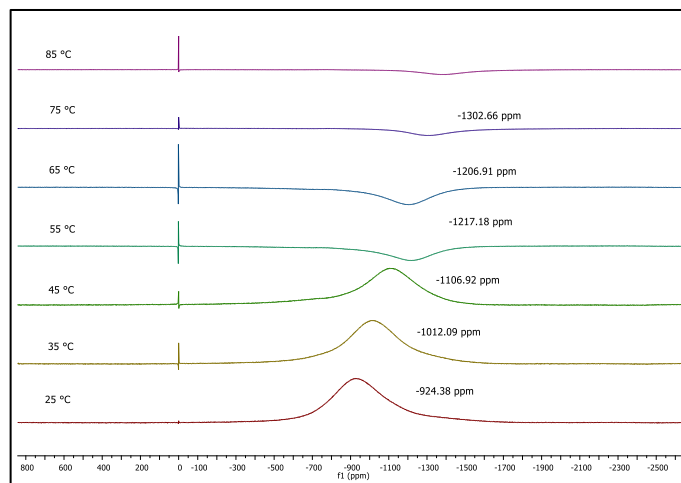


Figure 62 - VT  $^{59}\text{Co}$  NMR for the system  $[\text{Im}_{3\text{GA}}\text{4}]\text{I}/\text{Co}(\text{NTf}_2)_2/[\text{N}_2\text{224}][\text{NTf}_2]$  in the range 25 – 85 °C ( $^{59}\text{Co}$  signal for  $\text{K}_3[\text{Co}(\text{CN})_6]$  fixed at 0 ppm).

Figure 63 shows the trend of  $\Delta\delta$  values as a function of the temperature.

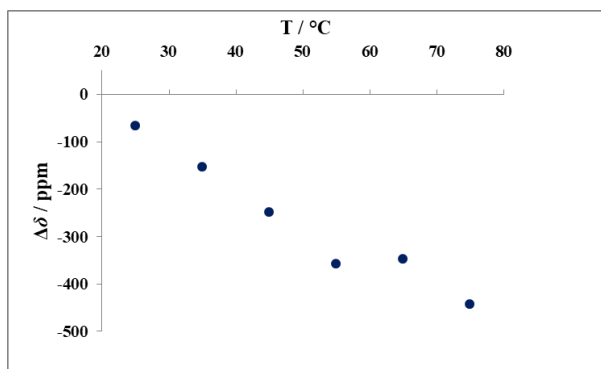


Figure 63 - Trend of  $\Delta\delta$  increasing the temperature in the range 20 – 90 °C for the system  $[\text{Im}_{3\text{GA}}\text{8}]\text{Br}/\text{Co}(\text{NTf}_2)_2/[\text{N}_2\text{224}][\text{NTf}_2]$ .

In this case  $\Delta\delta$  values stay constant between 55 and 65 °C. Although the reasons of phase inversion of the signals are not well understood, also in this case, the disappearance of the signal occurs at the temperature corresponding to the change in slope of the absorbance values (Figure 50).

#### 4.4.4 Designing a device: a thermochromic film

Among all systems investigated for their thermochromic behaviour, the best combination among ligand, metal and solvent was the  $[\text{N}_{11}2\text{GA}_8]\text{Br}/\text{Co}(\text{NTf}_2)_2/[\text{N}_{22}224][\text{NTf}_2]$ , with [ligand]/[metal] molar ratio equal to 3:1.

Taking into account its performance and the issue above mentioned about energy storage, we attempt to obtain homogenous film.

A thermochromic ILG film was studied and assembled by Lee et al.<sup>198</sup> Polyurethane polymeric ILGs were obtained by cross-linking between poly(propylene oxide) and imidazolium ILs. The film showed thermochromic reversible behaviour from transparent to an opaque state, in a convenient range of temperature. The device is based on the affinity between polyurethane and ILs, mixed in one phase at room temperature (transparent) and forming two phases (opaque) when the temperature is increased.

Zhu et al. took advantage of combining a thermochromic IL film and  $\text{VO}_2$  nanoparticles.<sup>199</sup> The thermochromic IL system was composed of di-(1-butyl-3-methylimidazolium tetrachloronickelate ( $[\text{C}_4\text{C}_1\text{im}]_2\text{NiCl}_4$ ) and 1-(3-hydroxyethyl)-3-methylimidazolium tetrafluoroborate ( $[\text{C}_2\text{OHmim}][\text{BF}_4]$ ). This film showed a thermochromic switch from colourless to blue upon increasing the temperature. The blue colour is due to a tetracoordinate complex  $\text{Ni}^{2+}$  and  $\text{Cl}^-$ . Initially, the hydroxyl group coordinates nickel, but the increase of temperature allows chloride to replace it.

Furthermore, the combination of the IL film with  $\text{VO}_2$  nanoparticles, gave a thermochromic composite film switching from brown to green in a range of temperature going from 20 up to 80 °C.

---

198. Lee, H. Y.; Cai, Y.; Velioglu, S.; Mu, C.; Chang, C. J.; Chen, Y. L.; Song, Y.; Chew, J. W.; Hu, X. M., Thermochromic Ionogel: A New Class of Stimuli Responsive Materials with Super Cyclic Stability for Solar Modulation. *Chem. Mater.* **2017**, 29 (16), 6947-6955.

199. Zhu, J.; Huang, A.; Ma, H.; Ma, Y.; Tong, K.; Ji, S.; Bao, S.; Cao, X.; Jin, P., Composite Film of Vanadium Dioxide Nanoparticles and Ionic Liquid–Nickel–Chlorine Complexes with Excellent Visible Thermochromic Performance. *ACS Appl. Mater. Interfaces* **2016**, 8 (43), 29742-29748.

These films find application in the design of devices for daily use, which could decrease the energy demand and, consequently, the environmental impact due to the energy production.

Chromogenic devices are not a utopia, and several industries are already working on it.

ENI, an Italian industry which produces and supplies energy, through a collaboration with the Polytechnic of Milan, is designing new devices called LSC (Luminescent Solar Concentrators). These new “smart windows” use solar energy to produce electricity and make the environment more comfortable and thermally controlled.

New Boeing's 787 Dreamliner (Air France) is another example of the application of chromogenic devices. The collaboration between PPG Aerospace and Gentex Corporation has recently given rise to the design and application of smart windows on airplanes. These windows can change the colour in different blue shades depending on the desire and necessity of passengers. The transmission of light is regulated, and as consequence, also the temperature of the cabin can be controlled.

This system is based on a gel medium fixed between two panels. An electric field applied across the gel determines the change of the colour, and obviously, the intensity of the colour depends on the voltage.

Considering the necessity to develop more application oriented systems, polymers were chosen as the base to obtain a thermochromic film. The incorporation of polymers to fabricate devices has been already investigated.<sup>200</sup> On the grounds of literature information, some polymers were considered, such as poly(methylmetachrylate) (PMMA), poly(ethylmetachrylate) (PEMA), nylon, poly(ethylene glycole) (PEG).

However, the best film was obtained with PMMA. The  $[\text{N}_1 \text{ 1 2GA}_8]\text{Br/Co(NTf}_2)_2$  mixture was incorporated into the polymer, obtaining a homogeneous pink film at room temperature. The pink coloration encouraged the investigation, so UV-Vis measurements were performed. The film rapidly

---

200. Seeboth, A.; Löttsch, D.; Ruhmann, R.; Muehling, O., Thermochromic Polymers—Function by Design. *Chem. Rev.* **2014**, *114* (5), 3037-3068.

changed the colour increasing the temperature, turning from pink to blue in the same range of temperature of the solution system (20-60°C) (Figure 63).

However, the absorbance in the case of the film is lower than the absorbance of the active compound in solution (Figure 65-a). The trend of absorbance versus temperature shows a linear trend over the 60 °C, that was the operational limit of the instrument (Figure 65-b). The above results seem to suggest the possibility of using the film also at higher temperatures.

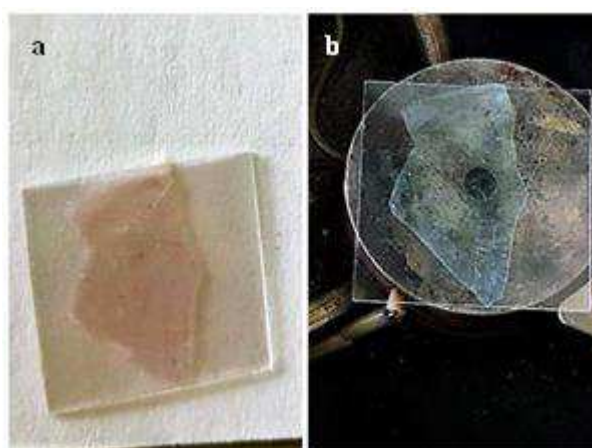


Figure 64 - Thermochromic polymeric film  $[N_{112GA8}]Br/Co(NTf_2)_2/PMMA$ : a) 25 °C; b) 60 °C.

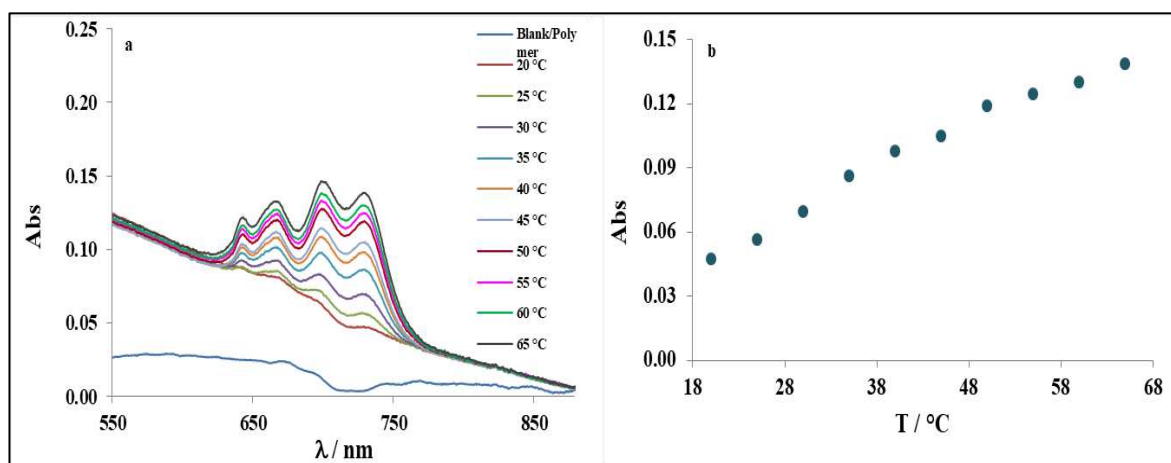


Figure 65 – VT UV-Vis measurement for the polymeric film  $[N_{112GA8}]Br/Co(NTf_2)_2/PMMA$ : a) spectra in the range of temperature 20-65 °C; b) trend of the absorbance increasing the temperature.

A film with PEMA was also obtained. However, the pink coloration already at room temperature was lighter than that of the PMMA film. Moreover, no significant changes in the absorbance were detected as a function of temperature.

The thermochromic system designed in this Ph.D research work shows encouraging performance and good chance to find application in thermo-devices.

## 4.5. Experimental Section

### 4.5.1 Materials

Poly(methyl methacrylate) (Sigma Aldrich, average Mw ~15,000 by GPC, powder), poly(ethyl methacrylate) (Sigma Aldrich, average Mw ~515,000 by GPC, powder), Nylon 6/6 (Sigma Aldrich, pellets), poly(ethylene glycol) (Sigma Aldrich, average Mw 6,000) were purchased and used without further purification.

### 4.5.2 Thermochromic solution

Co(NTf<sub>2</sub>)<sub>2</sub> salt (5.75 mg,  $9.28 \cdot 10^{-3}$  mmol) was dissolved in 600 mg of the IL solvent. In order to assist solubilisation, ultrasound irradiation (VWR ultrasonic cleaning bath and Decon ultrasonics Ltd.) was applied for 30 min. A pink homogeneous solution was obtained. To this solution the proper IL-ligand ( $2.78 \cdot 10^{-2}$  mmol) was added. The mixture was heated at 90 °C for 1.5 h.

### 4.5.3 Thermochromic film

[N<sub>1</sub> 1<sub>2GA</sub> 8]Br ligand (48 mg, 0.10 mmol) and Co(NTf<sub>2</sub>)<sub>2</sub> (23 mg, 0.03 mmol) were solubilised in DCM (3 mL). The polymer (390 mg) was solubilised in DCM (8 mL). In both cases, to obtain homogeneous solutions, the mixtures were sonicated for 30 min. Afterwards the solutions were cooled down and mixed, to obtain a pink solution was obtained. This solution was placed in a petri dish (diameter: 10 cm). The solvent slowly evaporated at room temperature. When an homogeneous film was obtained, it was subsequently removed from the glass by peeling.

#### 4.5.4 Evans sample

*t*-Butanol (0.2 mL) was added to the thermochromic solution described in section 5.5.2 and the mixture obtained was transferred into an NMR tube. Additionally, two capillaries containing the references (*t*-butanol and DMSO-*d*<sub>6</sub>) were placed inside the NMR tube. The  $X_m$  and the  $\mu_{\text{eff}}$  were calculated following a procedure previously reported.<sup>190,201</sup>

#### 4.5.5 VT UV-Vis measurements

Spectra at variable temperature of the solution were recorded with a Beckman Coulter DU 800 spectrophotometer equipped with a Peltier temperature controller. The solution was placed in a quartz cuvette with light path of 0.2 cm. The spectra were recorded in the wavelength range 250-900 nm, in a range of temperature between 15 and 90 °C.

Spectra at variable temperature of the film were recorded using the Agilent Cary 60 UV-Vis spectrophotometer equipped with a temperature control block, where the quartz cuvette was placed. The film was placed inside of the quartz cuvette with a light path of 0.2 cm. The spectra were recorded in the wavelength range 300-800 nm, in a range of temperature between 20 and 65 °C. The temperature was not increased over 65 °C due to mechanical limitation of the temperature control block.

#### 4.5.6 VT NMR measurements

The VT <sup>59</sup>Co NMR were recorded using the Ascend™ 600 Bruker with an external <sup>59</sup>Co reference (K<sub>3</sub>[Co(CN)<sub>6</sub>] in D<sub>2</sub>O in a sealed silica capillary). The spectra were recorded from 293.1 K (20 °C) to 363.1 K (90 °C); the investigation was performed using a 10 K gradient after equilibrating the sample for 20 min.

---

201. Johnson, B. J.; Antholine, W. E.; Lindeman, S. V.; Mankad, N. P., A Cu<sub>4</sub>S model for the nitrous oxide reductase active sites supported only by nitrogen ligands. *Chem. Commun.* **2015**, 51 (59), 11860-11863.



The VT  $^1\text{H}$  NMR spectra required for the Evans method were recorded using an Ascend<sup>TM</sup> 600 Bruker with two internal solvent references (DMSO- $d_6$  and *t*-butanol). The investigation was performed using a 10 K gradient after equilibrating the sample for 20 min.

## Conclusions

Results obtained in this Ph.D thesis perfectly matched the objectives of the initial research proposal.

In particular, the idea to synthesise novel more eco-compatible ILs has been achieved. The gluconic moiety is the crucial part of the IL structures. This moiety proved to be an amalgamation between biocompatibility and applications.

The characterisation of each organic salt was performed, highlighting attractive properties for different applications.

For this purpose, ILGs were obtained, taking advantage from the hydroxylated chain of the gluconate ILs, which through hydrogen bonds favour the formation of 3D-networks.

Moreover, ILGs were used as sorbent materials useful for applications aimed to preserve the environment. Indeed, the desulfurisation of fuel-systems, using the gelatinous matrix to adsorb thiophene, benzothiophene and dibenzothiophene was applied with satisfactory results. Furthermore, no mutual solubility of ILs and fuels, the main limitation of ILs application on fuel cleaning, was detected.

Taking into account preservation of the environment as the main objective of this Research Project, systems to store energy and to decrease the energy demand were designed.

To this aim, gluconic ILs were applied as ligands to coordinate metals, and in particular transition metals. The presence of hydroxyl groups on the ILs structures together with the amide functionality and halide anions provided the perfect mix of ligands to coordinate cobalt.

The characterisation of IL-Co system gave a thermochromic system which was able to switch its colour from pink to blue in a mild range of temperature, as a consequence of a change in the coordination geometry of cobalt. Temperature increase induced the reorganisation in the coordination sphere of cobalt that changed from octahedral to tetrahedral. The equilibrium between the corresponding complexes in solution, was investigated at variable temperature, obtaining a reversible system which could be applied in energy storage devices. A

thermochromic film was also prepared from the thermochromic solution, retaining the same phenomenon and achieving the production of a new handy device.

The leitmotif of the Project was resolutely preserved in all Chapters of the Thesis. This clarity of purpose was achieved not only in the interest of the Ph.D. experimental results, but rather for steadfast belief that Sustainable Chemistry is changing how we approach Chemistry.

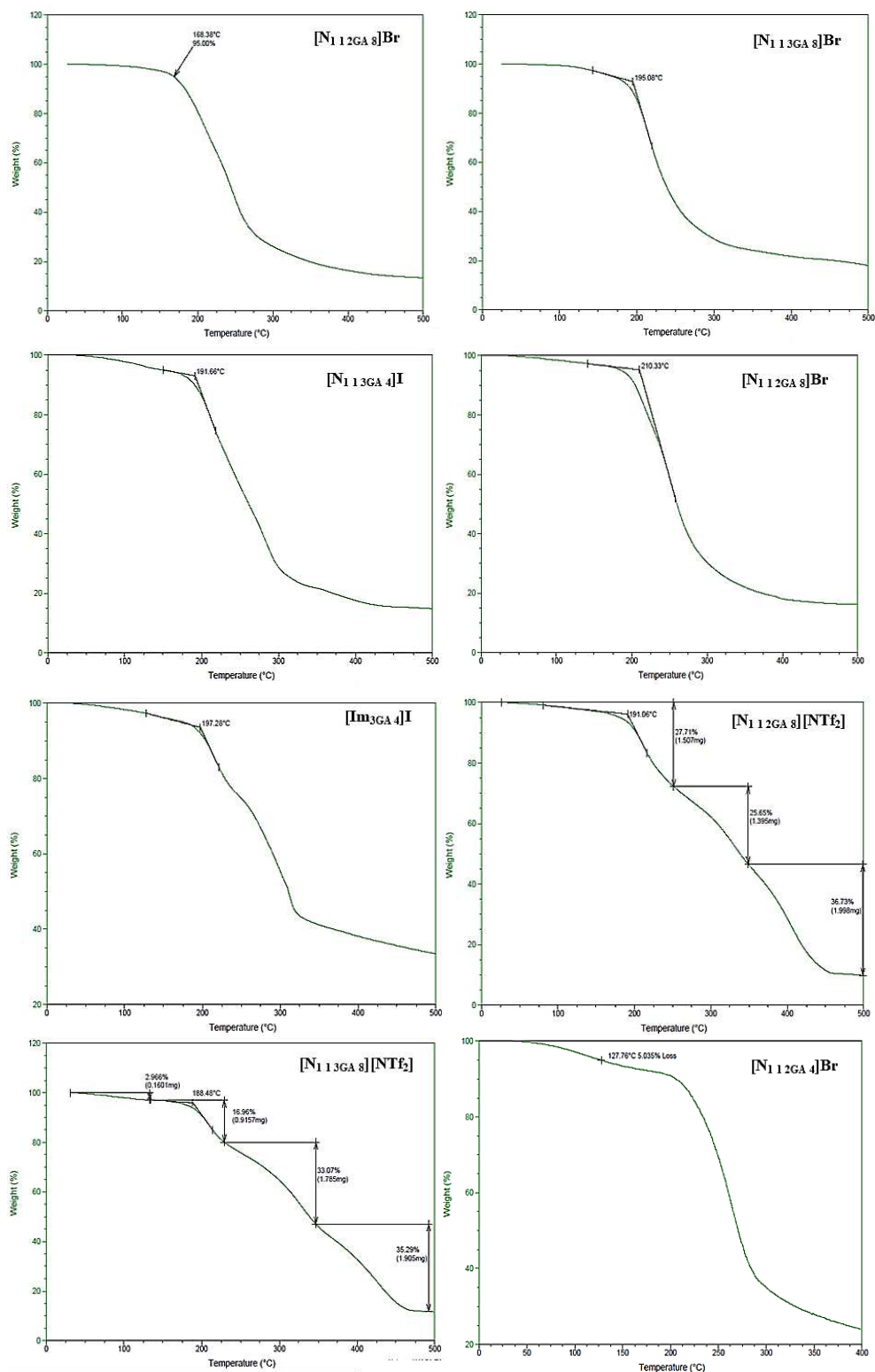
Taking it in the mind, the experimental work achieved in the triennium of the Ph.D. and exposed in this Manuscript represents a tale of a bigger Project. All the ILs here reported will be more studied and modified in order to obtain other organic molecules with desired physico-chemical properties, maintaining the essential characteristic of biodegradability and non-toxicity. At this purpose, the biological studies on eco-toxicity are necessary to develop future applications. Indeed, as already explained in the Introduction, the sustainable approach concerns each part of the process, from the synthesis of the reagents to the disposal of the “materials” at the end of the life-cycle. At this point, the knowledge of biological effects of these materials on the ecosystem is mandatory. Biological investigations of ILs reported in this Thesis are currently in progress. Preliminary results highlighted the safe nature of these organic salts. Moreover, new structural modification, improving the “natural” moiety and taking into account the biodegradation, will be designed. The future application will still concern environmental prevention and remediation, considering the promising results obtained during the Ph.D. research work. The applications already presented will be more investigate. The desulfurisation process will be studied with new gel systems, in the aim to substitute the  $[\text{NTf}_2]^-$  anion and make the ionic liquid gels more eco-friendly. Moreover, a “flow” system will be also taken into account to develop a more efficient desulfurisation process.

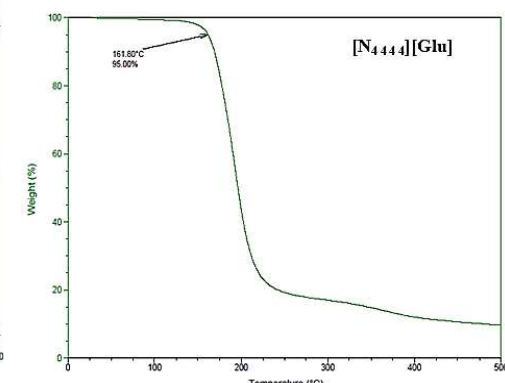
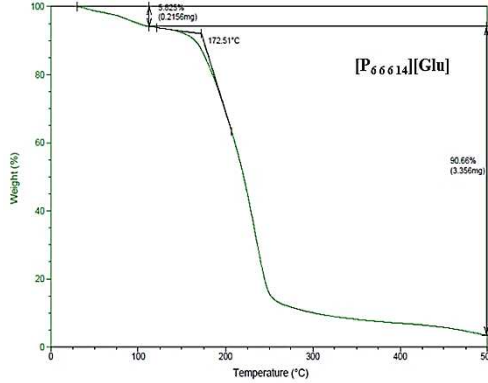
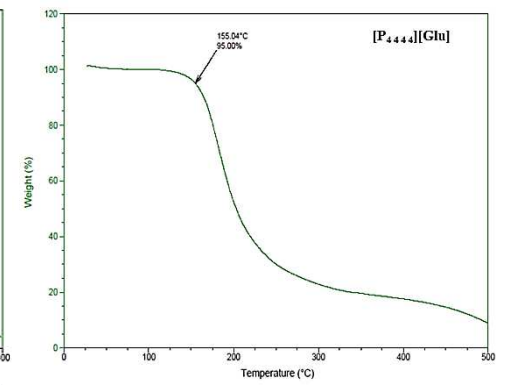
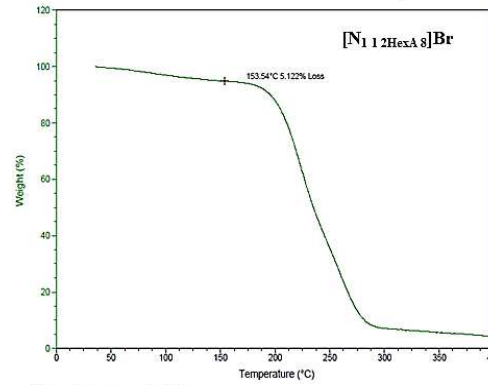
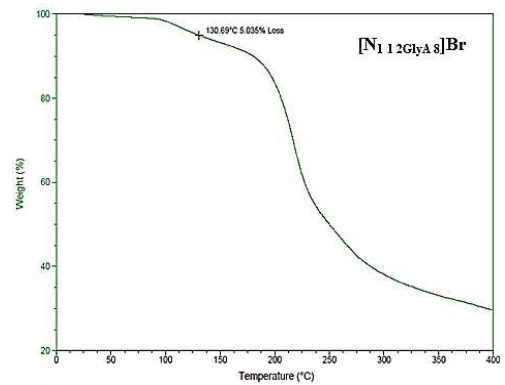
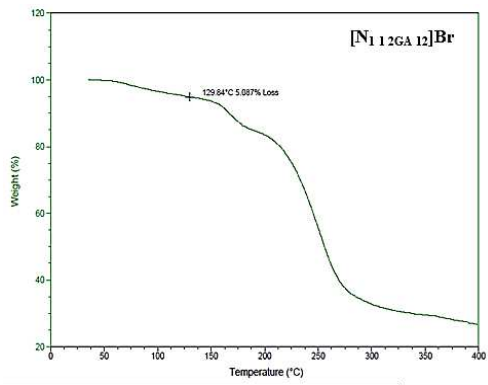
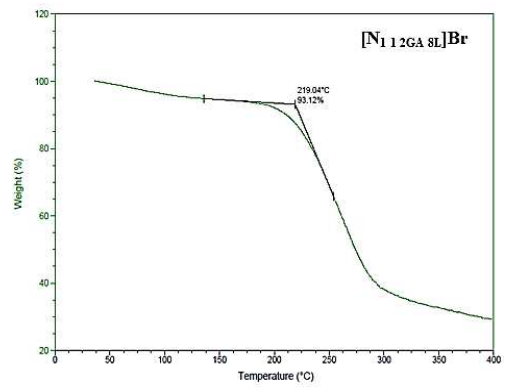
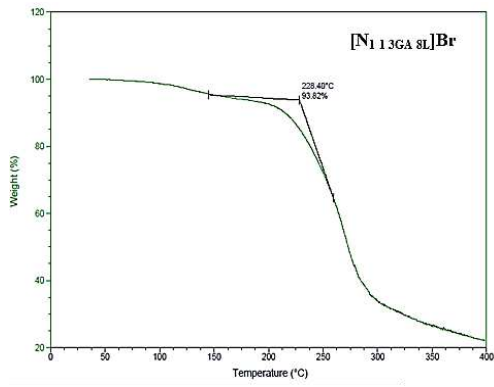
In Chapter 4 glucosamide ILs have been employed to fabricate polymer film for energy storage devices. On this way, more polymers will be considered in order to improve the film performances. Furthermore, also in this case, new molecules will be designed, respecting the fundamental eco-friendly characteristics.

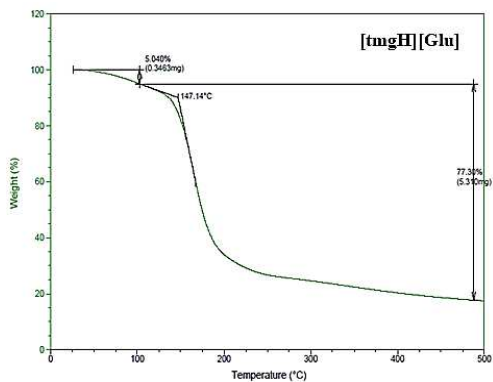
In the main, all future developments, whether or not they will regarding the environmental field, will be performed taking into account the ecosystem safety as an inescapable requirement.

# Appendix

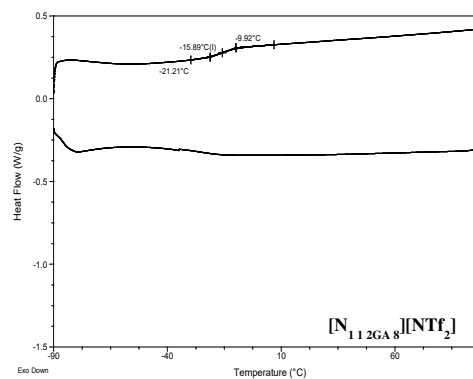
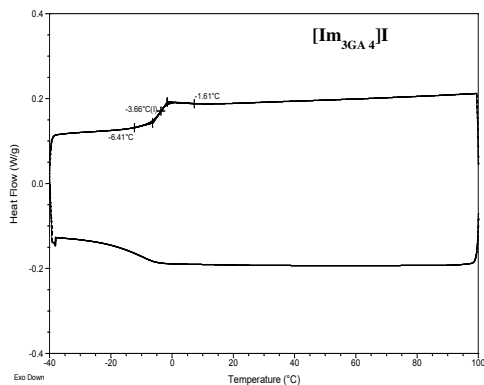
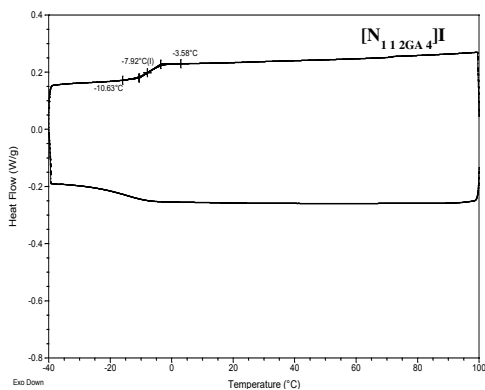
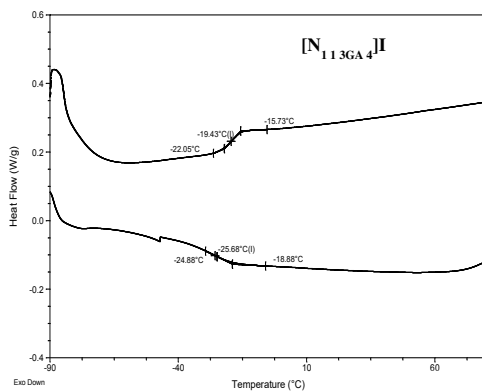
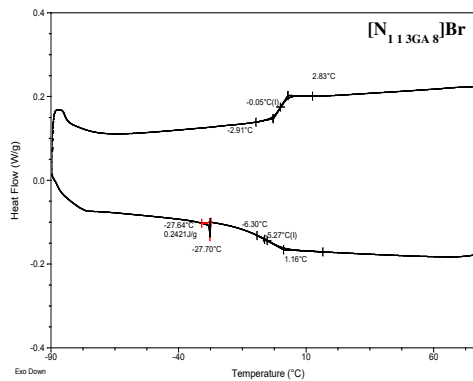
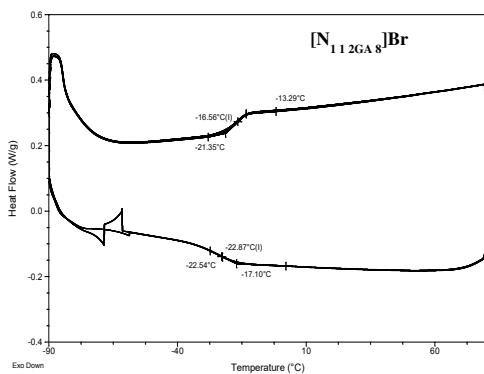
## A.1. TGA measurements

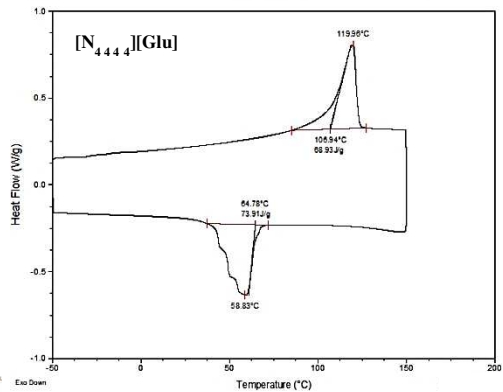
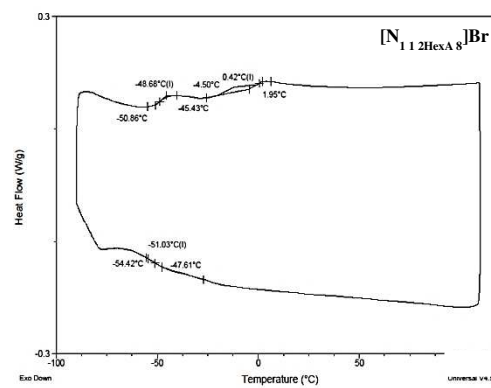
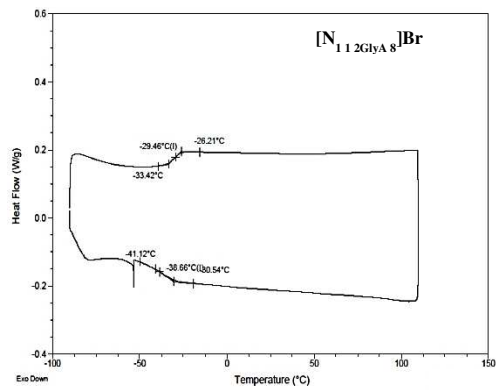
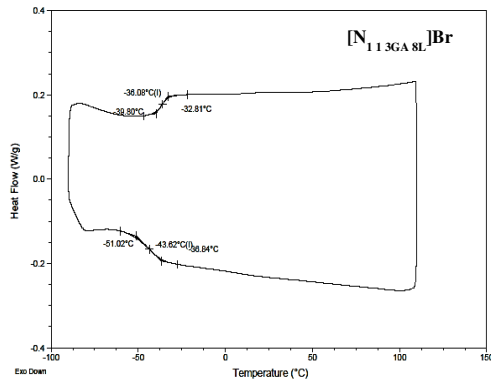
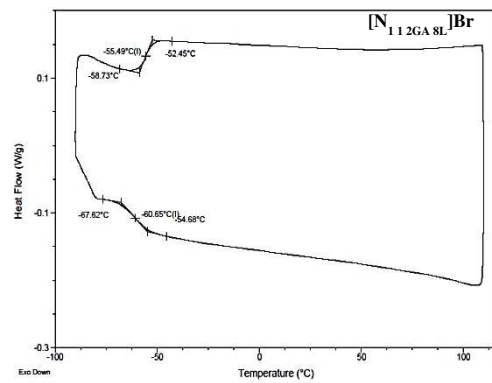
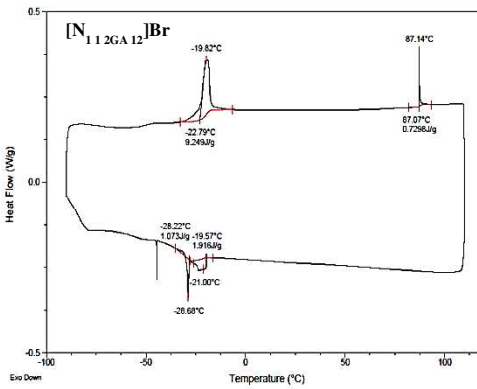
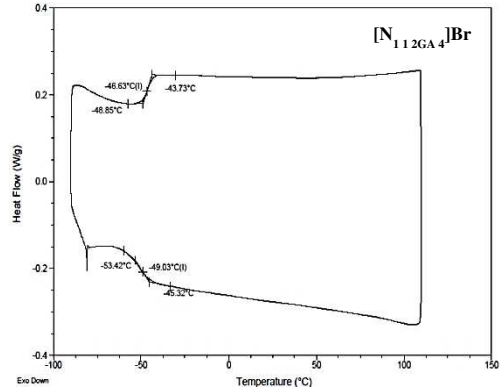
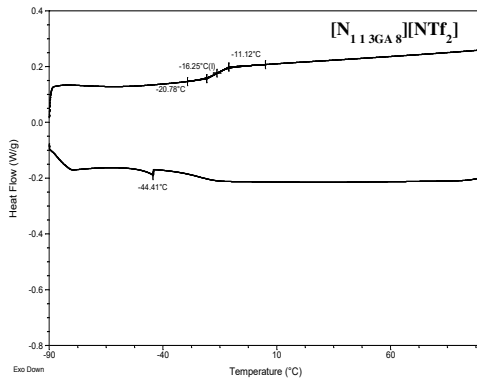




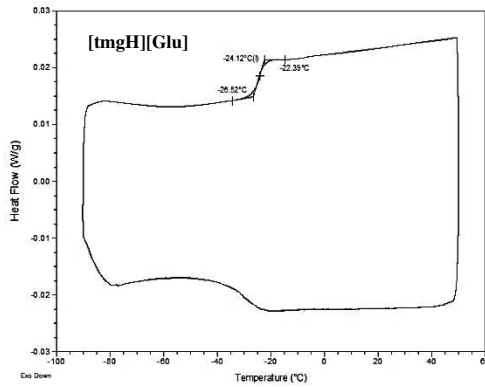
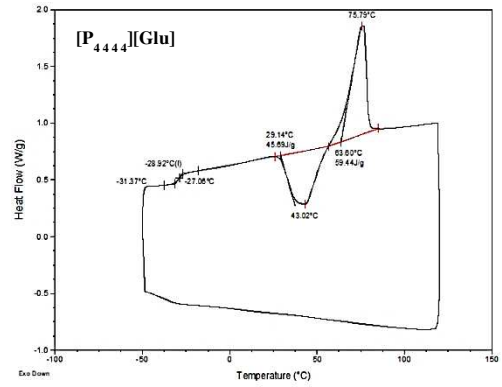
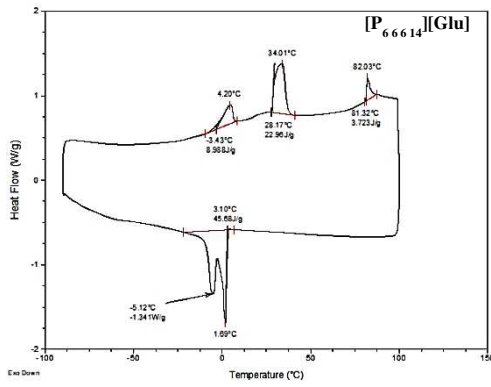


## A.2. DSC measurements

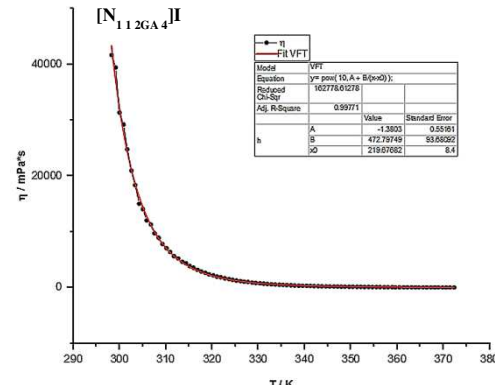
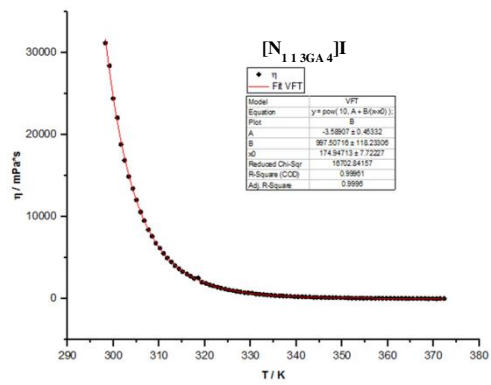
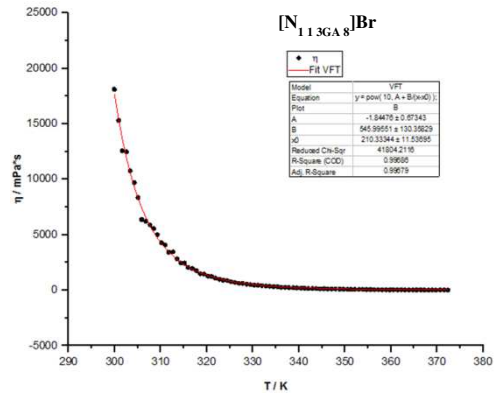
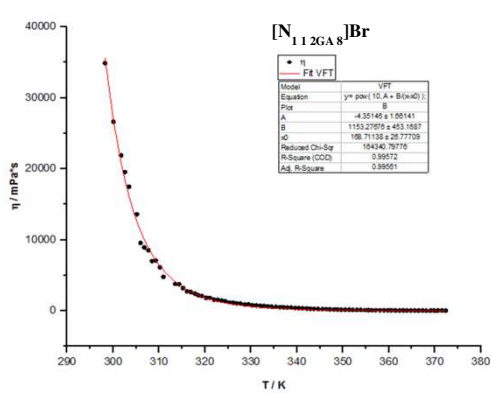


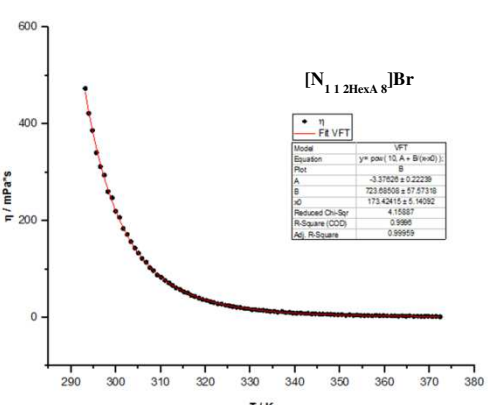
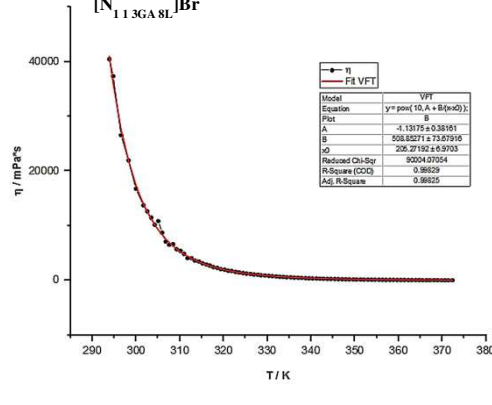
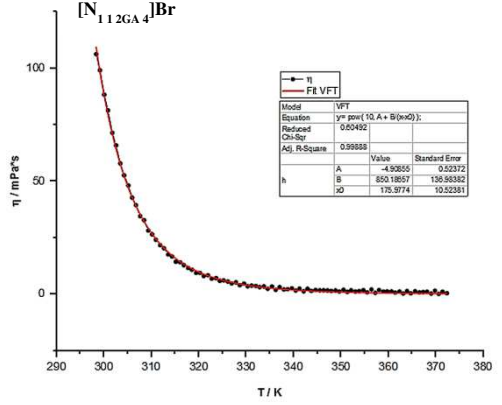
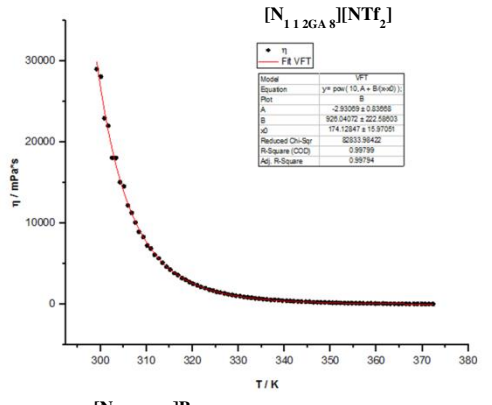
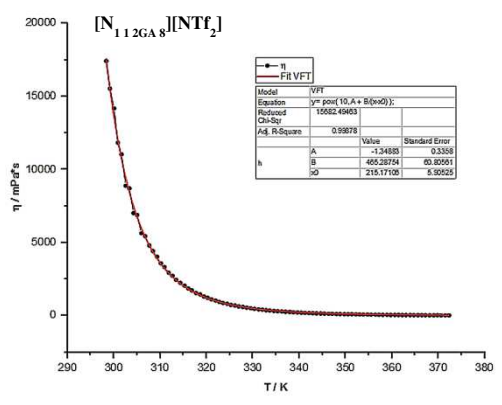
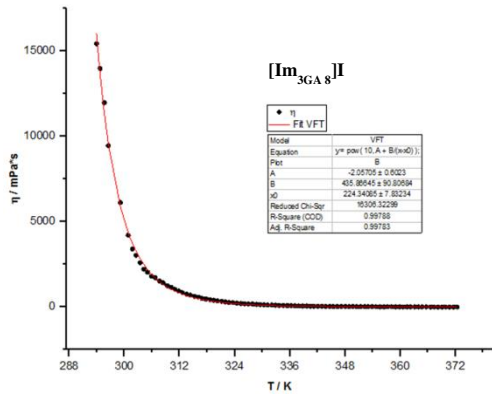




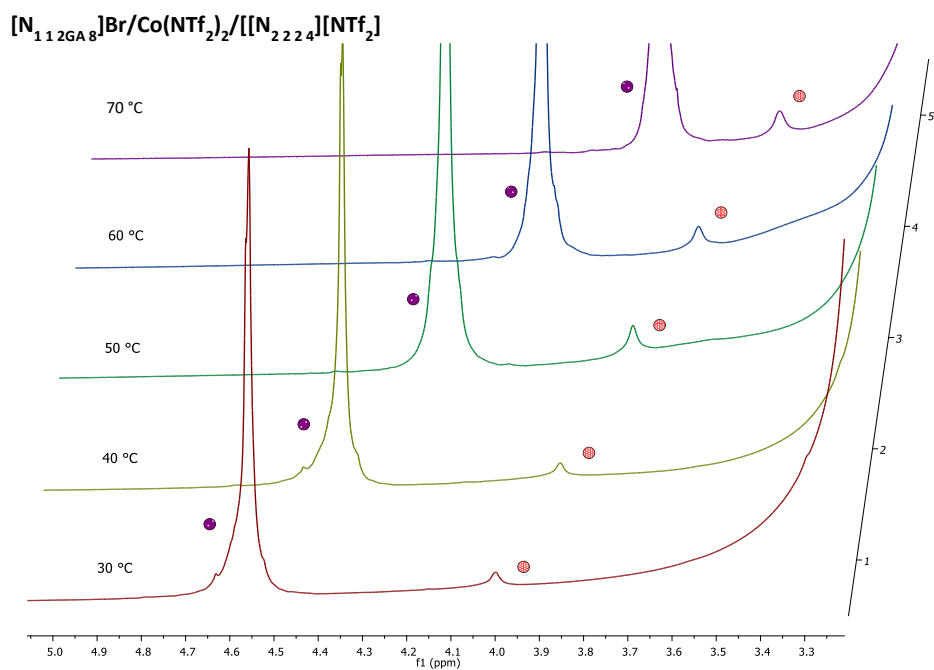


### A.3. Viscosity measurements fitted by VFT model

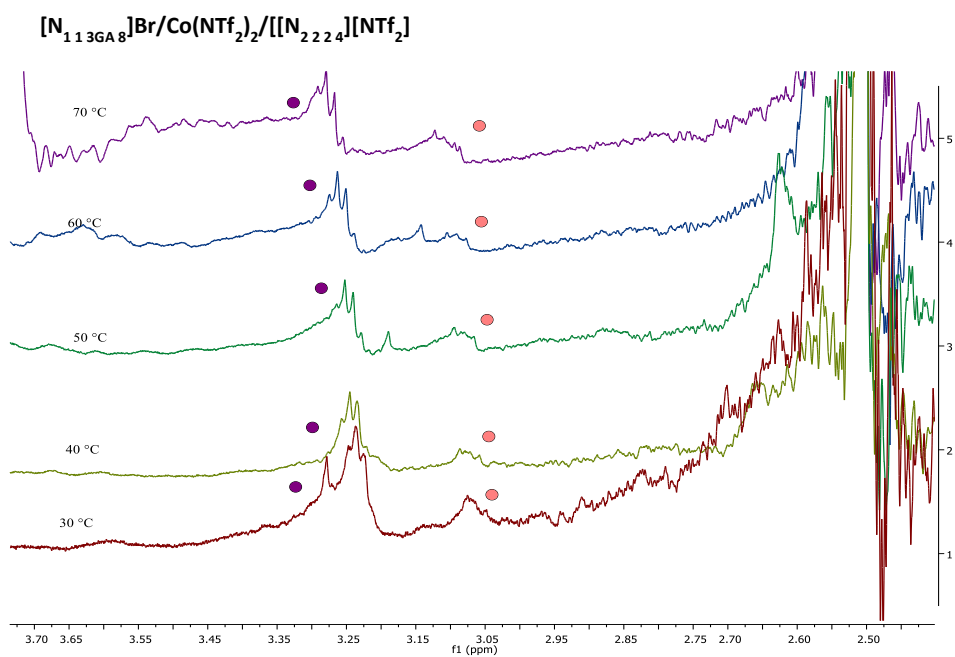




#### A.4. $^1\text{H}$ NMR Evans method

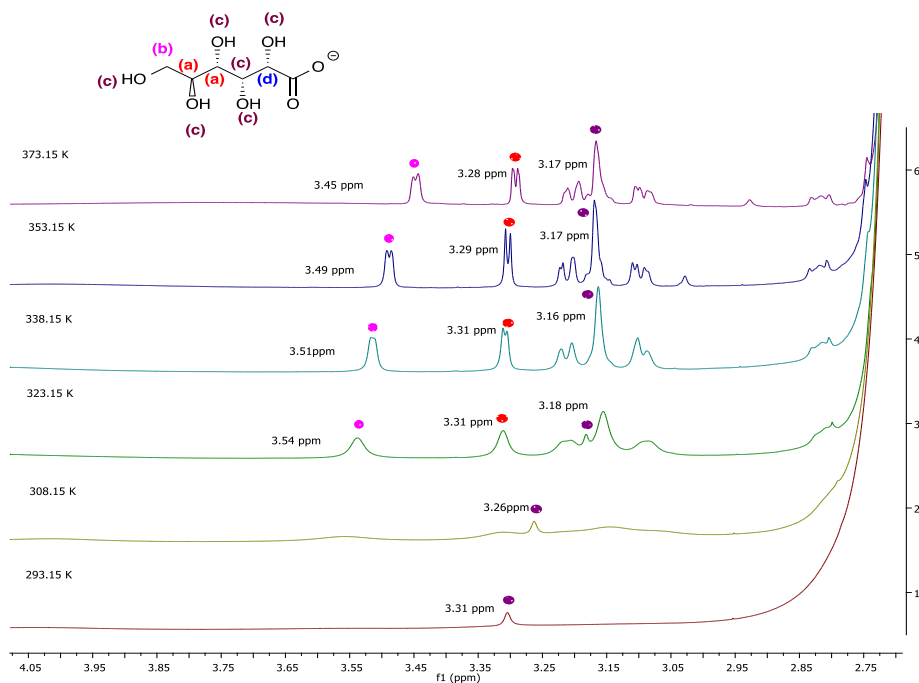


Purple dots: *t*-butanol in contact with the sample; red dots: *t*-butanol into the capillary.



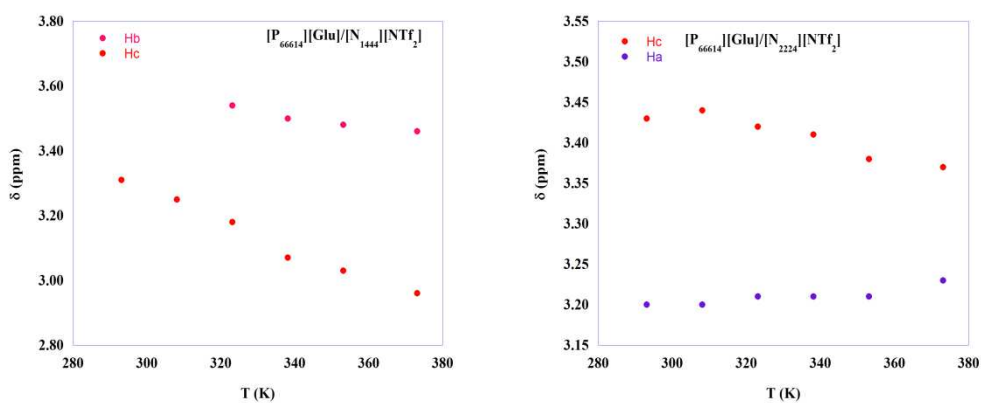
Purple dots: *t*-butanol in contact with the sample; red dots: *t*-butanol into the capillary.

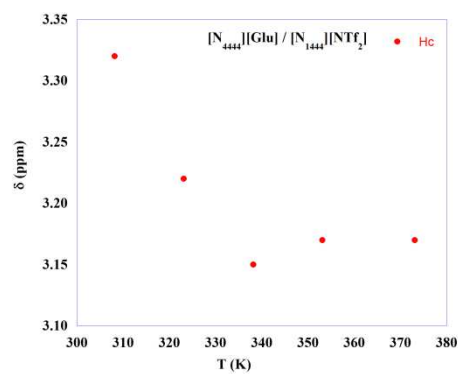
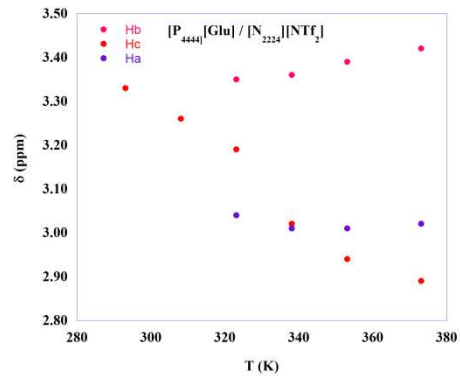
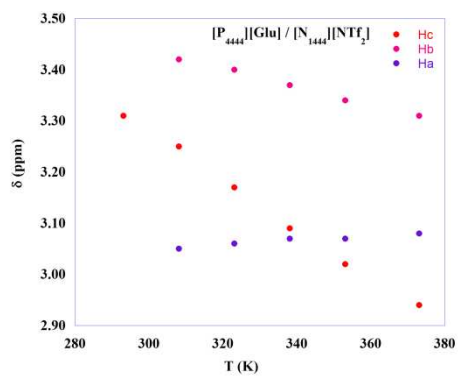
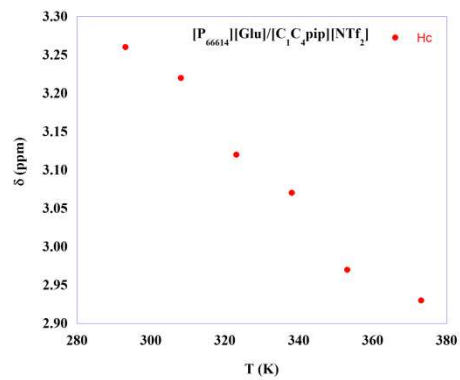
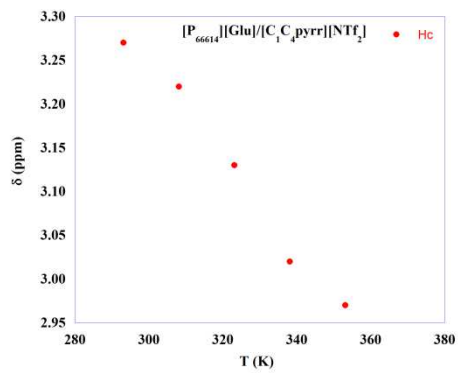
## A.5. VT $^1\text{H}$ NMR - spectra



Enlarged region of  $^1\text{H}$  NMR spectra of  $[\text{P}_{4444}][\text{Glu}]/[\text{N}_{1444}][\text{NTf}_2]$  at 3.0 % wt as a function of temperature.

## A.6. VT $^1\text{H}$ NMR – changes in chemical shift





## Acknowledgments

I would like to acknowledge MIUR for the financial support and the STEBICEF department for the success of this Research Project.

I would like also to thank all the people who were an active part, each in his own way, of this Ph.D..

Prof. Francesca D'Anna was the person, before me, has believed and still believes in my capacities. She was present all the time, for every necessity and question on Chemistry and on Life. I want to thank my supervisor for supported me in all, not just in the scientific life. Thank you for this Project and this Thesis and for what will come.

A special thank is for Prof. Kenneth Seddon. He believed in me from the beginning and he did a lot for me. This thesis is also his merit.

I want to thank Dr. Natalia Plechkova and Dr. Nimal Gunaratne. They were my scientific help in Belfast. They were helpful for each problem, not only in the lab.

I want to thank Prof. Renato Noto, who supported the Research Project and the Ph.D. development.

I want to thank my labmates Carla, Salvo and Alessandro. We are together every day, helping each other, chatting and laughing, all of this has made them friends, more than colleagues. In particular, Dr. Carla Rizzo and Dr. Salvo Marullo were precious during the thesis writing period, both practically and emotionally. Thank you.

Thank you to Dr. Marco Cascino and Casimiro Caruso, they were the essential technical support of all the work done in Palermo.

Thank you to Mrs. Deborah Poland, who was smiling all the time and was able to resolve every single problem I had!

Thanks to the technicians Richard Murphy, Connor McGrann and Angela Brownlie.

I want to thank friends I have met in Belfast - Marta has been the friend every person wishes to meet. Isa, who is a special person. Fede, who made my life in Belfast lighter and funny. Darius, my drinking friend in the last period. Albert and Ana, Fabio, Nati, Laura, Dani, Eris, all of them had a special part on my way. They were my full stops in this adventure, making my time in Belfast unforgettable.

Thanks to Elisa, Carla, Ciccio and Rosi. They were special colleagues in the beginning and became special friends. They made these years funny, happy and laughing. I know I have two families, one consists of them.

Thanks to my family. Nothing in my life would be without them. They were my guiding light in each new challenge of life. There to help, support, believe and love. This thesis is dedicated to them.

Thanks to Riccardo, because he has stayed close to me during my Ph.D., which was half time in another country. It was not easy, but I never felt loved less.

# Curriculum Vitae

**General information:** Floriana Billeci; address: Via Mariano D'Amelio, 3, 90143, Palermo; e-mail address: floriana.billeci@unipa.it; nationality: Italian; data of birth: 23/09/1989.

## **Education and Training:**

### **4 December 2018**

Qualifying examination to chemistry register obtained at University of Palermo.

### **February-April 2018**

Support as laboratory demonstrator, in the educational laboratory, for students training Inorganic Chemistry in the Bachelor's degree. Queen's University of Belfast.

### **1 November 2015 – 31 October 2018**

Ph.D. on Molecular and Biomolecular Chemistry. Supervision of Prof. Francesca D'Anna, University of Palermo; Prof. Kenneth R. Seddon, Dr. Natalia V. Plechkova and Dr. H. Q. Nimal Gunaratne, QUILL, Queen's University of Belfast.

Research Project: "Sweet" Ionic Liquids based materials for environmental applications. Several Ionic Liquids carrying natural moieties on the structure were synthesised, characterised, and applied in environmental remediation field and energy storage field.

### **March 2013 -October 2015**

Master's degree in Chemistry, 20 October 2015, 110/110 cum laude.

Specialist Curricula: Chemistry of molecular system. Degree Thesis: Self-assembly processes by fluorescent bis-imidazolium salts: analysis of alkyl chain effect. Supervision of Prof. Francesca D'Anna and Prof. Renato Noto. University of Palermo, Palermo.



**October – December 2011**

Training period at COFISE S.A.S. (Locorotondo Group), Palermo.

**October 2008 - March 2013**

Bachelor's degree in Chemistry, 27 March 2013, 102/110.

Degree Thesis: ultrasonic – ionic liquids synergy in “click-chemistry” reactions. Supervision of Prof. Francesca D’Anna and Prof. Renato Noto. University of Palermo, Palermo.

**27 September 2008**

passing the exam and obtaining the ECDL Certificate. AICA (Italian Association for Computer and Automatic Calculation).

**2007 – 2008**

Advanced Chemistry course. “Stanislao Cannizzaro” High School, Palermo.

**2006 - 2008**

Advanced Math course. “Stanislao Cannizzaro” High School, Palermo.

**September 2003 – July 2008**

Scientific High School leaving certificate, 08 July 2008, 93/100. “Stanislao Cannizzaro” High School, Palermo

**Publications:**

F. Billeci, F. D'Anna, H. Q. N. Gunaratne, G. Morgan, K.R. Seddon, N. V. Plechkova; *Green Chem.* submitted manuscript.

F. Billeci, F. D'Anna, H. Q. N. Gunaratne, N. V. Plechkova, K. R. Seddon, *Green Chem.* **2018**, 20, 4260-4276.

F. Billeci, F. D'Anna, I. Chiarotto, M. Feroci, S. Marullo, *New J. Chem.* **2017**, 41, 13889-13901.

F. Billeci, F. D'Anna, S. Marullo, R. Noto, *RSC Adv.* **2016**, 6, 59502-59512.

### **Conference Communications:**

Poster Communication to 27th Conference on Molten Salts and Ionic Liquids – EuCheMSIL 2018, Lisbon, Portugal, **7-12 October 2018**: F. D'Anna, F. Billeci, S. Marullo, N. Noto, C. Rizzo “Ionogels: Multifaced Materials”.

Poster Communication to 27th Conference on Molten Salts and Ionic Liquids – EuCheMSIL 2018, Lisbon, Portugal, **7-12 October 2018**: F. Billeci, F. D'Anna, H. Q. N. Gunaratne, N. V. Plechkova, K. R. Seddon “Ionic Liquid-cobalt complexes: a thermochromic interaction”.

Poster Communication to Quill meeting, **26-27 March 2018**, Queen’s University di Belfast. “Ionic Liquid: Materials for Desulfurisation processes”.

Poster Communication to E-Wisloc 2018: European Winter School on Physical Organic Chemistry, Bressanone, Italia, **28 January – 2 February 2018**: F. Billeci, F. D'Anna, H. Q. N. Gunaratne, N. V. Plechkova, K. R. Seddon ““Sweet” Ionic Liquid Gels: Properties and Applications”.

Oral Communication to Quill meeting, **27-28 March 2017**, Queens University di Belfast. ““Sweet” Ionic Liquids based on gluconic acid: properties”.

Oral Communication to 8th Green Solvents Conference, Kiel, Germany, **16-19 October 2016**: F. D'Anna, A. Meli, P. Vitale, F. Billeci, S. Marullo, C. Rizzo, R. Noto “Ionic liquids binary mixtures and zeolites: a combination to promote carbohydrates conversion into 5-hydroxymethylfurfural”.

Poster Communication to 8th Green Solvents Conference, Kiel, Germany, **16-19 October 2016**: F. Billeci, Francesca D'Anna, Salvatore Marullo, Renato Noto “Self-assembly of a fluorescent diimidazolium naphthalene diimide salt: The effect of increasing alkyl chain length”

Poster Communication to 8th Green Solvents Conference, Kiel, Germany, **16-19 October 2016**: S. Marullo, F. D'Anna, F. Billeci, C. Rizzo, P. Vitale, R. Noto “How mixing ionic liquids affects a Diels-Alder reaction”.

Poster Communication to 8th Green Solvents Conference, Kiel, Germany, **16-19 October 2016**: C. Rizzo, F. D'Anna, F. Billeci, S. Marullo, P. Vitale, R. Noto “Acidic imidazolium salts: catalysts for biomass transformation”.

Poster Communication to XV RSC-SCI Joint Meeting on Heterocyclic Chemistry, Taormina (Me), Italy, **12-15 May 2016**: F. Billeci, Francesca D'Anna, Salvatore Marullo, Renato Noto “Alkyl chain length effect on the self-assembly of diimidazolium naphthalene diimide salts”

Oral and Poster Communications to Quill meeting, **3-4 October 2016**, Queen’s University di Belfast. ““Sweet” Ionic Liquid based on gluconic acid”.